



Renata Marmo

NUMERICAL AND EXPERIMENTAL INVESTIGATION
ON SHEAR BEHAVIOUR OF RIVETED CONNECTIONS

*Tesi di Dottorato
XXIV ciclo*

*Il Coordinatore
Prof. Ing. Luciano ROSATI*

*Il Tutor
Prof. Ing. Raffaele LANDOLFO*

*Il co-Tutor
Dr. Ing. Mario D'Aniello*

On the front cover: Golden Gate Bridge – S. Francisco – California - USA
http://photoeverywhere.co.uk/west/usa/san_francisco/slides/golden_gate_bridge_details6334.htm

NUMERICAL AND EXPERIMENTAL INVESTIGATION ON SHEAR BEHAVIOUR OF RIVETED CONNECTIONS

Copyright © 2011 Università degli Studi di Napoli Federico II – P.le Tecchio 80, 80136 Napoli, Italy – web: www.unina.it

Proprietà letteraria, tutti i diritti riservati. La struttura ed il contenuto del presente volume non possono essere riprodotti, neppure parzialmente, salvo espressa autorizzazione. Non ne è altresì consentita la memorizzazione su qualsiasi supporto (magnetico, magnetico-ottico, ottico, cartaceo, etc.).

Benché l'autore abbia curato con la massima attenzione la preparazione del presente volume, Egli declina ogni responsabilità per possibili errori ed omissioni, nonché per eventuali danni dall'uso delle informazioni ivi contenute.

Finito di stampare il 01/12/2011

a Danilo

LIST OF CONTENTS

LIST OF CONTENTS	i
LIST OF FIGURES.....	v
LIST OF TABLES.....	xi
ABSTRACT	xiii
RINGRAZIAMENTI.....	xv
ABOUT THE AUTHOR.....	xvii
1 INTRODUCTION	1
1.1 Generalities on riveted connections.....	1
1.2 Objective of the research and methodology.....	2
1.3 Outline of the work.....	3
2 RIVETED CONNECTIONS IN HISTORIC METAL	
STRUCTURES.....	5
2.1 Riveted connections in historic metal constructions.....	6
2.1.1 Riveted Bridges.....	6
2.1.2 Riveted Monumental Constructions: the Eiffel Tower	15
2.2 History of riveted connections	16
3 RIVETED CONNECTIONS: STATE OF THE ART.....	23
3.1 Technology of riveted connections.....	23
3.1.1 General.....	23
3.1.2 Rivets: typologies and manufacturing.....	25
3.1.1 Manufacturing of steel plates.....	27
3.1.2 Manufacturing of hot driven riveted connections.....	28
3.1.3 Types of riveted connections.....	30
3.1.4 Failure modes of riveted connections	32
3.2 Resistance Verifications	33
3.2.1 The Eurocode resistance verifications	33
3.2.2 Long connections and long rivets.....	38
3.2.3 Nominal and actual stresses.....	39
3.3 State of the art: numerical studies and experimental activities on riveted connections.....	43
4 EXPERIMENTAL ACTIVITY ON RIVETED	
CONNECTIONS.....	69
4.1 Experimental programme.....	69

4.1.1	General.....	69
4.1.2	Programme of material tests.....	71
4.1.3	Testing programme on riveted connections and investigated parameters	71
4.1.4	Set-up of material and riveted connection tests.....	74
4.2	Experimental results.....	76
4.2.1	Test on materials	76
4.2.2	Tests on riveted connections.....	80
4.3	Interpretation of experimental results	83
4.3.1	Effect of load eccentricity.....	83
4.3.1	Effect of variation in A_n/A_g ratio.....	86
4.3.2	Effect of plate width.....	87
4.3.3	Effect of joint length	88
4.3.1	Effect of clamping forces.....	93
4.4	Theoretical vs. experimental strength.....	94
4.4.1	Effects of hot driven process	97
4.4.2	Effects of rivet clamping.....	99
4.4.3	Effects of net efficiency	99
4.5	Concluding remarks	100
5	NUMERICAL STUDY OF RIVETED CONNECTIONS.	103
5.1	Finite Element Analysis	104
5.1.1	Generalities.....	104
5.1.2	FEA by the Abaqus computer program	105
5.2	FE Models of riveted connections.....	106
5.2.1	Geometry of the models	106
5.2.2	The material modelling.....	108
5.2.3	The interaction between the component parts	113
5.2.4	Element type and mesh.....	116
5.2.5	Loads and boundary conditions.....	118
5.3	Calibration of the riveted connection FE model.....	120
5.3.1	Effect of hot-driven process.....	121
5.3.2	Effect of rivet clamping.....	126
5.4	Numerical results	129
5.4.1	Load-displacement curves.....	129
5.4.2	Collapse modes.....	134
5.5	Concluding remarks	136
6	THEORETICAL VS. NUMERICAL RESULTS	139
6.1	Hot-driven process.....	140
6.2	Rivet clamping.....	144

6.3	Conclusive remarks	147
7	CONCLUSIONS	149
8	FURTHER DEVELOPMENTS: CFRP-TO-STEEL	
	STRENGTHENING	153
8.1	Experimental activity.....	154
8.1.1	Preparation of specimens and application of CFRPs	154
8.1.2	Investigated parameters and experimental programme..	155
8.1.3	Set-up of adherence and riveted connection.....	156
8.2	Experimental results.....	158
8.2.1	Failure modes for simple bonding tests	158
8.3	Conclusive remarks	161
9	APPENDIX	163
	REFERENCES	293

LIST OF FIGURES

Figure 2.1 Coalbrookdale Bridge.	7
Figure 2.2 Eads bridge.	8
Figure 2.3 Forth bridge.	9
Figure 2.4 a. Baker's human cantilever; b. a rivet from Forth Bridge (Visitor centre trust Forth Bridge).	9
Figure 2.5 Forth bridge: construction phases.	10
Figure 2.6 Garabit viaduct.	10
Figure 2.7 Brooklyn bridge.	11
Figure 2.8 Golden Gate bridge.	13
Figure 2.9 Sydney Harbour bridge.	14
Figure 2.10 a. detail of riveted connections; b. rivet from the Sydney Harbour (Mackaness, 2006).	14
Figure 2.11 Eiffel tower.	15
Figure 2.12 NYC Railroad All-Riveted Lattice Trusses (Gasparini et al., 1997).	17
Figure 2.13 Canestota Station All-Riveted Lattice Bridge Designed by Charles Hilton (Gasparini et al., 1997).	18
Figure 2.14 Portable Hydraulic Riveter Patented by Chester B. Albree In 1896 (Gasparini et al., 1997).	20
Figure 2.15 The Boyer Long-Stroke Pneumatic Hammer (Gasparini et al., 1997).	21
Figure 2.16 PRR All-Riveted Bridge Built in 1909 (Gasparini et al., 1997).	21
Figure 3.1 Old steel section realised with riveted connections (Marrullier, 1925).	24
Figure 3.2 Types of rivet head.	25
Figure 3.3 Formation of holes: a) punching, b) drilling.	27
Figure 3.4 Heating of rivets: a) forge; b) red hot rivets (Vermes, 2007).	28
Figure 3.5 Phases of rivet formation: a) insertion of the rivet, b) formation of the rivet (Vermes, 2007).	28
Figure 3.6 "Bucking" bar (Fierro, 2009).	29
Figure 3.7 Loose rivets (Masi, 1996).	29

Figure 3.8 types of riveted connections: a) Lap joint, rivet in single shear, b) Butt joint, rivet in double shear, c) Rivet in multiple shear (Bresler et al. 1960).....	30
Figure 3.9 Rivet in tension (Bresler et al. 1960).....	31
Figure 3.10 Types of riveted connections: a) Eccentric load connection, b) Pure moment connection, c) Shear-moment connection (Bresler et al., 1960).....	31
Figure 3.11 Types of riveted connection failure: a) Tension failure in the plates b) Shearing failure in the rivet, c) Bearing failure, d) Shear-out failure in the plates (Bresler et al., 1960).....	32
Figure 3.12 Stresses in riveted connections: a) A riveted connection, b) Tensile stress, c) Shearing stress, d) Bearing stress (Bresler et al., 1960).....	33
Figure 3.13 Partial safety factor γ_M given by EN 1993-1-8.	34
Figure 3.14 Symbols for end and edge distances and spacing of fasteners given by EN 1993-1-8.....	36
Figure 3.15 Long connections (EN 1993-1-8).....	39
Figure 3.16 a) Elastic stress distribution, b) Plastic stress distribution (Bresler et al., 1960).....	41
Figure 3.17 Bearing stress distribution (Bresler et al., 1960).....	42
Figure 3.18 Sawed Sections of driven rivets (Kulak et al., 1987).	44
Figure 3.19 Sawed Sections of driven rivets (Kulak et al., 1987).	45
Figure 3.20 Typical fractures at four shear-tension ratios (Kulak et al., 1987).....	45
Figure 3.21 Interaction curve for rivets under combined tension and shear (Kulak et al., 1987).....	46
Figure 3.22 Distribution of slip condition for clean mill scale surfaces (Kulak et al., 1987).	48
Figure 3.23 Load partition in joint with a) four fasteners in line, b) ten fasteners in line (Kulak et al., 1987).....	49
Figure 3.24 Gusset plate connection (Kulak et al., 1987).....	50
Figure 3.25 Schematic of eccentricity in joints (Kulak et al., 1987).	50
Figure 3.26 Angle failure in built-up section (Kulak et al., 1987).....	51
Figure 3.27 Correlation of theoretical and test efficiencies (Kulak et al., 1987).....	52
Figure 3.28 Lap shear connection (Kulak et al., 1987).	52
Figure 3.29 Effects of secondary bending moment (Kulak et al., 1987).....	53
Figure 3.30 Details of riveted stiffened seat angle connections (Sarraf et al., 1996).....	54

Figure 3.31 a) Top angle deformation; b) Moment-strain curve measured near location of plastic hinge formed in vertical leg of top angle (Sarraf et al., 1996).....	54
Figure 3.32 Retrofit details: a) Ductile knee braces; b) Selective weldings (Sarraf et al., 1996).....	55
Figure 3.33 Hysteretic curves of retrofitted connection (Sarraf et al., 1996).....	56
Figure 3.34 Fatigue resistance of bolted and riveted connections (Valtinat et al., 2004).	57
Figure 3.35 Stress distribution in net section (Valtinat et al., 2004).....	57
Figure 3.36 Base material chemical composition (Fernandes et al., 2004).	58
Figure 3.37 Microstructure of base material (Fernandes et al., 2004).....	58
Figure 3.38 Macrostructure of rivet (Fernandes et al., 2004).....	59
Figure 3.39 Riveted beam used for the stress intensity factor determination (Moreno et al 2004).	60
Figure 3.40 Force transmission at the rivets due to the cracking of the web plate (Moreno et al 2004).	61
Figure 3.41 Geometrical configuration and loading of the analysed beam (Moreno et al. 2006).....	62
Figure 3.42 Experimental results and comparison with the numerical results (Moreno et al. 2006).	64
Figure 3.43 Finite element model used for analyse the tensile necking at the net section (Moreno et al. 2006).....	65
Figure 3.44 The riveted bridge parts that were tested: (a) test set-up; (b) detail of the connections (Moreno et al. 2006).	66
Figure 3.45 Out-of-plane distortion of a connection angle (Moreno et al. 2006).....	67
Figure 3.46 The distribution of bending stresses in the connection angle (Moreno et al. 2006).....	68
Figure 4.1 Riveted specimens: investigated typologies (D’Aniello et al. 2010).....	70
Figure 4.2 Coupon sampled from a plate of riveted specimen under testing (a); rivet coupon under testing (b) (D’Aniello et al. 2010).....	74
Figure 4.3 Dog-bone rivet shank (D’Aniello et al. 2010).	75
Figure 4.4 Test setup (a); the testing machine (b); the layout of LVDTs (c, d) (D’Aniello et al. 2010).....	76
Figure 4.5 The stress–strain response of plates of riveted specimens.....	77
Figure 4.6 The stress–strain response of rivet specimens.	77

Figure 4.7 The stress–strain response of rivet specimens (D’Aniello et al., 2010).....	81
Figure 4.8 Main types of failure mechanism and relevant response curve.	83
Figure 4.9 Rivet number vs. ultimate strength (unsymmetrical specimens). (D’Aniello et al., 2010).....	92
Figure 4.10 Rivet number vs. ultimate strength (symmetric specimens). (D’Aniello et al., 2010).....	92
Figure 4.11 Symmetric vs. unsymmetrical specimen shear capacity. (D’Aniello et al., 2010).....	92
Figure 4.12 Comparison of experimental results and predicted strength according to EC3. (D’Aniello et al. 2010).....	96
Figure 4.13 Comparison of experimental and predicted strength calculated with proposed equations. (D’Aniello et al. 2010).....	97
Figure 5.1 Types of finite elements available in Abaqus 6.10.....	106
Figure 5.2 Geometrical details of the four types of riveted connections FE models.	107
Figure 5.3 Geometry of numerical model.	107
Figure 5.4 Experimental curves for C16 rivets.	110
Figure 5.5 Refined curves and true stress-true strain curve for C16 rivets.	111
Figure 5.6 Experimental curves for C22 rivets.	111
Figure 5.7 Refined curves and true stress-true strain curve for C22 rivets.	112
Figure 5.8 Experimental curves for S10 plates.	112
Figure 5.9 Medium curve and true stress-true strain curve for S10 plates.	113
Figure 5.10 Interaction properties in contact interactions: (a) “hard” normal contact interaction; (b) frictional behaviour (ABAQUS, 2010).	114
Figure 5.11 Modelling assumptions: implemented contact conditions.	115
Figure 5.12 Mesh thickening in the parts in contact.	116
Figure 5.13 preliminary sensitivity study of the mesh.....	117
Figure 5.14 Simulation of the experimental load pattern.	118
Figure 5.15 Simulation of the rivet clamping with the displacement method.....	119
Figure 5.16 Simulation of the rivet clamping with the force method....	120
Figure 5.17 Increased stress-strain relationship for C16 and C22 rivets.	122

Figure 5.18 Stress-strain relationship for S10 plates.	123
Figure 5.19 Hot driven process effects on S-16-10-1-S joint response.	124
Figure 5.20 Hot driven process effects on U-16-10-1-S joint response.	124
Figure 5.21 Hot driven process effects on S-22-12-4-S joint response.	125
Figure 5.22 Hot driven process effects on U-22-12-4-S joint response.	125
Figure 5.23 Rivets clamping forces, from a value of 10% of f_{yd} to 80% of f_{yd}	126
Figure 5.24 Effects of the variation of the rivet clamping force on S-16-10-1-S joint response.	127
Figure 5.25 Effects of the variation of the rivet clamping force on U-16-10-1-S joint response.	128
Figure 5.26 Effects of the variation of the rivet clamping force on S-22-12-4-S joint response.	128
Figure 5.27 Effects of the variation of the rivet clamping force on U-22-12-4-S joint response.	128
Figure 5.28 Experimental vs. numerical load-displacement curve of S-16-10-1-S joint.	130
Figure 5.29 Experimental vs. numerical load-displacement curve of U-16-10-1-S joint.	130
Figure 5.30 Experimental vs. numerical load-displacement curve of S-22-14-4-S joint.	131
Figure 5.31 Experimental vs. numerical load-displacement curve of U-22-14-4-S joint.	131
Figure 5.32 Experimental vs. numerical PEEQ of S-16-10-1-S joint (the shank diameter is considered in the direction of applied load).	132
Figure 5.33 Experimental vs. numerical PEEQ of U-16-10-1-S joint (the shank diameter is considered in the direction of applied load).	132
Figure 5.34 Experimental vs. numericals PEEQ of S-22-14-4-S joint.	133
Figure 5.35 Experimental vs. numericals PEEQ of U-22-14-4-S joint.	133
Figure 5.36 Experimental vs. Numerical collapse mode for S-16-10-1-S.	134
Figure 5.37 Experimental vs. Numerical collapse mode for U-16-10-1-S.	135
Figure 5.38 Experimental vs. Numerical collapse mode for S-22-12-4-S.	136
Figure 5.39 Experimental vs. Numerical collapse mode for U-22-12-4-S.	136

Figure 6.1 Force-displacement curves for S-16-10-1-S.....	141
Figure 6.2 Force-displacement curves for U-16-10-1-S.	141
Figure 6.3 Increased stress-strain relationship for C16 and C22 rivets.	142
Figure 6.4 Hot driven process effects on S-22-12-4-S joint response...	143
Figure 6.5 Hot driven process effects on U-22-12-4-S joint response..	143
Figure 6.6 Effects of the variation of the rivet clamping force on S-16-10-1-S joint response.	144
Figure 6.7 Effects of the variation of the rivet clamping force on U-16-10-1-S joint response.	145
Figure 6.8 Effects of the variation of the rivet clamping force on S-22-12-4-S joint response.	146
Figure 6.9 Effects of the variation of the rivet clamping force on U-22-12-4-S joint response.	146
Figure 8.1 Test setup (a); the testing machine (b); the layout of LVDTs (c, d).....	157

LIST OF TABLES

Table 3.1 Minimum and maximum spacing, end and edge distances.....	35
Table 4.1 Bonding test programme matrix (D’Aniello et al. 2010).....	73
Table 4.2 Material characterization: BH measurements and CVN fracture toughness (D’Aniello et al., 2010).....	79
Table 4.3 Chemical composition of the plates (D’Aniello et al., 2010)...	79
Table 4.4 Chemical composition of the rivets (D’Aniello et al., 2010)...	80
Table 4.5 Single rivet specimens: parameters characterizing the mechanical response (D’Aniello et al., 2010).	84
Table 4.6 Specimens with rivets in row: parameters characterizing the mechanical response (D’Aniello et al., 2010).	88
Table 4.7 Specimens with rivets in row: parameters characterizing the mechanical response (D’Aniello et al., 2010).	91
Table 5.1 Mechanical properties of rivets.	113
Table 6.1 F_u/F_{EC3} values for specimens failed for rivet shear.....	140
Table 6.2 Different models for S-16-10-1-S.....	141
Table 8.1 Bonding test programme matrix.....	156
Table 8.2 Bonding test specimens.....	156
Table 8.3 Failure modes and load-displacement curves for B150.....	158
Table 8.4 Failure modes and load-displacement curves for B200.....	159
Table 8.5 Failure modes and load-displacement curves for B250.....	160

ABSTRACT

Hot-driven rivets were extensively used in iron and steel structures in the past. Nowadays, these constructions represent an important part of the architectural and cultural heritage that needs to be preserved and protected. The majority of historic steel structures is still in service and is exposed to loads larger than expected. The reliability of these structures is also affected by deterioration and the poor quality of material (Sustainable bridges 2006).

After several decades from their erection, this class of constructions reveals some damages and/or structural inadequacies (Guerrieri et al. 2005). These types of constructions are generally characterized by trussed structural schemes. Hence, the failure of connections can produce the overall failure of the structure, because the riveted connections represent the weaker elements of these structures.

These considerations lead to identify the vulnerability of connections as the crucial aspect concerning the structural capacity of ancient metal structures.

Hence, the present work is devoted to investigate the structural capacity of lapped riveted connections loaded in shear typically adopted in aged metal structures still in service. The aim is the development of a valid methodology of prevision of the existing riveted connections behaviour.

After a preliminary study on the technology of riveted connections and the rivet forming process, and in particular on the effects of hot driven process on the overall behaviour, a review of the actual codes prescriptions is reported, highlighting the approximations in the prescribed verifications and providing to a description of the local phenomena that characterizes the connection behaviour. An overview on the prior research on riveted connections is also presented, in which the experimental studies and the numerical simulations proposed and studied up to today are discussed and described. The literature experimental and numerical studies on riveted connections need to be extended to different materials, geometries and configurations, due to the sensitivity of the connection response to the manufacturing process (Hechtman, 1948; Schenker et al., 1954, Munse, 1970).

To this end, a large experimental investigation carried out within the framework of the European project PROHITECH. A detailed description of this campaign is reported: after a detailed illustration of the set-up of experimental tests and of the monitored parameters, the results are presented and discussed. On the basis of a careful revision of results, in the final part of the chapter a theoretical formulation on the failure verifications of these connections is proposed, by revising the EN 1993 1-8 2005 formula.

On the basis of the experimental results, a highly detailed riveted connections F.E. model is proposed. The geometries and the mechanical characteristics are described, and contact interactions are illustrated. The element type and the mesh sizing are highlighted, and the rivet clamping model is described. The calibration of the F.E. model is also illustrated. At last, the numerical results are reported and discussed.

The work ends with a comparison between numerical and proposed theoretical results to verify the reliability of the theoretical equations and F.E. results. In this manner, a useful tool to predict the behaviour of all types of riveted connections is provided. To this end, the magnitude of numerical results was compared with the proposed theoretical formulas, to ensure both the good accuracy of F.E. model and the reliability of the proposed equations. At last, the main conclusions of the work, together with possible further developments for future research, are illustrated.

RINGRAZIAMENTI

Only in the printed version

ABOUT THE AUTHOR

Renata Marmo was born in Naples, Italy, on January 19th, 1983. She graduated cum laude in Architecture at the University of Naples “Federico II” with a thesis in structural engineering named “About vulnerability of steel historic bridges: the case of a steel railways bridge on Gesso river”. She won with grant the PhD competition in Structural Engineering, XIV cycle, in December 2007. She studies riveted connections in historic metal structures. In fact, she takes part to the experimental activities, and she implemented a F. E. model representative of connections behaviour. She deepened also the fire behaviour of riveted connections. Furthermore, she studies tenon joints in timber structures. She is co-authoress of some scientific publications on all the above-mentioned topics:

1. Portioli F., Marmo R., Ceraldi C., Landolfo R. (2010). Numerical Modeling Of Connections With Timber Pegs. Proc. Of International Conference on Timber Engineering “WCTE 2010”, Riva del Garda, Trentino, Italy, 20-24 June 2010, paper n° 490.
2. Marmo R. (2010). The use of timber tenon joints with pegs: a sustainable solution for improving deconstruction. Proc. of International Symposium on Sustainability of Constructions – Integrated Approach to Life-time Structural Engineering. COST Action C25, Malta, 26 July – 1 August 2010, pp. 287-320.
3. Marmo R., D’Aniello M., Portioli F., Landolfo R. (2010). Finite element modelling of lap shear riveted connections in fire. Proc. of International Conference on Urban Habitat Constructions Under Catastrophic events Final Conference, COST Action C26, Napoli, 16-18 September.
4. Marmo R., D’Aniello M., Portioli F., Landolfo R. (2010). Historic Metal Elements Strengthened By Means Of Cfrp. Proc. Of International Conference EUROSTEEL 2011, August 31 - September 2, 2011, Budapest, Hungary

Renata Marmo è nata a Napoli, Italia, il 19/01/1983. Si è laureata con lode in Architettura presso l'Università degli Studi di Napoli "Federico II" il 09/11/2007 con tesi in tecnica delle costruzioni dal titolo "Sulla vulnerabilità dei ponti storici chiodati: il caso del ponte ferroviario sul fiume Gesso". Nel dicembre 2008 ha partecipato al concorso di ammissione al dottorato di ricerca in ingegneria delle costruzioni, XIV ciclo, ed ha vinto con borsa di studio. La principale tematica di studio riguarda il comportamento a taglio delle unioni chiodate nelle strutture metalliche storiche. A tal fine, ha seguito in maniera attiva la campagna di prove sperimentali sulle unioni chiodate ed ha implementato un modello agli elementi finiti che rappresenta in maniera significativa il loro comportamento. Di queste connessioni, poi, ha approfondito il comportamento a fuoco. Accanto alle unioni chiodate, la dottoranda studia inoltre il comportamento dei giunti a tenone nelle strutture in legno. Infine, è coautrice di alcune pubblicazioni scientifiche riguardanti tutte le tematiche sopra riportate:

1. Portioli F., Marmo R., Ceraldi C., Landolfo R. (2010). Numerical Modeling Of Connections With Timber Pegs. Proc. Of International Conference on Timber Engineering "WCTE 2010", Riva del Garda, Trentino, Italy, 20-24 June 2010, paper n° 490.
2. Marmo R. (2010). The use of timber tenon joints with pegs: a sustainable solution for improving deconstruction. Proc. of International Symposium on Sustainability of Constructions – Integrated Approach to Life-time Structural Engineering. COST Action C25, Malta, 26 July – 1 August 2010, pp. 287-320.
3. Marmo R., D'Aniello M., Portioli F., Landolfo R. (2010). Finite element modelling of lap shear riveted connections in fire. Proc. of International Conference on Urban Habitat Constructions Under Catastrophic events Final Conference, COST Action C26, Napoli, 16-18 September.
4. Marmo R., D'Aniello M., Portioli F., Landolfo R. (2010). Historic Metal Elements Strengthened By Means Of Cfrp. Proc. Of International Conference EUROSTEEL 2011, August 31 - September 2, 2011, Budapest, Hungary

1 INTRODUCTION

1.1 GENERALITIES ON RIVETED CONNECTIONS

Hot-driven rivets were extensively used in iron and steel structures in the past. Nowadays, these constructions represent an important part of the architectural and cultural heritage that needs to be preserved and protected. Historic metal structures include several typologies, as large span roofing of urban passages, gasholder structures and railway constructions (D’Aniello et al., 2010).

Railway structures represent a considerable part of construction heritage in many European countries. In Italy, the railway network includes approximately 3500 steel bridges and 14 000 lattice roof structures. The main part of these constructions were built in the period 1910–1960 and were assembled by riveting, although high-strength bolts started to be used in the 1930s (Batho et al., 1934).

The majority of historic steel structures is still in service and is exposed to loads larger than expected. The reliability of these structures is also affected by deterioration and the poor quality of material (Sustainable bridges, 2006).

After several decades from their erection, this class of constructions reveals some damages and/or structural inadequacies (Guerrieri et al., 2005). The ancient metal structures, generally made of puddled iron or wrought steel riveted plates, were built on the basis of the experience on timber constructions, consequently without an adequate knowledge and maturity about typical aspects of design of steel structures. These types of constructions are generally characterized by trussed structural schemes. Hence, the failure of connections can produce the overall failure of the structure, because the riveted connections represent the weaker elements of these structures.

These considerations lead to identify the vulnerability of connections as the crucial aspect concerning the structural capacity of ancient metal structures.

1.2 OBJECTIVE OF THE RESEARCH AND METHODOLOGY

The research presented in this work is framed in the experimental, theoretical and numerical studies aimed at the development of a valid methodology of prevision of the existing riveted connections behaviour. Indeed, despite many studies have investigated the behaviour of riveted connections, it is necessary to deepen the behaviour of these joints varying the geometries and the material characteristics.

Then, the first objective is the extension of the existing results that have been obtained in literature to different materials, geometries and configurations, due to the sensitivity of the connection response to the manufacturing process (Hechtman, 1948; Schenker et al., 1954, Munse, 1970). Moreover, the actual codes prescription for this kind of connections should be revised. The modern codes (EN 1993: 1-8) indeed treats the strength of riveted and bolted lap shear splices in a similar manner, despite the different manufacturing process, with the exception of slip-resistance. In EN 1993: 1-8 riveted connections are not considered as a slip-resistant type, but as a bearing type, owing to the variability and low average value of clamping force.

The second objective is the evaluation of the riveted connections local phenomena to propose corrective factors to the actual codes verifications. To this end, it is necessary to consider the different factors, including loading conditions, geometric and mechanical parameters and manufacturing procedures, which affect the capacity of hot-driven connections. Many variables concur in the installation of hot-driven rivets: the driving and finishing temperature, driving time and pressure. Indeed, as given by D'Aniello et al. (2010): “after the rivets have been heated to a high temperature, the manufacturing procedure requires that the plain end of the fastener is forged into a head by means of a pneumatic hammer. Then, when the hot rivet cools, it shrinks and pulls the parts tightly together. Thus, a residual clamping force and a pre-stressing in the rivet, with a partial slip resistance of the joint are obtained”. The grip length, the rivet diameter, the material and fabrication methodology, are some of the many parameters that influence the pre-stress state: for this reason a reliable calculation method to determine the pre-stress state of the rivet is not available. As well as the installation of rivets, the driving influences noticeably the strength of rivets and plates: as reported in Munse (1970), Fisher et al. (1969) and Schutz (1952), the results of existing tests showed that the

tensile strength of rivets could be increased by driving process by up to about 20% with respect to undriven rivets. Furthermore, beside the increase of strength, a considerable reduction in elongation capacity was observed, thus resulting in brittle behaviour. Another phenomenon that could be affect the riveted connections behaviour is the technique used to perforate the plates. As given by D'Aniello et al. (2010): “In old metal structures, holes were obtained by techniques such as: drilling, punching, sub-drilling and reaming, punching and reaming. Their effects on shear connections are important when splices fail by tearing in the net section”. With the aim to analyze the influence of different parameters on the shear capacity of typical lap shear connections representative of historic structural typologies in terms of structural verification according to the modern codes, a wide experimental investigation was carried out within the framework of the PROHITECH project (2005).

The third and last objective is the development of a reliable F.E. model of the tested connections, which could be extended to any other riveted connections. On the basis of the tests results, a 3D, highly detailed, finite element model of four different typologies of riveted connections is implemented, and the numerical results are compared with the experimental and theoretical ones, to ensure its reliability. In this way, the behaviour of all types of riveted connections could be derived, and a useful tool could be proposed for the evaluation of the vulnerability of ancient riveted connections.

1.3 OUTLINE OF THE WORK

This work is organized into eight chapters. After brief introductory remarks on the generalities of the riveted connections, on the main objectives of the research and on the followed study methodology, reported in Chapter 1, the history of riveted connections is described in Chapter 2. Since the riveted connections are proposed as a main connection system to join metallic members in historic metal structures, some considerations on the development of this technique during history are provided, focusing on the technological innovations in terms of field riveting process.

Chapter 3 deals with the features of riveted connections, focusing on their mechanical behaviour and on the related practical advantages. The

technology of riveted connections are illustrated, and the rivet forming process is described, focusing on the effects of hot driven process on the overall behaviour of these connections. A review of the actual codes prescriptions is reported, highlighting the approximations in the prescribed verifications and providing to a description of the local phenomena that characterizes the connection behaviour. The final part of the chapter is devoted to an overview on the prior research on riveted connections, in which the experimental studies and the numerical simulations proposed and studied up to today are presented and described.

Chapter 4 consists in a detailed description of a wide experimental campaign on aged riveted connections, devoted to determine the characteristics of aged steel materials and of historic riveted connections behaviour. After a detailed illustration of the set-up of experimental tests and of the monitored parameters, the results are presented and discussed. On the basis of a careful revision of results, in the final part of the chapter a theoretical formulation on the failure verifications of these connections is proposed, by revising the EN 1993 1-8 2005 formula.

Chapter 5 deals with the use of numerical analyses, based on the Finite Element Method, for the investigation of the behaviour of riveted connections. General information on the Finite Element Method is provided, and the main characteristics of the ABAQUS advanced computer program are briefly described. In the second part of the chapter, the attention is focused on the riveted connections F.E. model. The geometries and the mechanical characteristics are described, and contact interactions are illustrated. The element type and the mesh sizing are highlighted, and the rivet clamping model is described. The calibration of the F.E. model is also illustrated. At last, the numerical results are reported and discussed.

Chapter 6 deals with the comparison between numerical and proposed theoretical results to verify the reliability of the theoretical equations and F.E. results. In this manner, a useful tool to predict the behaviour of all types of riveted connections will be provided. To this end, the magnitude of numerical results was compared with the proposed theoretical formulas, to ensure both the good accuracy of F.E. model and the reliability of the proposed equations.

At last, the main conclusions of the work, together with possible further developments for future research, are illustrated.

2 RIVETED CONNECTIONS IN HISTORIC METAL STRUCTURES

Hot-driven rivets were extensively used in iron and steel structures in the past. Nowadays, these constructions represent an important part of the architectural and cultural heritage that needs to be preserved and protected. Historic metal structures include several typologies, as large span roofing of urban passages, gasholder structures and railway constructions (D'Aniello et al., 2010).

Railway structures represent a considerable part of construction heritage in many European countries. In Italy, the railway network includes approximately 3500 steel bridges and 14 000 lattice roof structures. The main part of these constructions were built in the period 1910–1960 and were assembled by riveting, although high-strength bolts started to be used in the 1930s (Batho et al., 1934).

The majority of historic steel structures is still in service and is exposed to loads larger than expected. The reliability of these structures is also affected by deterioration and the poor quality of material (Sustainable bridges, 2006).

After several decades from their erection, this class of constructions reveals some damages and/or structural inadequacies (Guerrieri et al., 2005). The ancient metal structures, generally made of puddled iron or wrought steel riveted plates, were built on the basis of the experience on timber constructions, consequently without an adequate knowledge and maturity about typical aspects of design of steel structures. These types of constructions are generally characterized by trussed structural schemes. Hence, the failure of connections can produce the overall failure of the structure, because the riveted connections represent the weaker elements of these structures.

These considerations lead to identify the vulnerability of connections as the crucial aspect concerning the structural capacity of ancient metal structures.

Hence this chapter provides an overview of the above mentioned connections, describing the most commonly used in the field of

constructions, the technology of riveting process, the actual codification guidelines, and the state of the art.

2.1 RIVETED CONNECTIONS IN HISTORIC METAL CONSTRUCTIONS

During the 18th century, the advent of new materials, such as steel and glass, allowed the development of new structural typologies and the decline of the masonry as unique structural material. This technological revolution changed the structural design, and determined a transformation of the methods and the types of constructions (Parrilli, 2010).

The replacement of the masonry buildings with cast iron columns represented the first main transformation. This replacement made possible to have more space to accommodate the bulky machines of new industries (Parrilli, 2010).

Moreover, at the end of 18th, in Britain, a lot of timber – floored factories burned due to disastrous fires. These structures were replaced with metallic frames, and allowed the development of the so-called fireproof buildings (Parrilli, 2010).

Another important transformation was represented by the development of new typologies of bridge structures. The mechanical properties of the metal material, such as the good response in terms of strength and the possibility to realise light structures, allowed the development of long span bridges.

2.1.1 Riveted Bridges

2.1.1.1 Coalbrookdale Bridge

The Coalbrookdale Bridge, denominated Ironbridge, was erected in the summer of 1779, and opened in the 1781. This bridge realised with the aim to cross the Severn River, represent the industrial revolution and the progress reached by the English industry.

This bridge, designed by Thomas Farnolls Pritchard and realised by two ironmasters, Abram Darby and John Wilkinson, traced the ancient

masonry arch bridges. The span is 30 m long and the height from the river level is 20 m. The Ironbridge presents also two main spans, and two secondary spans. The piles were strengthened to avoid problems with vibrations induced by the passage of trains. These vibrations, indeed, could determine instability problems in the iron elements.

Some years after the construction, this bridge presented cracks in the abutments and in the piles, some were repaired by means of wrought iron and steel belts, and others remained exposed. In 1934 the vehicular traffic were interrupted, nowadays this bridge represent an important historic heritage and it is included into UNESCO world heritage (Ryall et al., 2000).



Figure 2.1 Coalbrookdale Bridge.

2.1.1.2 Eads Bridge

The development of new structural typologies for long span bridges continued in USA, where in 1874 was erected the Eads bridge with the aim to join the Missouri with Illinois.



Figure 2.2 Eads bridge.

At that time, this bridge was the longest bridge ever built. Indeed, the entire structure was 1964 m long. Its name derived from the designer's name, James B. Eads. The structure is composed by three spans of upper deck arch bridge. The main span is the central one and has a length of 170 meters. The construction technique of the Eads bridge demonstrates a huge progress from the Ironbridge: the beams, indeed, are composed by two hollow sections joined each other by diagonals. All the joints are riveted connections. The piles are supported by reinforced concrete foundations. The marine traffic is ensured by an height from the waterline of 27 meters (Fierro, 2009).

2.1.1.3 Forth bridge

At the end of 17th century, a new construction technique was introduced: the cantilever beams. A cantilever bridge is formed by self-supporting arms anchored at and projecting toward one another from the ends; they meet in the middle of the span where they are connected together or support a third member.

The Firth of Forth Bridge (Fig. 2.3) in Scotland is a cantilever bridge, a complex version of the truss bridge. Rigid arms extend from both sides of two piers. Diagonal steel tubes, projecting from the top and bottom of each pier, hold the arms in place. The arms that project toward the middle are only supported on one side, like really strong diving boards. These "diving boards," called cantilever arms, support a third, central span. All the connections are riveted.



Figure 2.3 Forth bridge.

The initial designer of the Forth Bridge was Sir Thomas Bouch, a famous bridge engineer, known also for the construction of the railway bridge over the Firth of Tay with a total length of 3200 m. This multiple span truss bridge collapsed after a heavy storm in 1879, when a train was crossing the bridge (Fierro, 2009).

After this episode, Thomas Bouch lost all credibility with the railway company, his successors, J Fowler and B Baker, having to illustrate the statical principles of their design to the public (Fig. 2.4 a).

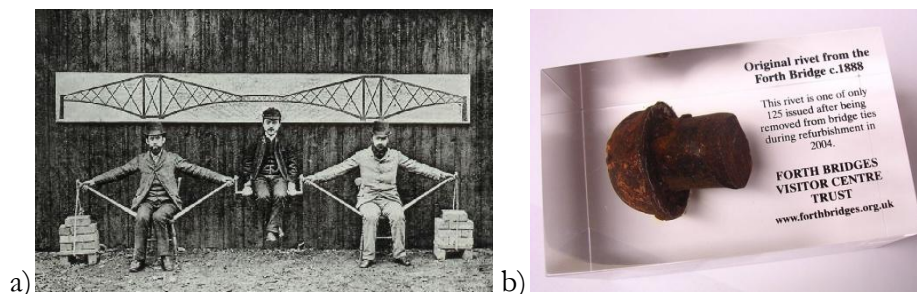


Figure 2.4 a. Baker's human cantilever; b. a rivet from Forth Bridge (Visitor centre trust Forth Bridge)

The bridge, which today is considered to be a unique and gigantic construction, is a masterpiece of engineering work. The depth of the truss above the piers is 106 m, the main tubular members are 3.7 m in diameter, and the whole bridge used 42.000 tons of steel and at times required up to 4.600 workers at the site to undertake the complex method of construction (Fig 2.5).

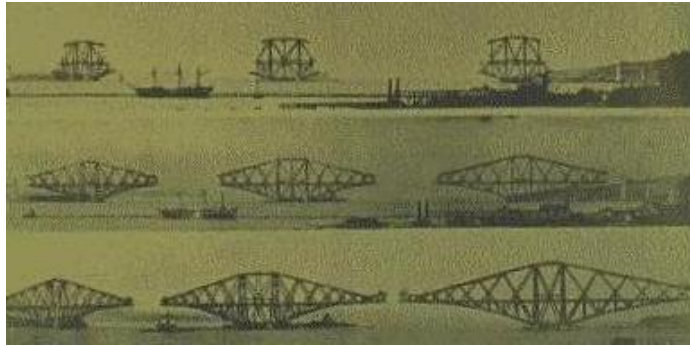


Figure 2.5 Forth bridge: construction phases.

2.1.1.4 Garabit viaduct

In the late 1800s, a mountainous barrier blocked the railways from reaching Southern France. For years, engineers tried to figure out a way to bridge the windy Garabit Valley in France's Massif Central.



Figure 2.6 Garabit viaduct.

Finally, one of the era's best engineers, Gustave Eiffel, came up with a brilliant solution. Indeed, the original designers, Boyer and Baudy, turned to Eiffel due to his huge experience in bridge construction (Fierro, 2009). To contrast the wind, Eiffel designs a truss arch, that offers a minimum surface to wind forces and allows the natural passage of the air. This arch was larger at the base, as the piles, to be more stable and to avoid swing problems. An ulterior technical progress was the huge height of the bridge from the waterline: 122 meters (Billington, 1983).

2.1.1.5 Brooklyn Bridge

One of the most important and innovative bridge was the Brooklyn bridge, one of the most ancient suspension bridges in USA. This Bridge, designed by John August Roebling in 1883, links Manhattan with Brooklyn, crossing the East River.



Figure 2.7 Brooklyn bridge.

The Roebling's idea was for a suspension bridge for railway and road traffic with a span of 486 m. But J. A. Roebling was not able to realise the project himself due to a mortal accident on site during surveying work, only 3 years after winning the contract. His son took over his position, but during the work in the pneumatic caissons for the foundation of the towers he suffered a serious collapse from caisson disease. From that time on he was an invalid, bound to his bed and suffering from a nervous disorder. He ran the project from his sickroom, located close to the site, watching the progress of the work through a field glass from his window (Fierro, 2009). His wife, Emily Warren Roebling dedicated her life to the bridge, became his assistant and kept contact with the workers and fellow engineers. When the Brooklyn or East River Bridge (Fig. 2.7) opened in 1883 it was a masterpiece of engineering work, the largest bridge in the world. The towers, built of masonry, were 107 m in height; the anchor blocks 60.000 tons in weight each; the 4 cables 40cm in diameter, consisting of 5358 wires each; stiffened by a deep trussed deck girder and a large number of diagonal stays.

After more than 100 years since it was opened, the Brooklyn Bridge is still in use.

2.1.1.6 Golden Gate Bridge

One of the masterpieces between suspension bridges is the Golden Gate Bridge, which links San Francisco with the Marin County. The idea to connect the Golden Gate straits was proposed by James Wilkins, who claimed the necessity of a new infrastructure to guarantee a faster and safer passage of the strait. In 1917, the bridge was called Golden Gate for the first time by the urban engineer M. H. O'Shaughnessy. The bridge has a total length of 2.71 km, the central span length is 1.282 m and the total height from the waterline is 67 m.

In this kind of bridge, the main beams are supported by suspension ties, connected to suspension cables; the diameter of the suspension cable is 91.34 cm. When the Golden Gate Bridge was built, in 1937, it was the longest suspension bridge ever built, and became the symbol of the city of S. Francisco.

The designer of the Golden Gate Bridge was Joseph Baermann Strauss, who initially designed a huge cantilever bridge, which was not approved. The final Golden Gate Bridge was erected thanks to the collaboration of

Irving Morrow, responsible of the decoration, the engineer Charles Alton Ellis and the bridge designer Leon Moisseiff (Fierro, 2009).



Figure 2.8 Golden Gate bridge.

The Golden Gate Bridge was opened in 1937, and, until the 1964, it was the longest suspended bridge in the world. The towers are 225 m high, and remained the tallest in the world until the construction of the Akashi-Kaikyo.

2.1.1.7 Sydney Harbour Bridge

Sydney Harbour Bridge is a steel arch bridge, for railway, cars and pedestrian traffic.



Figure 2.9 Sydney Harbour bridge.

This bridge was designed in 1923 by Bradfield, in collaboration with Laurence Ennis, Ralph Freeman and Arthur Plunkett. The construction began in 1928 and was assigned to Dorman Long & Co. The construction method was a cantilever-method: starting from the piles, the two half-part of the bridge was joined together in the mid-span.

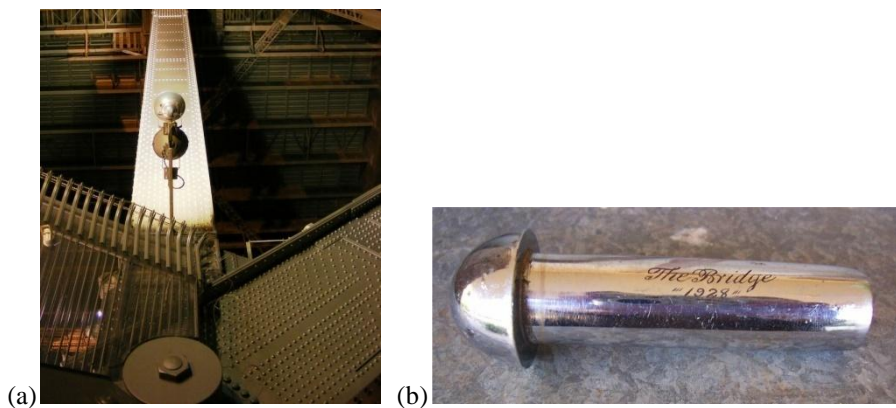


Figure 2.10 a. detail of riveted connections; b. rivet from the Sydney Harbour (Mackaness, 2006)

The bridge was opened in 1930; its safety was guarantee by testing the bridge vibration caused by the passage of trains.

A great part of the bridge steel, about the 79%, was produced in Middlesbrough, north England; the remaining part was produced in Australia. The total weight of Sydney Harbour bridge is 52800 tons, the total height from waterline is 134 m, and the length 503 m. For the connections, more than 6 millions rivet, realized in Lancashire (England), was used (Fierro, 2009).

2.1.2 Riveted Monumental Constructions: the Eiffel Tower

One of the most important metallic structures is represented by Eiffel tower, symbol of the industrial progress and icon of France. The tower was conceived in 1887 for the Universal Expo of 1889, and was designed by Eiffel.



Figure 2.11 Eiffel tower.

The main challenge of this construction was the wind resistance, due to the huge high. Eiffel conceived a truss tower, which allows the natural passage of the wind, with a pyramidal configuration, to guarantee the stability of the construction (Fierro, 2009).

The total weight of Eiffel tower is about 10000 tons, the metallic structure, instead, weighs 7200 tons. For the connections, more than 2 million and half rivets were used (Billington, 1983).

2.2 HISTORY OF RIVETED CONNECTIONS

One of the most important study of riveted connections, from the historical point of view, was performed by Dario Gasparini, ASCE member, and David Simons (1997). **“American truss bridge connections in the 19th century. II: 1850-1900”** is a chronicle of American metal bridges and of the use of riveted connections. Authors wrote that, after the introduction of iron, the construction field was interested in particular by the erection of bridges, as evidenced in “The Directory American bridge building companies” (Darnell, 1984). A recent study (Simmons, 1989) deepened the influences and the organization of one of the most important company in bridge construction.

The rise of company of construction entailed the decline of independent designer and builder: engineers began to affiliate themselves with bridge companies and railroad. Each company had a particular style of bridge and operated in a particular geographic area (Cooper, 1889).

After an accurate description of bridge structural innovation, authors deepened the riveted connections. The design of riveted connections remains largely empirical because stresses depend on many parameters that are highly uncertain. As described by authors (Gasparini et al., 1997): “Stresses depend not only on the loading and the geometry of the connection but also on the clamping force provided by each rivet, the friction between the plates, the actual details of the holes and rivets, and on the deformations of the plates being connected. Such complexity was very disheartening to mid-19th-century engineer. They had only recently developed the ability to compute stresses in beams and trusses and had adopted a working-stress design philosophy. Since stresses in riveted connections were impossible to compute, engineers were forced to measure or predict the strength of riveted connections and then limit loads to a fraction of it”. Richard DeJonge of the American Society of Mechanical Engineers (DeJonge, 1945) defines, in a bibliography of the technical literature on riveted connections, the steps of the development

of riveted connections, starting from the use of iron as a construction material until the development of investigations of the stress distribution in riveted plates.

The first period was dominated by British experimentation and by the fabrication of ships, lattice trusses, and bridges. William Fairbairn (with Eaton Hodgkinson) in 1849 and 1850 and by Edwin Clark (with Robert Stephenson) in 1850 published the first experimental results on riveted connections. As described by authors (Gasparini et al., 1997): “On the basis of these experiments Fairbairn estimated the ratio of strengths of a solid plate to the double-riveted lap joint and to the single-riveted lap joint as 100:70:56”.

Many other issues regarded riveted connections, as the best kind of rivet pattern, the best manufacturing of plate holes (punching or drilling), the optimum riveting process, the geometric details and so on. Only after the accumulation of experimental and field data engineers found an answer to all these questions.

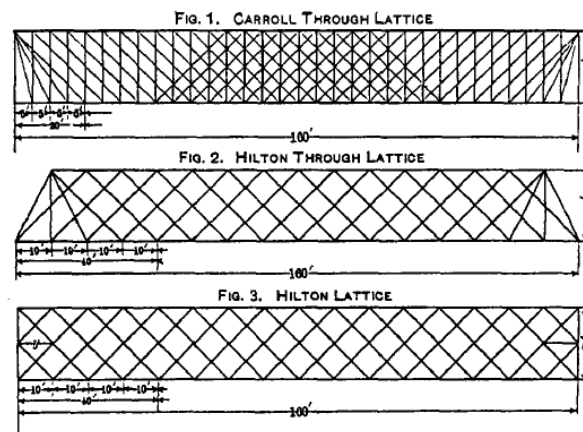


Figure 2.12 NYC Railroad All-Riveted Lattice Trusses (Gasparini et al., 1997).

The passage from hand or “snap” methods of riveting technology was documented by Wilfrid J. Lineham's 1902 Textbook of Mechanical Engineering. In his study, he described how hydraulic riveting was introduced in 1865 by Ralph H. Weddell, who developed also the “portable” hydraulic riveter in 1871, and was the first that applied it to bridge erection in 1873, on the Primrose Street Bridge in London.

The method of creating the holes for rivets was another American controversy revolved around. Drilling was preferred to punching, as described in the 1885 railway mechanics report, but, with “the leather-like ductile metal” then available, the expense of drilling was no longer justified. The riveting technique represented another issue revolved around. In the early 1870s, engineers not approved Machines that riveted “by a single squeeze”, and was preferred a multiple-stroke steam piston riveter. By the 1880s, shop riveting was done by a hydraulic piston, “having the merits of a single close squeeze and the adjustability of the steam piston”. The solid work produced by this hydraulic piston did not require any supplemental hand work in a process known as “caulking”.

A steady stream of activity on the design of all-riveted lattice bridges began in the United States from about 1857 to the late 1880s, principally for the New York Central (NYC) Railroad. Howard Carroll (a brilliant young Irish engineer, a Sir John MacNeil’s pupil, thoroughly imbued with English ideas), designed the earliest lattice trusses (Fig. 2.12). The Gray’s successor, Charles Hilton, working with George H. Thomson modified and improved the Gray/Carroll designs: they were employed in Americanizing the riveted lattice truss. A lattice truss designed by Charles Hilton for the NYC Railroad is shown in the next Figure.

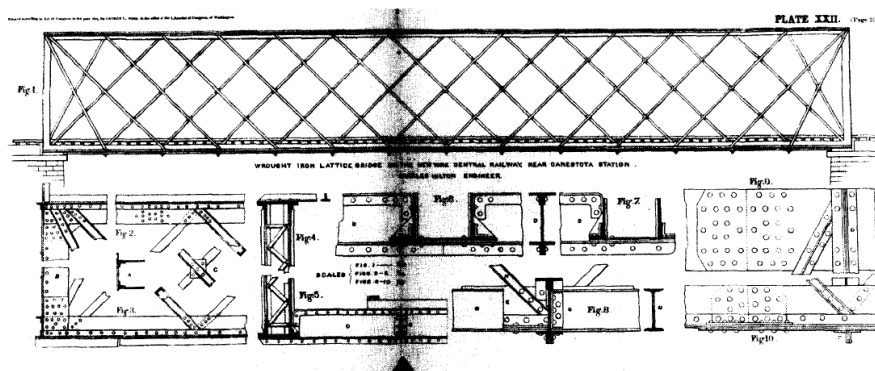


Figure 2.13 Canestota Station All-Riveted Lattice Bridge Designed by Charles Hilton (Gasparini et al., 1997).

The chief NYC engineer George E. Gray, with “assistance” from In 1877, Hilton wrote in a letter to the editor of *The Railroad Gazette* that “in the preceding seven years one builder had constructed over 8 m of lattice bridges and that this was probably less than half of the total length

of lattice bridges built in the United States” (Gasparini et al., 1997). T. C. Clarke and Walter Katte, in a discussion in Greiner’s paper (1895), noted the satisfactory performance of lattice bridges for over 20 years. In 1897, in an historical paper by Gray with a discussion by Thomson (Gray, 1897), Gray claimed that in 1859 the NYC was the first to build an all wrought iron, all-riveted railroad truss. Thomson notes that the “first design by Howard Carroll, was the bridge over the Mohawk River at Schenectady” which consisted of ten 20.4 m deck trusses, and that the “first specification for riveted bridgework known to the speaker as made by Carroll is dated 1857”. This, as reported by authors (Gasparini et al., 1997), “was the prototype for late-19th-century riveted-work specifications”. Thomson was considered the main proponent of all-riveted trusses, indeed, he wrote in 1888 a paper in *Engineering* on “American Bridge Failures”, decreeing that all-riveted designs are superior, particularly in case of accidents or “fault” conditions. Cooper (1889) and Waddell (1889) criticized strongly Thomson’s position. Cooper noted that “riveted lattice girders have been used quite generally on all our railroads for short spans and on certain lines of railroad for all spans”. He highlighted raised the old issue of field riveting to explain why a large span that necessitated “so much riveting of important connections at the bridge site, where that care and accuracy attainable at the shops cannot be depended upon,” would not be acceptable to many. In 1907, the collapse of Cooper’s pin-jointed Quebec Bridge accentuated the conflict between Thomson’s “all-riveted lattice truss school” and Cooper’s mainstream “American pin-jointed truss school”. Thomson deeply believed that more recognition to the pioneering NYC lattice bridges could be deserved, for the development of design procedures and construction practices for riveted joints. He also attacked “strain-sheet engineering”, maybe because lattice trusses were statically indeterminate, and bar forces had to be estimated using approximate methods. Probably the computation of bar forces in statically determinate trusses fell into disuse the lattice form, due to the hesitation of engineers to use approximate methods, even though lattice trusses had, in general, performed well. In the 1880s, in Britain and in the United States large-scale tests of riveted joints were performed, as described by De Jonge. In 1879 a research committee on riveted joints was formed by the London-based Institution of Mechanical Engineers. During the 1880s, the committee’s reports were issued periodically (DeJonge, 1945). In 1881, riveted connections began to be tested in the

United States by the Watertown Arsenal in Massachusetts. Many tests were performed by Watertown experimental facility for a lot of clients, such as the Berlin Iron Bridge Co. (in 1896) and George S. Morison (in 1901).

558,140. RIVETING AND PRESSING MACHINE CHESTER B. ALBREE, Allegheny, Pa. Filed Jan. 9, 1896. Serial No. 574,904. (No model)

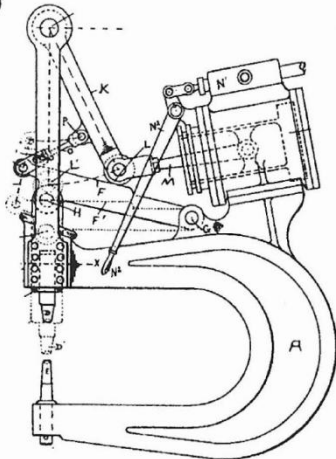


Figure 2.14 Portable Hydraulic Riveter Patented by Chester B. Albree In 1896 (Gasparini et al., 1997).

The bases for conservative methods for determining the number of rivets required to transfer a load was formed thanks to these and other tests. Lloyd's Register (Mercur, 1891), the British Board of Trade, Theodore Cooper (1888), and others published empirical rules for rivet sizes and spacing. In 1896, the first portable hydraulic riveters, patented by Chester B. Albree (Fig. 2.14), became widely available for shop riveting. In the late 1890s, pneumatic devices for field riveting were developed, as the Boyer long-stroke pneumatic hammer shown in Figure 2.15. The erection of grand all-riveted bridges such as the Firth of Forth Rail Bridge and Leffert Buck's Niagara Gorge trussed arch, completed in 1897, testified the growing ability to design and execute riveted connections. Gustav Lindenthal commented that Buck's use of riveted connections was an “a remarkable deviation from American practice”. The PRR truss bridge with riveted, gusset plate connections, shown in Figure 2.16, exemplifies the brutal endpoint of the evolution of 19th

century truss connections, very distant from the connections of the early pre-stressed trusses, the proprietary, crafted joint castings of the bridge companies, and the relatively delicate pinned joints.

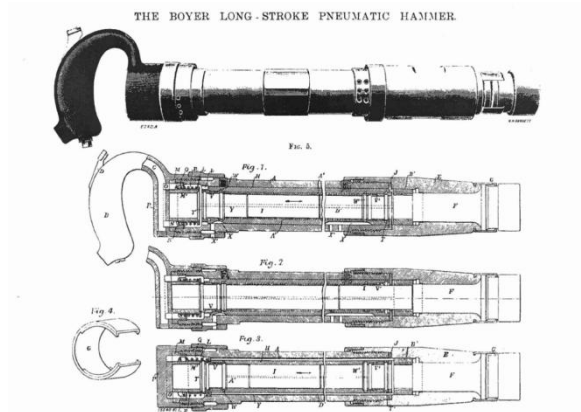


Figure 2.15 The Boyer Long-Stroke Pneumatic Hammer (Gasparini et al., 1997).

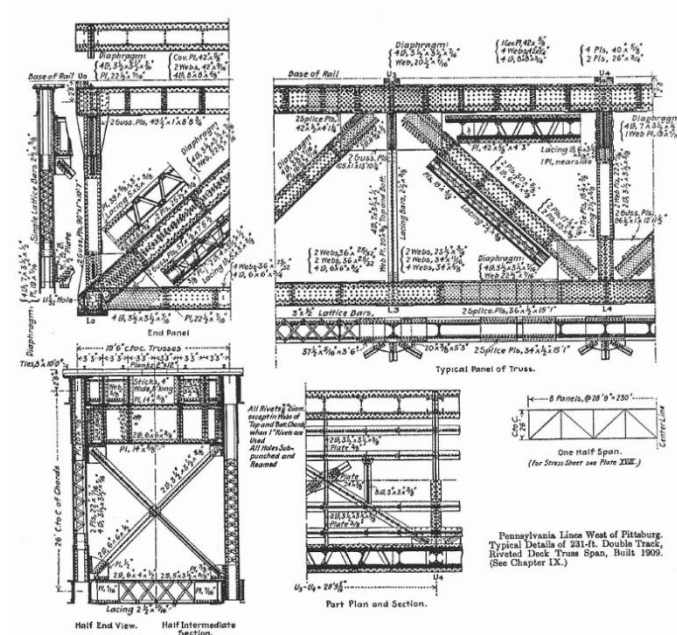


Figure 2.16 PRR All-Riveted Bridge Built in 1909 (Gasparini et al., 1997).

Chapter 2

3 RIVETED CONNECTIONS: STATE OF THE ART

3.1 TECHNOLOGY OF RIVETED CONNECTIONS

3.1.1 General

Connections represent the most important and the weakest part of metallic constructions. Indeed, an understanding of these joints represents an important and essential step.

Steel members and elements are connected each other by fasteners, that allow the transfer of forces by one element on another one. Connections are devices devoted to restore the continuity of metallic elements. Connections in metallic structures are subdivided into three different typologies: riveted, bolted and welded connections.

The joints, instead, are sets of connections, both of the same or different typologies.

The oldest typology of connection is riveted connections, used mainly from the end of 18th century to the half of 20th century. Today hot-driven rivet connections are not used anymore; cold-driven rivets, instead, are commonly adopted to join together thin plates and cold formed profiles. Cold-driven process is commonly used for rivets with a small diameter ($d < 6$ mm); hot-driven rivets, instead, are adopted when rivets have a large diameter ($d > 10$ mm). For diameters included from 6 to 10 mm both cold and hot-driven process are allowed.

Differently from bolts, hot-driven rivets cannot be separated from the connections. To disassemble the riveted connections, the rivets must be destroyed, removing the head with blowtorch or with chisel. The disassembling of connections is possible when bolts are used: this kind of connection is cheaply and easier to realise. Bolts were used also at the end of 18th century, when the thickness of the joint was huge or when rivets are subjected to tension (Fierro, 2009). The installation of rivets was performed after rivets were heated up to approximately 900 °C. This temperature was deemed to have been reached when the rivets in the

forge took on the so-called “cherry-red” colour. After installed, the rivet cooled off and returned in its original configuration. This phenomenon, contrasted by the thickness of the plates, induced tension stresses into the rivet shank and compressive forces on plates. This phenomenon is called clamping action. The amount of tension stresses was proportional to the length of the shank, and usually could reach the yield stress. Sometimes this phenomenon caused the break-up of the rivet for the separation of the head from the shank, especially when the rivet shank was very long. For this reason, bolts were preferred to rivets for huge lengths of the shank. To avoid an excessive amount of tension stresses into the rivet shank, bolts were also chosen when the shank could be subjected to tension. These were the only cases in which bolts were preferred to rivets, and for this reason bolts were considered as a second best (Fierro, 2009).

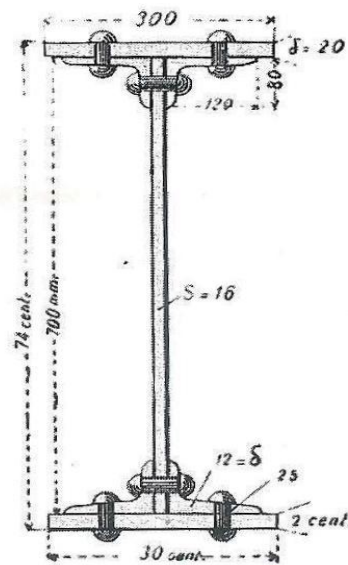


Figure 3.1 Old steel section realised with riveted connections (Marrullier, 1925).

Bolted and riveted connections do not permit the joining of plates in orthogonal arrangement, for this reason were designed and produced appropriate steel angle profiles (Fig. 3.1) that allow the connection of perpendicular plates (Marrullier, 1925).

3.1.2 Rivets: typologies and manufacturing

Rivets are made up of a head and of a shank. The shank is a round ductile steel bar piece, with a head at one end (Duggal, 2000).

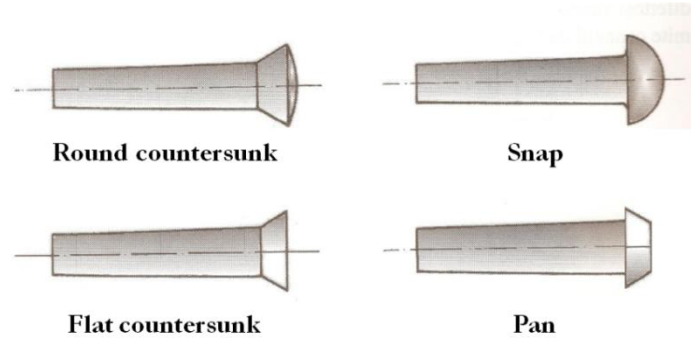


Figure 3.2 Types of rivet head.

There is four main typologies of head shape: snap head, pan head, round countersunk head, flat countersunk head (Fig. 3.2): the most common type of rivet head is the snap one. The main characteristic of the shank geometry is well described by Duggal (2000): “The shank is made of the length to extend through the parts to be connected and an extra length for a second head to be made at the other end”. The length of the shank is the sum of the grip (distance between the two heads) and the extra length required to make the second head. The total length of the rivet shank could be approximately calculated as:

$$l = 1.1s + 1.3d \quad (3.1)$$

where l is the shank length, s is the thickness of the plates to connect, and d is the hole diameter (Masi, 1996).

The formation of the second head is obtained when the rivet is heated up 900°C by hand hammering, hydraulic pressure driving or by pneumatic pressure driving. The diameter of the rivet shank is called nominal diameter. The holes in the plates to be connected present a diameter slightly greater than the shank diameter. The rivet is inserted into holes and the second head is formed on the other side. This process is called riveting (Duggal, 2000).

Hydraulic pressure driving and pneumatic pressure driving are performed by using riveting machines. Riveting machines are used to automatically set rivets and offer greater consistency, productivity, and lower cost when compared to manual riveting. Automatic feed riveting machines include a hopper and feed track which automatically delivers and presents the rivet to the setting tools which overcomes the need for the operator to position the rivet. The downward force required to deform the rivet with an automatic riveting machine is created by a motor and flywheel combination, pneumatic cylinder, or hydraulic cylinder. Manual feed riveting machines usually have a mechanical lever to deliver the setting force from a foot pedal or hand lever. Hydraulic cylinder machines have a low mobility. The applied force must be at least 90 N on mm² of rivet nominal cross section. The pneumatic hammer is particularly useful when it is impossible to use riveting machines (Masi, 1996).

Hand hammering is generally performed in the field, the hammer hits against a proper mould that allow the formation of the rivet head. During this operation, a special lock with a concave hemispherical end, called “bucking” bar, blocks the other rivet head. The force necessary to ensure the lock is usually provided by compressed air devices (Masi, 1996).

Riveting could be made when the rivet is in a cold state or in a red hot state. In the first case, the rivet is called *hot driven field rivet* or *hot driven shop rivets*, depending upon if the process is made in the field or in the workshop (Duggal, 2000).

The *cold driven rivets* have a limited application, due to the high pressure necessary to form the second head at ambient temperature that make this kind of rivets difficult to be formed in the field. The strength of cold driven rivets is higher than the hot driven ones. Their clamping force, however, is less due to the absence of shrinking.

If the rivet diameter is small, the second head could be formed manually by using an ordinary hammer: these rivets are called *hand driven rivets* (Duggal, 2000).

In the following, after a brief description of manufacturing of steel plates, a description of hot driven riveted connections is presented, to deepen the technology of this kind of rivets, which is the object of the presented study.

3.1.1 Manufacturing of steel plates

One of the most important operations during the manufacturing of riveted connections is the formation of holes on steel plates. This operation could be performed by using two different techniques: the punching or the drilling. In the first technique (Fig. 3.3 a)), a cylindrical puncher with a diameter equal to the diameter of the hole to be obtained is pressed strongly against the steel plate: in this manner the hole is obtained by removing a cylindrical piece of the material. Punching presents the disadvantage to damage the material around the hole, especially for holes with a big diameter. Punching the final hole diameter is permitted for thickness of plates smaller than 10 mm. For higher thickness, a punching of a smaller diameter is permitted. In this case, the final diameter could be obtained by boring. This technique guarantees perfectly cylindrical holes and allows the correction of the position of the hole. When the thickness of plate is bigger than the diameter of the hole, the unique technique allowed is drilling (Fig. 3.3 b)). The drilling consists in removing chips of base material from the plate with a helicoidal drill.

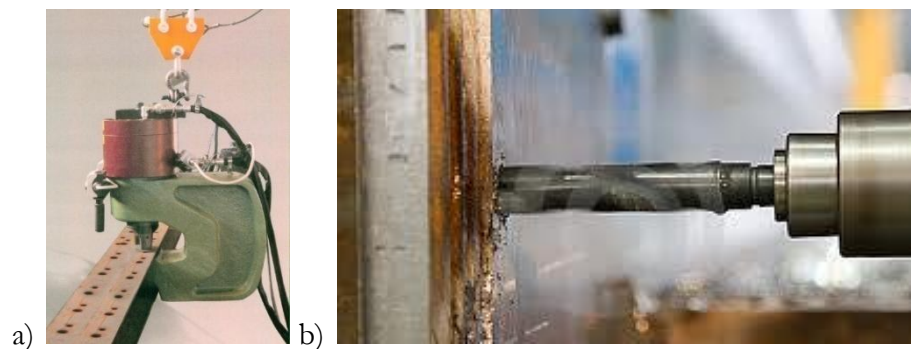


Figure 3.3 Formation of holes: a) punching, b) drilling.

No blowtorch is allowed for the holes formation. When more plates must be equal pierced, punching or drilling are performed contemporary on plates overlapped each other. This technique is particular convenient for precision of piercing and economy of manufacturing.

3.1.2 Manufacturing of hot driven riveted connections

The realization of hot driven riveted connections is subdivided into different steps, which will be described in the following.

Before their installation rivets are heated up to approximately 900 °C in a special forge (Fig. 3.4 a)). This temperature is deemed to have been reached when the rivets in the forge take on the so-called “cherry-red” colour (Fig. 3.4 b)). After heating, the rivet is inserted in the matching hole of the plates to be joined and a new head is then formed on the protruding end of the shank with a pneumatic hammer (see Fig. 1.15 a)–b)). The other head is blocked by using a “bucking” bar with a concave hemispherical end. The pneumatic hammer is provided of the same end of the “bucking bar”. When forming the head, the diameter of the rivet increases, thus filling the entire hole, which is generally 1 mm greater than the diameter of the undriven rivet (D’Aniello et al., 2010).

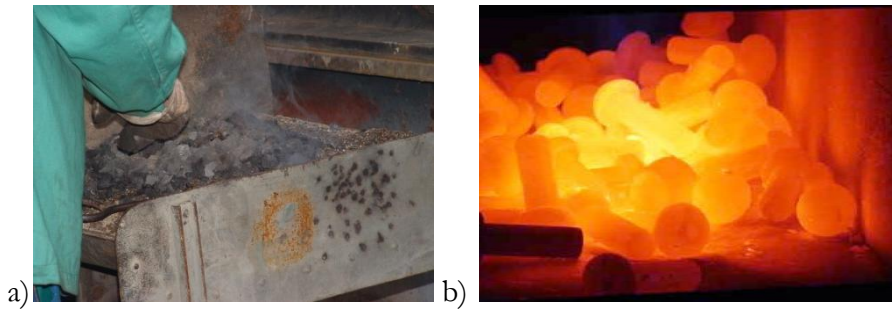


Figure 3.4 Heating of rivets: a) forge; b) red hot rivets (Vermes, 2007).

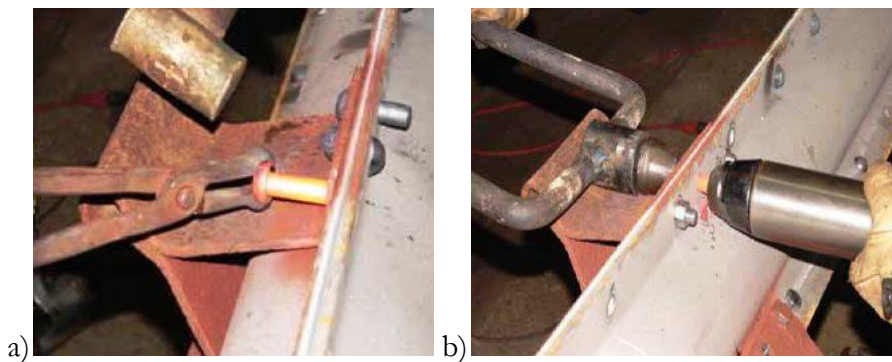


Figure 3.5 Phases of rivet formation: a) insertion of the rivet, b) formation of the rivet (Vermes, 2007).

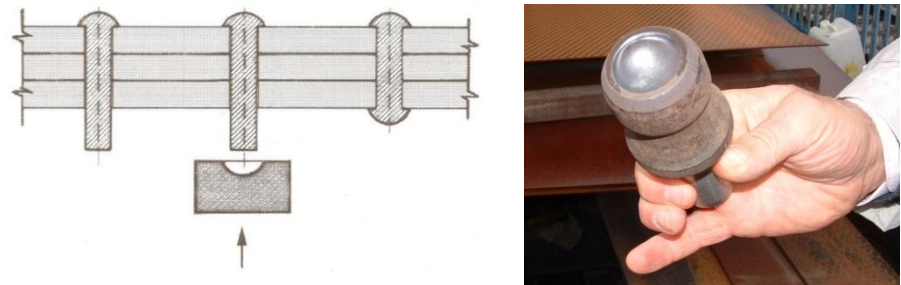


Figure 3.6 “Bucking” bar (Fierro, 2009).

The diameter of hot rivet is called gross diameter (Duggal, 2000). After this process no clearance is observed between the shank and the joined plates. During the riveting process the enclosed plates are drawn together with installation bolts and by the riveting equipment (D’Aniello et al., 2010). During the cooling, both rivet diameter and rivet length shrink: this shortening causes the tightening of the plates in contact and, consequently, an amount of residual tensile stresses in rivet shank and some compression in the plates to be connected. The friction to slide between parts caused by compression is called *clamping action*.

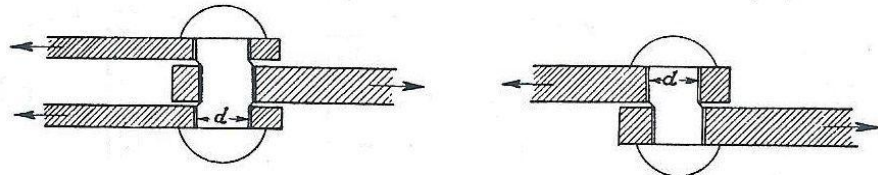


Figure 3.7 Loose rivets (Masi, 1996).

The quality of the riveted connections depends on the labour, which must be skilled. However, some imperfections are usual, like the imperfect shape of the second head, or the non alignment of the second head with the shank, or the presence of spaces between the rivet shank and the hole. This is the reason why a proper inspection must be performed at the end of riveting process: a defective rivet could be detected by tapping with a light hammer (Duggal, 2000). If the hammer gives a metallic or ringing sound, the rivet is loose, and needs to be

replaced. To remove a rivet, one head must be cut by using a chisel or a blowtorch.

3.1.3 Types of riveted connections

The classification of riveted connections depends on the mode of the load transmission by the rivets. There are two main categories of riveted connections (Bresler et al., 1960):

- *the rivet in shear*, when the load is transmitted through the bearing between the plates and the shank of the rivet, producing shear in the rivet;
- *the rivet in tension*, when the load is transmitted through the bearing between the plates and the shank of the rivet, producing tension in the rivet.

The rivets in shear are the most common type in riveted connections in structures. When only one section of the rivet is interested by the transmission of loads by shear, the connection is called *lap joint*, with rivets subjected to *single shear*. When the load is transmitted by shear in two rivet sections, the rivet is in *double shear*. Finally, when the loading on the rivet may be transmitted by shear in more than two planes, the rivet is in *multiple shear* (Bresler et al., 1960).

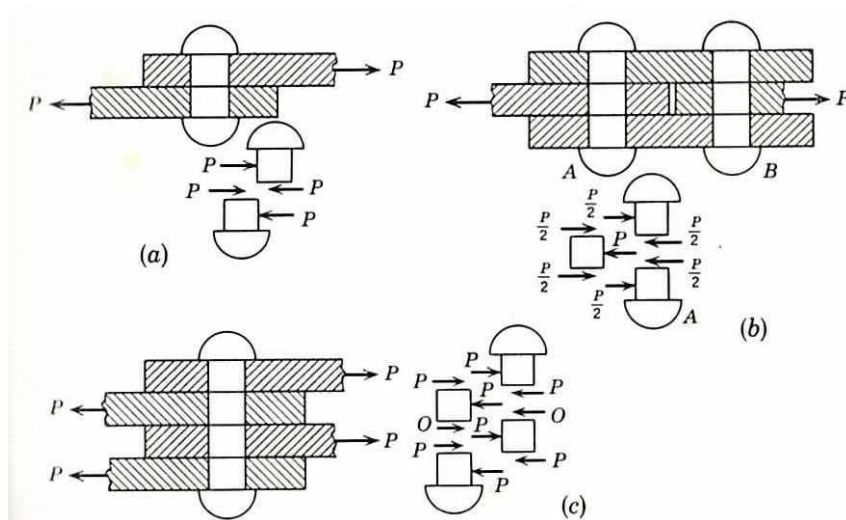


Figure 3.8 types of riveted connections: a) Lap joint, rivet in single shear, b) Butt joint, rivet in double shear, c) Rivet in multiple shear (Bresler et al. 1960).

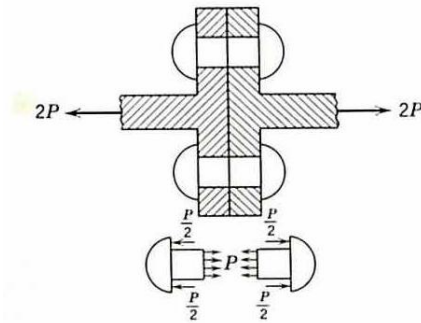


Figure 3.9 Rivet in tension (Bresler et al. 1960).

Another classification is based on the nature and on the location of load with respect to the rivet group. Indeed, the connection is considered to be carrying *direct load*, if the load passes through the centroid of the rivet cross-sectional areas. If the load does not pass through the centroid of the rivet group, the connection is called *eccentric load connection*. The connection is said *pure moment connection* when the load transmitted is a pure torque or a moment. Usually, the connection could be subjected to loads such that the rivets are both in tension and in shear. This is the case, for example, of the beam-to-column connections in which shear forces and a certain amount of bending moment are present. These connections are called *moment connections* or *shear-moment connections* (Bresler et al., 1960).

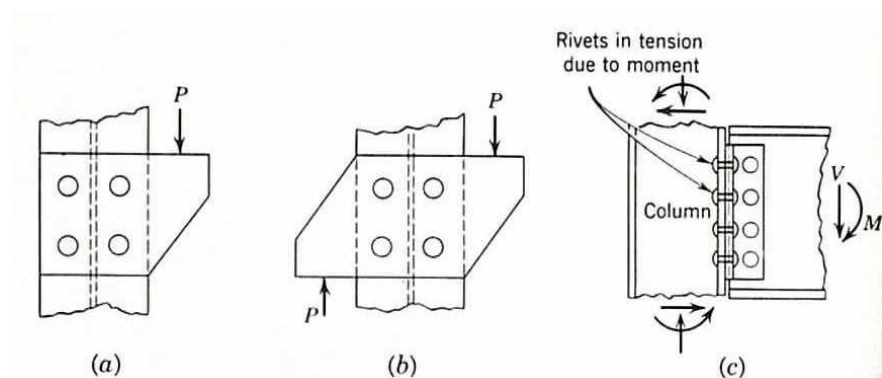


Figure 3.10 Types of riveted connections: a) Eccentric load connection, b) Pure moment connection, c) Shear-moment connection (Bresler et al., 1960).

3.1.4 Failure modes of riveted connections

The types of failure in riveted connections are mainly four:

1. *Tension failure* in the plates;
2. *Shearing failure* across one or more planes of the rivet;
3. *Bearing failure* between the plates and the rivets: this failure could involve the plates, the rivet or both;
4. *Shear-out failure* in the plates, this kind of failure could be avoided by providing a sufficient distance of the holes from edges.

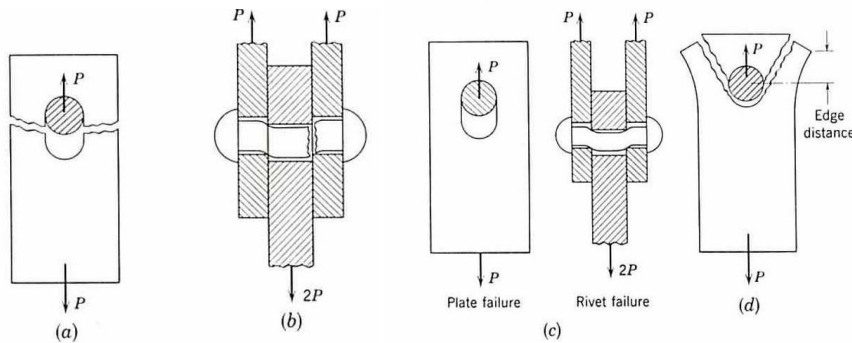


Figure 3.11 Types of riveted connection failure: a) Tension failure in the plates b) Shearing failure in the rivet, c) Bearing failure, d) Shear-out failure in the plates (Bresler et al., 1960).

The design of riveted joints is historically based on these failure criteria, with no regard to their elastic stresses. The calculation of the ultimate load of a riveted connection is defined as the multiplication of the ultimate stress of the material and the area involved in a particular type of failure, as illustrated in Figure (Bresler et al., 1960).

The definition of the ultimate load of riveted connections is defined in the actual codes, as the Eurocode 3 (UNI EN 1993-1-8: 2005), in which four resistance verifications are prescribed for riveted connections, one for each type of failure.

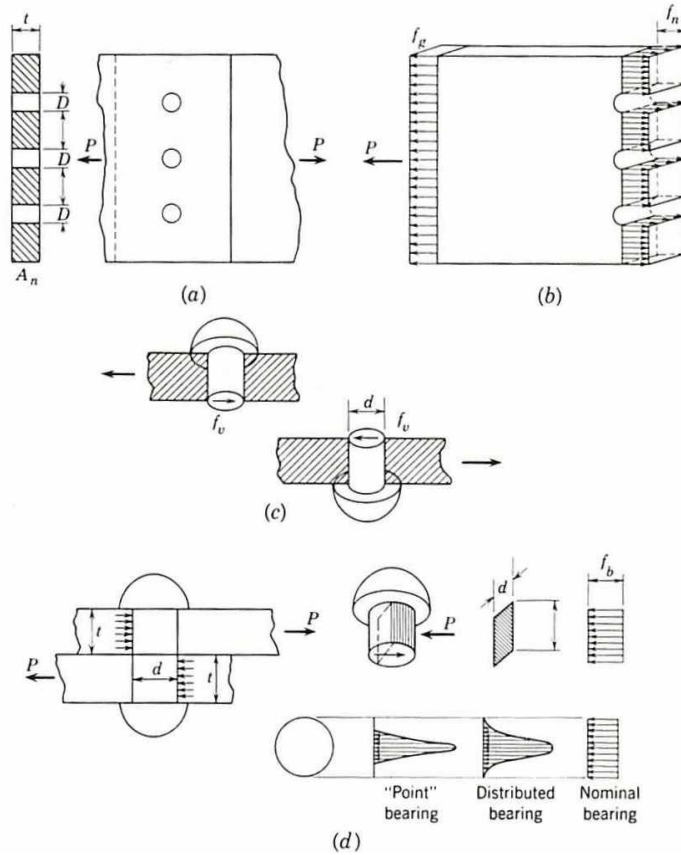


Figure 3.12 Stresses in riveted connections: a) A riveted connection, b) Tensile stress, c) Shearing stress, d) Bearing stress (Bresler et al., 1960).

3.2 RESISTANCE VERIFICATIONS

3.2.1 The Eurocode resistance verifications

The resistance verifications for riveted connections and the rules for material properties, tolerances and design guides are given by the European normative Eurocode 3 (UNI EN 1993-1-8: 2005).

In the normative, the first specification regards the definition of the basis of design. First of all, the partial safety factor γ_M for riveted connections according to EN 1993-1-1 is given (Fig. 3.13).

Resistance of members and cross-sections	γ_{M0} , γ_{M1} and γ_{M2} see EN 1993-1-1
Resistance of bolts	γ_{M2}
Resistance of rivets	
Resistance of pins	
Resistance of welds	
Resistance of plates in bearing	

Figure 3.13 Partial safety factor γ_M given by EN 1993-1-8.

The value of the partial safety factor γ_{M2} is equal to 1.25. Some indications on the type of calculation are also given. The EN 1993-1-8 established that: “The resistance of a joint should be determined on the basis of the resistances of its basic components. Linear-elastic or elastic-plastic analysis may be used in the design of joints.

Where fasteners with different stiffnesses are used to carry a shear load the fasteners with the highest stiffness should be designed to carry the design load”. Some design assumptions are also given: “Joints should be designed on the basis of a realistic assumption of the distribution of internal forces and moments. The following assumptions should be used to determine the distribution of forces:

1. the internal forces and moments assumed in the analysis are in equilibrium with the forces and moments applied to the joints,
2. each element in the joint is capable of resisting the internal forces and moments,
3. the deformations implied by this distribution do not exceed the deformation capacity of the fasteners or welds and the connected parts,
4. the assumed distribution of internal forces should be realistic with regard to relative stiffness's within the joint,
5. the deformations assumed in any design model based on elastic-plastic analysis are based on rigid body rotations and/or in-plane deformations which are physically possible, and
6. any model used is in compliance with the evaluation of test results (see EN 1990).”

Table 3.1 Minimum and maximum spacing, end and edge distances.

Distances and spacing	Minimum	Maximum ^{1) 2) 3)}		
		Structures made from steels conforming to EN 10025 except steels conforming to EN 10025-5	Structures made from steels conforming to EN 10025-5	Steel used unprotected
		Steel exposed to the weather or other corrosive influences	Steel not exposed to the weather or other corrosive influences	
End distance e_1	$1,2d_0$	$4t + 40 \text{ mm}$		The larger of $8t$ or 125 mm
Edge distance e_2	$1,2d_0$	$4t + 40 \text{ mm}$		The larger of $8t$ or 125 mm
Distance e_3 in slotted holes	$1,5d_0$			
Distance e_4 in slotted holes	$1,5d_0$			
Spacing p_1	$2,2d_0$	The smaller of $14t$ or 200 mm	The smaller of $14t$ or 200 mm	The smaller of $14t_{\min}$ or 175 mm
Spacing $p_{1,0}$		The smaller of $14t$ or 200 mm		
Spacing $p_{1,i}$		The smaller of $28t$ or 400 mm		
Spacing p_2 ⁴⁾	$2,4d_0$	The smaller of $14t$ or 200 mm	The smaller of $14t$ or 200 mm	The smaller of $14t_{\min}$ or 175 mm

¹⁾ Maximum values for spacing, edge and end distances are unlimited, except in the following cases:

- for compression members in order to avoid local buckling and to prevent corrosion in exposed members and;
- for exposed tension members to prevent corrosion.

²⁾ The local buckling resistance of the plate in compression between the fasteners should be calculated according to EN 1993-1-1 using $0,6 p_1$ as buckling length. Local buckling between the fasteners need not to be checked if p_1/t is smaller than 9ϵ . The edge distance should not exceed the local buckling requirements for an outstand element in the compression members; see EN 1993-1-1. The end distance is not affected by this requirement.

³⁾ t is the thickness of the thinner outer connected part.

⁴⁾ For staggered rows of fasteners a minimum line spacing of $p_2 = 1,2d_0$ may be used, provided that the minimum distance, L , between any two fasteners is greater or equal than $2,4d_0$.

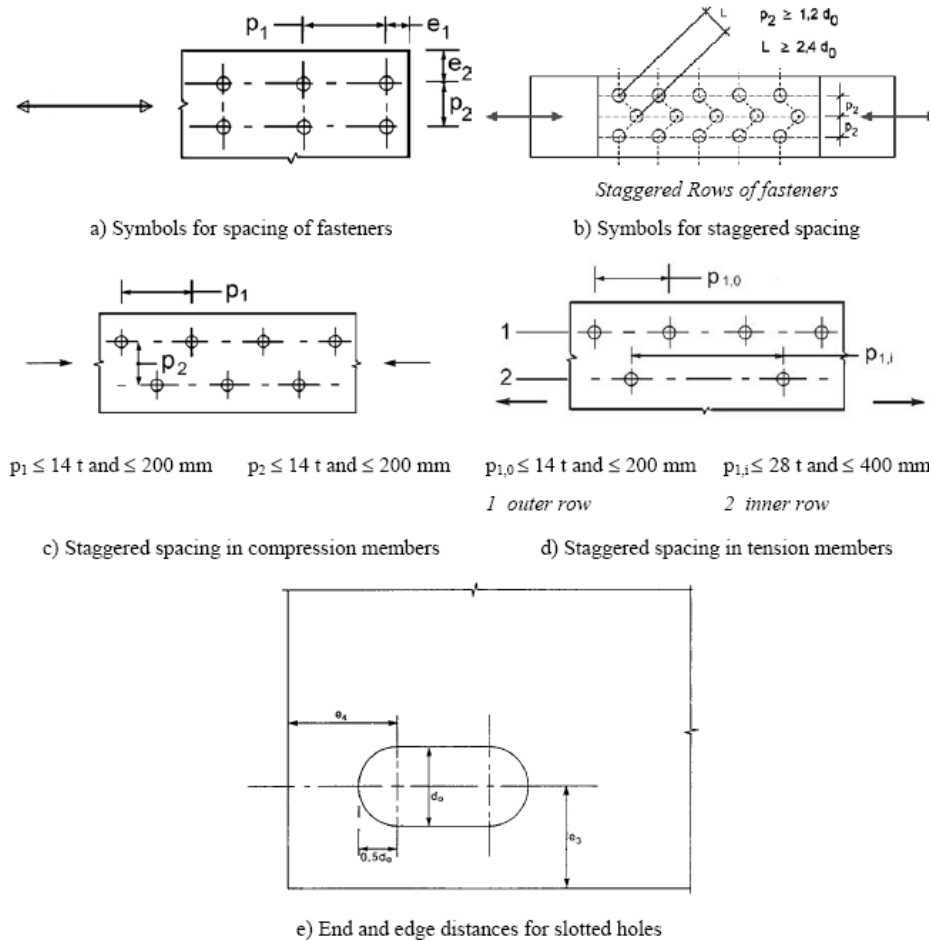


Figure 3.14 Symbols for end and edge distances and spacing of fasteners given by EN 1993-1-8.

The material properties, dimensions and tolerances of steel rivets should comply with the requirements given in the National Annex. As a general rule, the grip length of a rivet should not exceed $4.5d$ for hammer riveting and $6.5d$ for press riveting.

The positioning of holes for bolts and rivets is also given, and reported in Table 3.1.

The normative established the design resistance for individual fastener subjected to shear and/or tension according to the failure mode.

In case of a tension failure of the plate, the tension resistance is given by:

$$N_{u,Rd} = \frac{0.9 \cdot f_u \cdot A_{net}}{\gamma_{M2}} \quad (3.2)$$

where: f_u is the specified ultimate tensile strength of the plate;
 A_{net} is the net area of the plate subjected to tension;
 γ_{M2} is the rivet partial safety factor equal to 1.25.

In case of a shear failure of the rivet, the shear resistance for shear plane is given by:

$$F_{v,Rd} = \frac{0.6 \cdot f_{ur} \cdot A_0}{\gamma_{M2}} \quad (3.3)$$

where: f_{ur} is the specified ultimate tensile strength of the rivet;
 A_0 is the area of the rivet hole;
 γ_{M2} is the rivet partial safety factor equal to 1.25.

In case of a bearing failure of the plates, the bearing resistance is given by:

$$F_{b,Rd} = \frac{k_1 \cdot \alpha_b \cdot f_u \cdot d \cdot t}{\gamma_{M2}} \quad (3.4)$$

where: f_u is the specified ultimate tensile strength of the rivet;
 d is the nominal rivet diameter;
 t is the thickness of the plate;
 γ_{M2} is the rivet partial safety factor equal to 1.25;
 α_b is the smallest of α_d ; $\frac{f_{ub}}{f_u}$ or 1;
 α_d in the direction of the load transfer is:
 – for end bolts: $\alpha_d = \frac{e_1}{3d_0}$,
 – for inner bolts $\alpha_d = \frac{p_1}{3d_0} - \frac{1}{4}$;
 k_1 perpendicular to the direction of the load transfer is:
 – for edge bolts is the smallest of $2.8 \frac{e_2}{d_0} - 1.7$ or 2.5,

- for inner bolts is the smallest of $1.4 \frac{p_2}{d_0} - 1.7$ or 2.5.

For double shear connections with packing on both sides of the splice, t_p should be taken as the thickness of the thicker packing.

Riveted connections should be designed to transfer shear forces. If tension is present the design tensile force $F_{t,Ed}$ should not exceed the design tension resistance $F_{t,Rd}$ given by:

$$F_{t,Rd} = \frac{0.6 \cdot f_{ur} \cdot A_0}{\gamma_{M2}} \quad (3.5)$$

where: f_{ur} is the specified ultimate tensile strength of the rivet;

A_0 is the area of the rivet hole;

γ_{M2} is the rivet partial safety factor equal to 1.25.

In case of a combined shear and tension failure of the rivet, the resistance is given by:

$$\frac{F_{v,Ed}}{F_{v,Rd}} + \frac{F_{t,Ed}}{F_{t,Rd}} \leq 1.0 \quad (3.6)$$

The design resistance of a group of fasteners may be taken as the sum of the design bearing resistances $F_{b,Rd}$ of the individual fasteners provided that the design shear resistance $F_{v,Rd}$ of each individual fastener is greater than or equal to the design bearing resistance $F_{b,Rd}$. Otherwise the design resistance of a group of fasteners should be taken as the number of fasteners multiplied by the smallest design resistance of any of the individual fasteners.

3.2.2 Long connections and long rivets

When the distance L_j between the centres of the end fasteners in a joint, measured in the direction of force transfer (see Figure 3.15), is more than 15 d , the design shear resistance $F_{v,Rd}$ of all the fasteners calculated according to equation 3.7. should be reduced by multiplying it by a reduction factor β_{Lj} given by:

$$\beta_{Lf} = 1 - \frac{L_f - 15d}{200d} \quad (3.7)$$

but $\beta_{Lf} \leq 1.0$ and $\beta_{Lf} \geq 0.75$.

This provision does not apply where there is a uniform distribution of force transfer over the length of the joint, e.g. the transfer of shear force between the web and the flange of a section.

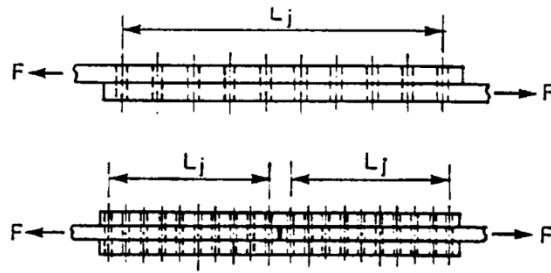


Figure 3.15 Long connections (EN 1993-1-8).

In case of rivets with an unusually long grip, the bending may be determinant. These cases are frequent when filler plates are required, necessitating use of long rivets. These rivets are considered to be weak in bending, and also less effective in transferring loads. The stress distribution in these connections is not easily to be determined, but practice demonstrated that the use of tight fillers helps to reduce the bending in the rivet. Loads, indeed, are transferred from the side plates to the fillers before it reached the main centre plate. In this case the addition of special or ulterior rivets when fasteners with unusual long grip are present is prescribed.

3.2.3 Nominal and actual stresses

The determination of the ultimate load of riveted connections is based on some assumptions that simplify the calculations. As well described by Bresler (1960): “Nominal stresses differ from the real stresses because of the following assumptions made in the calculation of nominal stresses:

- The frictional resistance to slip between plates is neglected,
- Deformation of the plates is neglected,

- Shearing deformation in the rivet is assumed proportional to the shearing stress,
- Tensile stress concentrations due to the rivet holes in the plates are neglected,
- Shearing stress in the rivets is assumed to be uniformly distributed over the rivet cross section,
- Bearing stress between rivets and plates is assumed to be uniformly distributed over the nominal contact surface between rivets and plates,
- Bending of rivets is neglected.

These assumptions are approximately valid when the connection is subjected to static loads approaching ultimate strength. The actual stresses in connections subjected to working loads, however, are not represented by these equations”.

3.2.3.1 Frictional resistance

The clamping action impressed to connection by the cooling of the hot-driven rivets determines on the joint a slip-resistant force. When the load is less than the frictional resistance determined by clamping action, the rivet is not subjected to shearing or bearing stresses, because the load is transferred between plates entirely through friction. Once the frictional resistance is exceeded, an initial slip occurs. After this slip, the loads are carried part by friction and part by shearing and bearing stresses on the rivets. In case of multi-rivets connections, the initial slip may not occur simultaneously, and may be noticeably load differential between first and last slippage (Bresler et al. 1960).

3.2.3.2 Effects of stress concentrations

The determination of the stresses along a plate with one or more holes can be determined by using the theory of elasticity since the stresses do not exceed elastic limit.

This distribution of stresses depends largely by the position of holes, the number of holes and the spacing. In the following Figure are shown the distribution of stresses in elastic range and in plastic range. The huge stress concentration around holes determines the yielding in these points, also for working loads. This yielding, however, does not determine the failure of the connection. The distribution of stresses becomes more uniform across the section with further increase in load, until the load reaches the ultimate strength. In this case the distribution of stresses in

the plate becomes uniform, justifying the use of the equation 3.2. (Bresler et al., 1960).

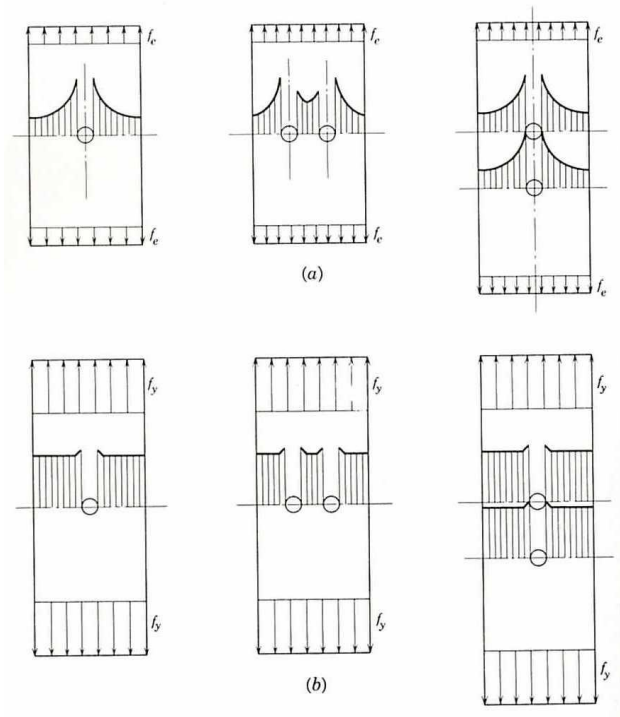


Figure 3.16 a) Elastic stress distribution, b) Plastic stress distribution (Bresler et al., 1960).

3.2.3.3 Shearing-stress distribution in the rivet

The shearing-stress distribution in the rivet cannot be easily determined, in particular when the stresses in the rivet are in the elastic range. Indeed, the elastic distribution of stresses in the rivet is certainly not uniform. When the ultimate load is acting on rivet, it is expected that the distribution of stresses becomes uniform, justifying the use of the equation 3.3. (Bresler et al., 1960).

3.2.3.4 Bearing-stress distribution

The bearing resistance verification proposed by EN 1993-1-8 considers the distribution of stresses along the net section as uniform. The real distribution differs a lot from the assumption made for the verifications: considering the “point” bearing contact, the actual stress is much higher

than the nominal one (Bresler et al., 1960). The distribution of bearing stresses in the rivet depends on the bending of the rivet. As reported by Bresler (1960): “the distribution is nearly uniform for that portion of the rivet which lies between two supporting plates, although for the portion bearing on the side plates there may be some variation in bearing stress”. In a lap joint, the variation in bearing stress is particularly pronounced. Indeed, for lap joints, the loads on the shank form a couple, equilibrated by an equal and opposite couple acting in the rivet head. That is why the resistance of the rivet heads is very important, and the resistance of countersunk rivet is reduced respect to the normal rivets. Also for lap joints, after excessive deformation occurs, the actual stress is much higher than the nominal one.

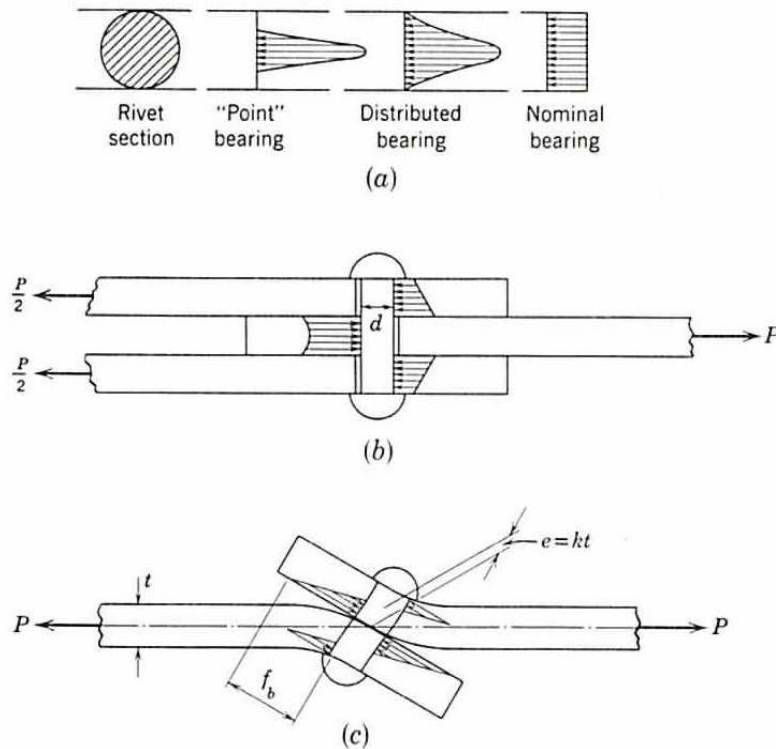


Figure 3.17 Bearing stress distribution (Bresler et al., 1960).

3.3 STATE OF THE ART: NUMERICAL STUDIES AND EXPERIMENTAL ACTIVITIES ON RIVETED CONNECTIONS

In the last years, many researches and studies were performed on this kind of connections to determine their strength capacity and their deformability. Experimental campaigns and FE analyses were carried out to establish which variables influence their behaviour.

In particular, the study conducted by G.L. Kulak, J.W. Fisher and J.H.A. Struik, “**Guide to design criteria for bolted and riveted joints**” (1987), is one of the most complete guide to designing and verifying these connections. In the 3rd chapter, exclusively devoted to riveted connections, authors highlighted how these joints represented one of the most important and ancient types of connecting steel elements, even if the introduction of welding and bolting declined steadily their use. The study of the riveted connections behaviour remains however an important and crucial challenge, to allow the rehabilitation of ancient steel structures.

After a brief but exhaustive description of the riveting process, authors explain how the formation of the rivet increases the shank diameter and consequently reduces the hole clearance. Authors describe also the effect of the shrinking of the shank, which involves a residual clamping force or internal tension in the rivet. The joint stiffness, critical installation conditions such as driving and finishing temperature, as well as the driving pressure determinate the magnitude of the residual clamping force. Authors observe that: “Measurements have shown that hot-driven rivets can develop clamping forces that approach the yield load of a rivet. A considerable variation in clamping forces is generally observed. Also, as the grip length is increased, the residual clamping force tends to increase”.

During the cooling process, the shank shrinks both diametrically and longitudinally. As written by authors: “the amount of hole clearance that results also depends on how well the rivet filled the hole prior to shrinkage”. Sawed sections of three hot-formed, hand pneumatic driven rivets are shown in the following Figure. As confirmed by many studies, the almost completely fill of holes is when the grip rivets are relatively short. When the grip length increases, also the clearance between rivet and plate tend to increase. One of the causes of this tendency is the

differences in working the material during driving. The following Figure shows some clearance for the longer grip rivets.

The mechanical properties of the rivet material before driving and the installation process determine the tensile strength of driven rivet. Many studies have investigated the influence of driving temperature on the tensile strength. The results of these studies indicated that varying the driving temperature and the soaking time (that is, the heating time of a rivet before driving) had a negligible effect on the tensile strength. Driving generally increases the strength of rivets, generally, for hot-driven rivets, the machine driving increased the rivet tensile strength by about 20%. The increase in strength involves a considerable reduction in elongation.

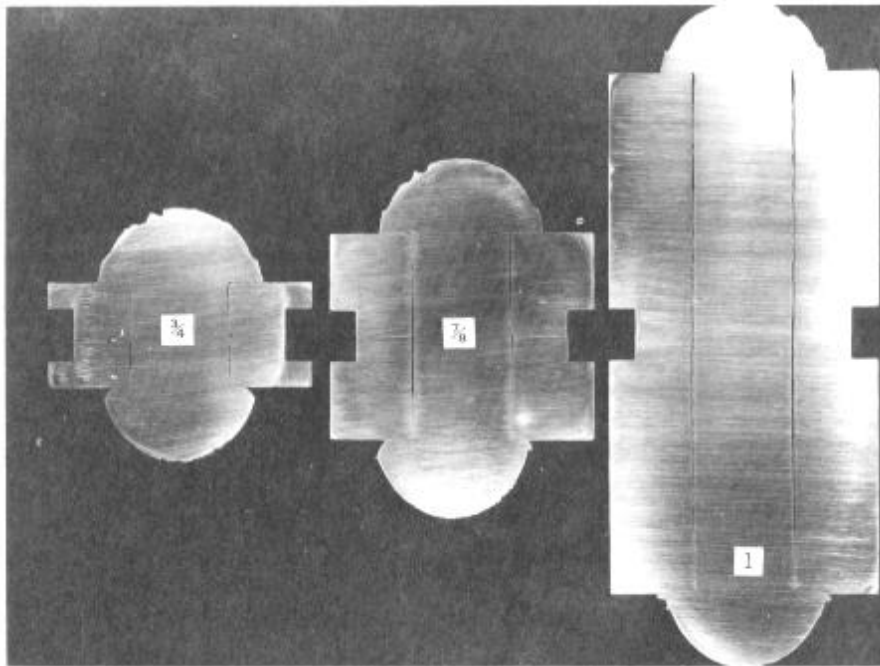


Figure 3.18 Sawed Sections of driven rivets (Kulak et al., 1987).

Most tension tests of driven rivets showed that the strength of the connection decreased as the grip length was increased. This difference in strength of short and longer rivets is neglected, for practical purposes. Besides, it was observed that the residual clamping force in driven rivets

has no influence on their strength. The effect of the clamping force was minimized by yielding of the rivet and does not affect the ultimate strength.

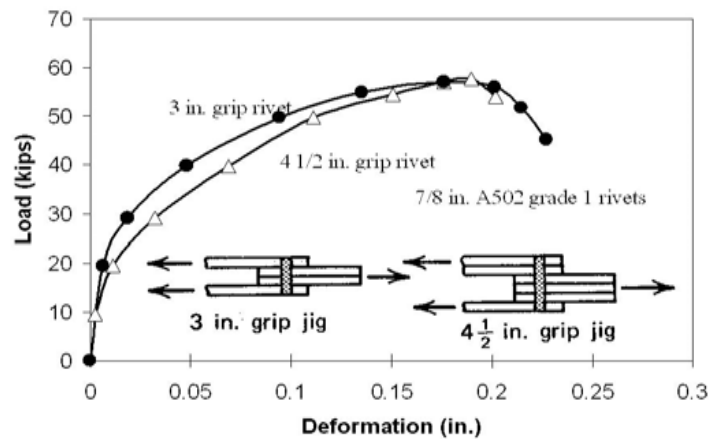


Figure 3.19 Sawed Sections of driven rivets (Kulak et al., 1987).

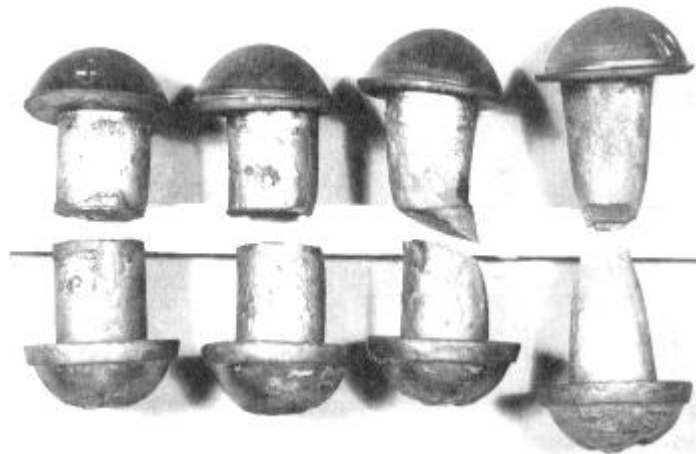


Figure 3.20 Typical fractures at four shear-tension ratios (Kulak et al., 1987).

The shear capacity of a rivet was also investigated by performing many experimental tests. As observed by authors: “an average shear strength to

tensile strength ratio of about 0.75 has been reported, and varied from 0.67 to 0.83". This variation is attributed to differences in testing methods, driving procedures, and test specimens. Figure 3.19 shows load versus deformation curves for double-shear tests on different lengths rivets. As expected, in the initial load stages the longer rivet shows a larger deformation, mainly for bending effects.

However, there are no significant decreases of shear strength. A slight decrease in strength for rivets in single shear compared with the double shear loading condition was observed. This phenomenon is caused by out-of-plane forces and secondary stresses on the rivet due to the eccentricity of the applied load. In most single shear test joints, the rivet is not subjected to a pure shear load condition. If the specimen is restrained, no secondary stresses and out-of-plane deformations are observed, and the difference in the single and double shear strength become insignificant. The driving process involves an increase in both rivet tensile strength and shear strength.

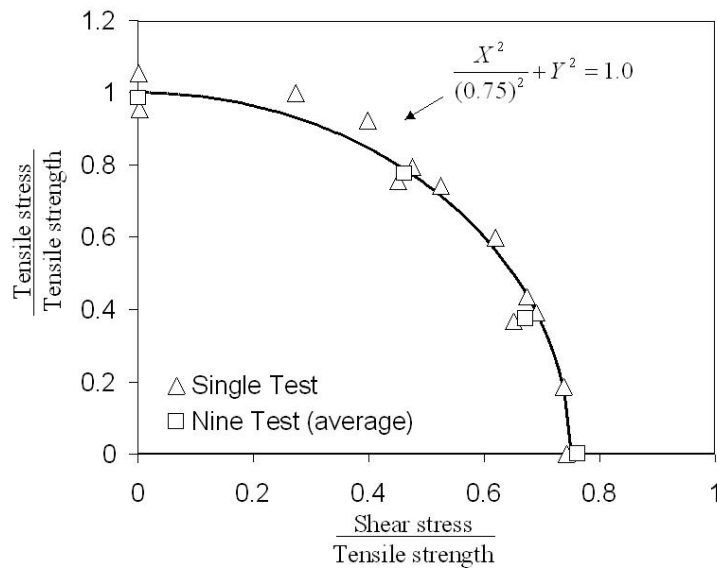


Figure 3.21 Interaction curve for rivets under combined tension and shear (Kulak et al., 1987).

The strength and behaviour of single rivets subjected to various combinations of tension and shear were also investigated by performing experimental tests. The variables were determined by varying grip length,

rivet diameter, driving procedure, and manufacturing process. Results demonstrated that these variables did not have a significant influence. Only the long grip rivets tended to show a decrease in strength.

The progressive variation in loads from pure tension to pure shear determined a significant decrease in deformation capacity. Figure 3.20 shows typical fractured rivets for different shear to tension load ratios. It is interesting to note how the fracture and the deformation capacity changed substantially as the loading condition changed from shear to combined shear and tension finally to tension.

An elliptical interaction curve that defined the rivet strength was fitted to the test results:

$$\frac{x^2}{0.75^2} + y^2 = 1.0 \quad (3.8)$$

where x is the ratio of the shear stress on the shear plane to the tensile strength of the rivet, and y is the ratio of the tensile stress to the tensile strength. In Figure the experimental results are compared with the elliptical interaction curve.

The behaviour of symmetrical connections before slip and after slip (when rivets work in shear) was also investigated by authors.

Before slip occurs, the connections behaviour is determined by the friction between plates in contact, which is function of the amount of pre-tension in rivets, of the type of material, of the number of rivets and of the number of plates. The total force developed by connection is:

$$P_{slip} = k_s \cdot m \cdot n \cdot T_i \quad (3.9)$$

where k_s is the friction coefficient, m the number of plates in contact, n the number of rivets and T_i is the rivet tension.

The friction coefficient could be determined only by performing experimental tests. To this end, different tests were performed for different kind of steel, different typologies of connections and different surface treatments. From the experimental tests, knowing the pre-tension in rivets, the friction coefficient is determined by:

$$k_s = \frac{P_{slip}}{m \cdot n \cdot T_i} \quad (3.10)$$

Tests results demonstrated that specimen with no surfaces treatments had a medium value of friction coefficient equal to 0.33, as reported in Figure 3.22. The geometry of connection, the number of plates and the number of rivets had no influence on friction coefficient. This value resulted equal for different types of steel, but it could be increased if the surfaces were treated.

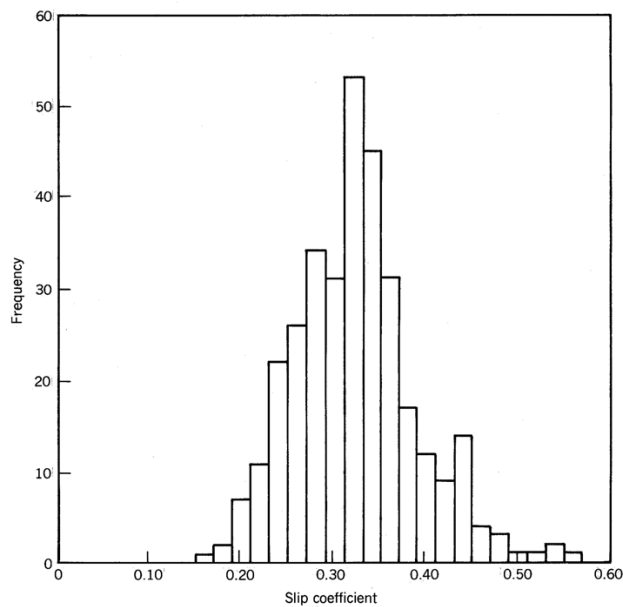


Figure 3.22 Distribution of slip condition for clean mill scale surfaces (Kulak et al., 1987).

Once the slip resistance of connection is overcome, a slip between plates was observed until the clearance between holes and shanks allows that. The shanks were subjected to shear, starting from the end rivet. Finally, all rivets absorbed a rate of shear. This phenomenon is not so evident in connections with few rivets, in which the force is equally distributed, but is more evident in joints with a lot of rivets, in which the distribution of shear could be happen after the end rivets reached their shear strength.

Next Figures show the rivet reactions to shear in case of connection with four rivets and in case of joint with ten rivets.

The failure of connection could be happen for rivet shear, for bearing or for tension fracture of the plate, if the strength of the net section is lower than the shear strength of rivets. The variables that influence the type of failure are: strength of plates and rivets, length of connection, pitch, edges distance, and kind of fasteners.

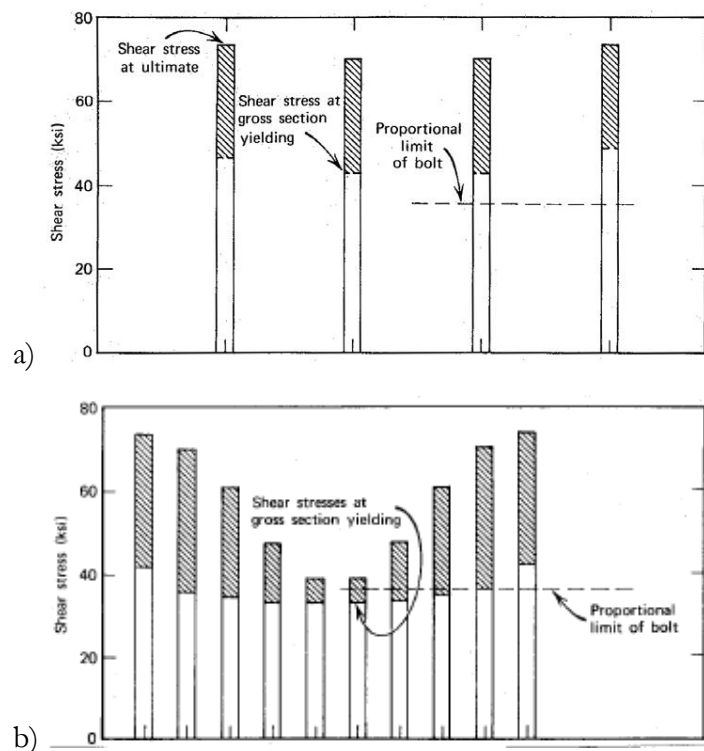


Figure 3.23 Load partition in joint with a) four fasteners in line, b) ten fasteners in line (Kulak et al., 1987).

Authors deepened also the behaviour of truss-type connections, which differ from the symmetrical connections because the centre of mass does not coincide with the point of application of forces.

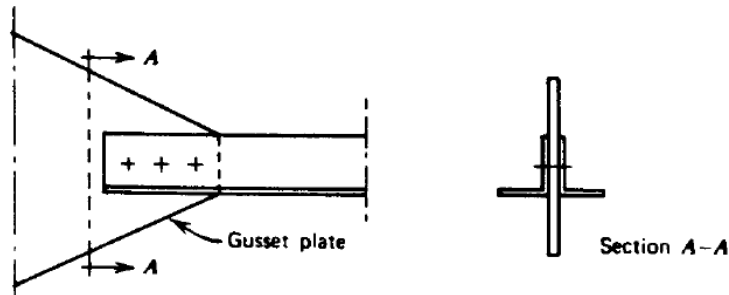


Figure 3.24 Gusset plate connection (Kulak et al., 1987).

In truss-type connections, not all the surfaces are connected. This aspect and the disalignment of centre of the mass and point of application of forces involve a reduction of strength of net section. In particular, the most important aspect that induces the reduction of strength is the x/L ratios, as illustrated in Figure 3.25.

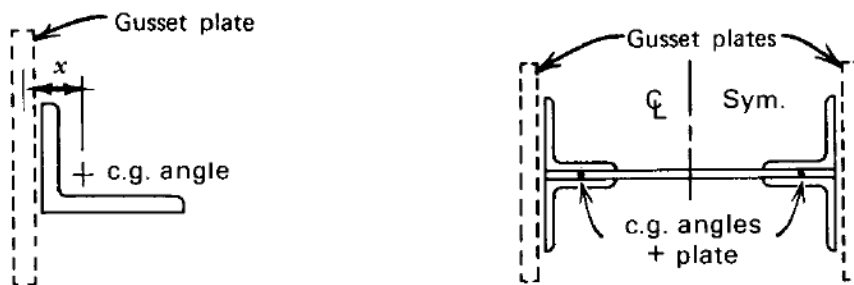


Figure 3.25 Schematic of eccentricity in joints (Kulak et al., 1987).

For higher x/L ratio, the behaviour of connection is more similar to symmetrical connections, with a different distribution of stresses in fasteners. If L decreases, the x/L ratio increases, and the strength of joint decreases.



Figure 3.26 Angle failure in built-up section (Kulak et al., 1987).

Failure of these joints involves always the end fasteners, and is a shear failure of the shank or a traction failure of plates, it depends from L . To take into account this phenomenon, a reduced area of net section is considered:

$$A_{eff} = A_n \left(1 - \frac{x}{L}\right) \quad (1.5)$$

The numerical results fitted well the experimental results, as shown in Figure 3.27.

The last type of connection studies by authors was the unsymmetrical ones, in which fasteners present a unique section subjected to shear (see Fig. 3.28). The main problem of unsymmetrical connections is the out of plane displacements, caused by the eccentricity of applied forces. To prevent this phenomenon, appropriate strengthening is advised.

Rivets and bolts, in these connections, are always subjected to a secondary traction force, but the main cause of collapse remains the shear. Tests demonstrated that secondary bending moments effects are more accentuate if the connection length is small. This aspect influences the overall strength of joint.

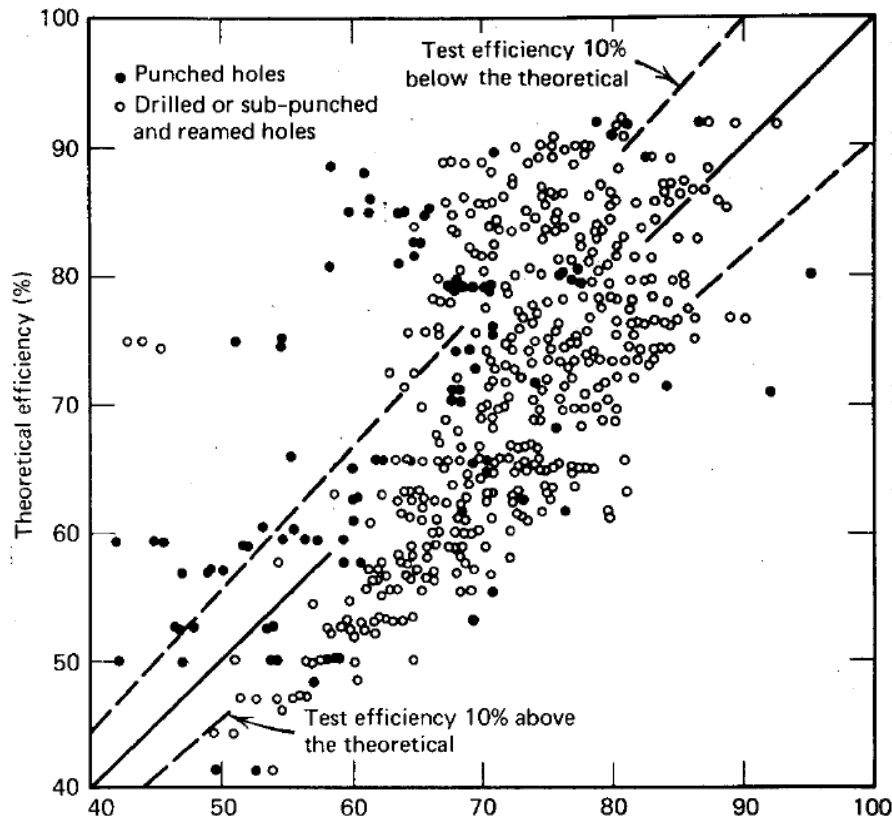


Figure 3.27 Correlation of theoretical and test efficiencies (Kulak et al., 1987).

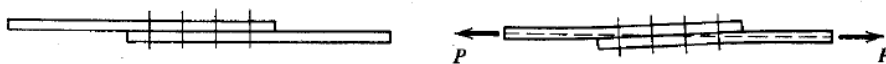


Figure 3.28 Lap shear connection (Kulak et al., 1987).

Results highlighted also that slip resistance is not influenced by the eccentricity of the load. Shear strength of fasteners is reduced of about 10% confronting that of symmetric specimens with similar properties. When the total length of the connection is relevant, effects of secondary bending moment are negligible.

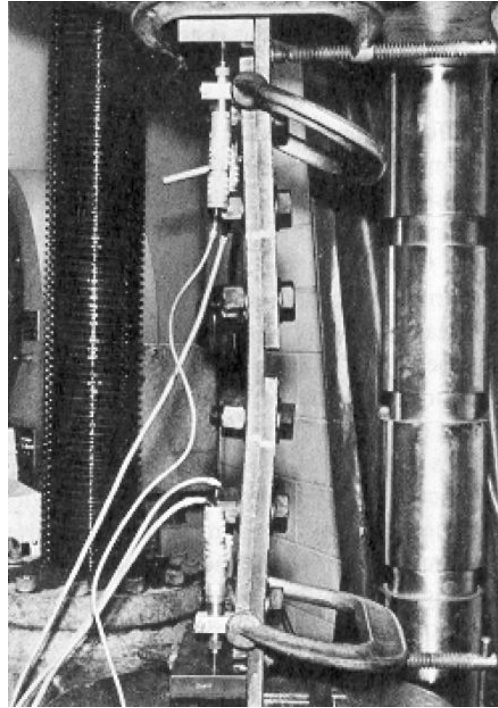


Figure 3.29 Effects of secondary bending moment (Kulak et al., 1987).

As denoted by authors: “lap joints may be subjected to a repeated type loading as well. The critical joint component under such loading conditions is not the fastener but the plate material. A severe decrease in the plate fatigue strength is apparent in unrestrained lap joints when compared with butt joints. The bending deformations cause larger stress ranges to occur at the discontinuities of the joint. The bending stress combines with the normal stress and results in high local stresses that reduce the fatigue strength. The reduction in fatigue strength depends on the joint geometry and the magnitude of the secondary bending. Hence, single shear splices subject to stress cycles should not be used unless the out-of-plane bending deformations are prevented”.

Another important work on riveted connections was carried out by Majid Sarraf and Michael Bruneau (1996), titled “**Cyclic testing of existing and retrofitted riveted stiffened seat angle connections**”. In this work, authors tested in laboratory a typical riveted connection taken

from an historic building. The aim of the experimental activity was the evaluation of the hysteretic behaviour and the estimation of the ultimate strength.

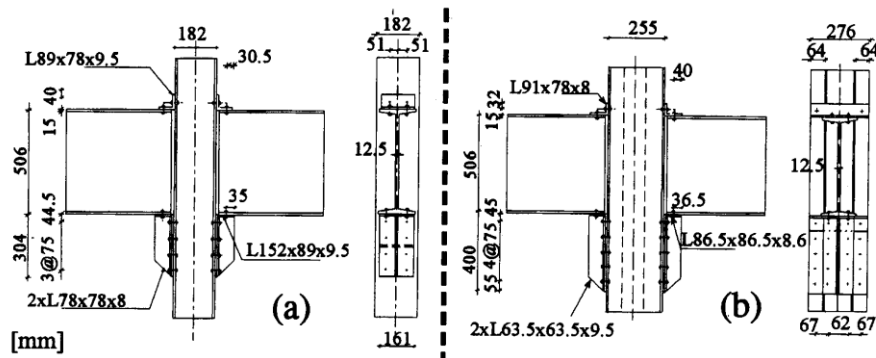


Figure 3.30 Details of riveted stiffened seat angle connections (Sarraf et al., 1996).

Experimental results showed a connection high strength, but the hysteretic curves demonstrated a low dissipative capacity. Authors developed also analytical models to calculate the ultimate strength: numerical results fitted well the experimental ones. A model that improves the hysteretic behaviour of the connection was also proposed. Indeed, the hysteretic curve moment-rotation of the investigated connections showed the pinching phenomenon, that involves a decrease of the ductility of the joint. Pinching could be determined by various factors.

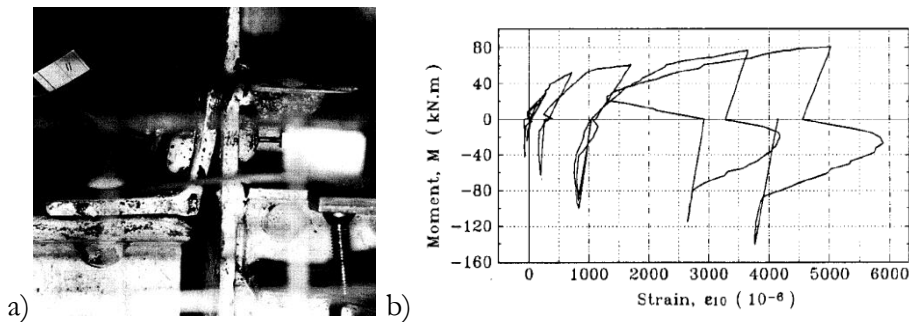


Figure 3.31 a) Top angle deformation; b) Moment-strain curve measured near location of plastic hinge formed in vertical leg of top angle (Sarraf et al., 1996).

In the early stages of loading when the connection is subjected to small shear forces generated by moment, one of the main causes of pinching is the slippage of rivet holes. This slippage is caused by two factors: one is the lack of tight fit inherent in ancient riveting practices; the other cause is the low friction resistance between connected parts. Another important cause of pinching is the rocking of top angles. Indeed, as showed in the hysteretic moment-strain curve (Fig. 3.31 b)), the response of top angles to cyclic loading determines the pinching phenomenon: when a positive moment is applied to the connection, the tension force causes the formation of plastic hinges and tension stresses in rivets.

The last cause of pinching is the separation of the seat angles and stiffener angles. As noted by authors: “negative moments induce the plastic deformation of both seat and stiffened angles, i.e., flexural resistance is provided by two separate connection components”.

To improve the ductility of riveted connections, authors proposed the addition of braces, as reported in Figure 3.32. The hysteretic behaviour of retrofitted joints is shown in Figure 3.33.

Authors concluded their work highlighting the high strength of these retrofitted connections and their good hysteretic behaviour, particularly recommended in case of structures in seismic areas.

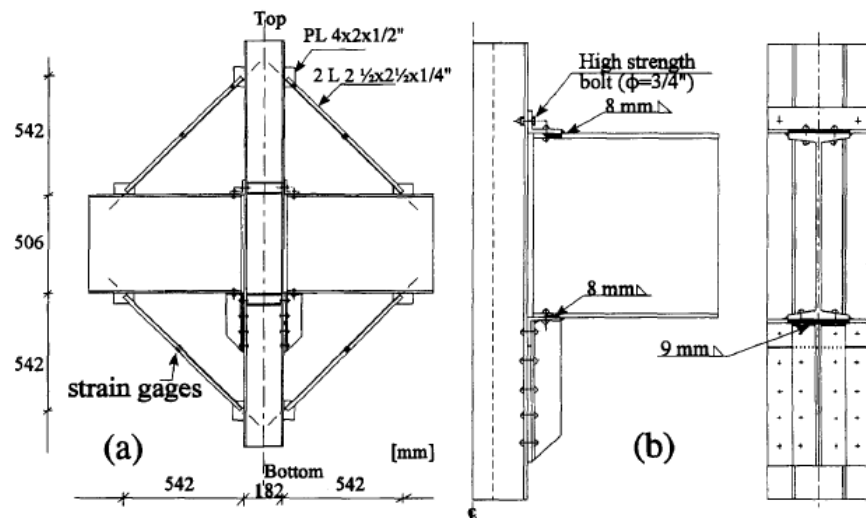


Figure 3.32 Retrofit details: a) Ductile knee braces; b) Selective weldings (Sarraf et al., 1996).

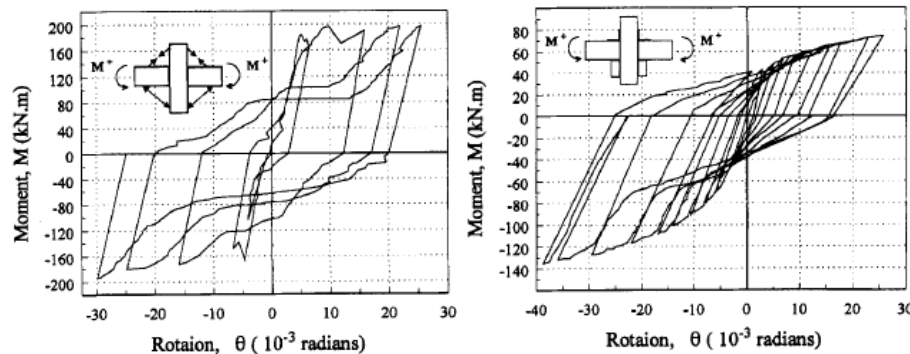


Figure 3.33 Hysteretic curves of retrofitted connection (Sarraf et al., 1996).

An important study on fatigue resistance of riveted connections under cyclic loading was carried out by Günther Valtinat, Ingo Hadrych and Holger Huhn: **“Strengthening of riveted and bolted steel constructions under fatigue loading by preloaded fasteners - experimental and theoretical investigations”** (2004).

This study was carried out due to the presence in Germany of many historical bridges, still in use today. In 1930's, experimental campaigns demonstrated that riveted bridges are subjected to a huge decrease of fatigue resistance in case of cyclic loading. In 1950's, was demonstrated that bolted bridges have a higher fatigue resistance than the riveted bridges, as showed in Figure 3.34, where the fatigue resistance of bolted and riveted connections respect to the number of cycles is illustrated.

As illustrated by authors: “The increase in capacity which means in stress range $\Delta\sigma$ or load cycles N was so immense that sometimes the fatigue behaviour of plain bars could be reached”. This increase was caused by the high pressure under the washers of the bolts around the hole. The effect of this high pressure is a certain protection of the hole area, indeed the stress distribution in the net section became much more favourable than for example with fitted bolts without preload (Figure 3.35).

The main scope of the work was the knowledge of the crack propagation velocity in preloaded bolt joints to non preloaded bolted connections until riveted connections. From experimental results, it can be concluded that riveted connections have a fatigue resistance equal to non preloaded bolted joints, so a certain margin of service life was observed for these connections.

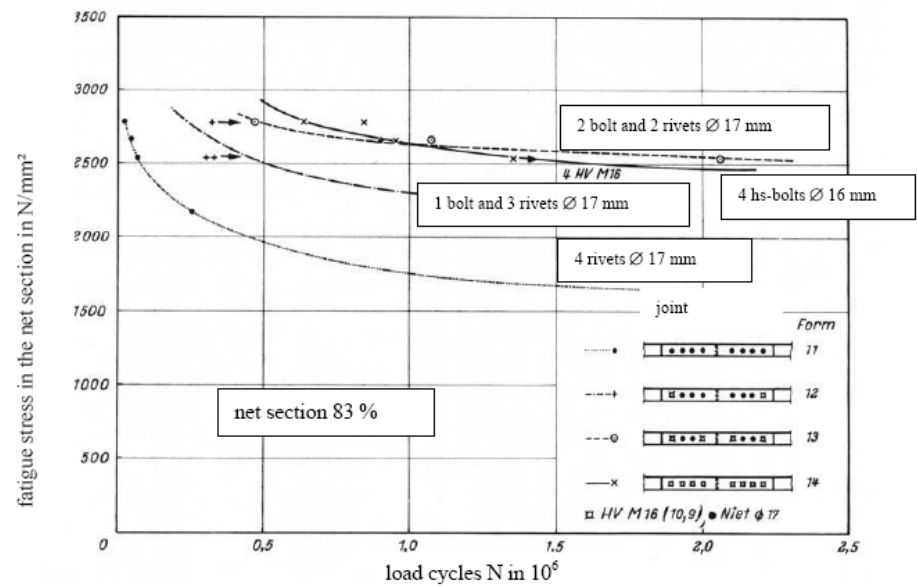


Figure 3.34 Fatigue resistance of bolted and riveted connections (Valtinat et al., 2004).

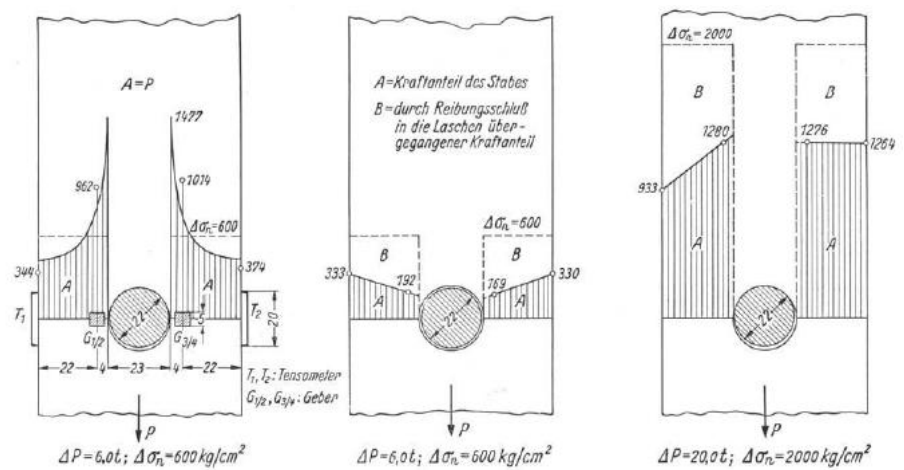


Figure 3.35 Stress distribution in net section (Valtinat et al., 2004).

Another important work on existing bridges was carried out by A.A.Fernandes, P.T. de Castro, M. Figueiredo, F. Oliveira: “**Structural integrity evaluation of highway riveted bridges**”, in which the Luís I bridge, located in Porto, was studied. The bridge was designed by the Belgian Engineer Téophile Seyrig, former partner of Gustav Eiffel, and built between 1881 and 1886.

First of all, the study started with the sampling of base material and riveted joints from the bridge. To perform the fatigue testing of the joints, a riveted T section cross beam was also removed. The sampling ended with the replacement of the base material with new material. The base material chemical composition was evaluated. The average values measured in three samples are illustrated in Figure 3.36.

Sample	C	Mn	Si	P	S
1	0.24	0.26	1.49	>0.15	>0.15
2	0.21	0.52	2.07	>0.15	>0.15
3	0.81	0.24	2.71	>0.15	>0.15

Figure 3.36 Base material chemical composition (Fernandes et al., 2004).

The chemical composition is typical of carbon steel with low carbon and manganese contents, with low volume fraction of perlite, as can be observed in Figure 3.37 a).

Higher carbon content was measured; this is due to local segregations. The use of Si in the steel desoxidation/desulphurization process caused the high silicon content, as shown by the large volume of inclusions (of Mn S type), as seen in Figure 3.37.

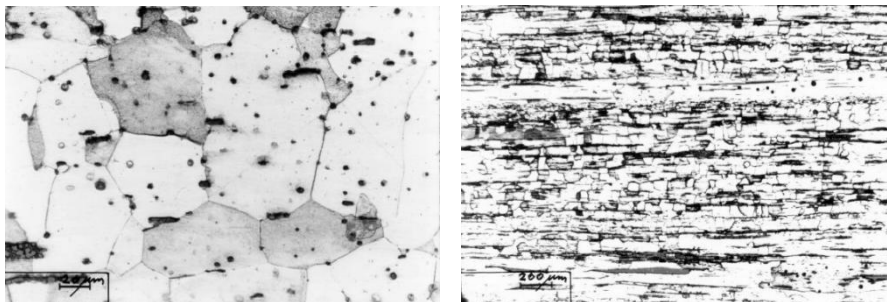


Figure 3.37 Microstructure of base material (Fernandes et al., 2004).

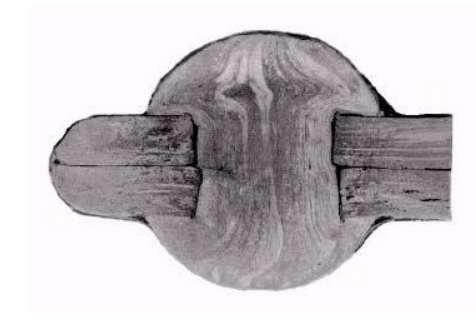


Figure 3.38 Macrostructure of rivet (Fernandes et al., 2004).

The rivet has a similar metallographic structure, due to a large density of inclusions in the most deformed parts of the rivet head. The mechanical properties evaluated are typical of carbon steel.

To evaluate the residual life of the bridge, the load history caused by the vehicles passage is necessary. Usually, according to the codes, is assumed the assumption that each vehicle with a weigh major than 30 kN induces a fatigue damage.

Authors concluded the work declaring that:

- “- The bridge base material showed mechanical properties similar to other European bridges built in the same period.
- The notch toughness properties, although lower than those required by modern codes of practice, are considered acceptable, given the heterogeneity of the material.
- The fatigue tests conducted in a riveted joint removed from the bridge are in conformance with current codes of practice requirements.
- The crack growth studies, due to the number of specimens available were not conclusive and so a crack growth law derived for carbon steels similar to the bridge material was used in the calculations.
- The best estimate of the remaining fatigue life, based on available data of truck traffic flow and data published in the international literature, is greater than 100 years”.

To ensure the security grade of the structure under actual loads, an evaluation of the effective bearing capacity of the structure is necessary. J. Moreno and A. Valiente are the authors of two important studies on this topic. The first work is “**Stress intensity factors in riveted steel beams**” (Moreno et al 2004), in which a model that takes into account

the effective bearing capacity of a beam in presence of a fracture is presented. This model evaluates also the contribution of near-cracking rivets, which transfer the loads to other intact elements.

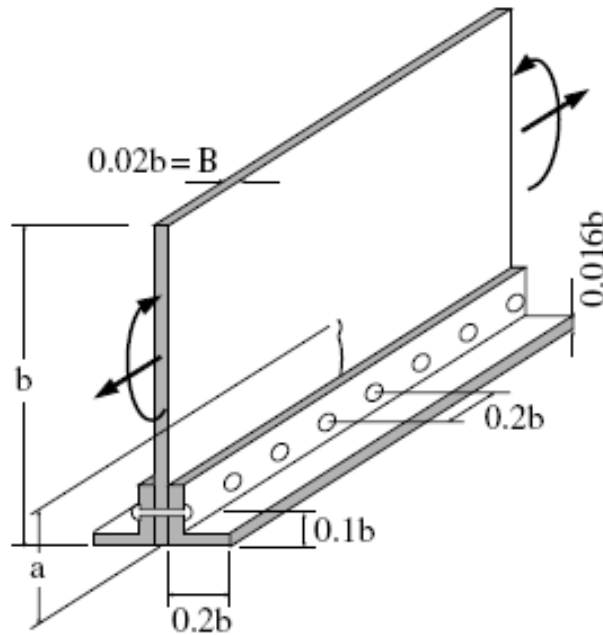


Figure 3.39 Riveted beam used for the stress intensity factor determination (Moreno et al 2004).

At the beginning of the 20th century, technology did not offer manufactured hot rolled beams or welding techniques for making welded connections. The most common structural member of steel bridges was riveted built-up beams, which consisted of angles and plates of puddled iron. The method presented in this work was applied on a one flanged and one webbed T section with a plate forming the web, two angles forming the flange, and a single row of rivets connecting them.

Axial and flexural loading were considered acting on the riveted beam so that the web is under the action of a bending moment when uncracked. In this phase, the distribution of these force and moment between the web and the angles follows the stress field of the theory of Strength of Materials. When the crack occurs, the forces alter this distribution near the crack due to the lower stiffness of the web, and the presence of rivets ensures the forces transfer to the angles. The proposed method to

calculate the rivets forces is based on the displacement equality. The formulation of this method leads to an expression of the stress intensity factor K , that is:

$$K = K_m + \sum_j K_j = \frac{1}{B\sqrt{b}} \left[\frac{M}{b} H^m(\bar{a}) + \sum_j P_j H^p(\bar{a}, \bar{s}_j) \right] \quad (1.6)$$

where: K_m is the stress intensity factor;

P_j is the rivet generic j -reaction;

K_j is the stress intensity factor of the rivet generic j -reaction;

H^m and H^p are a -dimensional function dependant by s_j and a ;

a is the distance of the generic j -rivet from the crack;

s_j is the crack dimension.

The variation of results for different a and s_j values highlights how the rivets reactions reduce the opening of the crack. Authors demonstrated also that the rivets reaction decrease sharply with the distance to the crack, and concentrate at the first rivet, since the force transmitted by the fifth rivet is only about 5% of the total transmitted force.

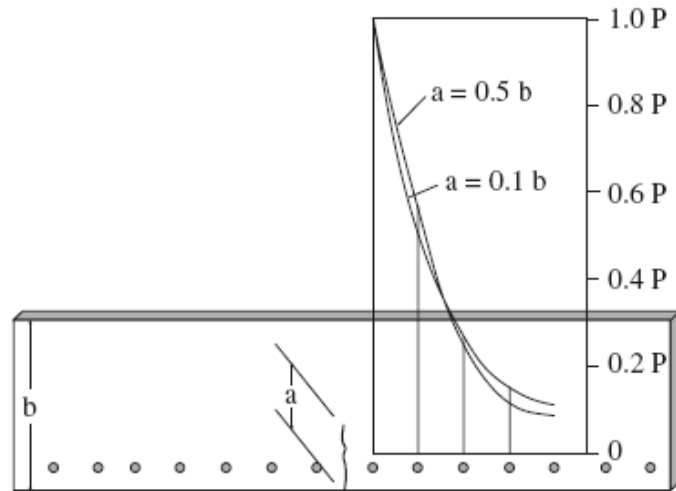


Figure 3.40 Force transmission at the rivets due to the cracking of the web plate (Moreno et al 2004).

As denoted by authors: “the difference between the stress intensity factors K and K_m is the error attributable to the neglect of the interaction of the cracked component of the beam with the remaining ones. This difference increases with the crack size, its relative value ranging from 50% to 90% as the cracked part of the cross-section of the web ranges from a fifth to the half. Even more striking is the fact that K_m increases with the crack size whereas K decreases: the effect of the interaction is so significant that the general trend of decrease of structural safety as damage grows becomes reversed in the riveted beam considered”. The conclusion of this work highlights that the structural assessment of riveted bridge could not neglect the effect of the rivets: this due to the fact that neglecting the contribution of rivets is excessively conservative.

Finally, the results show that the stress intensity factor can be a decreasing function from a given crack size, and not a monotonically increasing function of the crack size. This highlights the importance of none neglecting the contribution of rivets in these connections.

The same authors, in another work titled “**Cracking induced failure of old riveted steel beams**” (Moreno et al 2006), analysed which factor influences the collapse of connections and the type of failure.

In many cases, indeed, different types of failure, i.e. rivet shear failure or plates bearing failure, could be determinant.

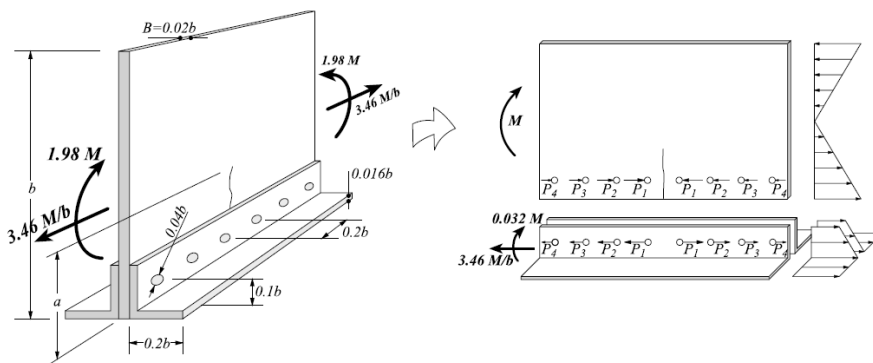


Figure 3.41 Geometrical configuration and loading of the analysed beam (Moreno et al. 2006).

The analysed riveted beam is shown in Figure 3.41. Authors determined its failure criterion considering the cracked plate and the riveted joints as potential origins of the collapse.

The three failure modes of riveted connections are:

- shearing of the rivet shank;
- tensile necking of the cross-sections weakened by the connection holes;
- crushing of the contact surface between the rivet and the connected pieces through which force transmission occurs.

For what concern the shearing of rivet shank, the limit value F_L^s of Eurocode 3 is:

$$F_L^s = 0.6R_m^r \pi R^2 \quad (1.7)$$

where: R is the rivet radius;

R_m^r is the rivet yielding stress.

In the plate's net area, the tensile necking of the resistant ligaments is avoided by limiting the tensile force at each cross-section of the connected pieces. The limit value is defined by codes as the product of the tensile strength of the steel and the resistant area of the cross-section (net section) decreased of a factor that takes into account for possible stress concentration effects produced by the holes. This formulation is appropriate in case of pieces that end at the joint and are loaded at the side of the other end. In this case, the considered joints connect pieces in the middle of their lengths and are loaded at both sides of the connected cross-section. Consequently, authors calculated the ultimate strength by a finite element calculation able to predict it reliably.

The failure of the joint due to the crushing of the contact between the rivet and the surface of the insertion hole is called bearing failure. It is a highly nonlinear phenomenon that, since the material is confined and cannot fracture, is valued rather arbitrary and based on judgments as to when the deformation due to crushing becomes excessive. For this reason, authors investigated the crushing of riveted joints in constructional steel both experimentally and numerically. The specimens used for the two crushing tests were rectangular plates with two holes. The specimens were tensile loaded along the longer symmetry axis. The tensile crushing forces were applied on the surfaces of the holes by means of two matching cylinders inserted in them. Some clip gauge

extensometers were used to measure the relative displacement of the loading cylinders. The finite element modeling of the two crushing tests was performed by considering the loading cylinders acting as rivets as rigid rough surfaces of the Coulomb type with a friction coefficient equal to 0.3. Loading was applied by increasing the relative displacement of the loading cylinders up to a value of 5 mm.

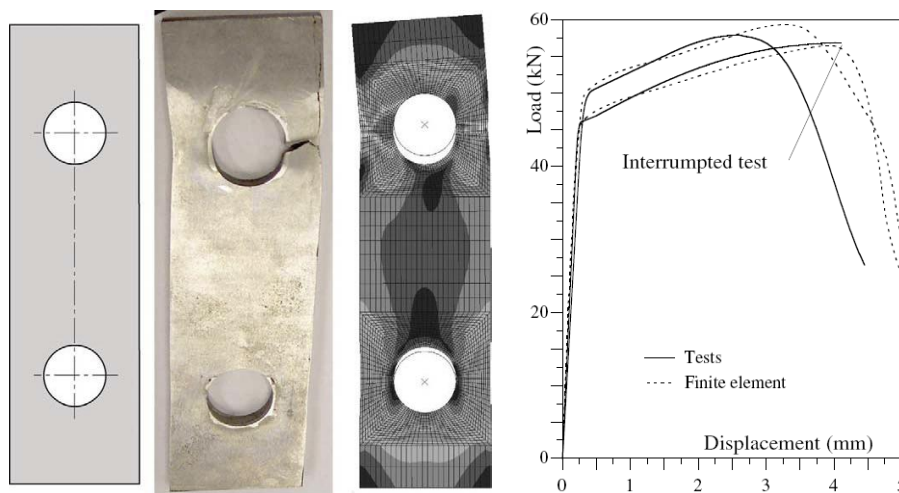


Figure 3.42 Experimental results and comparison with the numerical results (Moreno et al. 2006).

The lack of agreement between experiments and numerical modelling of necking can be attributed to the fact that in the ligament small, uncontrollable geometrical imperfections or material in-homogeneities are present in the highest degree. To reproduce the necking in the finite element modelling, a slightly diminishing of the area of one ligament was performed: as expected, necking occurred in this ligament. The F.E. model was also used to test the reliability of the formulas proposed in the precedent work for the calculation of the stress intensity factor and the determination of the rivet reactions. From the comparison of results, authors deduced that, for the calculation of the stress intensity factor, formulas fit well the numerical results. Also the sum of reaction of the rivets is similar, but a huge difference was noted for the single rivet reaction. The formulae proposed in the precedent work resulted inadequate to predict the failure mechanism of this type of connection in

presence of a crack, because the collapse depends mainly by the near-crack rivet reaction.

For the crushing failure of a riveted joint, authors proposed the limit load of the transmitted force given by Eurocode.

These formulae are not appropriate to limit the forces transmitted by the rivets to prevent the failure of the angles by tensile necking of the net section. For that reason, authors analysed this kind of failure by means of a new finite element modelling, showed in the next Figure.

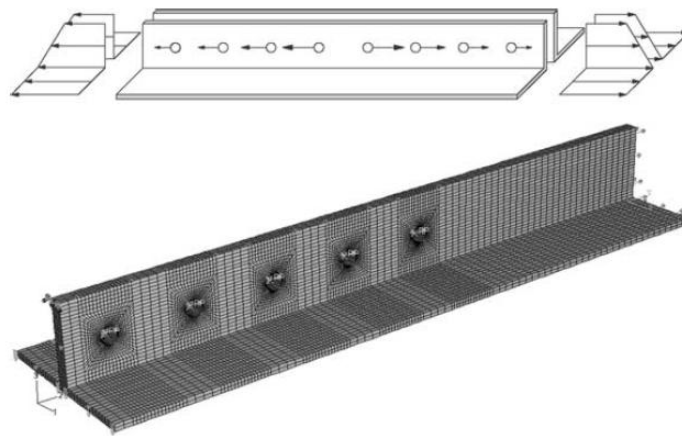


Figure 3.43 Finite element model used for analyse the tensile necking at the net section (Moreno et al. 2006).

The last collapse mechanism analysed was the fracture of the cracked web plate. Authors, in this case, reported a number of experimental data about the fracture behaviour of old structural steels present in literature.

One of the most important study on riveted connections is “**FE analysis of stringer-to-floor-beam connections in riveted railway bridges**”, carried out by M. Al-Emrani and R. Kliger (Al-Emrani et al 2003). In this work, the results of a wide experimental activity on stringer-to-floor-beam riveted connections and a highly detailed F.E. model of these joints were performed. To make the experimental tests, three full-scale bridge parts were taken from the old riveted railway bridge over the river Vindela“lven in northern Sweden, built in 1896. Tests were performed using four hydraulic jacks, each placed at the centre line of a stringer, as illustrated in the next Figure.

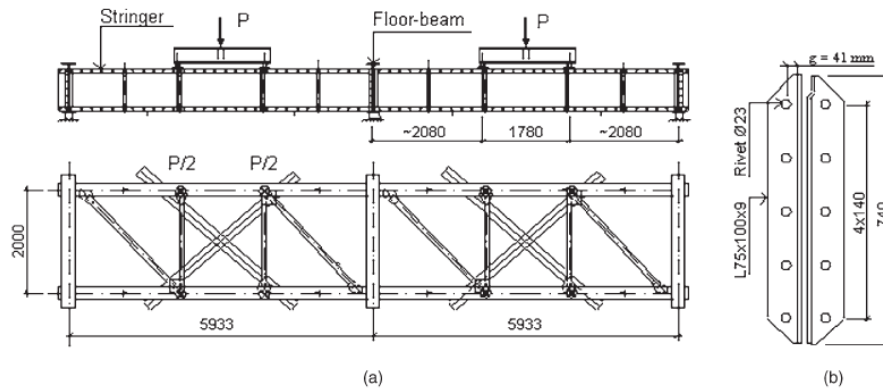


Figure 3.44 The riveted bridge parts that were tested: (a) test set-up; (b) detail of the connections (Moreno et al. 2006).

The FE model is characterized by symmetry with respect to two perpendicular planes passing through the centre lines of both the central floor beam (plane XZ) and the stringer. Authors adopted some other simplifications and assumptions to facilitate the building of the FE model, reduce the calculation costs and ease the post-processing of the results. These simplifications are, mainly, the adoption of nominal dimensions, the assumption of rivets initially ‘perfect’ shape, the modelling of material according to tension tests. Three different mesh densities were performed in the first step: solid elements were used for the angle and the rivets in the connection, shell elements were used for the stringer. Rigid contact surface, meshed with linear quadratic rigid elements (R3D4), was used to simulate contact between the back-face of the outstanding leg of the connection angle and the floor-beam web. All the contact pairs in the model was characterized by using a classical Coulomb-friction model, with an assumed friction coefficient ($\mu = 0.3$). The FE models were verified with two main criteria. As described by authors: “First, the ability of the model to ‘reproduce’ the correct stiffness of the connection was checked against displacement and strain measurements made at the top of the connection angles and at the mid-span of the stringers, respectively. Secondly, strain gauges installed at different locations along the stringer depth near the connection were used to register the distribution of local stresses in these locations. The measured values were compared with the corresponding values obtained

from the FE analysis". The magnitude of the clamping force in the rivets was also taken into account: three different rivet pre-tension values (30, 65, and 140 MPa) were considered and the results are compared with and related to strain measurements made on one of the rivets in the connections. Two types of finite element were used, C3D8 and C3D20. Both the finite element reproduced the effective behaviour of the connection, but C3D8 reduced the computational costs.

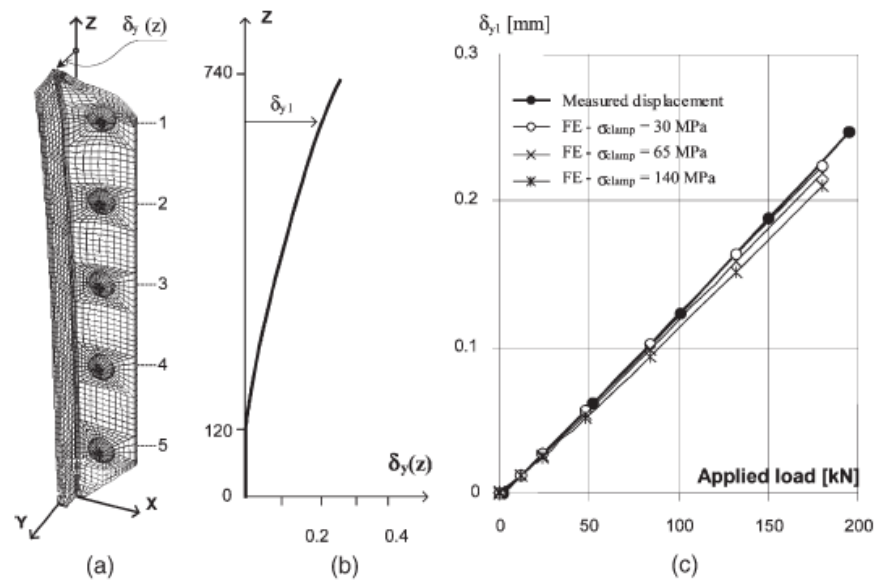


Figure 3.45 Out-of-plane distortion of a connection angle (Moreno et al. 2006).

The results of the FE analysis and the comparison between these results and the experimental ones are showed in Figure 3.45. The dominant role in the behaviour of these connections is the gauge distance between the rivets and the fillet of the angle. The outstanding leg of the angle along the gauge length is subjected to bending stresses, which reached a maximum near the fillet of the angle. These parts reached the experienced plastic strains but to a very limited extent. The stresses in the rivets were, however, fully elastic. Authors highlighted also that the influence of the rivet-clamping force on the magnitude of maximum bending stresses near the fillet of the angle is negligible. On the other hand, a higher clamping force determined higher bending stresses in the outstanding leg near the rivet. Clamping forces influenced the

connections in terms of stiffness: for higher values of clamping forces, indeed, the connection behaved like a rigid body, due to the effect of the rivet head on angles.

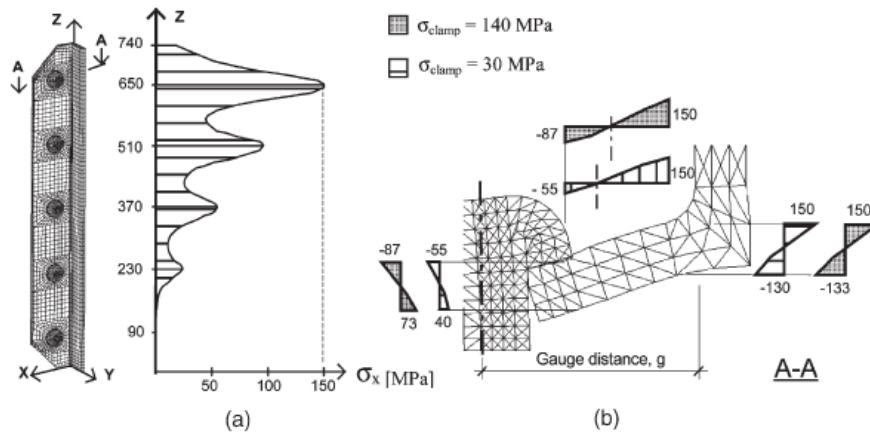


Figure 3.46 The distribution of bending stresses in the connection angle (Moreno et al. 2006).

Strain gauge specially designed for uniaxial strain measurements in bolts were used to make strain measurements, in order to obtain information about the magnitude of the clamping forces. These forces could be determined by comparing the nominal tensile stresses obtained from the FE analyses using different rivet-clamping stresses with the measured values (superimposed by the same presumed initial clamping stresses). A good correlation was obtained between measured and calculated axial stresses for the model with a rivet-clamping stress of 30 MPa.

Finally, the benefice of higher clamping force was demonstrated: if this force is high, the bending in rivet when the load increases is low, and the ultimate strength increases noticeably.

4 EXPERIMENTAL ACTIVITY ON RIVETED CONNECTIONS

In order to provide a tool for structural safety assessment of the historical steel structures that are still in service, this chapter is devoted to investigate the structural capacity of the riveted connections under actual service loads. A wide experimental activity was carried out within two research project:

1. the international research project PROHITECH on ‘Earthquake protection of historical buildings by reversible mixed technologies’ within the Sixth Framework Programme FP6 of EU,
 - WP 7 – Experimental analysis
 - WP 8 – Numerical analysis
 - WP 9 – Development of calculation models
2. the national Research Project PRIN prot. 2005087058_004 “Vulnerability and reversible consolidation techniques for historical metal structures”.

The experimental campaign was carried out in collaboration with RFI (Rete Ferroviaria Italiana) to determine the chemical and mechanical response of the ancient steel, and to investigate the overall behaviour of different types of riveted connections. The experimental results were also presented and discussed.

4.1 EXPERIMENTAL PROGRAMME

4.1.1 General

The main scope of the testing programme was to investigate the influence of different parameters on the shear response of riveted

connections. Several lap shear tests have been planned in order to study the mechanical behaviour of riveted connections. In detail, it is possible to subdivide this activity into two phases:

1. Test on steel riveted joints made up with plates and rivets gained from warehouse of Italian railways and characterized by geometric properties similar to those of the ancient riveted connections;
2. Test on ancient joints sampled by a real historic metal structure, dated from the second half of 19th century.

All specimens were dimensioned and detailed by the Steel Structure Division of RFI, which is based in Naples, in order to be representative of connections typically used for its lattice roofing and bridge. According to precedent studies on historic metal constructions, a total of 66 specimens, representing 22 different typologies of riveted connections, were realized. Each type of connection differed from the others for number of rivets, rivet diameter, plate dimensions and load symmetry.









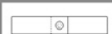



































			U-16-10-2		
			U-16-10-4		
S-16-10-1			S-19-10-2		
U-16-10-1			U-19-10-2_90		
S-19-10-1			U-19-10-2_60		
U-19-10-1			S-19-10-4		
S-19-12-1			U-19-10-4_90		
U-19-12-1			U-19-10-4_60		
S-22-10-1			S-22-12-2		
U-22-10-1			U-22-12-2		
S-22-12-1			S-22-12-4		
U-22-12-1			U-22-12-4		

Figure 4.1 Riveted specimens: investigated typologies (D'Aniello et al. 2010).

The specimen material was gained from Italian railways warehouse and is dated from the first half of the 20th century. Tests were performed to determine their mechanical characteristics and were also described by D’Aniello et al., 2010.

To investigate the behaviour of real ancient riveted connections, four specimens were sampled from a dismantled bridge, dated from the second half of 19th century (1984). Specific manufacturing were performed on these specimens to allow the correct execution of tests.

Before testing the riveted connections, a wide experimental campaign was performed to determine the mechanical characteristics of the base material. Indeed, the research activity was divided into two main steps: tests on materials and tests on steel riveted connections (D’Aniello et al., 2010).

4.1.2 Programme of material tests

The first step of the experimental activity regarded the planning and the execution of material tests: the scope of this campaign was the determination of the properties of steel plates and rivets constituting the connections being examined. Tensile coupon tests, Brinell hardness (BH) tests, chemical analysis and Charpy-V notch (CVN) tests were performed, obtaining both the chemical and the mechanical properties (D’Aniello et al., 2010).

4.1.3 Testing programme on riveted connections and investigated parameters

Once the material was characterized, a series of tests on riveted connections were performed, and different parameters were controlled to investigate their influence on the connection response (D’Aniello et al., 2010).

First of all, the influence of load eccentricity was analyzed by testing both symmetrical and unsymmetrical connections. Hence, the effects of secondary bending moments induced by load eccentricity on joint deformation and shear strength (D’Aniello et al., 2010).

In order to induce the yielding at the gross cross-section before the failure by fracture at the net cross-section, different values of the normalized net area A_n/A_g were considered during the testing

programme. To obtain the yielding in the gross cross section, indeed, the ratio $A_n f_u / A_g f_y$ must be larger than 1, where $A_n f_u$ being the ultimate strength of the net section and $A_g f_y$ the yield strength of the gross section. In this case, considering the specified average yield and tensile strengths of the tested steel, the value of the normalized net area A_n / A_g could be equal or greater than 0.67 (D'Aniello et al., 2010). This requirement allows yielding of the gross section before failure of the net section occurs. The tested riveted connections presented a normalized net area that varies in the range 0.68–0.79, which corresponds to a ratio of $A_n f_u / A_g f_y$ in the range 1.02–1.17 (D'Aniello et al., 2010).

An important parameter that influences the failure in tension of the plates is the plate width (w). In this case, different values of the ratios w/d were considered, where w is the width of plates and d is the nominal diameter of the rivet, namely 3.16, 3.18, 4.38 and 4.74 (D'Aniello et al., 2010). The influence of the plate width becomes remarkable when the ratio (w/d) is lesser than 8, according to the literature (Schenker 1954; Munse 1956; Munse 1970).

In order to characterize the riveted connections behaviour, different joint lengths were considered and the influence of the length on the connection behaviour was studied. Indeed, the length of the joint could vary according to the number of rivets, the rivet spacing p and the distance from the centre of the end rivet hole to the adjacent edge (e_1) in the direction of shear load. In order to take into account different joint lengths, specimens made of one, two and four rivets were tested during the experimental campaign. Four different p/d ratios (4.09, 6.32, 8.75 and 9.21) were tested. These ratios satisfy the geometric limits of EN 1993:1-8 with the exception of specimens U19-10-2_60 and U19-10-4_60, in which $p/d = 9.21$ while the corresponding Eurocode limit is 7.37 (being the maximum allowable spacing equal to 14 times the plate's thickness). In addition, in this study three different e_1/d ratios (1.59, 2.19 and 2.37) were analyzed (D'Aniello et al., 2010).

Another parameter that influences the strength of riveted connections is the clamping force induced by the cooling of the rivet: the influence of this parameter on the slip resistance was also analysed.

A total of 64 lap shear tests were performed, as summarized in the programme matrix reported in Table 4.1.

The geometries of the investigated connections are shown in Figure 4.1. Specimens were labelled as C–D–TH–N, where:

C is the splice configuration (i.e. S: Symmetrical joint; U: Unsymmetrical joint);

D is the rivet diameter (16, 19 or 22 mm);

TH is the steel plate thickness (10 or 12 mm);

N is the number of rivets per specimen (D'Aniello et al., 2010).

Table 4.1 Bonding test programme matrix (D'Aniello et al. 2010).

Specimen tag	S	U	Rivet diam. (mm)	Thickness plate (mm)	Width plate (mm)	Dist. from edge (mm)	Rivet pitch (mm)	Rivet no.	Test no.
Single rivet									
S-16-10-1	✓		16	10	70	35	–	1	3 (a, b, c)
U-16-10-1		✓	16	10	70	35	–	1	3 (a, b, c)
S-19-10-1	✓		16	10	70	35	–	1	3 (a, b, c)
U-19-10-1		✓	19	10	90	45	–	1	3 (a, b, c)
S-19-12-1	✓		19	10	90	45	–	1	3 (a, b, c)
U-19-12-1		✓	19	12	90	45	–	1	3 (a, b, c)
S-22-10-1	✓		22	10	70	35	–	1	3 (a, b, c)
U-22-10-1		✓	22	10	70	35	–	1	2 (a, b)
S-22-12-1	✓		22	12	70	35	–	1	2 (a, b)
U-22-12-1		✓	22	12	70	35	–	1	3 (a, b, c)
Rivets in row									
U-16-10-2		✓	16	10	70	35	140	2	3 (a, b, c)
U-16-10-4		✓	16	10	70	35	140	4	3 (a, b, c)
S-19-10-2	✓		19	10	90	45	120	2	3 (a, b, c)
U-19-10-2		✓	19	10	90	45	120	2	3 (a, b, c)
U-19-10-2		✓	19	10	60	30	175	4	3 (a, b, c)
S-19-10-4	✓		19	10	90	45	120	4	3 (a, b, c)
U-19-10-4		✓	19	10	90	45	120	4	3 (a, b, c)
U-19-10-4		✓	19	10	60	30	175	4	3 (a, b, c)
S-22-12-2	✓		22	12	70	35	90	2	3 (a, b, c)
U-22-12-2		✓	22	12	70	35	90	2	3 (a, b, c)
S-22-12-4	✓		22	12	70	35	90	4	3 (a, b, c)
U-22-12-4		✓	22	12	70	35	90	4	3 (a, b, c)
									Tot. tests
									64

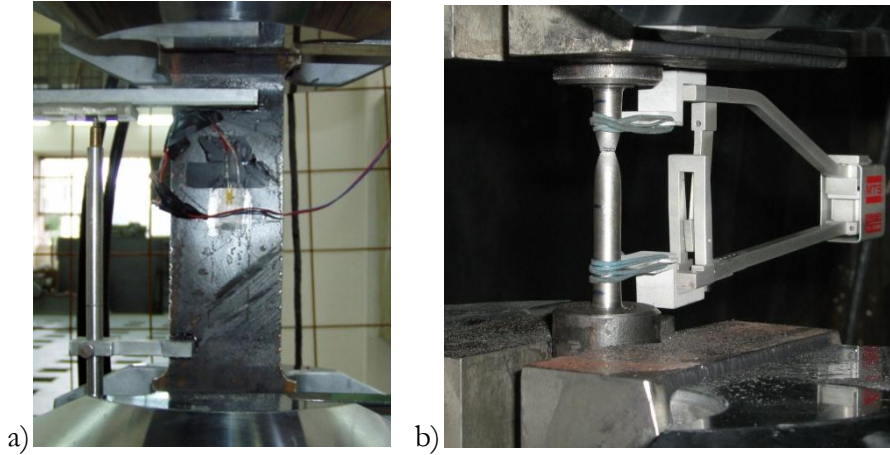


Figure 4.2 Coupon sampled from a plate of riveted specimen under testing (a); rivet coupon under testing (b) (D’Aniello et al. 2010).

Due to the fact that connections could be affected by the manual riveting, similar riveted connections can show a different capacity response (Fisher et al., 1969). To take into account this phenomenon, three nominally identical specimens have been built up for every type of riveted connection. In two cases (U19-10-2 and U19-10-4) RFI asked us to investigate the influence of two different values of the distance from the edge to the centre of the rivet in the transverse direction. Hence, the same tag has been adopted twice for specimens having two different widths (D’Aniello et al, 2010) .

4.1.4 Set-up of material and riveted connection tests

Tensile, CVN, BH tests and chemical analysis were the tests performed to characterize the material. The testing machine was a universal electro-mechanical MTS 500. The strains were measured using both strain gages and a linear deformometer (Fig. 4.2(a) and (b)).

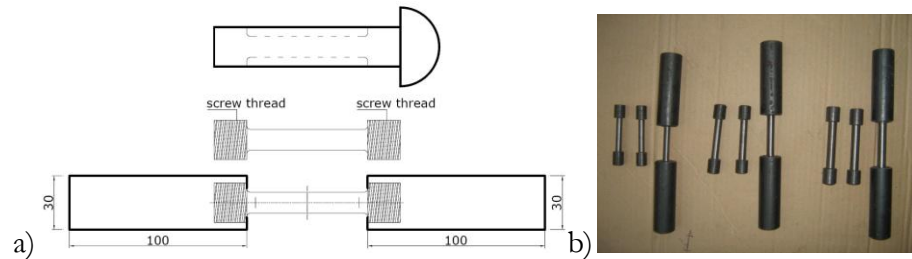
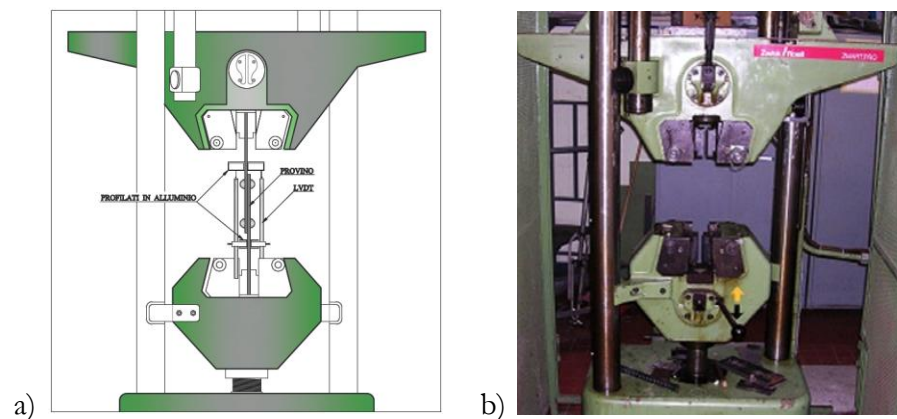


Figure 4.3 Dog-bone rivet shank (D'Aniello et al. 2010).

To perform the uniaxial tensile tests, all the rivet shanks were arranged in a dog-bone configuration, as shown in Figure 4.3. Moreover, both ends of the coupons were screw-threads and two cylindrical threaded sleeves were used to fix the specimens into the test machine (D'Aniello et al, 2010).

The CVN tests of plates and rivets were performed by using an impact tester Zwick 5113. An ELBO TH-3000-OB universal hardness test machine was used for BH measurements. Finally, to identify the chemical composition of both plates and rivets, a glow discharge atomic emission spectrometer LECO model GDS850A was employed. The experimental setup used for riveted connections is shown in Figure 4.4(a). In particular, lap shear tests were carried out with a universal electro-mechanical Zwick/Roell testing machine (Fig. 4.4(b)). The specimens were loaded in tension under displacement control until failure, i.e. after the load decreased (D'Aniello et al, 2010).



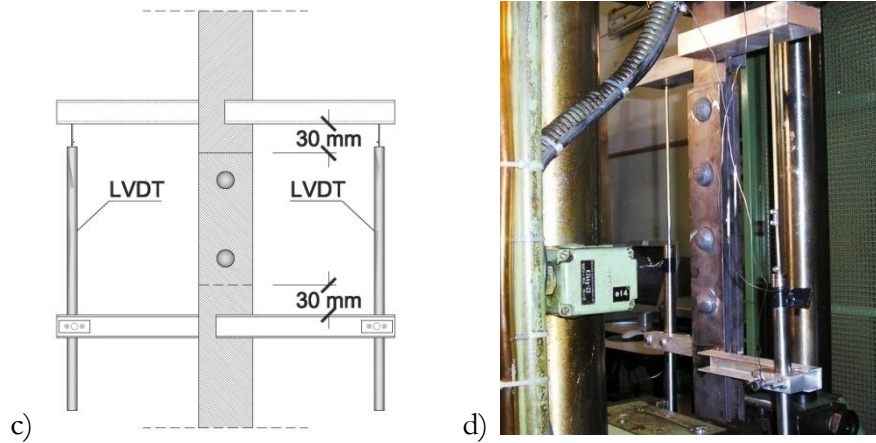


Figure 4.4 Test setup (a); the testing machine (b); the layout of LVDTs (c, d) (D'Aniello et al. 2010).

For each test, the maximum load reached and the types of failure mode were observed. A pair of LVDT (Linear Variable Differential Transformer) measured the relative in-plane displacement of tested specimens. The LVDTs were characterized by a displacement range of ± 150 mm and were positioned 30 mm from both ends of the regions where plate discontinuities occur in all specimens (Fig. 4.4(c) and (d)). The displacement rate was fixed at 0.1 mm/s and an acquisition frequency of 10 Hz was assumed (D'Aniello et al, 2010).

4.2 EXPERIMENTAL RESULTS

4.2.1 Test on materials

4.2.1.1 Tensile tests

Tensile tests were performed, as mentioned above, both on rivet specimens and plate samples.

The tensile tests on plates were executed on two different plate thicknesses: 10 and 12 mm. For each thickness, five plate specimens were sampled, for a total of 10 specimens. A pair of LVDTs and a strain gage was used to measure both the displacement and the strain, as showed in Figure 4.2 a).

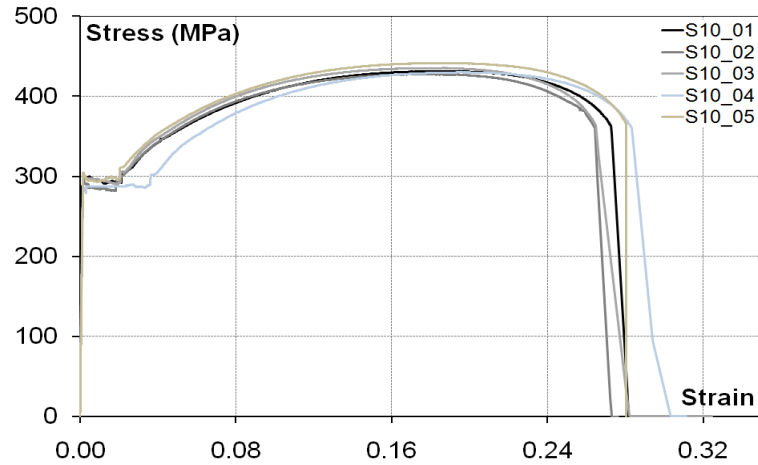


Figure 4.5 The stress–strain response of plates of riveted specimens.

The stress–strain curves of the plates are shown in Figure 4.6. The average yield stress of steel plate was 291 MPa (Standard Deviation “SD”= 5.63 MPa and Coefficient of Variation “CV” = 0.02), while the average ultimate stress was 433 MPa (SD = 5.48 MPa, CV = 0.01) and there was an average ultimate strain (corresponding to necking) of about 28% (SD = 1%, CV = 0.04). This material was identified as a modern steel S 275 (D’Aniello et al, 2010).

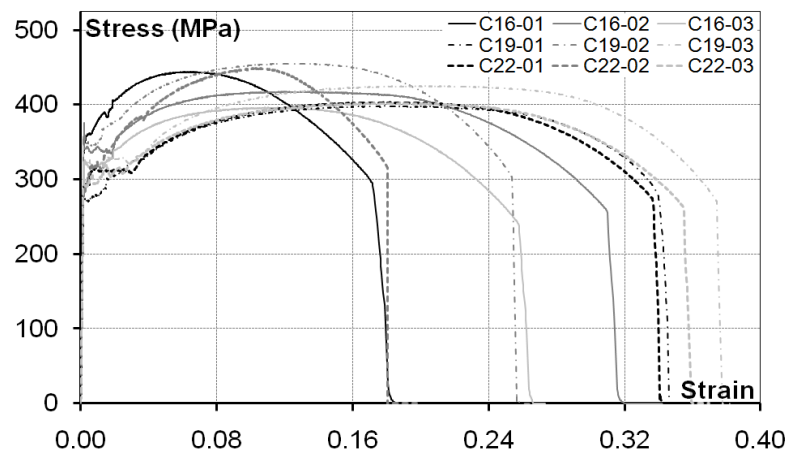


Figure 4.6 The stress–strain response of rivet specimens.

Tensile tests on rivet specimens were executed on three different rivet diameters: 16, 19 and 22 mm. For each investigated diameter, three identically specimens were sampled, for a total of 9 specimens. A pair of LVDTs and a strain gage was used too to measure both the displacement and the strain, as showed in Figure 4.2 b).

Considering the experimental results, a considerable variability in the base material properties of the rivets was noted. This phenomenon is probably determined by the lack of adequate quality control in the industrial processes of that period. Indeed, it was not possible to set a specific trend per rivet diameter in terms of yield and ultimate strength, as shown in Figure 4.6. However, the average value of yield stress was 315 MPa (SD = 26.03 MPa, CV = 0.08), the average ultimate stress was about 412 MPa (SD = 17.85 MPa, CV = 0.04), while the average ultimate strain (corresponding to necking) was 16% (SD = 6%, CV = 0.36) (D'Aniello et al, 2010). These data appear to be more consistent with steel produced by a Martin–Siemens process (Sustainable bridges, 2006).

4.2.1.2 Impact strength tests

The impact strength tests were performed at ambient temperature (20°C) on four specimens sampled from plates having a cross-section of 10×10mm and a V notch. Table 4.2 shows the results. It should be noted that the average Charpy-V-Notch (CVN) fracture toughness is equal to 15 J, which is lower than the reference value of 27 J at 0 °C or +20 °C as suggested in EN 10025 for modern steel (D'Aniello et al, 2010). However, this discrepancy is reported also in literature (Sustainable bridges, 2006). The experimental CVN values are in accordance with the literature, and highlight that this type of aged steel is more brittle than modern ones (D'Aniello et al, 2010).

4.2.1.3 Hardness tests

The base material used for the riveted connections was also characterized by performing BH tests on plates and rivet shanks. These tests are in accordance with the necessity of more and detailed information on ancient steel. All the results are reported in Table 4.2. In particular, it is possible to note that the average value of BH is 121 for plates and 137 for rivets. These results are in agreement with the strength obtained from the tensile tests (D'Aniello et al, 2010).

Table 4.2 Material characterization: BH measurements and CVN fracture toughness (D’Aniello et al., 2010).

	Brinell Hardness measurements				Charpy-V-Notch fracture toughness			
	BH	Average BH	SD	CV	CVN (+20°C)	Average CVN (+20°C)	SD	CV
	(500 kgf load, 10 mm ball)				(J)	(J)	(J)	
plate 1	119				23			
plate 2	121	121	1.71	0.01	36	31	7.59	0.25
plate 3	123				38			
plate 4	120				25			
rivet 1	146							
rivet 2	139							
rivet 3	115	137	12.52	0.09	–	–	–	–
rivet 4	140							
rivet 5	144							

4.2.1.4 Chemical analysis

Chemical analyses were also performed on base material, in order to evaluate the composition of the ancient steel. In Tables 2.3 and 2.4 are reported all the results of the chemical analyses. It should be noted that both the plate and rivet metal is characterized by a high percentage of sulphur, about twice the maximum value of the quantity commonly present in modern steel EN 10025 (D’Aniello et al, 2010).

Table 4.3 Chemical composition of the plates (D’Aniello et al., 2010).

	C (%)	Si (%)	Mn (%)	P (%)	S (%)	Cu (%)	Cr (%)	Ni (%)	V (%)	Mo (%)	N (%)	Ceq (%)
plate 1	0.07	0.15	0.54	0.014	0.059	0.41	0.06	0.12	0.004	0.02	0.0104	0.212
plate 2	0.08	0.18	0.5	0.012	0.061	0.37	0.06	0.11	0.004	0.02	0.0099	0.212
plate 3	0.09	0.19	0.56	0.017	0.061	0.38	0.11	0.12	0.004	0.02	0.0091	0.243
plate 4	0.08	0.17	0.54	0.01	0.048	0.3	0.06	0.1	0.003	0.02	0.0092	0.213
Average value	0.08	0.17	0.54	0.01	0.06	0.37	0.07	0.11	0.00	0.02	0.0097	0.220
SD	0.01	0.02	0.03	0.00	0.01	0.05	0.03	0.01	0.00	0.00	0.0006	0.015
CV	0.10	0.10	0.05	0.23	0.11	0.13	0.34	0.09	0.13	0.00	0.0636	0.070

Table 4.4 Chemical composition of the rivets (D’Aniello et al., 2010).

	C (%)	Si (%)	Mn (%)	P (%)	S (%)	Cu (%)	Cr (%)	Ni (%)	V (%)	Mo (%)	N (%)	Ceq (%)
rivet 1	0.41	0.02	0.22	0.04	0.07	0.06	0.09	0.24	0.00	0.00	0.0146	0.485
rivet 2	0.39	0.03	0.20	0.06	0.08	0.08	0.08	0.19	0.00	0.00	0.0197	0.457
rivet 3	0.35	0.03	0.23	0.05	0.07	0.08	0.15	0.21	0.00	0.00	0.0239	0.438
rivet 4	0.40	0.02	0.22	0.04	0.07	0.07	0.07	0.22	0.00	0.00	0.0149	0.470
rivet 5	0.42	0.02	0.21	0.04	0.07	0.07	0.08	0.24	0.00	0.00	0.0151	0.491
Average value	0.39	0.02	0.22	0.05	0.07	0.07	0.09	0.22	/	/	0.0176	0.47
SD	0.03	0.00	0.01	0.01	0.00	0.01	0.03	0.02	/	/	0.0041	0.02
CV	0.07	0.10	0.05	0.18	0.06	0.14	0.34	0.10	/	/	0.2316	0.05

On the other side, the carbon content is different in plate and rivet steel. In particular, rivets present a high carbon percentage, about 0.39%, while the plates have a low carbon percentage (0.08%).

Confronting the experimental results in terms of equivalent carbon percentage (Ceq) with the values given by Mang et al. (1996), Hohlwegler et al. (1993), Stier et al. (1983), it is possible to note that the tested ancient steel is similar to the modern mild steel, with the exception of the tensile strength characteristics. Furthermore, it should be asserted that the corrosion resistance and the metal toughness are both penalized by the high sulphur content. This phenomenon is particularly evident for rivets, where the high carbon content implies low ductility, and difficulty in machining (D’Aniello et al, 2010).

4.2.2 Tests on riveted connections

4.2.2.1 Monitored mechanical parameters

During the riveted connection tests, some parameters were monitored, in order to describe the experimental connection behaviour. These parameters are illustrated in Figure 4.6, and are reported in D’Aniello et al. (2010) as described below:

- “ $s = (s_{LVD1} + s_{LVD2})/2$: average displacement (s_{LVDi} is the displacement recorded by the i th LVDI);
- F_u : strength, which is the maximum recorded average load;

- s_u : slip corresponding to F_u ;
- F_e : conventional elastic strength. The yield force is conventionally measured on an idealized bi-linear response curve obtained from the experimental one by assuming that the areas under the actual curve and its bi-linear idealization, which has the same initial stiffness and the same peak point of the actual curve, are equal;
- s_e : slip corresponding to F_e ;
- $K_e = F_e/s_e$: elastic stiffness;
- s_{max} : displacement corresponding to a load equal to $0.80F_u$ on the post-peak branch of response curve;
- $\mu = s_{max}/s_e$: maximum ductility”.

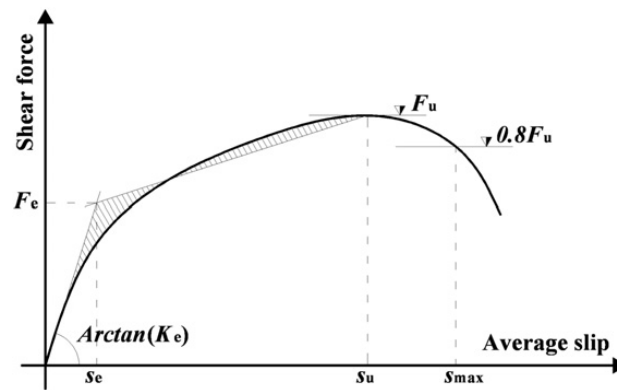


Figure 4.7 The stress–strain response of rivet specimens (D’Aniello et al., 2010).

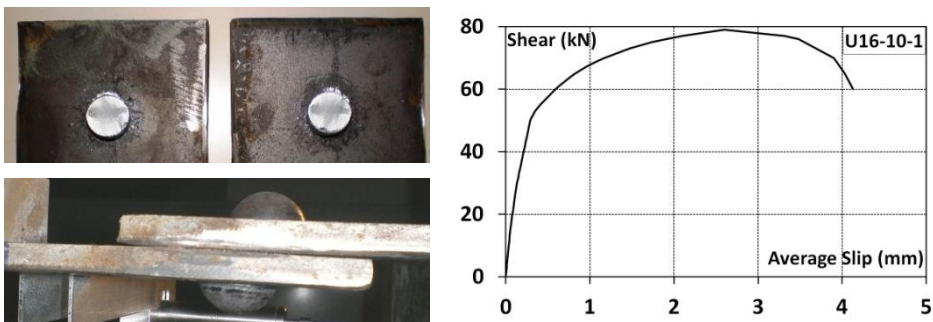
4.2.2.2 Failure modes

After tests, it was possible to observe the different failure modes of the tested connections. In particular, three main failure modes were noted:

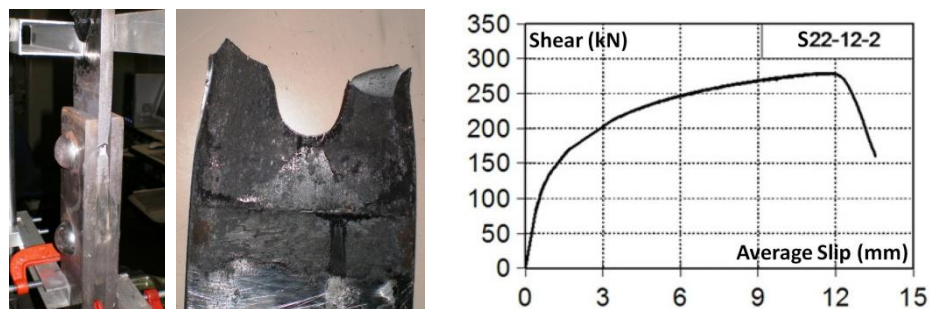
- (I) rivet shear failure;
- (II) bearing at rivet holes of thinner plates;
- (III) failure in tension on the net section of the steel plate.

In most cases, the connection exhibited a combination of failure mechanisms. In particular, the unsymmetrical joints showed mixed failure modes, combining types I and III. On the other side, symmetrical

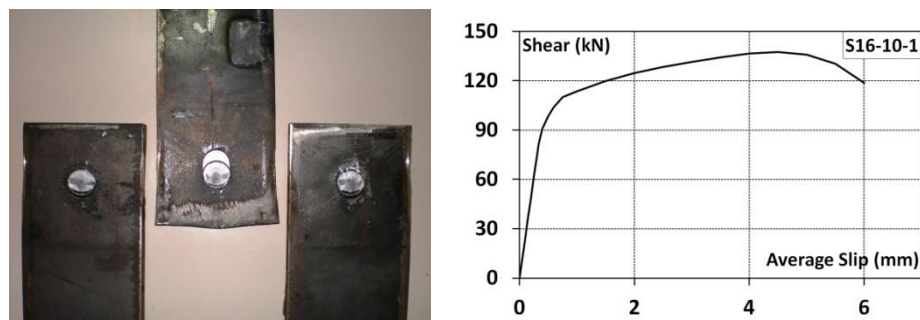
connections are prone to collapse following the single failure mode, as the rivet shear failure (I) or the bearing at rivet holes of thinner plates (II). The main types of failure mechanism and the relevant force–displacement response curves obtained by the tests are shown in Figure 4.8. The mechanical parameters monitored during the tests are reported in Tables 2.5 for riveted connection with a single rivet, and in Table 4.6 for joints with rivets in a row (D’Aniello et al, 2010).



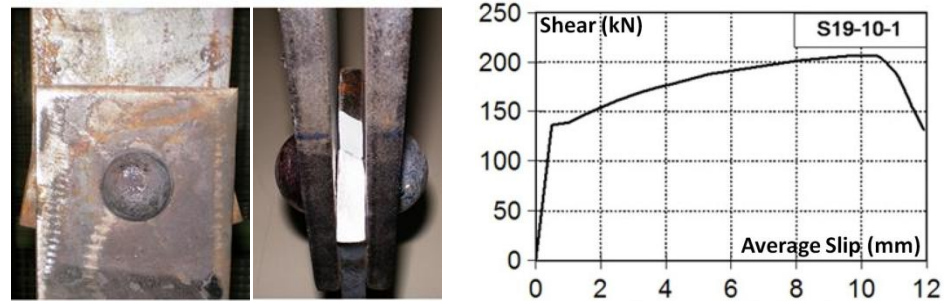
(a) Rivet shear failure (U16-10-1).



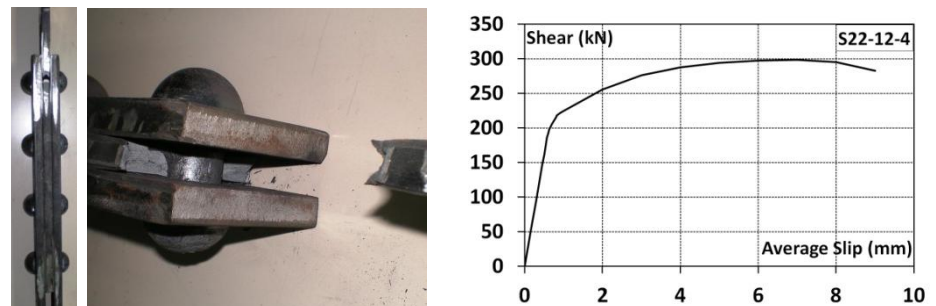
(b) Plastic bending and tearing of the steel plate in net section (S22-12-2).



(c) Rivet shear failure and yield in bearing of inner plate (S16-10-1).



(d) Yield in bearing of inner plate and material upset in front of the rivet (S19-10-1).



(e) Net cross-section failure (S22-12-4).

Figure 4.8 Main types of failure mechanism and relevant response curve.

4.3 INTERPRETATION OF EXPERIMENTAL RESULTS

The mechanical parameters, monitored during experimental tests, influenced the riveted connections overall behaviour. The effects of these selected parameters on the response of the connections are analyzed below.

4.3.1 Effect of load eccentricity

On the basis of the experimental results, it should be noted that the most important factors that influence the joints overall behaviour are the geometry of the connection and the loading conditions. Indeed, these factors determine the connection shear behaviour.

Table 4.5 Single rivet specimens: parameters characterizing the mechanical response (D’Aniello et al., 2010).

Single rivet	specimen	F_p	s_u	s_{max}	F_e	s_e	k_e	$\mu=s_u/s_e$
S-16-10-1	A	146.08	5.51	7.00	107.01	0.39	274.38	14.13
	B	147.99	6.26	7.59	109.22	0.43	253.56	14.53
	C	131.43	3.90	5.34	90.06	0.35	257.87	11.17
	Average	141.83	5.22	6.64	102.10	0.39	261.94	13.28
	SD	1.35	0.53	0.42	1.57	0.03	14.73	0.29
	CV	0.01	0.10	0.06	0.02	0.07	0.06	0.02
U-16-10-1	A	80.02	2.50	3.39	66.94	0.41	163.27	6.10
	B	83.95	3.83	4.36	64.41	0.42	153.36	9.12
	C	76.71	3.06	3.91	62.30	0.45	138.44	6.80
	Average	80.23	3.13	3.89	64.55	0.43	151.69	7.34
	SD	46.97	1.74	2.14	37.48	0.21	87.43	4.48
	CV	0.59	0.56	0.55	0.58	0.49	0.58	0.61
S-19-10-1	A	180.45	5.80	11.17	136.01	0.46	295.67	12.61
	B	232.35	12.08	14.80	141.70	0.46	311.43	26.55
	C	207.12	10.10	11.40	130.02	0.53	247.66	19.23
	Average	206.64	9.33	12.46	135.91	0.48	284.92	19.46
	SD	109.20	5.20	6.91	70.84	0.13	154.12	11.47
	CV	0.53	0.56	0.55	0.52	0.27	0.54	0.59
U-19-10-1	A	86.99	3.04	3.85	47.36	0.43	110.14	7.07
	B	108.93	2.85	3.68	95.34	0.46	207.26	6.18
	C	108.52	5.12	6.04	64.00	0.47	137.63	11.00
	Average	101.48	3.67	4.52	68.90	0.45	151.68	8.08
	SD	51.65	1.90	2.60	40.40	0.15	87.81	4.47
	CV	0.51	0.52	0.57	0.59	0.34	0.58	0.55
S-19-12-1	A	225.16	6.54	7.86	126.70	0.31	415.41	21.43
	B	207.17	6.93	7.95	125.35	0.50	250.70	13.86
	C	217.19	6.43	7.14	149.00	0.60	270.91	11.68
	Average	216.51	6.63	7.65	133.68	0.29	1125.07	50.70
	SD	111.96	3.24	3.74	63.06	0.14	183.31	9.40
	CV	0.52	0.49	0.49	0.47	0.49	0.16	0.19
U-19-12-1	A	100.63	3.65	4.15	60.07	0.41	148.32	9.00
	B	145.28	5.55	6.57	87.37	0.61	143.23	9.10
	C	106.84	3.81	4.72	73.36	0.80	91.70	4.76
	Average	117.58	4.34	5.15	73.60	0.61	127.75	7.62
	SD	62.34	2.09	2.50	36.93	0.20	81.04	4.49
	CV	0.53	0.48	0.49	0.50	0.33	0.63	0.59
S-22-10-1	A	173.59	8.00	10.77	133.35	0.30	444.50	26.67
	B	184.57	4.93	10.94	138.70	0.42	330.24	11.73
	C	190.89	6.77	10.62	136.01	0.46	298.92	14.87

4. Experimental activity on riveted connections

	Average	183.02	6.57	10.78	136.02	0.39	357.89	17.76
	SD	89.01	3.31	5.47	69.38	0.09	208.04	11.50
	CV	0.49	0.50	0.51	0.51	0.23	0.58	0.65
U-22-10-1	A	143.13	9.33	10.14	79.34	0.78	102.37	12.03
	B	146.43	10.32	11.09	76.02	0.67	113.46	15.40
	Average	144.78	9.83	10.62	77.68	0.73	107.92	13.72
	SD	2.33	0.70	0.67	2.35	0.08	7.84	2.38
	CV	0.02	0.07	0.06	0.03	0.11	0.07	0.17
S-22-12-1	A	236.18	4.32	6.11	156.72	0.48	329.94	9.08
	B	238.23	6.02	10.05	153.36	0.56	273.86	10.74
	Average	237.21	5.17	8.08	155.04	0.52	301.90	9.91
	SD	1.45	1.20	2.79	2.38	0.06	39.65	1.17
	CV	0.01	0.23	0.34	0.02	0.11	0.13	0.12
U-22-12-1	A	143.39	3.83	4.46	94.67	0.48	197.23	7.97
	B	128.74	5.47	6.38	84.70	0.49	172.86	11.16
	C	148.61	3.93	4.73	137.36	0.93	147.70	4.23
	Average	140.25	4.41	5.19	105.58	0.63	172.60	7.79
	SD	78.37	2.40	2.56	51.26	0.23	97.22	5.33
	CV	0.56	0.54	0.49	0.49	0.37	0.56	0.68

Considering the two different analysed configuration, it is possible to note that unsymmetrical joints are subjected to secondary bending moment induced by the load eccentricity. This phenomenon causes significant out-of-plane displacements, which tend to lift off one plate from the adjacent one at each connection. On the basis of the experimental results, it should be noted also that the effects of bending are mainly confined to the regions where plate discontinuities occur. The effects of the secondary bending moment are strictly dependant by the joint length: indeed, as the joint length increases bending will become less pronounced and the influence on the behaviour of the connection should decrease (D'Aniello et al., 2010). These effects are traceable in bolted connections, which present the same configuration (Shoukry et al, 1970). Another parameter that influences the magnitude of secondary bending moment is the number of rivets: in case of a single rivet in the direction of the applied shear load, the effects induced by the bending moment are most pronounced; on the contrary, the influence of bending is less pronounced in specimens with more rivets. In the first case, the rivet is subjected to single shear and also to a secondary tensile component, which transmits the flexural action (D'Aniello et al., 2010). Furthermore, the plate material is also affected by high bending stresses,

caused by load eccentricity: for this reason, secondary bending moment slightly reduces the ultimate strength of short connections.

For what concern longer unsymmetrical joints, the incidence of secondary bending moment is less evident, so that in connections with a maximum of two rivets in line, the collapse is assignable to rivets. This phenomenon is probably caused by a complete equalization of the load before rivet failure, so the collapse appears like a simultaneous shearing of all rivets (D'Aniello et al., 2010).

The symmetrical specimens, on the contrary, are characterized by a perfect centred applied load, so that secondary bending moment not occurs. Obviously, these connections are not subjected to flexural deformation. Tests demonstrated that the differential elongations are greater at the ends of the joint, so that while the centre plate fails, the lap plates are still elastic. This phenomenon is well described by D'Aniello et al., 2010, that wrote: "This is due to the low level of the applied load with respect to their plastic strength, which was confirmed by the absence of Lüder lines on the plates' surfaces. It follows that the applied load is concentrated at the end rivets." Indeed, as the length of the joint increases, the plates become less stiff and resistant and not allow the equal redistribution of stresses in all rivets: this causes the failure of the centre plate in the net section, with large plastic elongation of the end holes (D'Aniello et al., 2010).

4.3.1 Effect of variation in An/Ag ratio

One of the monitored parameter during tests was the stress evolution in the net section of plates. It was observed that, when failure occurs in the net section, the ultimate tensile strength of the plate was greater than the ultimate stress obtained by the uniaxial coupon tests. This discrepancy was also founded and studied by other researchers (Schenker et al; 1954, Munse, 1970; Schutz, 1952; Koegler et al, 1943) and it is known as the "net efficiency". D'Aniello et al., 2010, wrote that: "This phenomenon may be attributed to the fact that the presence of the hole also gives rise to transverse stresses generating a sort of multiple-stress effect (Schenker et al; 1954), emphasized by the presence of clamping force in the rivets, which avoid free lateral contractions in their vicinity."

The examined cases showed an average increase of the tensile strength equal to 13% (SD = 33.10 MPa, CV = 0.07); however, the maximum calculated value was considerably larger and was 23% for specimens

U22-12-4 and S22-12-4. The net efficiency was considerably higher when the specimen has a small A_n/A_g ratio, that means a small gauge width. This phenomenon is caused by the high stress concentration and by the effect of the clamped rivet head. It was also observed that these effects are less evident when the gauge width increases (D’Aniello et al., 2010).

4.3.2 Effect of plate width

Another important parameter that influences the net efficiency is the plate width. Experimental tests were carried out considering different plate width to evaluate the effect on the overall behaviour and on the net efficiency. Indeed, two different plate widths for the same geometric parameters were tested for U19-10-4, which failed in tension in the net area. On the basis of the experimental results, it can be asserted that the ultimate strength of the connection increases as the plate width increases. D’Aniello et al, 2010, observed also that: “In general, it was recognized that the ultimate tensile strength of specimens failed in tension on the net section increased with an average scatter of 10%, varying the plate width from the minimum to the maximum w/d ratio.”

Sometimes, the failure mechanism could vary if the plate width changes. On the basis of the tests, it was observed that for U19-10-2, varying the plate width, the collapse mechanism changes from rivet shear to net section failure. The specimen was prepared considering two different plate widths, 90 and 60 mm, and being equal all other geometric parameters.

D’Aniello et al, 2010, observed also that the actual codes, as EN1993:1-8, introduced e_2/d ratios, where e_2 is the distance from the centre of a hole to the adjacent edge in the transverse direction of the applied load, to take into account the influence of the plate width on single row riveted connections. The examined samples presented e_2/d ratios equal respectively to 1.08, 1.09, 1.69 and 1.87. The first two cases, that are the smaller values of e_2/d ratios, corresponded to the smaller values of normalized net areas, and it is possible to note that in these cases the limiting edge distance e_2 is less than the limiting value $e_2 \leq 1.2d_0$ prescribed by EN 1993:1-8, 2005. Nevertheless, the observed ultimate strength of these specimens is greater than the one calculated according to the EN 1993:1-8 formulas (D’Aniello et al.2010)

4.3.3 Effect of joint length

The joint length represents one of the most important parameters that affect the connection ultimate strength. This characteristic is particularly significant for the unsymmetrical joints, in which secondary bending moment plays a determinant rule for the collapse. As mentioned above, the incidence of the secondary bending moment strictly depends by the joint length. Together with these considerations, some remarks could be done on the influence of pitch on shear capacity of connections, although the experimental tests did not explicitly aim to investigate its influence on joints behaviour and specific parametric tests were not performed. However, it is possible to note that, for the investigated specimens, spacing did not appreciably influence the shear strength.

For what concern the influence of e_1/d ratios on the joint behaviour, the specimens presented that ratio larger than 1.2, which is the EN 1992:1-8 limits. Nevertheless the end distance resulted insufficient when the joint collapse in bending, and the rivet split out through the end of the plate. This phenomenon occurred for S19-10-1, S22-10-1 and S22-12-1.

Tests results demonstrated how the shear strength varies according to the rivet number and the A_n/A_g ratio. As the rivet number increases, both symmetrical and unsymmetrical joints do not present a linear increase in strength. On the contrary, the increase of the number of rivets determines a decrease of connection strength, due to the fact that, considering the particular configuration of the examined joints, failure modes different from the rivet shear occurs (D'Aniello et al., 2010).

Table 4.6 Specimens with rivets in row: parameters characterizing the mechanical response (D'Aniello et al., 2010).

Rivets in row	specimen	F_p	s_u	s_{max}	F_e	s_e	k_e	$\mu=s_u/s_e$
U-16-10-2	A	141.87	2.78	3.97	98.68	0.48	207.75	5.84
	B	162.23	3.84	4.61	105.36	0.56	189.84	6.91
	C	161.37	2.88	3.69	110.68	0.53	210.82	5.49
	Average	155.16	3.17	4.09	104.91	0.52	202.80	6.08
	SD	14.40	0.75	0.45	4.72	0.06	12.66	0.76
	CV	0.09	0.24	0.11	0.05	0.11	0.06	0.12
U-16-10-4	A	236.56	18.97	22.40	166.69	0.99	169.23	19.25
	B	241.13	23.51	27.30	168.69	1.01	167.02	23.27
	C	242.85	23.41	26.60	170.68	0.96	178.72	24.51
	Average	240.18	21.96	25.43	168.69	0.99	171.66	22.34
	SD	133.85	12.12	14.33	95.46	0.53	93.54	12.13

4. Experimental activity on riveted connections

	CV	0.56	0.55	0.56	0.57	0.54	0.54	0.54
S-19-10-2	A	336.63	14.24	16.80	236.69	0.84	281.77	16.95
	B	346.02	16.27	18.75	240.71	0.60	404.55	27.34
	C	332.60	10.46	13.45	230.69	0.63	366.17	16.60
	Average	338.42	13.66	16.33	236.03	0.69	350.83	20.30
	SD	167.40	7.04	8.23	116.72	0.15	182.16	11.12
	CV	0.49	0.52	0.50	0.49	0.21	0.52	0.55
U-19-10-2 (width 90 mm)	A	201.55	4.35	5.29	128.68	0.62	207.55	7.01
	B	196.22	4.36	5.17	126.69	0.66	193.42	6.66
	C	232.35	5.22	6.40	126.70	0.64	197.97	8.16
	Average	210.04	4.64	5.62	127.36	0.64	199.65	7.28
	SD	95.14	2.68	3.19	61.99	0.27	97.48	4.36
	CV	0.45	0.58	0.57	0.49	0.42	0.49	0.60
U-19-10-2 (width 60 mm)	A	190.09	13.12	17.38	128.68	0.53	245.10	24.99
	B	184.23	13.30	17.51	123.36	0.52	237.23	25.59
	C	188.92	13.83	18.29	121.34	1.10	110.81	12.63
	Average	187.75	13.42	17.73	124.46	0.72	197.71	21.07
	SD	89.30	6.74	9.05	60.25	0.12	117.85	13.26
	CV	0.48	0.50	0.51	0.48	0.17	0.60	0.63
S-19-10-4	A	354.63	10.69	14.30	254.04	0.74	345.63	14.54
	B	353.27	11.02	13.85	251.45	0.62	405.56	17.77
	C	352.96	9.69	12.45	256.67	0.64	404.20	15.26
	Average	353.62	10.47	13.53	254.05	0.67	385.13	15.86
	SD	182.09	4.89	6.40	130.69	0.31	190.40	7.52
	CV	0.51	0.47	0.47	0.51	0.47	0.49	0.47
U-19-10-4 (width 90 mm)	A	356.61	23.12	26.15	250.01	1.29	193.81	17.92
	B	355.52	22.04	25.10	243.38	1.30	187.94	17.02
	C	355.12	25.28	28.40	246.67	1.06	232.71	23.84
	Average	355.75	23.48	26.55	246.69	1.22	204.82	19.59
	SD	169.89	11.64	13.04	117.32	0.53	95.14	8.30
	CV	0.48	0.50	0.49	0.48	0.43	0.46	0.42
U-19-10-4 (width 60 mm)	A	184.37	14.53	18.45	122.69	0.82	149.62	17.71
	B	178.42	11.84	17.00	121.34	0.76	160.72	15.68
	C	183.07	10.98	14.65	130.70	0.72	182.80	15.36
	Average	181.95	12.45	16.70	124.91	0.77	164.38	16.25
	SD	88.74	6.23	8.16	60.03	0.19	73.19	7.86
	CV	0.49	0.50	0.49	0.48	0.24	0.45	0.48
S-22-12-2	A	278.89	2.75	4.56	257.38	0.32	804.31	8.58
	B	298.35	6.71	8.39	212.70	0.50	425.40	13.42
	C	296.89	7.68	9.44	210.02	0.55	385.36	14.08
	Average	291.38	5.71	7.46	226.70	0.46	538.36	12.03
	SD	145.63	2.95	3.71	122.08	0.14	369.03	5.34
	CV	0.50	0.52	0.50	0.54	0.30	0.69	0.44

U-22-12-2	A	279.05	10.46	11.63	170.02	1.6	106.26	6.54
	B	255.24	8.88	10.13	184.03	1.63	112.90	5.45
	C	280.77	11.60	13.49	170.72	1.64	104.10	7.07
	Average	271.69	10.31	11.75	174.92	1.62	107.75	6.35
	SD	127.12	4.73	5.27	83.42	0.81	156.56	2.72
	CV	0.47	0.46	0.45	0.48	0.50	1.45	0.43
S-22-12-4	A	308.94	9.76	12.17	249.26	0.75	334.46	13.10
	B	298.54	9.76	12.00	250.06	0.85	293.58	11.46
	C	303.50	7.24	8.95	247.68	0.66	373.88	10.93
	Average	303.66	8.92	11.04	249.00	0.75	333.97	11.83
	SD	147.93	4.49	5.68	124.61	0.16	150.66	6.29
	CV	0.49	0.50	0.51	0.50	0.21	0.45	0.53
U-22-12-4	A	308.94	15.67	18.60	201.34	0.85	236.87	18.43
	B	303.59	13.16	15.40	200.68	1.07	188.43	12.36
	C	303.66	15.23	17.90	202.69	0.88	230.33	17.30
	Average	305.40	14.69	17.30	201.57	0.93	218.54	16.03
	SD	146.89	7.14	8.40	94.64	0.46	102.06	7.72
	CV	0.48	0.49	0.49	0.47	0.49	0.47	0.48

As mentioned above, increasing length of joint plates, which are not sufficiently stiff, do not allow an equal redistribution of shear stresses in rivets. This phenomenon causes an onset of yielding in the gross section of the plate. Indeed, the tested specimens that have a large number of rivets do not present a high shear stress concentration in the rivets shanks. D’Aniello et al., 2010, also wrote that: “longer joints having the larger A_n/A_g ratio showed a lesser decrease in average shear strength when compared with the shear strength of a single rivet”. This is particularly true for unsymmetrical joints with up to two rivets, while this was not true for symmetrical specimens (D’Aniello et al., 2010).

The strength capacity of riveted connections is particularly influenced also by the A_n/A_g ratio. Depending on the magnitude of this parameter, the shear strength could not differ appreciably from unsymmetrical joints, in which rivet is loaded only in one shear plane, to symmetrical joints, that are characterized by rivet loaded in two shear planes. This phenomenon occurs for a low A_n/A_g ratio, due to the fact that in symmetrical joints the inner plate is the weaker one, and it is not sufficiently stiff to permit shear distribution among the rivets. On the contrary, as A_n/A_g ratio increases, the inner plate becomes stiffer, and allow the shear distribution among rivets.

Table 4.7 Specimens with rivets in row: parameters characterizing the mechanical response (D'Aniello et al., 2010).

	F_u Average Strength	Failure mechanism (Test)	F_{EC3} Calc. strength (EN 1993 1-8)	Failure mechanism (EN 1993 1-8)	F^* Calc. strength (proposed formulas)	Failure mechanism (proposed formulas)	F_u/F_{EC3}	F_u/F^*
	[kN]		[kN]	[kN]	[kN]			
S-16-10-1	141.83	V + B (sec.)	99.31	V	148.97	V	1.43	0.95
U-16-10-1	80.22	V	49.66	V	74.49	V	1.62	1.08
S-19-10-1	206.64	B	140.05	V	243.38	B	1.48	0.85
U-19-10-1	101.48	V	70.02	V	105.04	V	1.45	0.97
S-19-12-1	216.51	V + B (sec.)	140.05	V	210.07	V	1.55	1.03
U-19-12-1	117.58	V	70.02	V	105.04	V	1.68	1.12
S-22-10-1	183.02	B	126.20	B	189.30	B	1.45	0.97
U-22-10-1	144.78	V	93.88	V	140.82	V	1.54	1.03
S-22-12-1	237.21	B	151.44	B	227.16	B	1.57	1.04
U-22-12-1	140.25	V	93.88	V	140.82	V	1.49	1.00
U-16-10-2	155.16	V	99.31	V	148.97	V	1.56	1.04
U-16-10-4	240.18	T	187.46	V	259.61	T	1.28	0.93
S-19-10-2	338.41	T	280.10	V	341.34	T	1.21	0.99
U-19-10-2 (width 90 mm)	210.04	V	140.05	V	210.07	V	1.50	1.00
U-19-10-2 (width 60 mm)	187.74	T	140.05	V	197.11	T	1.34	0.95
S-19-10-4	353.62	T	307.21	T	341.34	T	1.15	1.04
U-19-10-4 (width 90 mm)	355.75	T	275.01	V	341.34	T	1.29	1.04
U-19-10-4 (width 60 mm)	181.96	T	177.40	T	197.11	T	1.03	0.92
S-22-12-2	291.37	T	249.23	T	276.92	T	1.17	1.05
U-22-12-2	271.69	V	187.77	V	281.65	V	1.45	0.96
S-22-12-4	303.66	T	249.23	T	276.92	T	1.22	1.10
U-22-12-4	305.40	T	249.23	T	276.92	T	1.23	1.10
Average							1.40	1.01
SD							0.17	0.07
CV							0.12	0.07

Legend: V= rivet shear failure, B = plate bearing, T= failure in tension in the net section

In this case the presence of two shear planes implies a benefit for the shear capacity, even if failure modes other than rivet shearing may limit this effect.

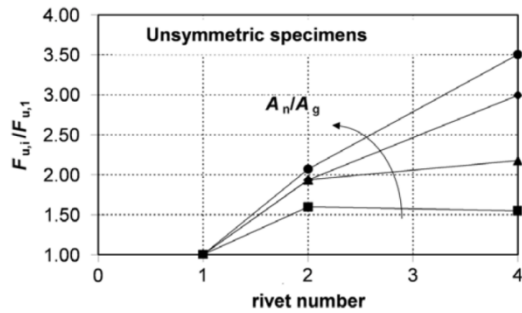


Figure 4.9 Rivet number vs. ultimate strength (unsymmetrical specimens). (D'Aniello et al., 2010).

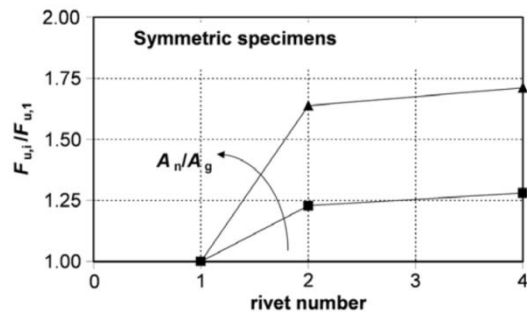


Figure 4.10 Rivet number vs. ultimate strength (symmetric specimens). (D'Aniello et al., 2010).

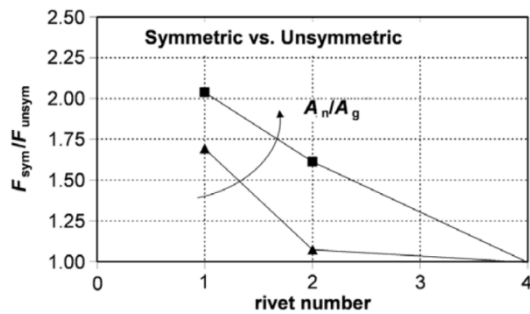


Figure 4.11 Symmetric vs. unsymmetrical specimen shear capacity. (D'Aniello et al., 2010).

Finally, it should be noted, as mentioned by D'Aniello et al. (2010), that: “these charts were provided to RFI inspectors as a quick and easy tool with which to assess the shear capacity of the connections of RFI lattice structures. Therefore, they cannot be extended to connections having different geometries”.

4.3.1 Effect of clamping forces

Another important parameter that influences the shear strength of riveted connections is the rivet clamping force, caused by the cooling of the rivet after the formation. Experimental tests were not planned to monitor the entity of the rivet clamping force, because it was not measured directly. However, from the analysis of experimental results, it is possible to evaluate the effects on joint behaviour of variability of clamping forces on slip resistance. Confronting the load-slip curves of each specimen, it is possible to note that some joints, as specimens U16-10-1, U22-12-2, S 16-10-1 shown in Figure 4.8 a) and c), present a gradual slip when the load is applied. On the contrary, specimens S19-10-1 and S22-12-4, shown in Figure 4.8 d) and e), are subjected to a sudden slip when load was applied. This different behaviour is probably caused by the variability of clamping forces, considering that the inner surfaces of plates were not specifically treated to increase the friction. The variability of clamping forces, as well described by D'Aniello et al., 2010, “implies different and unknown levels of pre-stressing of the surfaces of the plates in contact and an unreliable threshold for slip-resistance”.

Furthermore, it was observed that specimens of the same type presented different slip behaviour. Taking into account these considerations, it is possible to suppose that the variability of the joints measured initial stiffness, reported in Tables 5 and 6, is related to the degree of pre-stressing of the rivets.

D'Aniello et al. (2010) well summarized the results saying that: “However, the slips were so small that they are not expected to have a significant effect on real structures. These results confirmed that the investigated connections can be considered as a bearing-type. The possible initial slip should not affect the shape of the force–displacement curve to an appreciable extent”.

4.4 THEORETICAL VS. EXPERIMENTAL STRENGTH

On the basis of experimental results, a comparison between Eurocode formulas and the experimental strength of riveted connections was carried out. This comparison is useful to evaluate the reliability of the codes strength provisions of riveted joints. As mentioned in the first chapter, the strength of the lap shear connections calculated in accordance with EN 1993 1-8 2005 is the minimum of the following formulas (see chapter 1):

1. **tensile strength of the critical net section** (EN 1993:1-1 clause 6.2.3(2b)),

$$N_{u,Rd} = \frac{0.9 \cdot f_u \cdot A_{net}}{\gamma_{M2}} \quad (4.1)$$

where: f_u is the specified ultimate tensile strength of the plate;
 A_{net} is the net area of the plate subjected to tension;
 γ_{M2} is the rivet partial safety factor equal to 1.25.

2. **shear strength of the rivets** (EN 1993:1-8 clause 3.6.1(1)),

$$F_{v,Rd} = \frac{0.6 \cdot f_{ur} \cdot A_0}{\gamma_{M2}} \quad (4.2)$$

where: f_{ur} is the specified ultimate tensile strength of the rivet;
 A_0 is the area of the rivet hole;
 γ_{M2} is the rivet partial safety factor equal to 1.25.

3. **bearing strength of the thinner plate** (EN 1993:1-8 clause 3.6.1(1)).

$$F_{b,Rd} = \frac{k_1 \cdot \alpha_b \cdot f_u \cdot d \cdot t}{\gamma_{M2}} \quad (4.3)$$

where: f_u is the specified ultimate tensile strength of the rivet;
 d is the nominal rivet diameter;
 t is the thickness of the plate;

γ_{M2} is the rivet partial safety factor equal to 1.25;

α_b is the smallest of α_d ; $\frac{f_{ub}}{f_u}$ or 1;

α_d in the direction of the load transfer is:

- for end bolts: $\alpha_d = \frac{e_1}{3d_0}$,
- for inner bolts $\alpha_d = \frac{p_1}{3d_0} - \frac{1}{4}$;

k_1 perpendicular to the direction of the load transfer is:

- for edge bolts is the smallest of $2.8 \frac{e_2}{d_0} - 1.7$ or 2.5,
- for inner bolts is the smallest of $1.4 \frac{p_2}{d_0} - 1.7$ or 2.5.

where: d_0 is the hole diameter of a rivet;

e_1 is the end distance from the centre of a rivet hole to the adjacent end of any part, measured in the direction of load transfer;

e_2 is the edge distance from the centre of a hole to the adjacent edge of any part, measured at right angles to the direction of load transfer;

p_1 is the spacing between the centres of rivets in a line in the direction of load transfer;

p_2 is the spacing measured perpendicular to the load transfer direction between adjacent lines of rivets.

For double shear connections with packing on both sides of the splice, t_p should be taken as the thickness of the thicker packing.

In case of a combined shear and tension failure of the rivet, the resistance is given by:

$$\frac{F_{v,Ed}}{F_{v,Rd}} + \frac{F_{t,Ed}}{F_{t,Rd}} \leq 1.0 \quad (4.4)$$

The design resistance of a group of fasteners may be taken as the sum of the design bearing resistances $F_{b,Rd}$ of the individual fasteners provided that the design shear resistance $F_{v,Rd}$ of each individual fastener is greater than or equal to the design bearing resistance $F_{b,Rd}$. Otherwise the design resistance of a group of fasteners should be taken as the number of fasteners multiplied by the smallest design resistance of any of the individual fasteners.

Furthermore, increasing the joint length, the assumption that each rivet carries an equal rate of the applied load become less accurate. In particular, Eurocode prescribes that, when the distance L_f between the centres of the end rivets, measured in the direction of force transfer, is more than $15d$, a reduction factor β_{Lf} must be applied on the design shear resistance $F_{v,Rd}$. That factor is given by EN 1993:1-8 3.8(1) as:

$$\beta_{Lf} = 1 - \frac{f_u - 15d}{200d} \quad (4.5)$$

Some assumptions were made in order to compare the experimental results to that obtained by EN 1993:1-8 formulas: indeed, the theoretical strengths were calculated assuming that:

1. the average experimental strengths of materials is equal to unity,
2. the partial safety factors γ_{M2} is equal to unity.

The results of this comparison between experimental results and theoretical formulas in terms of ultimate strength and expected failure modes are reported in Table 4.7. Figure 4.12 shows the ratio between the average experimental strength (F_u) and that calculated in accordance with EN 1993:1-8 (F_{EC3}) (D'Aniello et al., 2010).

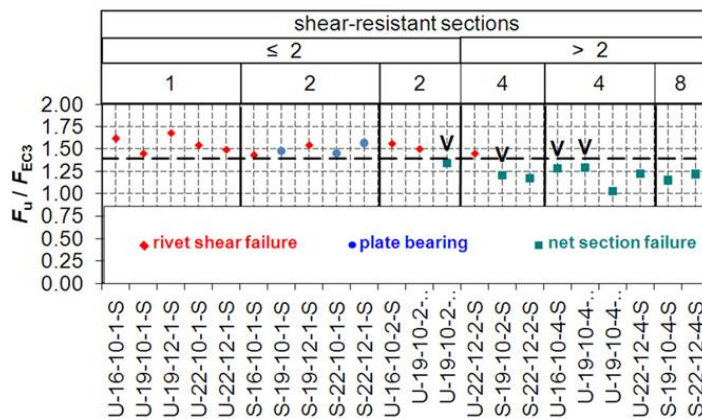


Figure 4.12 Comparison of experimental results and predicted strength according to EC3. (D'Aniello et al. 2010).

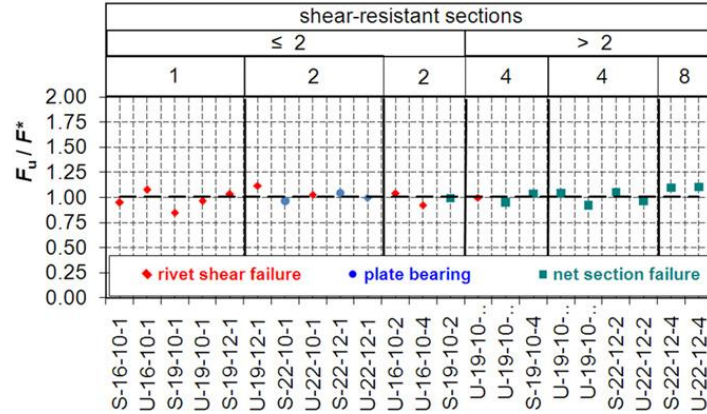


Figure 4.13 Comparison of experimental and predicted strength calculated with proposed equations. (D’Aniello et al. 2010).

As observed by D’Aniello et al. (2010): “in four cases the failure mechanisms predicted by EN 1993 1-8 differ from those shown by the tests. In particular, net section failure occurred instead of rivet shear failure. The reason may be found in the large increase in ultimate shear strength induced by hot-driven process”.

Considering the magnitude of the ultimate strength, a great discrepancy could be observed between the values obtained with the Eurocode formulas and the experimental one. Indeed, the average value of F_u/F_{EC3} ratio for all specimens is bigger than the unity, and assumes, generally, a value of 1.40 (SD=17%, CV=0.12). In Table 4.7, these cases are highlighted by a letter that indicates the appropriate failure mode. The reasons of that discrepancy were studied by D’Aniello et al. (2010), and will be discussed below.

4.4.1 Effects of hot driven process

Observing the amount of the average F_u/F_{EC3} ratio, that results equal to 1.53 for specimens whose rivets failed in shear, it is possible to declare that the monotonic shear strength of this type of connection may be noticeably higher than that calculated according to EN 1993:1-8 (D’Aniello et al., 2010). Considering that the hot driven process improves the ultimate tensile strength of the rivet of about 20%, the amount of the ultimate tensile strength calculated according to the EN

1993:1-8 formulas still differs a lot from the experimental values. Reducing the average over-strength, ratio, equal to 1.53, by the factor for the effect of the hot-driven that may be assumed to be $1.20 = 1.28$, with 1.20, a residual over-strength ratio equal to $1.53/1.2 = 1.28$ still remains. As denoted by D’Aniello et al. (2010): “This implies that the ultimate rivet shear stress $f_{ur,v} = 0.6f_{ur}$ calculated according to Eurocode (Equation 4.2) is underestimated”.

In the past, Schenker 1954; and Munse 1956 analyzed the results of different driving procedures on different types of joint configurations, and they observed that the rivets’ shear strength to tensile strength ratio ($f_{ur,v}/f_{ur}$) may vary within the range 0.67–0.83, with an average value of 0.75.

Taking into account these observations, it was calculated $f_{ur,v}$ for the presented cases as follows:

$$f_{ur,v} = \frac{F_u}{1.2 \cdot \eta_r \cdot \eta_s \cdot A_0} \quad (4.6)$$

where: η_r is the number of rivets;

η_s is the number of shear planes.

Confronting the rivets’ shear strength to tensile strength ratio $f_{ur,v}/f_{ur}$ for the examined cases, a range of values equal to $(0.71 \div 0.84)$ with an average value of 0.76 (SD=0.04, CV=0.05) was obtained, confirming the values given in Schenker (1954); and Munse (1956).

Thus, D’Aniello et al. (2010) proposed a more appropriate formula to calculate the rivets’ shear strength as follows:

$$F_{v,Rd} = \frac{\Omega_1 \cdot \Omega_2 \cdot f_{ur} \cdot A_0}{\gamma_{M2}} \quad (4.7)$$

where: Ω_1 takes into account the effect of the hot-driven process, which can be assumed to be equal to 1.20 for rivets driven in analogous manner to those examined;

Ω_2 is the rivets’ shear strength to tensile strength ratio, which can be assumed to be equal to 0.75 in accordance to (Kulak et al. 1987, Schenker 1954; Munse 1956).

4.4.2 Effects of rivet clamping

An important contributor to the overstrength of the riveted connections respect to the Eurocode provisions is the rivet clamping force (Kulak et al. 1987). This phenomenon, indeed, induces an additional shear force on the connection that becomes on the faying surfaces as an additional friction resistance. This phenomenon is particularly evident in all the specimens that failed in bearing. In these cases, indeed, the average over-strength F_u/F_{EC3} ratio is equal to 1.50. However, as observed by D’Aniello et al. (2010): “because the friction resistance is related to the clamping force in the rivet, the actual influence of this effect is uncertain and further investigation is needed”.

4.4.3 Effects of net efficiency

The average over-strength F_u/F_{EC3} ratio equal to 1.21 is observed in all specimens failing in tension on the net section. This large amount of resistance is caused by the above mentioned net efficiency effect. On the basis of these observations, D’Aniello et al. (2010) modified the Eurocode formula by assuming no reduction factor:

$$N_{u,Rd} = \frac{f_u \cdot A_{net}}{\gamma_{M2}} \quad (4.8)$$

The values of strength calculated according to this formula are reported in Figure 4.10 and are indicated as F^* : it can be observed that these values are nearer to the experimental strengths (F_u) than those given by EN 1993:1-8. To confirm that observation, the average values of the F_u/F^* ratio are reported in Table 4.7. These values are slightly larger than 1.00, with an average value equal to 1.01. On the contrary, the values obtained using Eurocode formulas present a more pronounced deviation ($SD = 7\%$, $CV = 0.07$). Moreover, all the predicted failure mechanisms correspond to those obtained experimentally (D’Aniello et al., 2010).

4.5 CONCLUDING REMARKS

This chapter describes the results of a large experimental investigation carried out within the framework of the European project PROHITECH. The main objective is the evaluation of the riveted connections strength and the comparison with the actual codes provisions, as the EN 1993:1-8. Due to the fact that the majority of riveted structures in Italy are railway constructions, the present activity was undertaken in co-operation with Italian railway agency (RFI), which was interested in developing verification tools for those riveted splices in aged steel structures which are still in service.

For this reason, the investigation was performed on riveted specimens made of aged steel, manufactured with the techniques in use in Italian railway practice. Specimen geometry was detailed as required by RFI. The steel constituting plates and rivets was characterized by performing both mechanical and chemical tests. Tests showed good mechanical and chemical properties (strength, chemical composition).

The results of the lap-shear tests are reported and discussed, and the main characteristics of the riveted connections behaviour are reported and confronted with the existing literature.

The experimental results highlighted that unsymmetrical joints are subjected to a considerable amount of out-of-plane deformation. The effects of bending were mainly confined to the regions where plate discontinuities occurred. Obviously, as the joint length increased, bending was less pronounced. The splice with only a single fastener in the direction of the applied load are most influenced by secondary bending. In this case, a secondary tensile component may also be present. Furthermore, the plate material in the direct vicinity of the splice was subjected to high bending stresses due to the eccentricity of the load. Hence, the ultimate strength of short connections tended to slightly decrease due to the bending. This phenomenon not influences significantly the shear strength of longer asymmetric lap joints.

At last, a comparison between the experimental strengths and the failure modes and the results predicted by applying the formulas given in EN 1993:1-8 was made. It was recognized that the approach given in the code is conservative in all examined cases. However, the scatter between experimental and calculated strength seems excessively precautionary.

The theoretical prediction of shear strength of rivets was improved taking into account two parameters:

1. the increase of ultimate tensile strength of rivets due to hot-driven process;
2. the actual rivet shear strength to tensile strength ratio.

Furthermore, the contribution made by friction resistance between the faying surfaces constituting the splices could be concur in the experimental over-strength in the bearing failure. Considering the uncertainties about the clamping in the rivets, this effect needs further investigation.

Another phenomenon was observed in experimental tests of specimen failed in tearing at the net section, in these cases, the ultimate strength showed an increase of about 20%, larger than that calculated according to EN 1993:1-8. This result should be ascribed to the net efficiency effect.

In some cases tests showed a different failure mechanisms from those predicted by EN 1993:1-8. This phenomenon was due to the large increase in ultimate shear strength induced by the hot-driven process, which is not taken into account by EN 1993:1-8.

On the basis of the obtained experimental results, some modifications to EN 1993:1-8 prediction formulas are proposed. The influence of the hot-driven process and of the net efficiency effect were considered to formulate the provided equations. The results obtained by applying these proposed formulas are closer to the experimental strengths than those given by EN 1993:1-8, in terms of both the ultimate strengths and the failure mechanisms.

However, it is necessary to deepen some aspects not considered during this experimental activity, such as the effect of the friction resistance on the bearing mechanism and the presence of more rows of rivets in the connection.

To ensure the reliability of these formulas, a wide campaign of numerical simulations was carried out, that will be discussed in the next chapter

5 NUMERICAL STUDY OF RIVETED CONNECTIONS

The characterization of connections behaviour cannot be obtained by using the classical St. Venant hypotheses in linear elasticity, due to the stress concentration that usually is present in connections.

“Suitable models can be obtained on the basis of plastic theory, looking for equilibrated solutions which are consistent with strength criteria” (Esposto, 2008). Indeed, the determination of stiffness, strength, and deformations of connections must be obtained with experimental analyses and numerical investigations (Ballio and Mazzolani, 1983).

This is suitable in particular for riveted connections, which are influenced by hot driven process due to the formation of the rivet, friction and contact interactions and large displacements.

As briefly described in chapter 2, the riveted connections are commonly studied by using Finite Element Analyses (FEA), as a useful tool to support experimental activities or to predict their behaviour varying some parameters once the model is calibrated.

Indeed, Finite Element Analyses are usually adopted in the product development cycles, as a complementary tool to the experimental activity, to reduce the overall cost of the products and to rationalize the design cycle (Esposto, 2008).

In addition, FEA often are the only way to get an answer in the case of particular problems, such as, for example, the mechanical behaviour of a system subjected to extreme loading conditions which are impossible to duplicate in an experiment (ABAQUS, 2006).

Finite Element Analysis is also a useful tool to investigate aspects that are difficult to measure or to monitor during the experimental tests: so, when a system is already investigated by experimental tests, its FE model could be used to obtain complementary information.

When a FE model is calibrated according to the experimental results, it could be used to “perform numerical analyses in which several parameters of interest may be varied, without the necessity of additional expensive experimental campaigns” (Esposto, 2008).

According to the above considerations, the research here presented is devoted to define and implement a FE numerical model of four types of riveted connections, corresponding to four kind of tested specimens. In details, they are the specimens:

- a) S16-10-1;
- b) U16-10-1;
- c) S22-12-4;
- d) U22-12-4.

According to the experimental results, four calibrated FE models are presented, as a useful tool to predict the behaviour of riveted connections.

5.1 FINITE ELEMENT ANALYSIS

5.1.1 Generalities

The Finite Element Method tends to subdivide complex systems into their individual components, or “elements”, whose behaviour is easily understandable, and then it rebuilds the original system for studying its whole behaviour (Zienkiewicz et al., 2004).

In general, a model may be defined as a simplified representation of reality. Systems and objects, in a macroscopic perspective, appear like continuous. To obtain a model that reproduces the continuity, the above mentioned subdivision is continued indefinitely, and the elements are infinite. To solve the problem, it is necessary to define it in terms of infinitesimal concepts and to solve it through sets of differential equations. These problems cannot be solved using computers but only by mathematical manipulations, which are often possible only in case of oversimplified problems (Esposto, 2008).

The continuity, however, could be reproduced with a good accuracy also by using a finite number of elements: the problem become “discrete” and it can be solved by means of computers also in the case of very large number of elements. Obviously, the approximation of the results is better as far as the number of finite elements increases (Zienkiewicz et al., 2004). In general, as mentioned before, a continuous problem is defined on a continuous physical domain and is governed by differential equations (Esposto, 2008).

There are different discretization approaches that depend on which “object” is selected for the discretization: the finite difference methods operate on the differential equations that govern the problem; the finite element method operates on the physical domain.

A possible simple definition of the Finite Element Method may be the following (Zienkiewicz et al., 2004): “a method of approximation to continuous problems such that the continuum is divided into a finite number of parts (elements), the behaviour of which is specified by a finite number of elements follows precisely the same rules as those applicable to standard discrete problems”.

The continuum domain is subdivided into a finite number of elements, separated by imaginary lines and connected each other at the vertices, or nodes, forming the finite element mesh.

The displacements are the unknown of the problem, so a set of equations, which univocally define the displacements, characterizes each finite element. The displacements of each finite element are computed at the nodes. The stresses and the strains of each element are put in relation with the element displacements. Starting from the equations related to the single finite element, the whole equation system is assembled, leading to the definition of a global matrix governing the problem; the prescribed boundary conditions are eventually imposed.

The displacements, the stresses and the strains of the system are consequently determined once the problem equation system is solved (Esposto, 2008).

5.1.2 FEA by the Abaqus computer program

Numerical analyses of the present research have been carried out by means of the finite element program ABAQUS 6.10.

The analysis in ABAQUS program is subdivided into three main steps:

- Pre-processing
- Simulation
- Post-processing

The discretized geometry, the element section properties, the material data, the loads and boundary conditions, the analysis type, and the output requests are defined into the pre-processing phase. The solving of

the problem occurs into the simulation phase. The results of the analysis are obtained in the post-processing phase.

In order to take in consideration all the possible physical problems, the number of available finite elements in ABAQUS is very huge. Each finite element, in ABAQUS, is characterized by five features (Esposito, 2008):

- Family
- Degrees of freedom
- Number of nodes
- Formulation
- Integration

In the Figure 5.1 are shown the most commonly used families of finite available in ABAQUS.

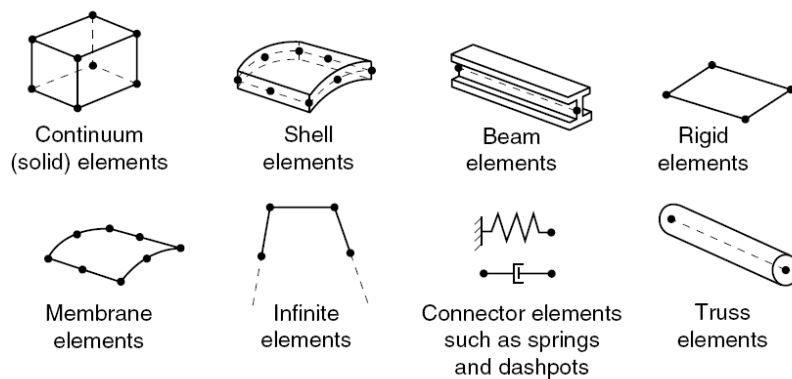


Figure 5.1 Types of finite elements available in Abaqus 6.10.

5.2 FE MODELS OF RIVETED CONNECTIONS

5.2.1 Geometry of the models

Four specimens have been numerically analyzed and investigated. Their geometrical properties are reported in Figure 5.2.

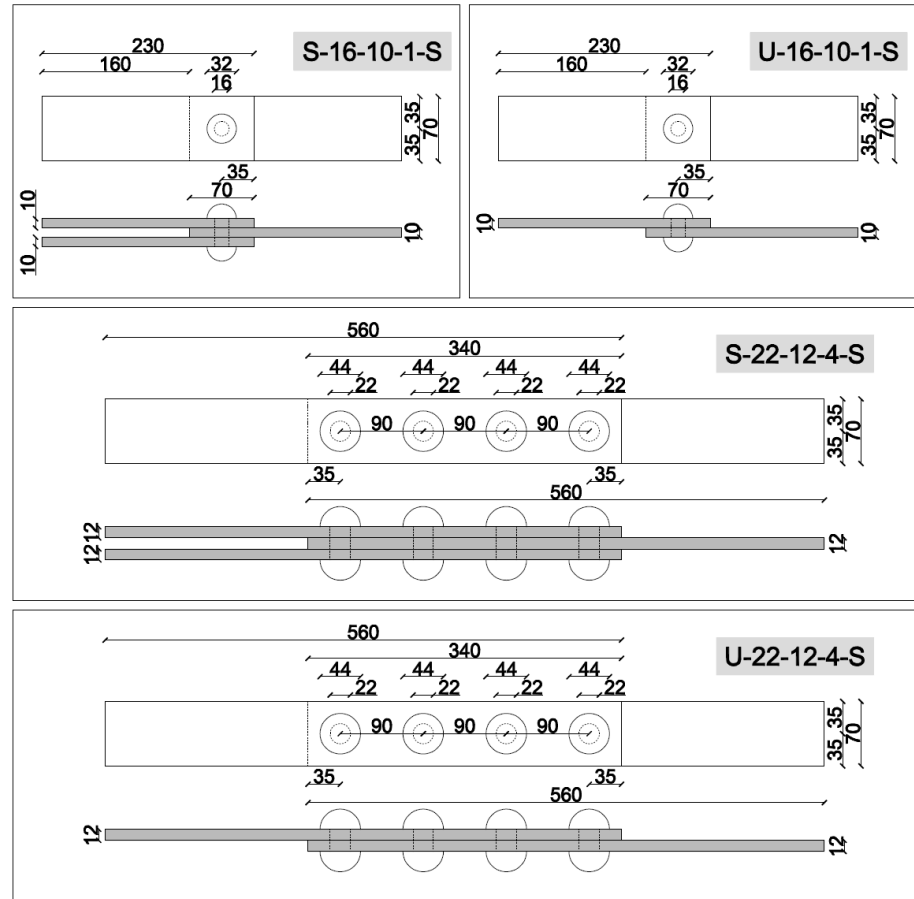


Figure 5.2 Geometrical details of the four types of riveted connections FE models.

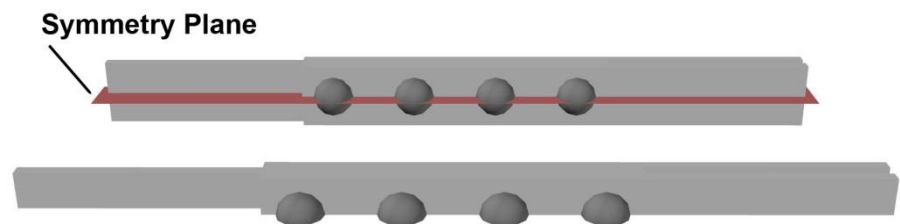


Figure 5.3 Geometry of numerical model.

The numerical model is composed by two main parts: plates and rivets. Each element is defined as a single part, and is first treated as a volume, which is then meshed into elements.

All models are simplified by assuming an exploiting of the system symmetry with respect to the mid plane of connection (Fig. 3.3). This simplification makes the analysis computationally cheaper.

The symmetry condition includes additional boundary conditions, which are necessary to avoid the out of plane displacements and rotations of points along the symmetry plane: this assumption prevents the elements mutual penetration. The symmetry condition does not allow the out-of-plane buckling phenomena to be caught. However, during the experimental tests, no buckling phenomena were observed, so this aspect does not influence the results.

The assumptions related to the other modelling issues are the same in the four models and they are presented in the following sections.

5.2.2 The material modelling

5.2.2.1 Generalities

A wide range of material types are available in ABAQUS, that cover all the possible problems related to metals, concrete, masonry, and so on. For what concerns ductile materials, the plasticity could be taken into account considering also hot driven process phenomena and non-linearity characteristics of the material.

Usually, during the experimental tests, the strains and the stresses are measured referring to the initial geometry of the specimen. These measures are called “nominal strain” (ϵ_{nom}) and “nominal stress” (σ_{nom}).

The nominal strain is defined as the ratio between the total elongation (Δl) of the specimen in tension and the initial length (l_0):

$$\epsilon_{nom} = \frac{\Delta l}{l_0} \quad (5.1)$$

Nominal stress is defined as the ratio between the value of the force (F) and the initial cross section area of the specimen (A_0):

$$\sigma_{nom} = \frac{F}{A_0} \quad (5.2)$$

In ABAQUS, the material must be defined in terms of “true stress” (σ) “true strain” (ϵ), to take into account the occurrence of finite deformations and the nearly incompressible nature of the plastic deformations in ductile materials. True strain is derived from nominal strain by considering the limit $\Delta l \rightarrow dl \rightarrow 0$. True stress is obtained by imposing that the actual volume of the part undergoing plastic deformations is the same as the initial one (Esposto, 2008):

$$A_0 \cdot l_0 = A \cdot l \quad (5.3)$$

On the basis of the above considerations, the nominal vs. true relationships are the following ones (Esposto 2008):

$$\epsilon = \ln(1 + \epsilon_{nom}); \quad \sigma = \sigma_{nom}(1 + \epsilon_{nom}) \quad (5.4)$$

For the definition of the plastic range, ABAQUS requires the value of the plastic true strain, which is obtained by subtracting the elastic true strain (σ / E) from the total true strain (ϵ):

$$\epsilon_{pl} = \epsilon - \sigma/E \quad (5.5)$$

In case of metal plasticity, the incompressible nature of plastic deformations imposes some limitations on the selection of the finite elements. Indeed, additional kinematic constraint on the finite element are involved in incompressibility, in particular, the volume at the integration points must remain constant. In some kinds of elements, this limitation makes the finite element over-constrained, with consequent stiffer behaviour. The phenomenon is usually called “volumetric locking”. In particular, the most susceptible elements to volumetric locking are the fully integrated second-order solid elements. On the contrary, reduced integration solid elements, characterized by fewer points at which the incompressibility constraints must be satisfied, are not over-constrained and so they can be used for most elastic-plastic simulations (Esposto, 2008).

5.2.2.2 Mechanical characterization

Steel material, in this particular case, was defined by using the mechanical properties obtained from the experimental tests on rivets (C16, C22) and on plates (S10).

For what concern rivets, three tests were performed for each rivet diameter. The experimental curves obtained from tests on rivets C16 are reported in Figure 5.4, the experimental curves obtained from tests on rivets C22 are reported in Figure 5.6 After a refining procedure of the experimental curves, a medium curve was obtained (Fig. 3.5, Fig. 3.7). That constitutive law does not take into account the effect of hot driven process induced by the formation of the rivet: this phenomenon was considered by increasing the stress-strain relationship by means of an experimental factor (D'Aniello et al., 2010) and will be discussed in the next section. The curves were transformed in true stress-true strain.

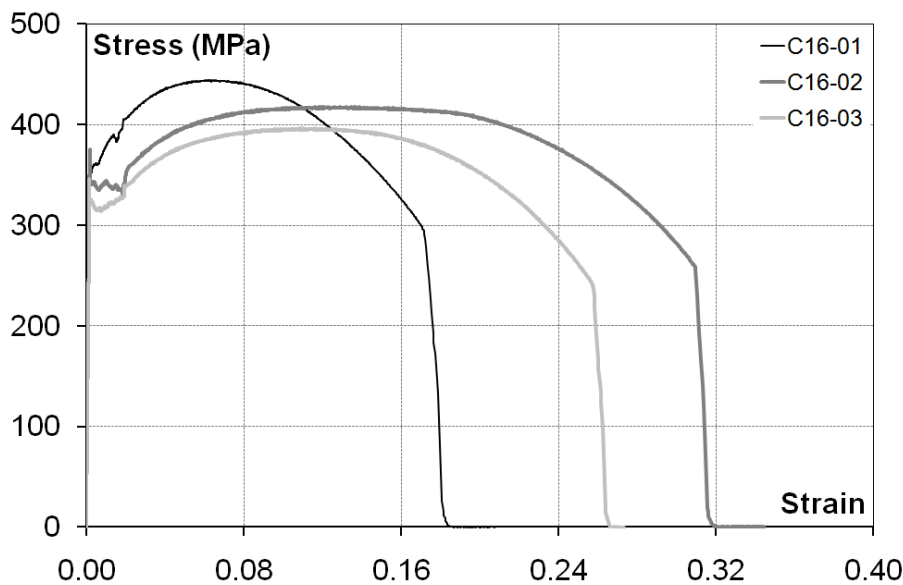


Figure 5.4 Experimental curves for C16 rivets.

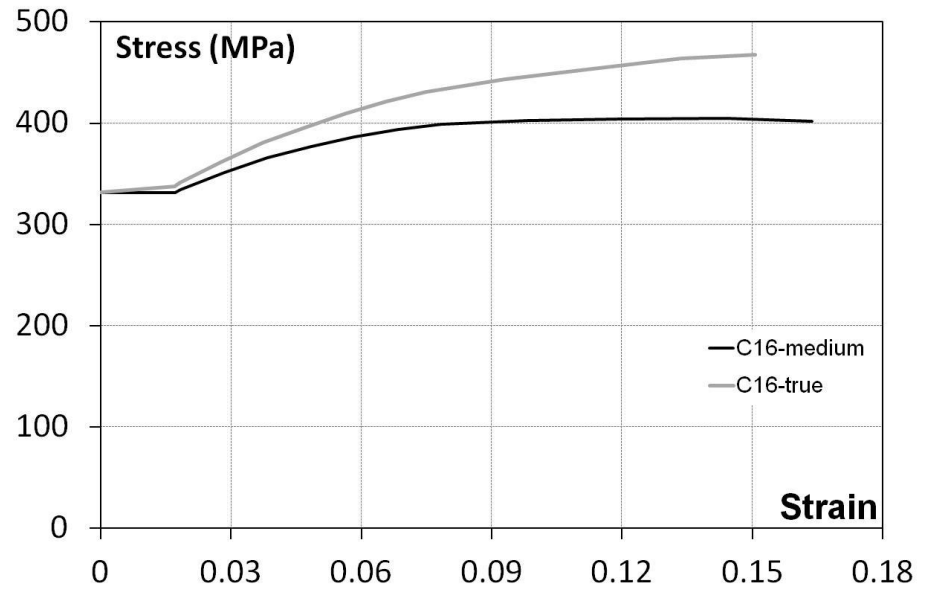


Figure 5.5 Refined curves and true stress-true strain curve for C16 rivets.

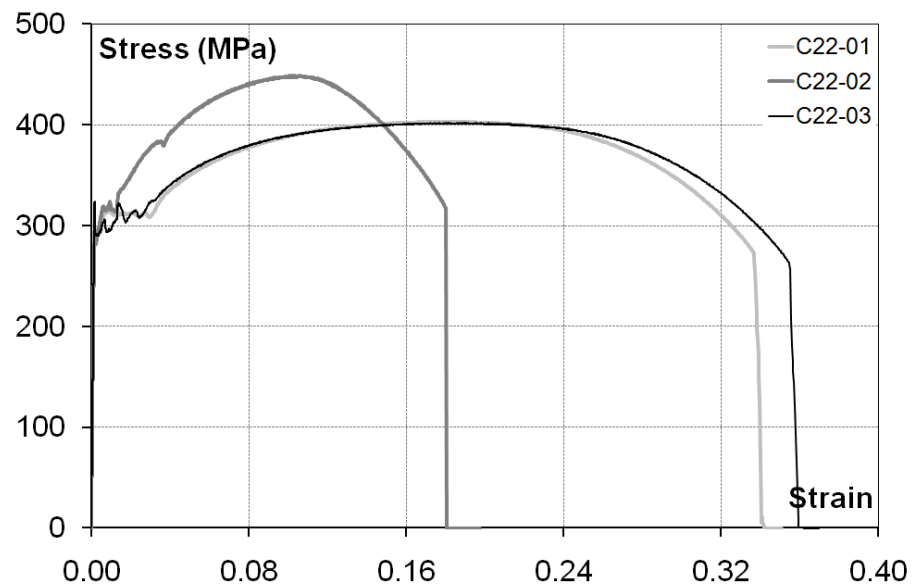


Figure 5.6 Experimental curves for C22 rivets.

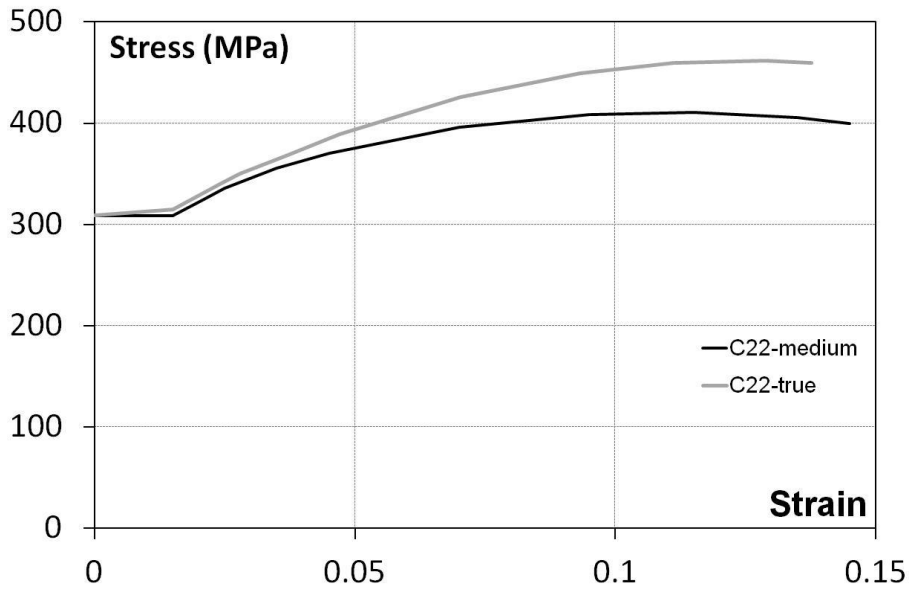


Figure 5.7 Refined curves and true stress-true strain curve for C22 rivets.

The some procedures were performed for the constitutive law of plates.

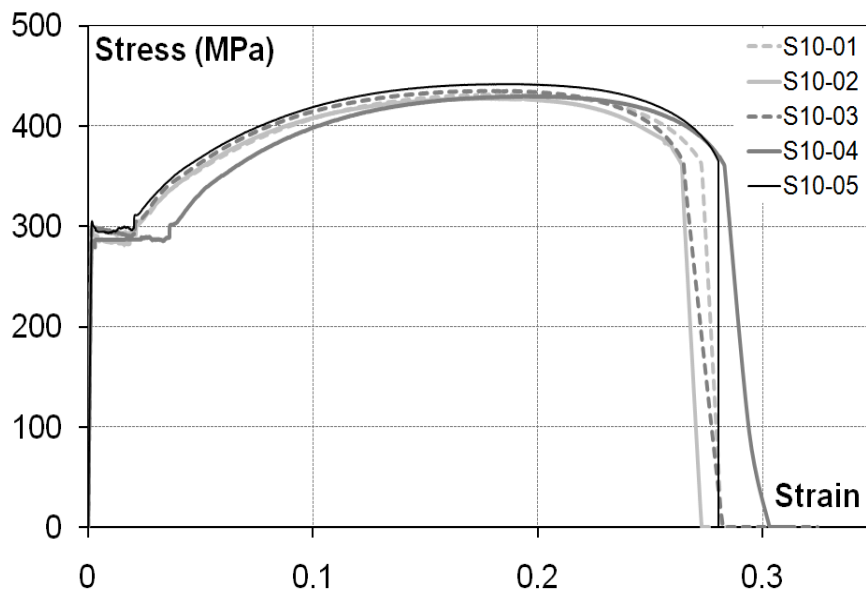


Figure 5.8 Experimental curves for S10 plates.

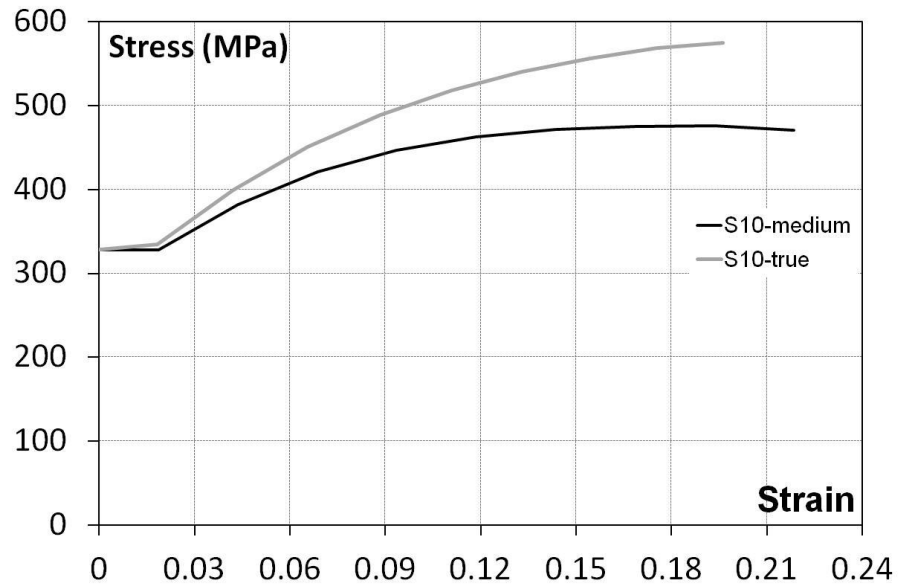


Figure 5.9 Medium curve and true stress-true strain curve for S10 plates.

Table 5.1 Mechanical properties of rivets.

Elastic properties		Plastic properties	
Rivets	E	210000 MPa	f_{yd} 331.5 MPa
	ν	0.3	ϵ_u 0.225
Plates	E	206436 MPa	f_{yd} 328 MPa
	ν	0.3	ϵ_u 0.27

5.2.3 The interaction between the component parts

Contact problems, in which two adjacent surfaces may be either in close contact or not during the simulated physical process, are suitably treated by ABAQUS/Standard. To define a contact interaction, the identification of the surfaces in contact and the interaction properties must be identified. The contact properties characterize the behaviour in the normal and tangential direction, referred to the contact surfaces.

Regarding the normal behaviour, the “clearance” is the distance separating two surfaces. When the clearance between two surfaces becomes equal to zero, the contact constraint is applied (Fig. 3.10a). In the contact formulation, there is no limit to the contact pressure magnitude which can be transmitted between the surfaces (Esposto, 2008). The contact constraint is removed when the surfaces separate: this phenomenon occurs when the contact pressure between the surfaces in contact becomes equal to zero or negative. This behaviour is called “hard” contact (Esposto, 2008).

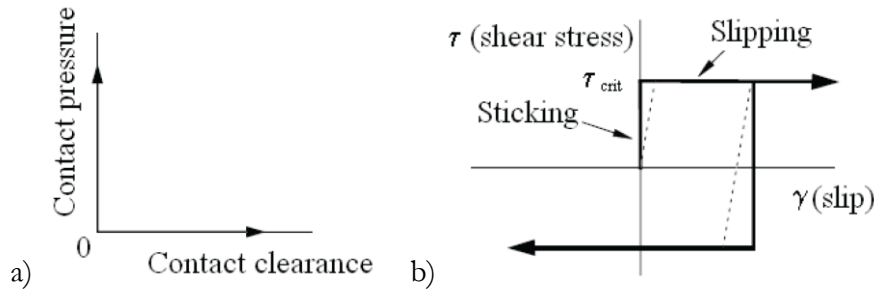


Figure 5.10 Interaction properties in contact interactions: (a) “hard” normal contact interaction; (b) frictional behaviour (ABAQUS, 2010).

Regarding the tangential behaviour, the relative sliding between the contact surfaces and the related friction forces are calculated. Both “finite sliding” and “small sliding” formulations can be adopted to solve this complex type of calculation. Regarding the computational time, the “small sliding” formulation is much less expensive, but not as accurate as the “finite sliding” one. The Coulomb formulation is the most common model for describing tangential friction forces. In this formulation, as well known, the tangential motion is zero until the shear stress reaches a critical value (τ_{crit}), related to the normal contact pressure (p) according to the following equation:

$$\tau_{crit} = \mu \cdot p \quad (5.6)$$

where μ is the friction coefficient (Esposto 2008). The behaviour of the Coulomb friction model is summarized in Figure 5.10b, where it is plotted by a thick line.

In the riveted connection model, surface-to-surface contacts are used to model the following interactions: a) between the internal surfaces of the hole and rivet shank (Fig. 11a,b,c); b) between the rivet heads and the external plate surfaces (Fig. 11a,b,c); c) at interface between the plates (Fig. 11d) (Marmo et al. 2010).

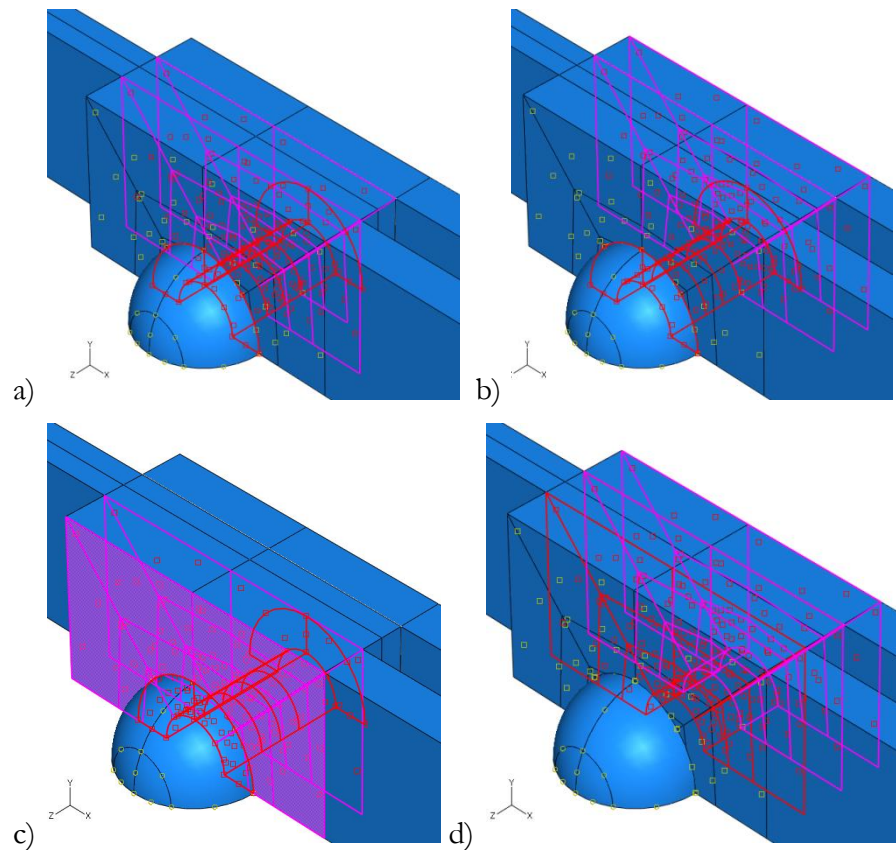


Figure 5.11 Modelling assumptions: implemented contact conditions.

In general, the master surface of the surface-to-surface contact must be the stiffer element; consequently the slavery surface is the surface of the most deformable part. In this case, the master surface is always the rivet, and the plates are the slavery ones.

Surface-to-surface contacts model the behaviour of parts that can be in contact or not, depending on configuration of the system. ABAQUS permits also the setting of friction properties between the parts in

contact. In particular, a “penalty friction tangential contact” is used for modelling the interaction between plates and rivet, which allows transmitting both shear and normal forces: the considered friction coefficient is equal to 0.3.

5.2.4 Element type and mesh

The 8-node brick continuum element C3D8R, with 8 nodes per element, 3 degrees of freedom per node and a linear interpolation function was adopted for modelling both rivet and plates. This kind of element matches the requirements typical of problems involving material plasticity, contact interactions and large size models (Esposto, 2008).

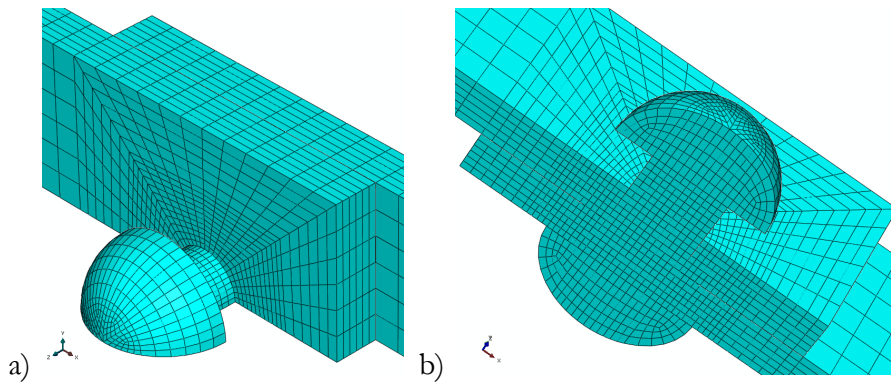


Figure 5.12 Mesh thickening in the parts in contact.

After a preliminary sensitivity study of the mesh, in order to minimize numerical discrepancy due to the contact boundary conditions, it needed to thicken the mesh sizing, making refined partitions of plates and rivet as shown in Figures 3.12 a,b (Marmo et al., 2010). The mesh refinement of the surfaces involved in contact interactions derives from the rigid master-slave algorithm used in contact by ABAQUS/Standard, which implies that slave surfaces must be meshed exactly as the master ones: it allows achieving a good accuracy of the results. The mesh of cylindrical parts, such as the rivet shank, derives from a calibration of the model (Marmo et al., 2010).

In order to optimize the accuracy of the analysis and the CPU time for calculation, a sensitivity study of the mesh was also performed. The investigated mesh subdivisions are showed in Figure 5.13.

The responses of the different models are plotted in Figure 5.13. It is possible to note that, in case of smaller plate's elements, the response is stiffer than the model with larger elements. The subdivision of the plates in thickness does not affect the response of the model. Model 3 was chosen for fire analysis, due to the most accurate response.

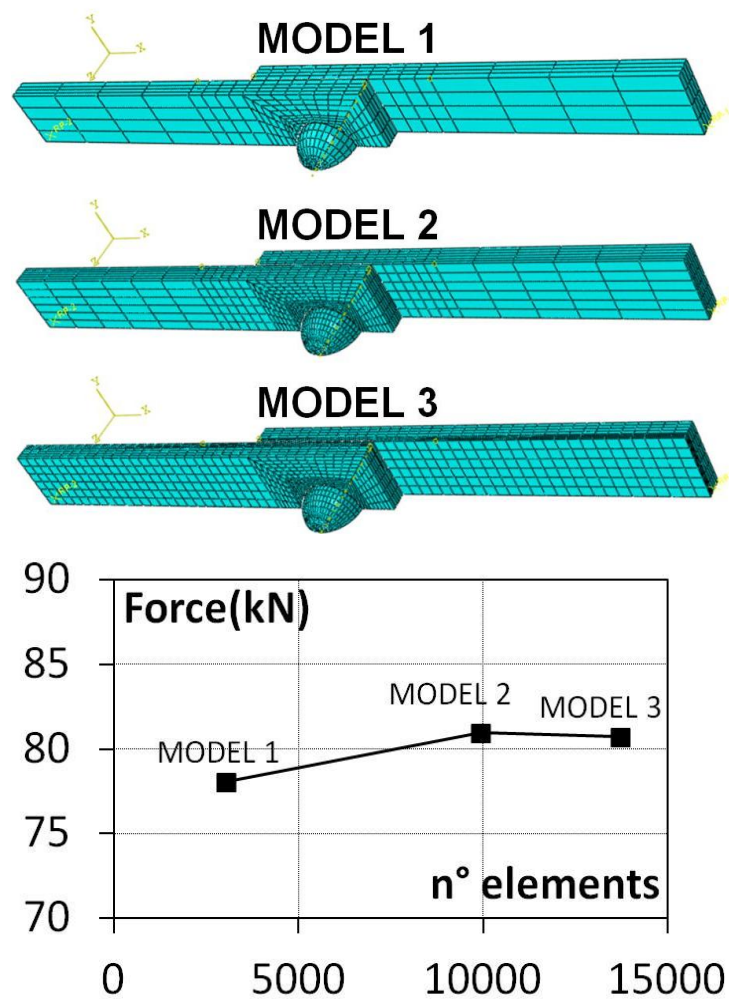


Figure 5.13 preliminary sensitivity study of the mesh.

5.2.5 Loads and boundary conditions

The simulation of the riveted connection behaviour reproduces initially the cooling of rivet and the consequently shortening of the rivet shank, then the pull out of the plates. The analysis is subdivided into a number of static steps, the first one corresponding to the rivet shortening, and the second one corresponding to the application of the load.

The load pattern has been simulated by applying a relative displacement between the two opposite terminal ends of each connected plates, as shown in Figure 5.13.

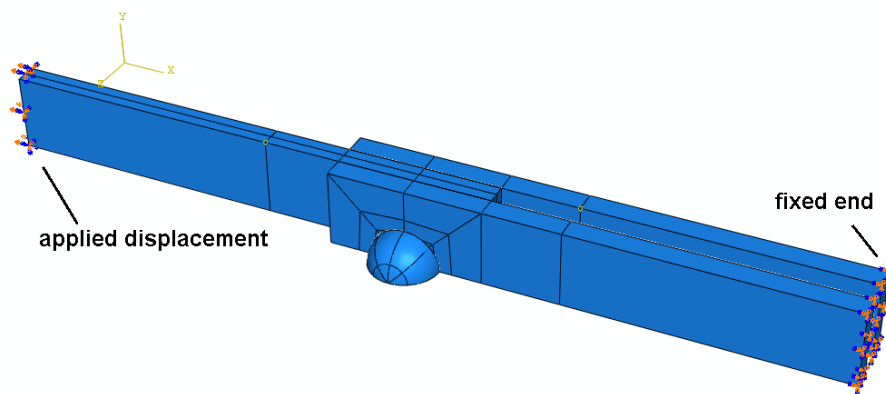


Figure 5.14 Simulation of the experimental load pattern.

The rivet cooling has been simulated in two different ways:

- applying a relative displacement between the two heads of the rivet;
- applying a load to the shank.

5.2.5.1 *Relative displacement method*

In order to take into account the rivet clamping, the rivet shank was modelled with an initial length smaller than the nominal length in the actual configuration. The rivet clamping was introduced imposing a relative elongation in tension to the rivet shank that was initially modelled with a length shorter than its nominal value, as illustrated in Figure 5.14.

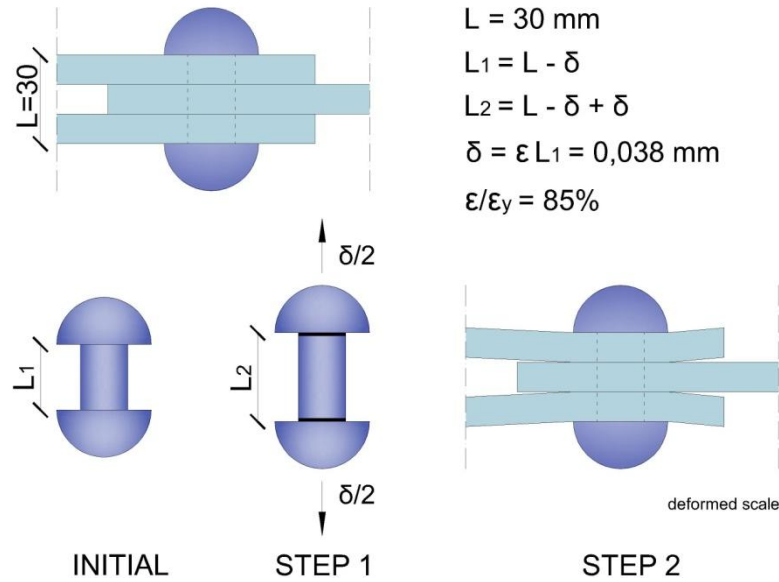


Figure 5.15 Simulation of the rivet clamping with the displacement method.

The modified initial length was L_1 . A relative elongation of 0,038 mm, corresponding to a strain equal to the 80% of the yield one, was given to the rivet shank. The shank shrinking due to the cooling process after the riveting was simulated by the re-release of the rivet shank. (Marmo et al., 2010).

5.2.5.2 Bolt Load method

ABAQUS permits the simulation of the tightening forces or length adjustments in bolts or fasteners by using the “bolt load” command.

The tension in the tightened bolts can be modelled by applying a bolt load to each one in the first step of the analysis.

The load can be defined in terms of either a concentrated force or a prescribed change in length, and it can be applied across a rivet cross-section surface (Fig. 3.15).

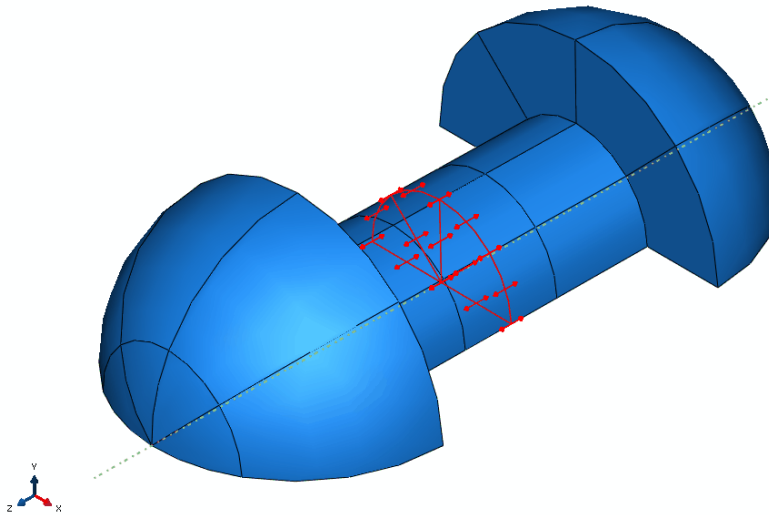


Figure 5.16 Simulation of the rivet clamping with the force method.

The bolt load was applied on rivets by choosing:

- a surface that defines the rivet cross-section. In this case, the surface cut through the rivet geometry. Abaqus/CAE creates an “internal” surface at that location;
- a rivet axis that indicates the rivet clamping force direction (it need not be normal to the cross-section);
- a method for applying the loading: in this case, the “apply force” method was chosen. That method models tightening the rivet so that it carries a specified load;
- a magnitude for the chosen method: in this case, it was set the force magnitude (ABAQUS, 2010).

5.3 CALIBRATION OF THE RIVETED CONNECTION FE MODEL

Once the four models of four different types of riveted connections were implemented, a calibration of the material model and of the rivet clamping force was performed, to analyse the influence of these uncertain parameters on the overall behaviour of the connections.

The riveted connections behaviour, indeed, is particularly influenced by the rivet forming process, that involves a drastic change of temperature and a hot driven process. That phenomenon induces in the material a hot driven process, which involves a strengthening sometimes up to 50%.

The shank shrinking due to the cooling process after the riveting induces on connection an additional force, which could vary about the 10% of the ultimate strength of the material up to 80 %. This clamping force deeply influences the connection behaviour, and its magnitude is not so simply to determine.

In this paragraph, a sensitive study of these values is performed, and the different responses on the connection behaviour are discussed. Finally, a calibrated model of riveted connection is proposed, that can easily predict their behaviour.

5.3.1 Effect of hot-driven process

Analyzing the results of different experimental tests (Munse et al., 1970; Fisher et al., 1969, Schutz, 1952, D’Aniello et al., 2010), the strength of rivets and plates is strongly influenced by the driving process. Indeed, this process could increase the tensile strength of rivets by up to about 20% with respect to undriven rivets. A considerable reduction in elongation capacity was observed with the increase in strength, thus resulting in brittle behaviour (D’Aniello et al., 2010). Tests performed by Hechtman (Hechtman, 1948) on rivets hot-driven at different temperatures showed that the strength increases with the temperature. This effect could be recognized up to a threshold of 900 °C. No appreciable variation was found by varying the temperature within the range 900–1200 °C. This phenomenon is related to the modification induced in the steel grain microstructure, which typically occurs in the steel after thermo-mechanical treatments (Bailey et al., 1979; Nack et al., 1983; Malina et al., 2005).

This particular behaviour could be taken into account during the FE modelling by increasing the stress-strain relationship of rivet steel, subjected to heat variation. The increasing factor is evaluated by considering the average F_u/F_{EC3} ratio of all specimens failed for rivet shear. The amount of the ultimate tensile strength calculated according to the EN 1993:1-8 formulas differs a lot from the experimental values. This is due to the rivets’ shear strength to tensile strength ratio ($f_{ur,v}/f_{ur}$),

that usually assumes an average value of 0.75 (Ω_2), and due to the hot driven process, that improves the ultimate tensile strength of the rivet of about 20% (Ω_1). As mentioned above, D'Aniello et al. (2010) proposed two corrective factors, to take into account these phenomena (4.7):

$$F_{v,Rd} = \frac{\Omega_1 \cdot \Omega_2 \cdot f_{ur} \cdot A_0}{\gamma_{M2}}$$

This value could vary slightly, due to the uncertainty of the hand-made riveting process, and then due to the uncertainty of the forming rivet temperature.

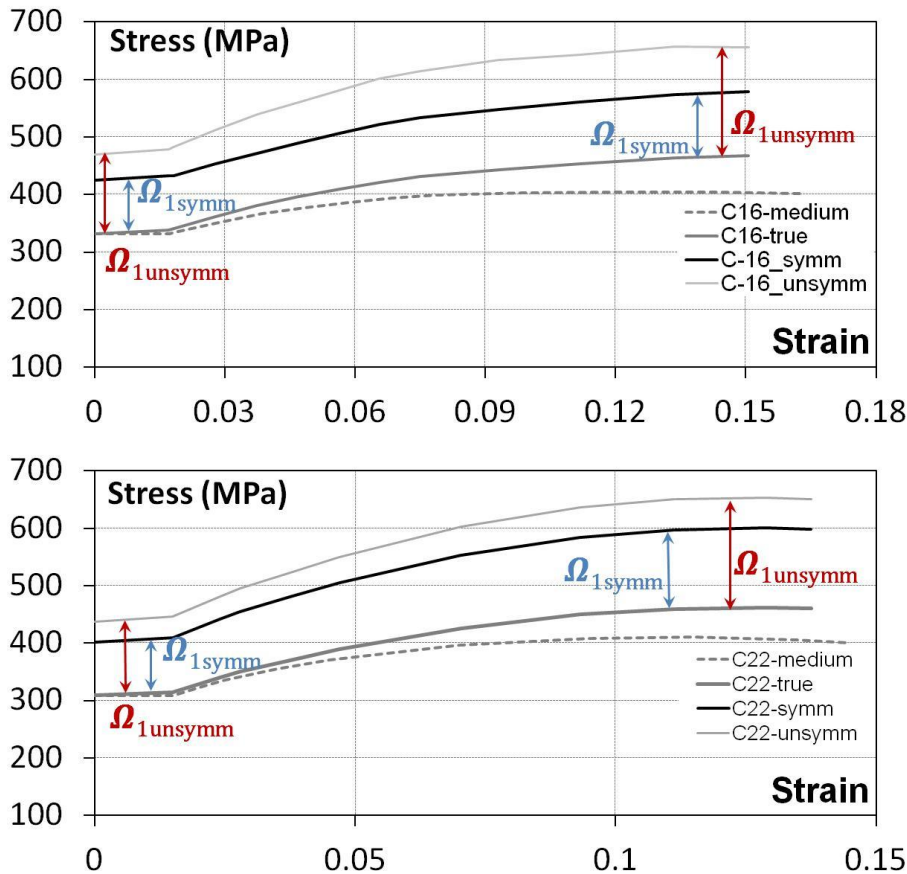


Figure 5.17 Increased stress-strain relationship for C16 and C22 rivets.

Furthermore, the effects of hot driven process could slightly vary also according to length, and then its magnitude could differ from symmetrical to unsymmetrical joints. In the F.E. model, these phenomena were taken into account by increasing the stress-strain relationship of the $\Omega_{1\text{symm}}$ factor for the symmetrical joints, and of the $\Omega_{1\text{unsymm}}$ factor for the unsymmetrical joints as shown in Figure 5.17. In the next chapter, a sensitivity study on the response of riveted connections varying this increasing factor is carried out, confronting the F.E. model results with the proposed theoretical formulas.

In case of long joints, the hot driven process effects involve also the plate steel, due to the presence of more rivets. The plates, already weakened by the presence of holes and by the formation process of the holes, are subjected also to hot driven process effects induced by rivets. In this case, indeed, this effect is not negligible, and induces on the plate steel a reduction of the ultimate strain of about the 45%.

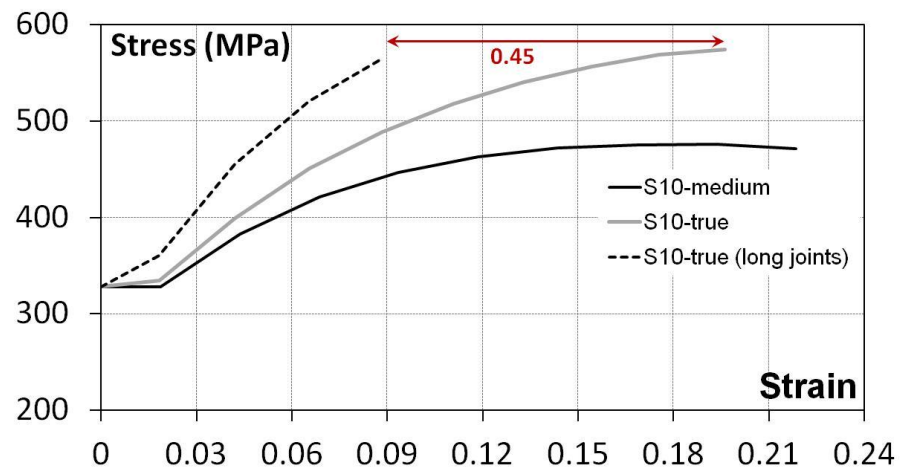


Figure 5.18 Stress-strain relationship for S10 plates.

The results on one rivet joints (S-16-10-1-S and U-16-10-1-S) demonstrate that the hot driven process effects are not negligible; indeed the response of the numerical model approaches the experimental one especially in terms of ultimate strength.

For what concern the four rivets connections (S-22-12-4-S and U-22-12-4-S), the hot driven process effects of rivets increase the ultimate

strength of the connection, and the reduction of plate's ultimate strain induces the failure in the inner plate net section according to the experimental curves.

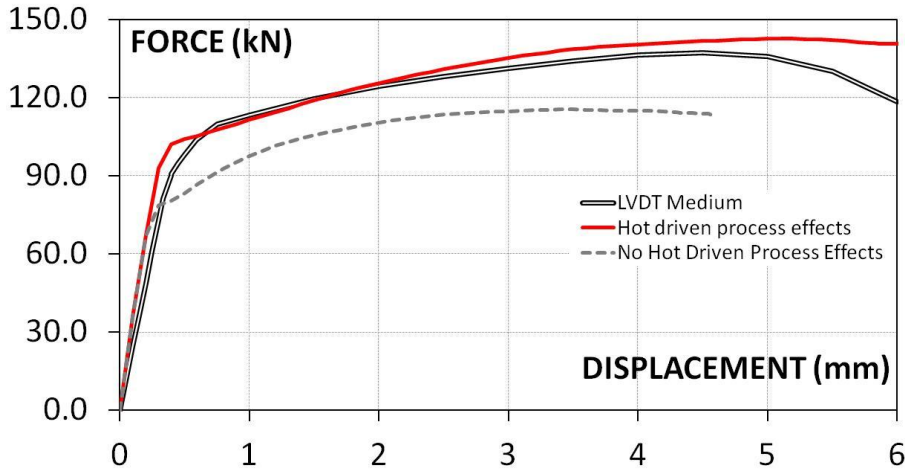


Figure 5.19 Hot driven process effects on S-16-10-1-S joint response.

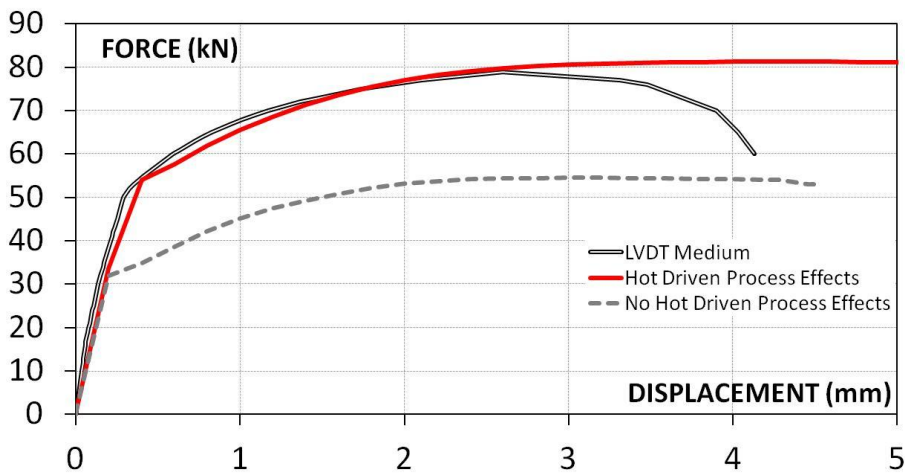


Figure 5.20 Hot driven process effects on U-16-10-1-S joint response.

As shown in the Figure 5.21 and the Figure 5.22, the F. E. Model without the hot driven process effects underestimate the ultimate strength of the joint, but in this case the failure occurs for displacements bigger than the experimental ones. Taking into account the hot driven

process effects, the response of the numerical model approaches the experimental one both in terms of ultimate strength and ultimate displacement.

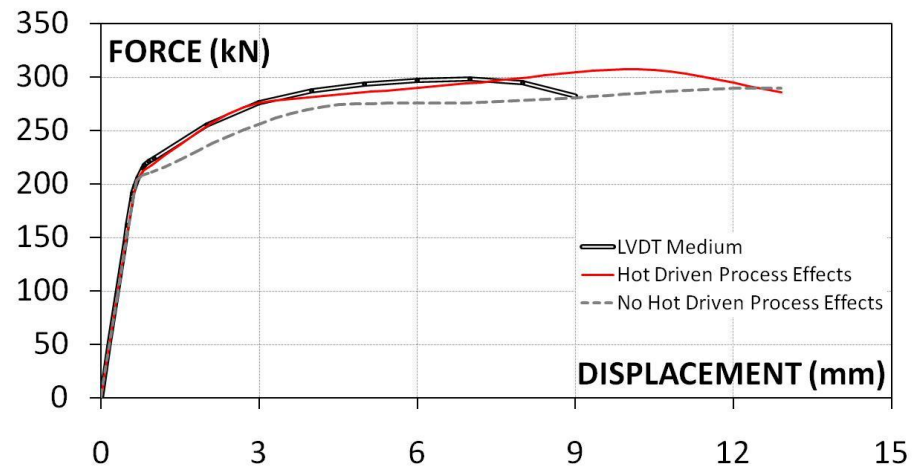


Figure 5.21 Hot driven process effects on S-22-12-4-S joint response.

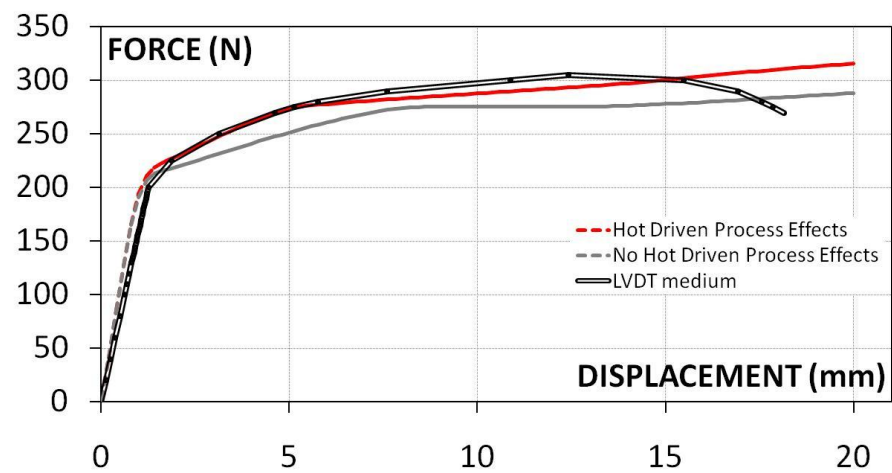


Figure 5.22 Hot driven process effects on U-22-12-4-S joint response.

5.3.2 Effect of rivet clamping

Once the material was calibrated, taking into account also the effects of hot-driven process, a sensitivity study on probably values of rivet clamping forces was carried out. The magnitude of these forces depends on the shank shrinking induced by the cooling process. Obviously, these values are not univocally determinable.

To evaluate the effect of different values of rivet clamping, a parametric analysis on riveted connections was performed. The values of rivet clamping were set starting from a value of 10% of the nominal yielding stress of the rivet steel to a value of 80%.

S-16-10-1-S					U-16-10-1-S					S-22-12-4-S					U-22-12-4-S								
0.1 f_{td}	F clamping				3330.912	0.1 f_{td}	F clamping				4996.368	0.1 f_{td}	F clamping				5889.07	0.1 f_{td}	F clamping				8833.605
	f_{td}	d	π	A/2	f_{td}		d	π	A/2	f_{td}	d		π	A/2	f_{td}	d	π		A/2				
	331.5	16	3.14	100.48	331.5		16	3.14	100.48	310	22		3.14	189.97	310	22	3.14		189.97				
0.2 f_{td}	F clamping				6661.824	0.2 f_{td}	F clamping				9992.736	0.2 f_{td}	F clamping				11778.14	0.2 f_{td}	F clamping				17667.21
	f_{td}	d	π	A/2	f_{td}		d	π	A/2	f_{td}	d		π	A/2	f_{td}	d	π		A/2				
	331.5	16	3.14	100.48	331.5		16	3.14	100.48	310	22		3.14	189.97	310	22	3.14		189.97				
0.3 f_{td}	F clamping				9992.736	0.3 f_{td}	F clamping				14989.104	0.3 f_{td}	F clamping				17667.21	0.3 f_{td}	F clamping				26500.815
	f_{td}	d	π	A/2	f_{td}		d	π	A/2	f_{td}	d		π	A/2	f_{td}	d	π		A/2				
	331.5	16	3.14	100.48	331.5		16	3.14	100.48	310	22		3.14	189.97	310	22	3.14		189.97				
0.4 f_{td}	F clamping				13323.648	0.4 f_{td}	F clamping				19985.472	0.4 f_{td}	F clamping				23556.28	0.4 f_{td}	F clamping				35334.42
	f_{td}	d	π	A/2	f_{td}		d	π	A/2	f_{td}	d		π	A/2	f_{td}	d	π		A/2				
	331.5	16	3.14	100.48	331.5		16	3.14	100.48	310	22		3.14	189.97	310	22	3.14		189.97				
0.5 f_{td}	F clamping				16654.56	0.5 f_{td}	F clamping				24981.84	0.5 f_{td}	F clamping				29445.35	0.5 f_{td}	F clamping				44168.025
	f_{td}	d	π	A/2	f_{td}		d	π	A/2	f_{td}	d		π	A/2	f_{td}	d	π		A/2				
	331.5	16	3.14	100.48	331.5		16	3.14	100.48	310	22		3.14	189.97	310	22	3.14		189.97				
0.6 f_{td}	F clamping				19985.472	0.6 f_{td}	F clamping				29978.208	0.6 f_{td}	F clamping				35334.42	0.6 f_{td}	F clamping				53001.63
	f_{td}	d	π	A/2	f_{td}		d	π	A/2	f_{td}	d		π	A/2	f_{td}	d	π		A/2				
	331.5	16	3.14	100.48	331.5		16	3.14	100.48	310	22		3.14	189.97	310	22	3.14		189.97				
0.7 f_{td}	F clamping				23316.384	0.7 f_{td}	F clamping				34974.576	0.7 f_{td}	F clamping				41223.49	0.7 f_{td}	F clamping				61835.235
	f_{td}	d	π	A/2	f_{td}		d	π	A/2	f_{td}	d		π	A/2	f_{td}	d	π		A/2				
	331.5	16	3.14	100.48	331.5		16	3.14	100.48	310	22		3.14	189.97	310	22	3.14		189.97				
0.8 f_{td}	F clamping				26647.296	0.8 f_{td}	F clamping				39970.944	0.8 f_{td}	F clamping				47112.56	0.8 f_{td}	F clamping				70668.84
	f_{td}	d	π	A/2	f_{td}		d	π	A/2	f_{td}	d		π	A/2	f_{td}	d	π		A/2				
	331.5	16	3.14	100.48	331.5		16	3.14	100.48	310	22		3.14	189.97	310	22	3.14		189.97				

Figure 5.23 Rivets clamping forces, from a value of 10% of f_{yd} to 80% of f_{yd} .

Indeed, the clamping force on rivet shank was determined as:

$$F_{clamp} = \beta \cdot f_{yd} \cdot \frac{A}{2} \quad (5.7)$$

where: f_{yd} is the yielding stress of rivet steel;

A/2 is a half of the shank cross section, in this case was considered only half of the cross section because all models are simplified by assuming an exploiting of the system symmetry with respect to the mid plane of connection.

β is a reduction factor that varies in the range of 0.1-0.8.

In case of one rivet joints (S-16-10-1-S and U-16-10-1-S), the increasing of clamping force induces a reduction of joint ultimate strength. This phenomenon is due to the presence, in one rivet connections failure modes, of secondary effects. These effects, that are secondary bending moment in unsymmetrical connections and bearing in the inner plate for symmetric connections, are penalized by the presence of higher clamping forces, and determined a decrease of the ultimate strength of connection.

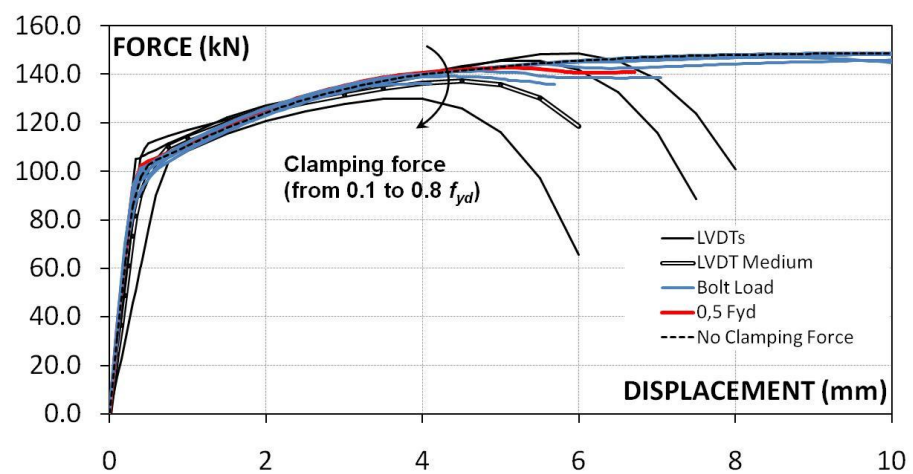


Figure 5.24 Effects of the variation of the rivet clamping force on S-16-10-1-S joint response.

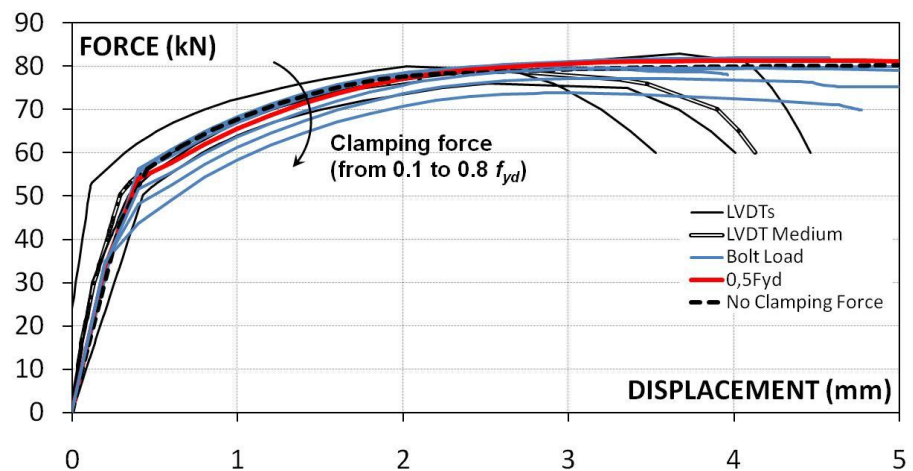


Figure 5.25 Effects of the variation of the rivet clamping force on U-16-10-1-S joint response.

In case of four rivets joints (S-16-10-1-S and U-16-10-1-S), the increasing of clamping force induces an increase of joint ultimate strength.

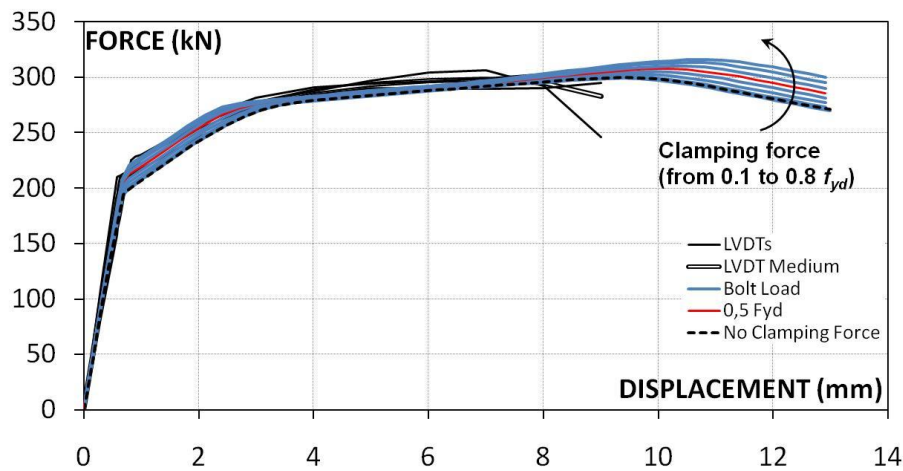


Figure 5.26 Effects of the variation of the rivet clamping force on S-22-12-4-S joint response.

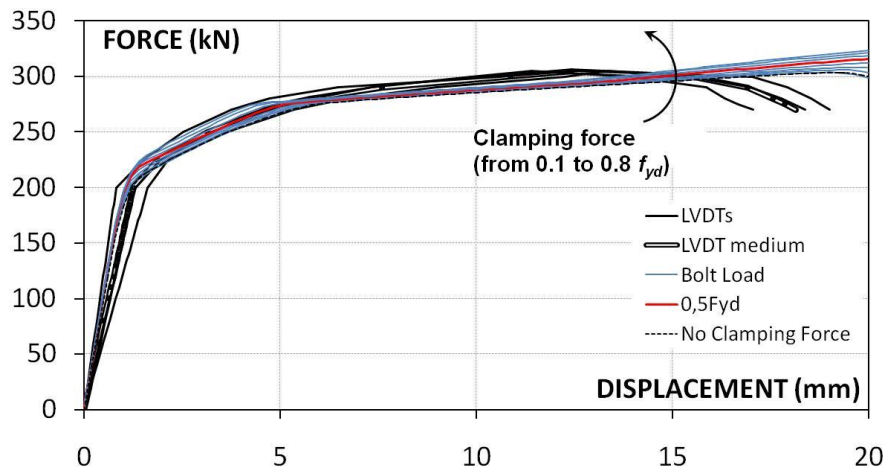


Figure 5.27 Effects of the variation of the rivet clamping force on U-22-12-4-S joint response.

At last, an average value of clamping equal to $0.5 f_{yd}$ was considered as the optimal value to describe the riveted connection behaviour in all the four models presented.

5.4 NUMERICAL RESULTS

5.4.1 Load-displacement curves

The reliability of the numerical models is highlighted by the comparison of the obtained analytical results with the experimental ones. In particular, the numerical load-displacement curves are well superimposed to the experimental ones, as shown in Figures 3.28, 3.29, 3.30, 3.31. The main characteristics of the connection in terms of global behaviour, namely the initial stiffness, the strength corresponding to the end of linear behaviour, the post-yielding stiffness and the strength corresponding to the collapse are successfully caught by the finite element models.

The connection behaviour is linear elastic up to the strength corresponding to the end of linear phase, when the friction between plates is exceeded. After the friction resistance is exceeded, a sudden slip occurs and the connection stiffness noticeably reduces, as expected on the basis of both the theoretical predictions and the experimental evidence. At last, both the expected ultimate capacity of the connection is well caught by the finite element model, as demonstrated by the response curves obtained from the numerical analyses.

For what concern the S-16-10-1-S, it is interesting to note how the curve obtained by imposing a bolt load equal to the 50% of the yielding stress of the rivet steel is able to predict the ultimate strength and the deformation of the connection according to the experimental curve, while the curve obtained by imposing a relative displacement overestimates the ultimate strength and deformation of the connection (Fig. 3.28). The maximum load achieved for this joint is approximately equal to 100 kN, while the ultimate displacement is approximately equal to 6.7 mm.

On the contrary, for U-16-10-1-S the bolt-load curve overestimates the ultimate displacement of the connection, but it catches the ultimate

strength. The relative-displacement curve, instead, underestimates both the strength and the deformability of the real connection. The maximum load achieved for this joint is approximately equal to 50 kN, a half respect to the relative symmetrical connection S-16-10-1-S, while the ultimate displacement is approximately equal to 4.13 mm.

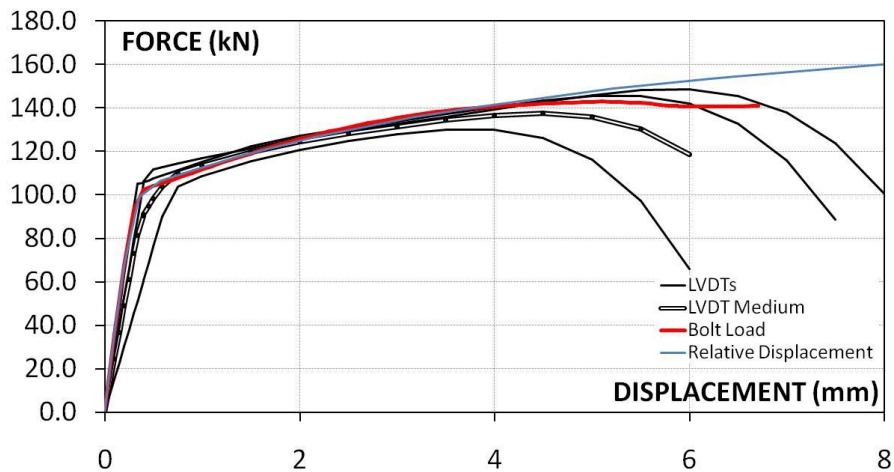


Figure 5.28 Experimental vs. numerical load-displacement curve of S-16-10-1-S joint.

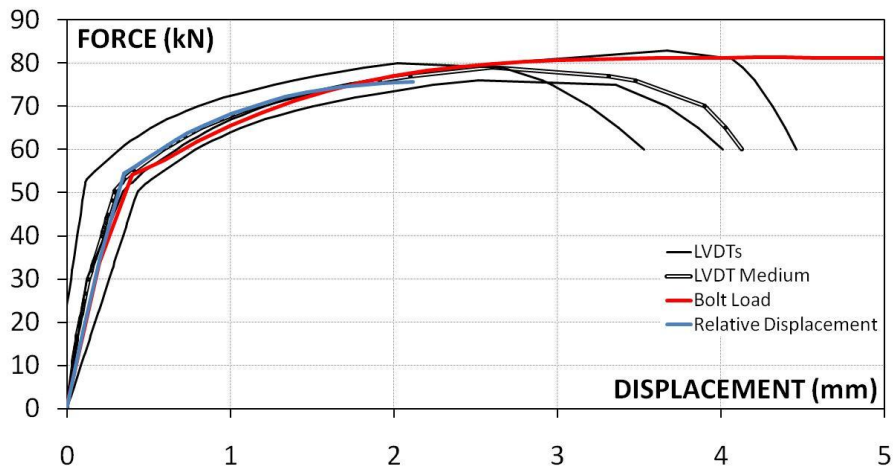


Figure 5.29 Experimental vs. numerical load-displacement curve of U-16-10-1-S joint.

For what concern the four rivets joints, in case of S-22-12-4-S the bolt-load curve overestimates the ultimate displacement of the connection, but it catch the ultimate strength.

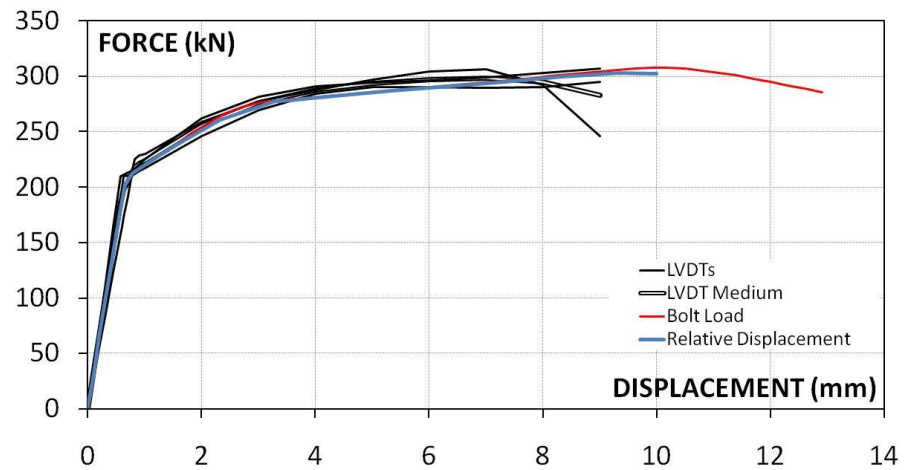


Figure 5.30 Experimental vs. numerical load-displacement curve of S-22-14-4-S joint.

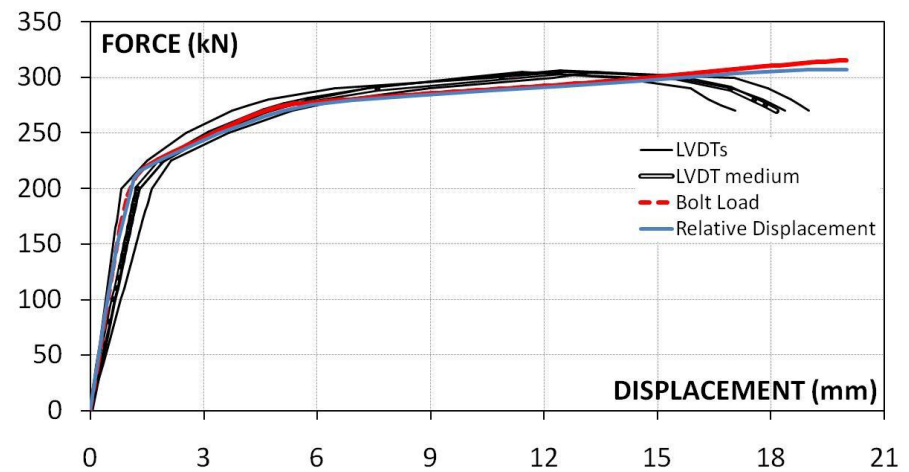


Figure 5.31 Experimental vs. numerical load-displacement curve of U-22-14-4-S joint.

The relative-displacement curve, instead, is able to predict the ultimate strength and the deformation of the connection according to the experimental curve. The maximum load achieved for this joint is approximately equal to 310 kN, while the ultimate displacement is approximately equal to 9 mm.

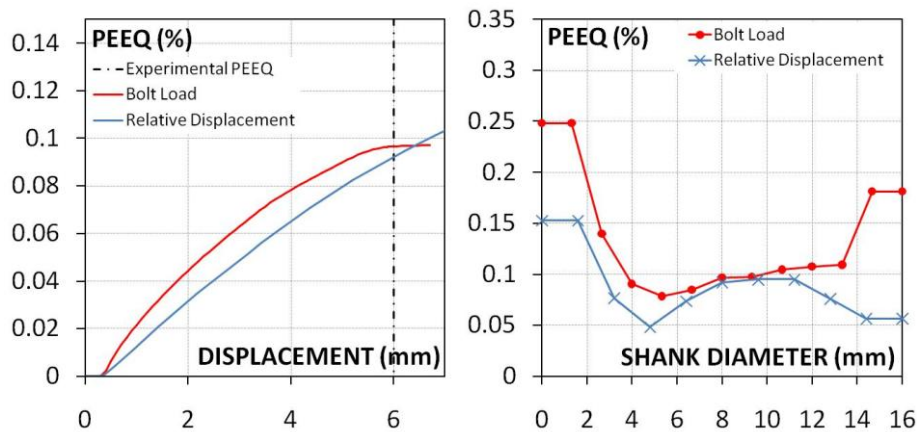


Figure 5.32 Experimental vs. numerical PEEQ of S-16-10-1-S joint (the shank diameter is considered in the direction of applied load).

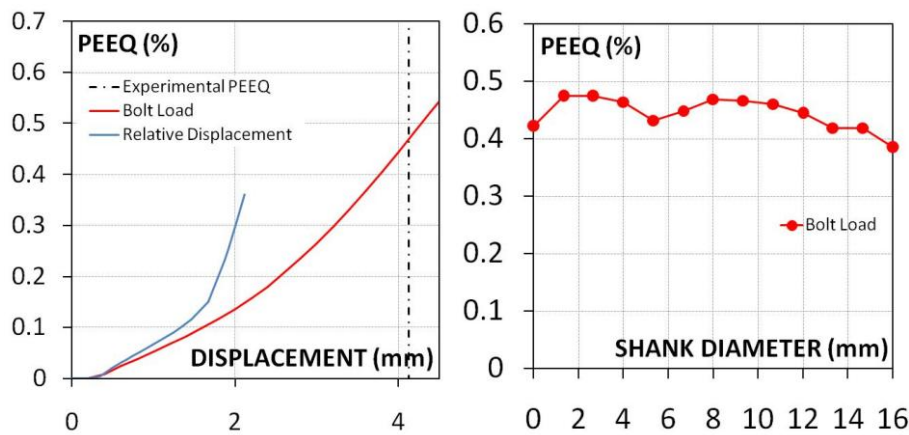


Figure 5.33 Experimental vs. numerical PEEQ of U-16-10-1-S joint (the shank diameter is considered in the direction of applied load).

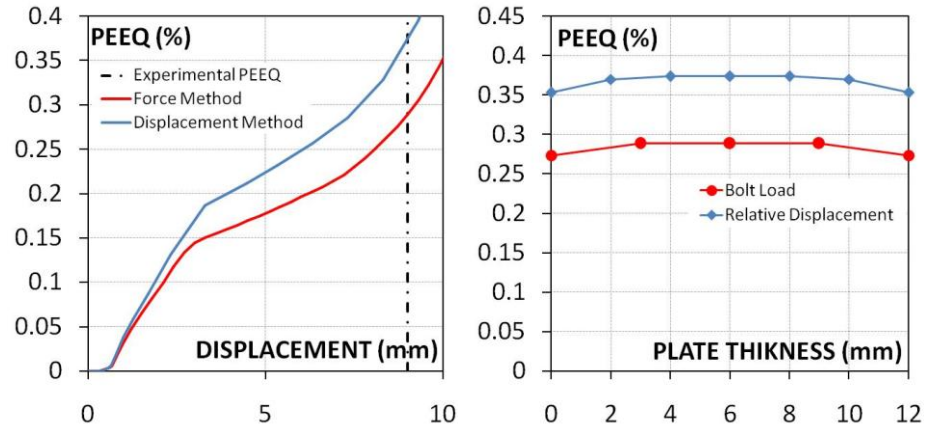


Figure 5.34 Experimental vs. numericals PEEQ of S-22-14-4-S joint.

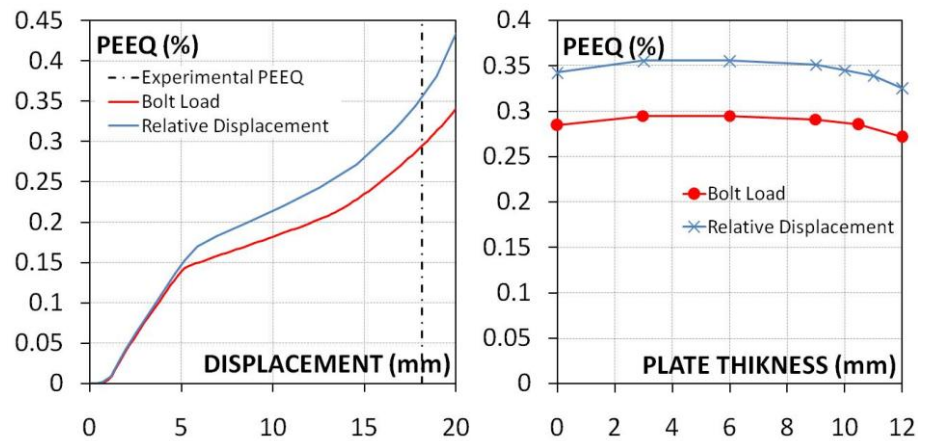


Figure 5.35 Experimental vs. numericals PEEQ of U-22-14-4-S joint.

Likewise, in case of S-22-12-4-S both the bolt-load curve and the relative-displacement curve slightly overestimates the ultimate displacement of the connection, but it catch the ultimate strength. The maximum load achieved for this joint is approximately equal to 300 kN, while the ultimate displacement is approximately equal to 18 mm.

5.4.2 Collapse modes

The numerical models exhibit exactly the failure modes observed after tests. The main failure mode observed for one-rivet joints is the rivet shear. At failure, the joints present always secondary phenomena, as secondary bending moment for unsymmetrical connections, or bearing of plates in symmetrical connections.

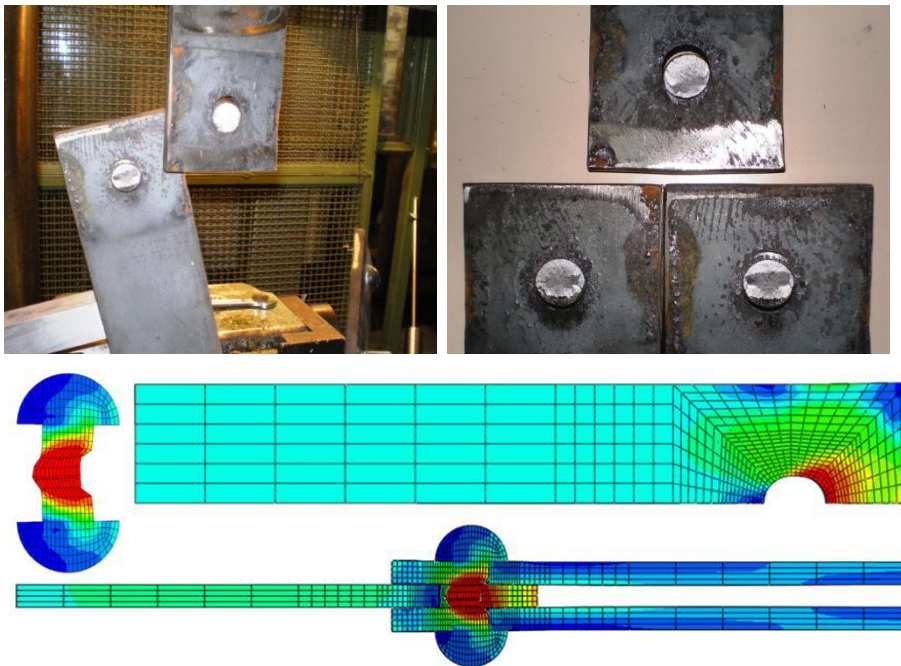


Figure 5.36 Experimental vs. Numerical collapse mode for S-16-10-1-S.

Figure 5.36 shows a comparison between a failed symmetrical specimen and the F.E. model results. It is possible to note how the numerical model catches the failure of rivet in shear and also the bearing of the inner plate, which is the weakest plate in this kind of joints.

The results of U-16-10-1-S are reported in Figure 5-37. The failure of this joint is imputable to the rivet in shear, as shown in Figure 5.37, but also the secondary phenomena, as the secondary bending moment caused by the eccentricity of the load, plays an important role in the collapse of this kind of connection. The numerical model catches both the main failure mode and the secondary bending moment.

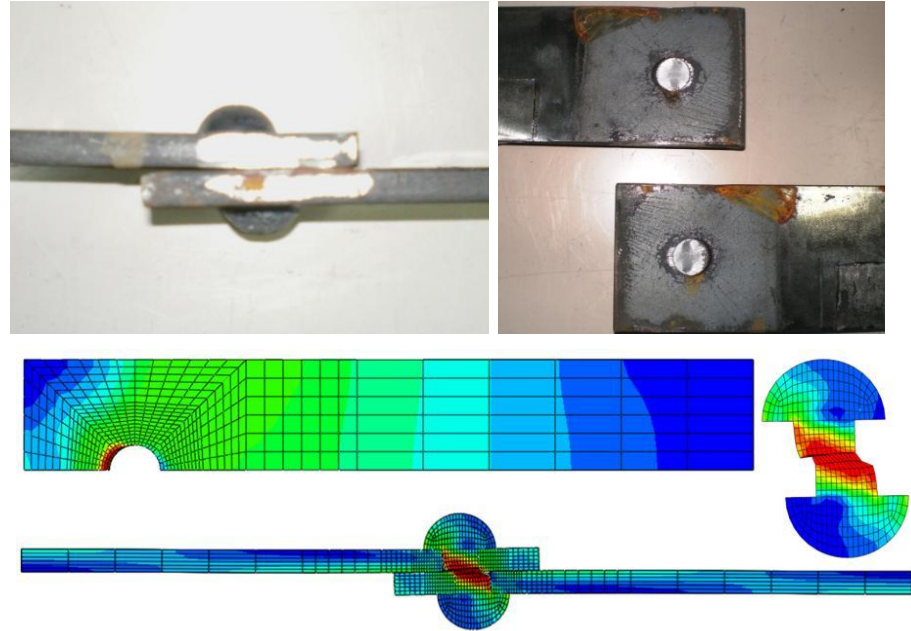


Figure 5.37 Experimental vs. Numerical collapse mode for U-16-10-1-S.

The main failure mode observed for four-rivet joints is the tension in the net section. This kind of joints does not present secondary phenomena at failure, as well as the secondary bending moment in unsymmetrical connections is negligible. Figure 5.38 shows the comparison between the numerical results and a failed symmetrical four-rivet specimen: the F.E. model presents a reduction of the net section with a high concentration of stresses in the inner plate, reproducing faithfully the real behaviour of the joint at collapse.

The unsymmetrical four-rivets numerical results are shown in Figure 5.39, in comparison with the failed relative specimen: the F.E. model presents a reduction of the net section with a high concentration of stresses in one of the two plates, reproducing faithfully the real behaviour of the joint at collapse.

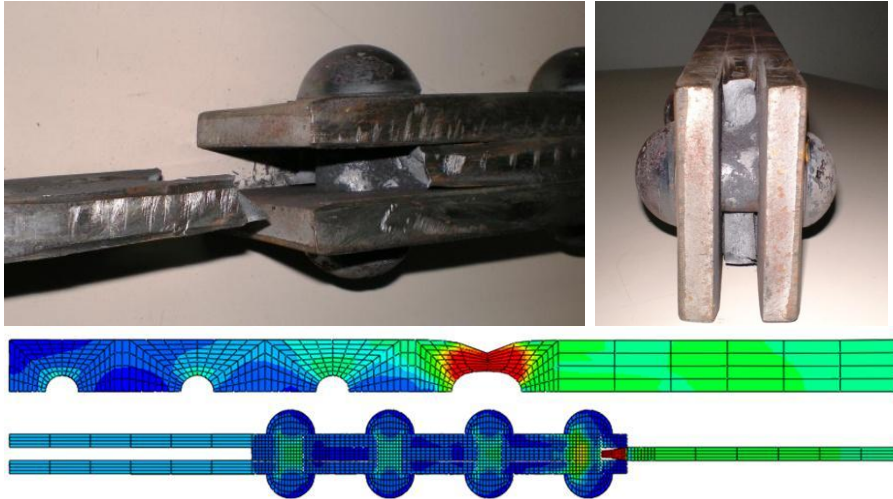


Figure 5.38 Experimental vs. Numerical collapse mode for S-22-12-4-S.

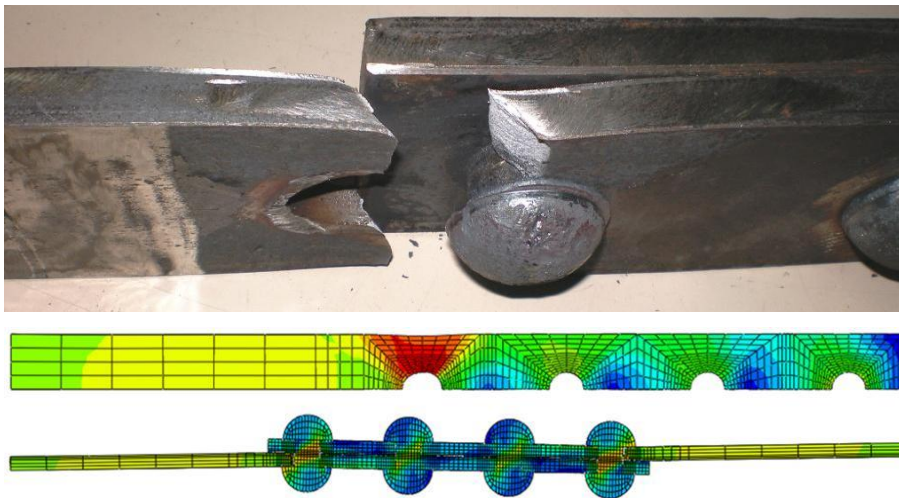


Figure 5.39 Experimental vs. Numerical collapse mode for U-22-12-4-S.

5.5 CONCLUDING REMARKS

In this chapter, on the basis of a wide experimental research a numerical study aimed to analyse the response of lap shear riveted connection typically present in historic metal structures is summarized. Moreover,

the results of the predictive numerical analyses performed on some representative specimens have been shown. The 3-D FE models presented have simulated the shearing and bearing behaviour in simple symmetric lap shear connection. The models incorporate non-linear material properties for all the connection components, geometric non-linearity and contact interaction by means of the ABAQUS/Standard code. In most cases, contact elements were crucial for modelling the steel connection performance, and so creation of the fin plate connection model was a big challenge. However, the contact interaction between the connection components was introduced and successfully achieved on all the interfaces.

The hot driven process was taken into account by increasing the material stress strain relationship by a factor, determined according to literature and the average values obtained by experimental tests. This factor increases the ultimate strength and decreases the ultimate strain of the rivet material, which is subjected to heat variation due to the formation of the second head. In longer joints, where more than two rivets are present, the plate material presents a weakening caused by the formation of holes and a reduction of the ductility due to the influences of heat deriving by the hot driven process of rivets. These phenomena were taken into account by decreasing the plate stress-strain relationship of about the 45%, according to literature.

The clamping action caused by the cooling of rivet was modelled in two different ways:

1. by applying a relative displacement between the two ends of the rivet and then by releasing the shank;
2. by applying a bolt load in the middle of the rivet shank.

Both the methods described well the connections behaviour and reproduce their effective failure modes, observed during experimental tests. In detail the clamping force in the first method is variable during the analysis, reproducing the real behaviour of the rivet forming process. However, the F.E. model is complicated and less rational. In the second method, the clamping force remains constant during the analysis, but the model presents less steps and force, resulting more rational.

The effects of hot driven process and of rivet clamping on rivet connections behaviour are not negligible, as observed confronting the experimental and numerical results. In the next chapter, the magnitude

of these phenomena is confronted with the numerical formulas proposed in the previous chapter by D’Aniello et al. (2010).

6 THEORETICAL VS. NUMERICAL RESULTS

On the basis of the experimental results, the theoretical formulation and the numerical model response, a comparison has been made to verify the reliability of the theoretical equations and F.E. results.

In this manner, a useful tool to predict the behaviour of all types of riveted connections will be provided.

To this end, the magnitude of numerical results was compared with the proposed theoretical formulas, to ensure both the good accuracy of F.E. model and the reliability of the proposed equations.

In particular, two main effects could be verified:

1. The magnitude of hot driven process;
2. The effects of rivet clamping on the net efficiency.

These two phenomena, indeed, were compared with the experimental results and the literature values, and then were computed into the theoretical formulation to correct the reductive factors of EN 1993:1-8 formulas. Considering these two effects, the tension failure of plates (eq. 3.2) and the rivet shear failure (eq. 3.3):

$$N_{u,Rd} = \frac{0.9 \cdot f_u \cdot A_{net}}{\gamma_{M2}}$$

$$F_{v,Rd} = \frac{0.6 \cdot f_{ur} \cdot A_0}{\gamma_{M2}}$$

respectively became equation 4.8 and equation 4.7:

$$N_{u,Rd} = \frac{f_u \cdot A_{net}}{\gamma_{M2}}$$

$$F_{v,Rd} = \frac{\Omega_1 \cdot \Omega_2 \cdot f_{ur} \cdot A_0}{\gamma_{M2}}$$

In the next paragraphs, these equations will be confronted with the F.E. model results, in order to verify the reliability of numerical model.

6.1 HOT-DRIVEN PROCESS

The hot driven process effects were taken into account during the FE modelling by increasing the stress-strain relationship of rivet steel. The increasing factor is evaluated by considering the average F_u/F_{EC3} ratio of all specimens failed for rivet shear.

Table 6.1 F_u/F_{EC3} values for specimens failed for rivet shear.

	F_u	Failure mechanism	F_{EC3}	F_u/F_{EC3}
	[kN]		[kN]	
S-16-10-1	141.83	V + B (sec.)	99.31	1.43
U-16-10-1	80.22	V	49.66	1.62
Average value				1.53

Generally, as mentioned above, the amount of the average F_u/F_{EC3} ratio results equal to 1.53 for specimens whose rivets failed in shear. This is due to the rivets' shear strength to tensile strength ratio ($f_{ur,v}/f_{ur}$), that usually assumes an average value of 0.75 (Ω_2), and due to the hot driven process, that improves the ultimate tensile strength of the rivet of about 20% (Ω_1). This value could vary slightly, due to the uncertainty of the hand-made riveting process, and then due to the uncertainty of the forming rivet temperature. Furthermore, the effects of hot driven process could vary also according to length, and then its magnitude could differ from symmetrical (Ω_{1symm}) to unsymmetrical joints ($\Omega_{1unsymm}$). As mentioned above, in the F.E. model, these phenomena were taken into account by increasing the stress-strain relationship of the Ω_1 factor, that could slightly varies from symmetrical to unsymmetrical joints, but his values is always about 20%. A sensitive study was carried out to verify the reliability of these considerations, and to ensure the correspondence between numerical model and theoretical formulations.

Table 6.2 Different models for S-16-10-1-S.

S-16-10-1, U-16-10-1	Increasing factor
Model 1	No increasing factor
Model 2	F_u/F_{EC3}
Model 3	$\Omega_1=(F_u/F_{EC3})/\Omega_2$

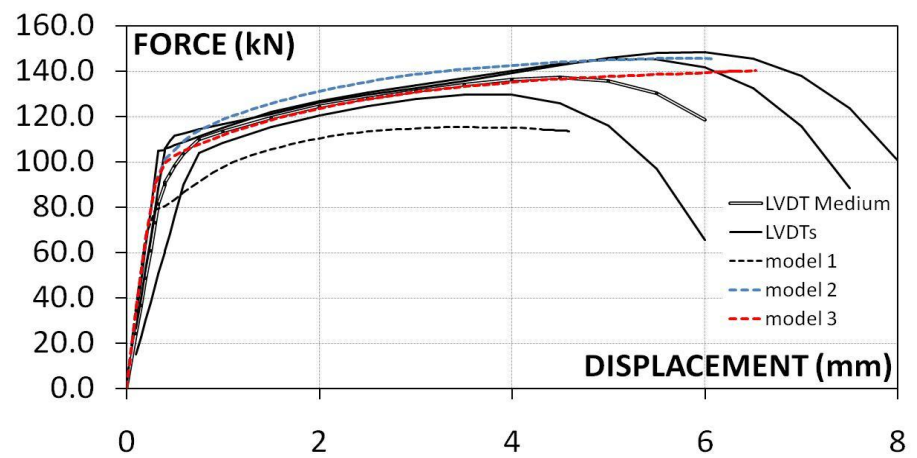


Figure 6.1 Force-displacement curves for S-16-10-1-S.

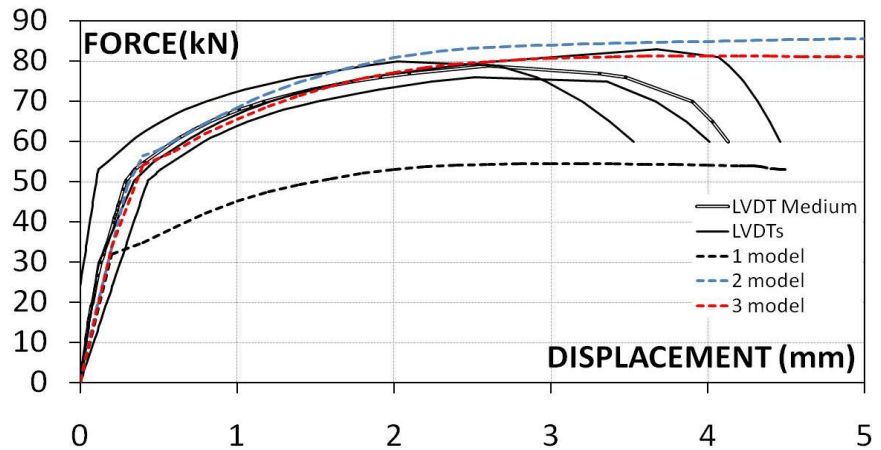


Figure 6.2 Force-displacement curves for U-16-10-1-S.

The sensitivity analyses demonstrated that the hot driven process are not negligible, indeed the increased stress-strain relationship has produced a

response that underestimates the real behaviour of connections. Furthermore, the increasing factor equal to F_u/F_{EC3} needs to be reduced of the rivets' shear strength to tensile strength ratio ($f_{ur,v}/f_{ur}$), that usually assumes an average value of 0.75 (Ω_2). Taking into account the hot driven process effects with the Ω_1 factor, the response of the numerical model approaches the experimental one especially in terms of ultimate strength. Indeed, on the basis of this comparison, the Ω_1 factor, that varies in the range of 1.1-1.3, with an average values of 1.2, is assumed to increase the stress-strain relationship of riveted connections, confirming the equation 4.7 proposed by D'Aniello et al. (2010).

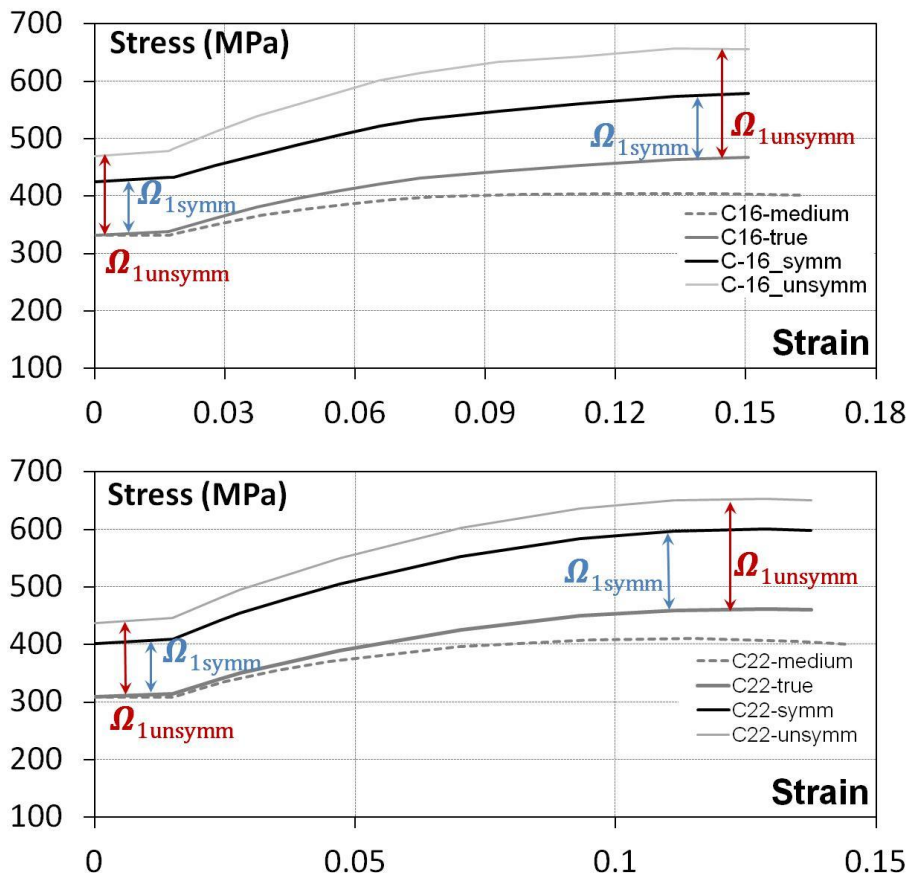


Figure 6.3 Increased stress-strain relationship for C16 and C22 rivets.

The same consideration could be done for what concern the four-rivet connections, which are joined with C22 rivets. The stress-strain relationship of C22 rivets were increased of the same increasing factor Ω_1 adopted for the one-rivet connections (Fig. 6.3). For long connections, however, some consideration must be done for the calibration of the plate's stress-strain relationship.

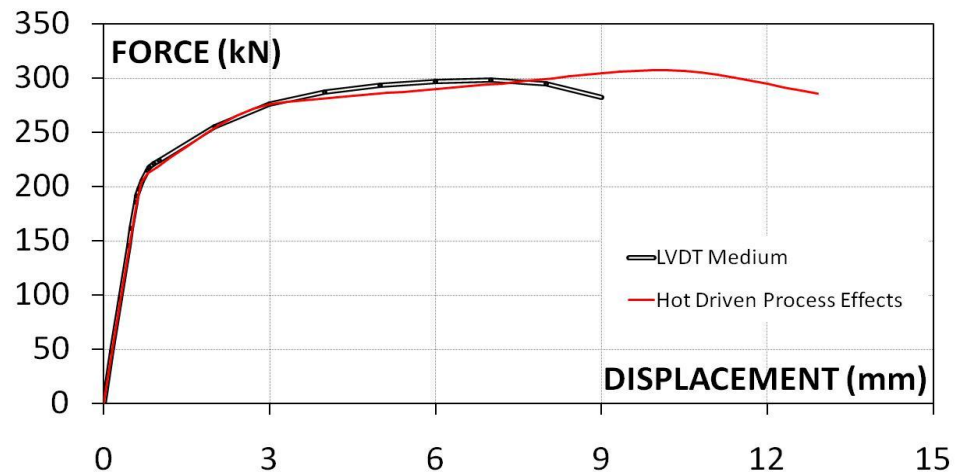


Figure 6.4 Hot driven process effects on S-22-12-4-S joint response.

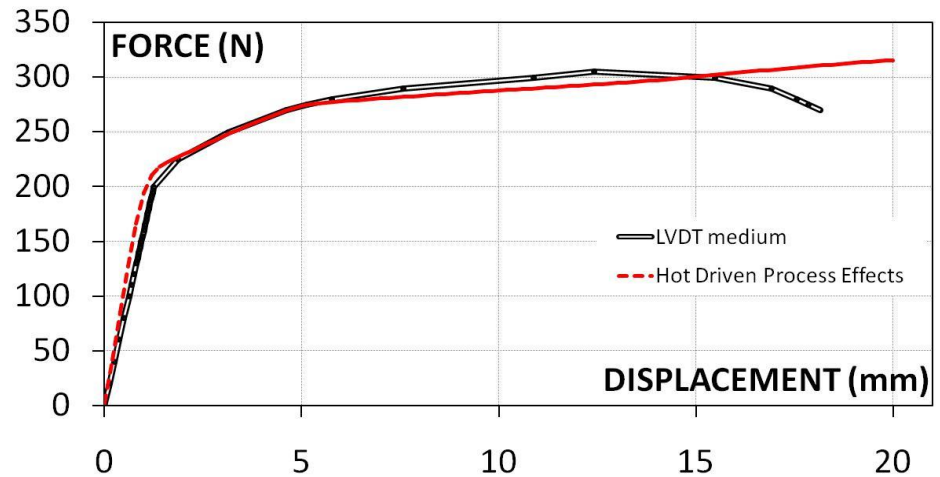


Figure 6.5 Hot driven process effects on U-22-12-4-S joint response.

As described in the chapter 5, the ductility of the plate material must be reduced of about 45% to take into account the presence of more rivets, that influence the mechanical properties of the plates during the cooling, and to consider the influence of the forming process of more holes, that weak the plates.

The response of F.E. models with the increasing factor are reported in the next Figures. It is possible to note that, varying the geometries and the typologies of connections, the responses always catch the experimental curves increasing the stress-strain relationship by Ω_1 factor. On the basis of these considerations, the reliability of both F.E. Models and theoretical formulas are confirmed.

6.2 RIVET CLAMPING

The magnitude of rivet clamping is uncertain, due to the uncertainty of hand driving. In the previous chapter, once the material was calibrated, a sensitivity study on probably values of rivet clamping forces was carried out. To evaluate the effect of different values of rivet clamping, a parametric analysis on riveted connections was performed. The values of rivet clamping were set starting from a value of 10% of the nominal yielding stress of the rivet steel to a value of 80%.

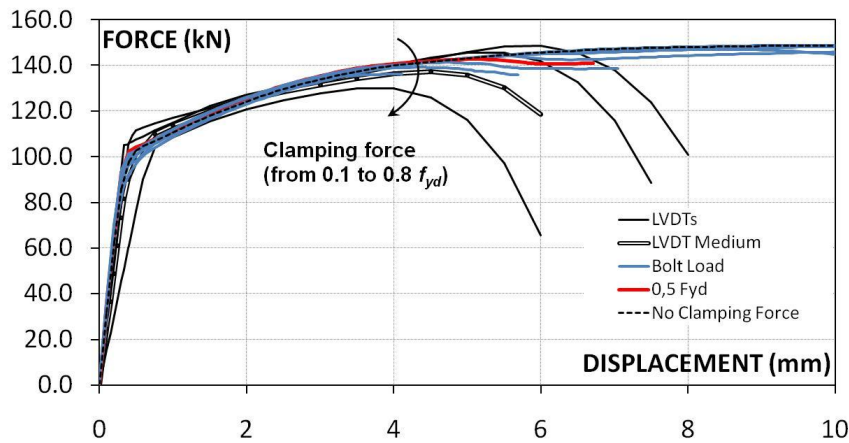


Figure 6.6 Effects of the variation of the rivet clamping force on S-16-10-1-S joint response.

In case of one rivet joints (S-16-10-1-S and U-16-10-1-S), the increasing of clamping force induces a reduction of joint ultimate strength. This phenomenon is due to the presence, in one rivet connections failure modes, of secondary effects. These effects, that are secondary bending moment in unsymmetrical connections and bearing in the inner plate for symmetric connections, are penalized by the presence of higher clamping forces, and determined a decrease of the ultimate strength of connection.

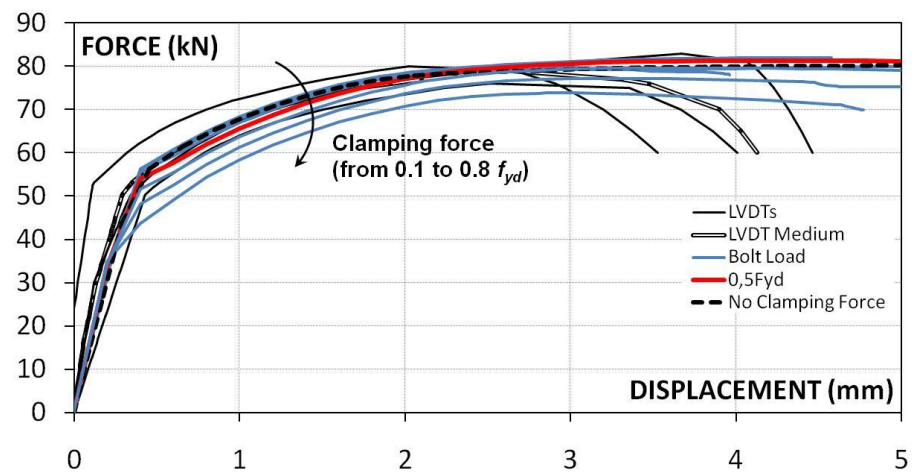


Figure 6.7 Effects of the variation of the rivet clamping force on U-16-10-1-S joint response.

In case of four rivets joints (S-16-10-1-S and U-16-10-1-S), the increasing of clamping force induces an increase of joint ultimate strength. This phenomenon confirms the above considerations on net efficiency, which occurs in case of collapse for tension in the net section. These connections, indeed, failed for tension in the net section.

As given by D’Aniello et al. (2010), “This phenomenon may be attributed to the fact that the presence of the hole also gives rise to transverse stresses generating a sort of multiple-stress effect (Schenker et al; 1954), emphasized by the presence of clamping force in the rivets, which avoid free lateral contractions in their vicinity.”

The magnitude of clamping force, indeed, emphasizes the net efficiency, as illustrated in the next Figures, increasing of about 10% the ultimate strength of the connection.

For what concern the S-22-12-4-S, the ultimate strength obtained without clamping forces is equal to 299 kN; instead, the ultimate strength of the connection with a rivet clamping force equal to $0.8 f_{yd}$ is equal to 316 kN. The increase from the model without clamping force to the model with a clamping force equal to $0.8 f_{yd}$ is about 10%. The ratio between these two strengths is equal to 0.95.

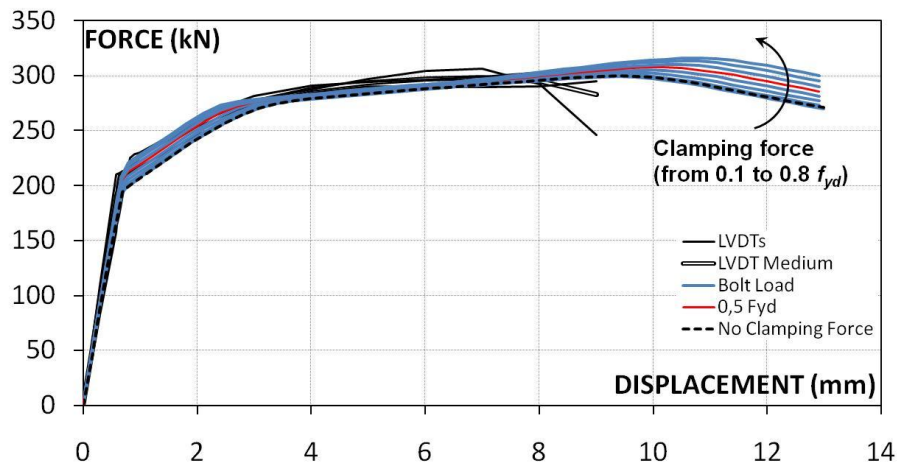


Figure 6.8 Effects of the variation of the rivet clamping force on S-22-12-4-S joint response.

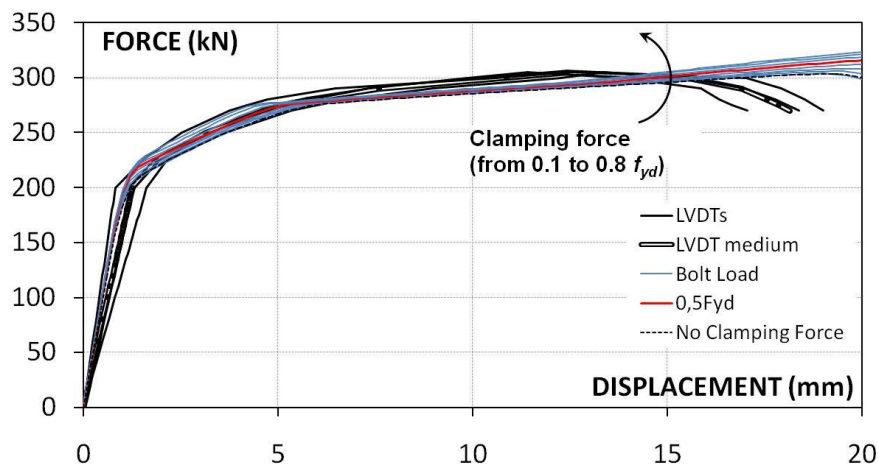


Figure 6.9 Effects of the variation of the rivet clamping force on U-22-12-4-S joint response.

For what concern the U-22-12-4-S, the ultimate strength obtained without clamping forces is equal to 303 kN; instead, the ultimate strength of the connection with a rivet clamping force equal to $0.8 f_{yd}$ is equal to 324 kN. The increase from the model without clamping force to the model with a clamping force equal to $0.8 f_{yd}$ is about 10%. The ratio between these two strengths is equal to 0.93.

These considerations confirm the important role of clamping forces in terms of determination of the ultimate strength of the riveted connections. When the failure occurs for tension in the net section, the presence of rivet clamping force determines a higher or not resistance of the joint.

The variation of the ultimate strength from joints without clamping force and joints with a clamping force equal to $0.8 f_{yd}$ confirms the reliability of the proposed theoretical formulas. Indeed, D'Aniello et al. (2010) modified the Eurocode formula (4.1):

$$N_{u,Rd} = \frac{0.9 \cdot f_u \cdot A_{net}}{\gamma_{M2}}$$

by assuming no reduction factor (4.8):

$$N_{u,Rd} = \frac{f_u \cdot A_{net}}{\gamma_{M2}}$$

The average value of the ratio between the numerical model without clamping force and the numerical model with a clamping force equal to $0.8 f_{yd}$ is about 0.94, as proposed by D'Aniello et al. in their formula.

6.3 CONCLUSIVE REMARKS

In this chapter, a comparison of numerical and theoretical results was performed, to ensure the reliability of both the F.E. models and the proposed formulas. On the basis of sensitivity studies, the entity of the hot driven process effects was confirmed. The rivets constitutive material, indeed, is increased of about 20%, according to the

experimental results and the theoretical formulation. The numerical results demonstrated that the different configurations of riveted connections modelled with this increasing factor give a good response, which is well superimposed to the experimental curves. This comparison confirms the good accuracy of the numerical model, and the good agreement between experimental results, theoretical formulation and F.E. model.

The same considerations have been made for what concern the rivet clamping forces. A sensitivity study on the value of this force has been made, and a average value of clamping equal to $0.5 f_{yd}$ was considered as the optimal value to describe the riveted connection behaviour. Furthermore, the variation of the clamping force from a value equal to 0 to a value equal to $0.8 f_{yd}$ confirms the corrective theoretical formula for evaluate the ultimate strength in case of traction failure in the net section, and the effects of the net efficiency on the overall behaviour of these joints, as observed during the experimental activity. These considerations confirm the good accuracy of the numerical model, and the good agreement between experimental results, theoretical formulation and F.E. model.

7 CONCLUSIONS

In this work a wide experimental, theoretical and numerical research is presented. The study is aimed to investigate the behaviour of lapped riveted connections loaded in shear typically adopted in aged metal structures still in service. The final objective is the development of a valid methodology of prevision of the existing riveted connections behaviour.

The present work was framed in different steps, each of them devoted to the achievement of a partial objective.

In detail, the first step has the objective of the extension of the literature experimental and numerical results on riveted connections to different materials, geometries and configurations, due to the sensitivity of the connection response to the manufacturing process (Hechtman, 1948; Schenker et al., 1954, Munse, 1970). Indeed, despite many studies have investigated the behaviour of riveted connections, it is necessary to deepen the behaviour of these joints varying the geometries and the material characteristics.

To achieve this partial objective, a large experimental investigation carried out within the framework of the European project PROHITECH. This investigation was performed on riveted specimens made of aged steel, manufactured with the techniques in use in Italian railway practice. Specimen geometry was detailed as required by RFI. The steel constituting plates and rivets was characterized by performing both mechanical and chemical tests. Tests showed good mechanical and chemical properties (strength, chemical composition).

The results of the lap-shear tests are reported and discussed, and the main characteristics of the riveted connections behaviour are reported and confronted with the existing literature.

Furthermore, a comparison between the experimental strengths and the failure modes and the results predicted by applying the formulas given in EN 1993:1-8 was made. It was recognized that the approach given in the code is conservative in all examined cases. However, the scatter between experimental and calculated strength seems excessively precautionary.

On the basis of the obtained experimental results, the second step was planned and carried out, with the aim to evaluate the riveted connections local phenomena and propose corrective factors to the actual codes verifications.

To achieve this partial objective, some modifications to EN 1993:1-8 prediction formulas are proposed. The influence of the hot-driven process and of the net efficiency effect were considered to formulate the provided equations. The results obtained by applying these proposed formulas are closer to the experimental strengths than those given by EN 1993:1-8, in terms of both the ultimate strengths and the failure mechanisms. However, it is necessary to deepen some aspects not considered during this experimental activity, such as the effect of the friction resistance on the bearing mechanism and the presence of more rows of rivets in the connection.

Due to the fact that no distinction is made in EN 1993 between riveted and bolted connections, new design equations are proposed to verify both the rivet shear and net area resistance, preserving the same simplicity of Eurocode verification procedure and providing more reliable control on the behaviour of riveted connections.

The third and last objective is the development of a reliable F.E. model of the tested connections, which could be extended to any other riveted connections. On the basis of the tests results, a 3D, highly detailed, finite element model of four different typologies of riveted connections is implemented, and the numerical results are compared with the experimental and theoretical ones, to ensure its reliability.

The models incorporate non-linear material properties for all the connection components, geometric non-linearity and contact interaction by means of the ABAQUS/Standard code.

The hot driven process was taken into account by increasing the material stress strain relationship by a factor, determined according to literature and the average values obtained by experimental tests. In longer joints, where more than two rivets are present, the plate material presents a weakening caused by the formation of holes and a reduction of the ductility due to the influences of heat deriving by the hot driven process of rivets. These phenomena were taken into account by decreasing the plate stress-strain relationship of about the 45%, according to literature (Bailey et al., 1979; Nack et al., 1983; Malina et al., 2005).

The clamping action caused by the cooling of rivet was modelled in two different ways:

1. by applying a relative displacement between the two ends of the rivet and then by releasing the shank;
2. by applying a bolt load in the middle of the rivet shank.

Both the methods described well the connections behaviour and reproduce their effective failure modes, observed during experimental tests. In detail the clamping force in the first method is variable during the analysis, reproducing the real behaviour of the rivet forming process. However, the F.E. model is complicated and less rational. In the second method, the clamping force remains constant during the analysis, but the model presents less steps and force, resulting more rational.

Finally, to achieve the final objective of the development of a valid methodology of prevision of the existing riveted connections behaviour, a comparison of numerical and theoretical results was performed.

On the basis of sensitivity studies, the entity of the hot driven process effects was confirmed.

A sensitivity study on the value of clamping force has been also made, and the variation of this force from a value equal to 0 to a value equal to $0.8 f_{yd}$ confirms the corrective theoretical formula for evaluate the ultimate strength in case of traction failure in the net section, and the effects of the net efficiency on the overall behaviour of these joints, as observed during the experimental activity.

These considerations confirm the good accuracy of the numerical model, and the good agreement between experimental results, theoretical formulation and F.E. model.

8 FURTHER DEVELOPMENTS: CFRP-TO-STEEL STRENGTHENING

As described above, Historic metal structures are an important part of the architectural and cultural heritage that needs to be preserved. The majority of historic steel structures are still in service and are exposed to loads that are larger than was expected. After several decades from their erection, this class of constructions reveals some damages and/or structural inadequacies (Guerrieri et al., 2005). These types of constructions are generally characterized by trussed structural schemes. Hence, the failure of connections can produce the overall failure of the structure, because the riveted connections represent the weaker elements of these structures.

The present work is devoted to determine a reliable and simple tool for the individuation of the resistance of the existent riveted connections. An important development, which is already start, regards the possibility of strengthening these connections by using innovative techniques. The traditional strengthening method for steel structures is to cut and replacing steel plates or to attach additional plates to existing members. However, these techniques do not preserve the structure by deterioration, since steel plates are prone to corrosion and fatigue (Zhao et al., 2007).

A promising and increasingly economic method for strengthening historic steel structure is the application of externally bonded composite material plates. This technique allows increasing both the strength and buckling capacity of steel members and also the fatigue-life extension (Stratford et al., 2005) and crack patching (Bassetti et al., 2000).

The effectiveness and reliability of this strengthening/repairing method is mainly guaranteed by the anchorage of the fibers, which typically fails before the plate's tensile capacity is achieved. Therefore, debonding of FRP from the steel elements must first be addressed in order to obtain a fully composite action.

The present chapter focuses on the study of the influence of different bonding length on the type of failure of the joint and its influence on the ductility of the failure process. The aim is to develop a reliable bond-slip

model that does not require the measurements of local strains and based on the forces from pull-tests that can be measured accurately.

8.1 EXPERIMENTAL ACTIVITY

The main scope of the testing programme is to analyze the influence of different arrangements on the bonding strength of CFRP laminates on steel elements.

Tests on CFRP bonded butt steel plates both simple and wrapped are planned first. In particular, tests on simple bonded specimens allow: i) the characterization of the adhesive properties; ii) to analyse on the influence of different bonding length (Zhao et al. 2007), (Liu et al. 2009). Tests on wrapped specimens will give the possibility to investigate the importance of wrapping width on the anchorage strength.

Once the material characteristics and the optimal values for bonding length and wrapping depth are established, tests on symmetric and unsymmetrical lapped joints will be performed to study the effect of tapering and discontinuity on the bonding capacity of CFRP strengthening, which should be adopted for typical historic steel elements, as the riveted connections (D'Aniello et al. 2010).

8.1.1 Preparation of specimens and application of CFRPs

The surfaces of the steel plates were sandblasted to remove any rust patina, residues and grease to enhance the bonding capacity.

The composite materials are furnished by BASF–The Chemical Company. In particular, the thixotropic adhesive used for bonding the CFRP laminas is the MBRACE LAMINATE, which is a bicomponent resin with a mixing ratio 4/1 and an average pot-time of 20 minutes.

The CFRP laminas used for tests are the MBT HM 5/1,4, having ultimate tensile strength $f_{tk}=2050\text{MPa}$, mean elastic modulus $E_f=200000\text{MPa}$, 50mm width and 1.4 mm thickness.

The mean thickness of adhesive layer was 1 mm. The CFRP bond is obtained by applying an adhesive layer, placing CFRP laminas and pressing-down the lamina to steel plate until the adhesive is sufficiently dried. The adhesive is cured for seven days.

A double layer of MBRACE FIBRE HM sheets ($f_{tk}=2500\text{MPa}$, $E_f=390000\text{MPa}$, 0.165 mm thickness) are used for wrapping. The wrapping sheets were applied by means of the bicomponent epoxy resin MBRACE SATURANT, having a mixing ratio 3/1 and an average pot-time of 30 minutes.

8.1.2 Investigated parameters and experimental programme

The investigated parameters are explained as follows:

1. *Bonding length*: different lamina lengths were considered; in particular 150 mm, 200 mm (recommended by Italian code CNR-DT 200/2004) and 250 mm lengths were adopted.
2. *Adhesive behaviour*: the bonding capacity is directly influenced by the type of adhesive.
3. *Presence of wrapping*: the effects of the wrapping on the slip resistance were analyzed. To this end, different wrapping depths were considered, according to literature (CNR-DT 200/2004; Cadei et al. 2004): 100 mm and 150 mm.
4. *Load eccentricity*: both symmetric and unsymmetrical specimens were considered in order to analyze the effects of secondary bending moments induced by load eccentricity on adhesive deformation and strength (D'Aniello et al. 2010).

A total of 45 simple bonding tests are prepared, as summarized in the programme matrix reported in Table 8.1, but until now only simple bonding specimens are performed.

The geometries of the investigated connections are shown in Table 8.2. Specimens were labelled as C-B-W, where:

C is the splice configuration (e.g. Bu: Butt; S: Symmetric; U: Unsymmetrical);

B is the bonding length (e.g. 150, 200, 250 mm);

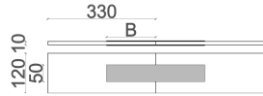

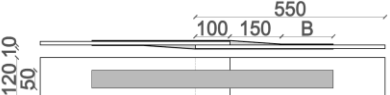
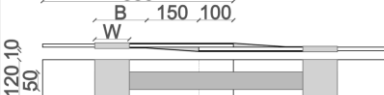
W is the wrapping depth (e.g. 100, 150 mm);

Three nominally identical samples were built up for every type of specimen.

Table 8.1 Bonding test programme matrix.

Specimen tag	Butt	Symm.	Unsymm.	B (mm)	W (mm)	Test no.
Unwrapped						
B150	✓	✓		150		3 (a, b, c)
B200	✓	✓		200		3 (a, b, c)
B250	✓	✓		250		3 (a, b, c)
U-B150			✓	150		3 (a, b, c)
U-B200			✓	200		3 (a, b, c)
U-B250			✓	250		3 (a, b, c)
Wrapped						
B150W100	✓	✓		150	100	3 (a, b, c)
B150W150	✓	✓		150	150	3 (a, b, c)
U-B150W100			✓	150	100	3 (a, b, c)
U-B150W150			✓	150	150	3 (a, b, c)

Table 8.2 Bonding test specimens.

	Unwrapped	Wrapped
Butt		
Lapped		
Unsymmetrical		

8.1.3 Set-up of adherence and riveted connection

The experimental setup is shown in Figure 8.1(a). In particular, tests were carried out with a universal electro-mechanical Zwick/Roell testing machine (Fig. 8.1(b)). The specimens were loaded in tension under displacement control until failure, i.e. after the load decreased.

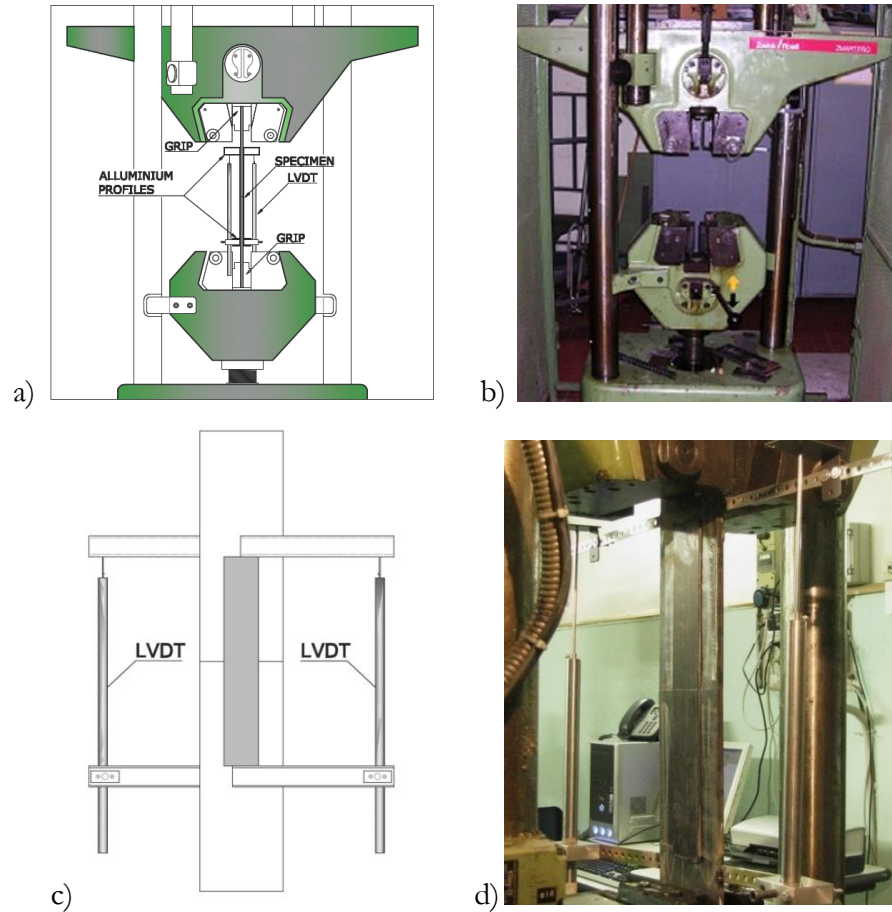


Figure 8.1 Test setup (a); the testing machine (b); the layout of LVDTs (c, d)

The maximum load reached and the types of failure mode were observed for each test. The relative in-plane displacement of tested specimens was measured by means of a pair of LVDT (Linear Variable Differential Transformer) characterized by a displacement range of ± 150 mm and positioned on both ends of the CFRP lamina (Fig. 8.1(c) and (d)). The displacement rate was fixed at 0.1 mm/s and an acquisition frequency of 10 Hz was assumed (D’Aniello et al. 2010).


8.2 EXPERIMENTAL RESULTS

8.2.1 Failure modes for simple bonding tests

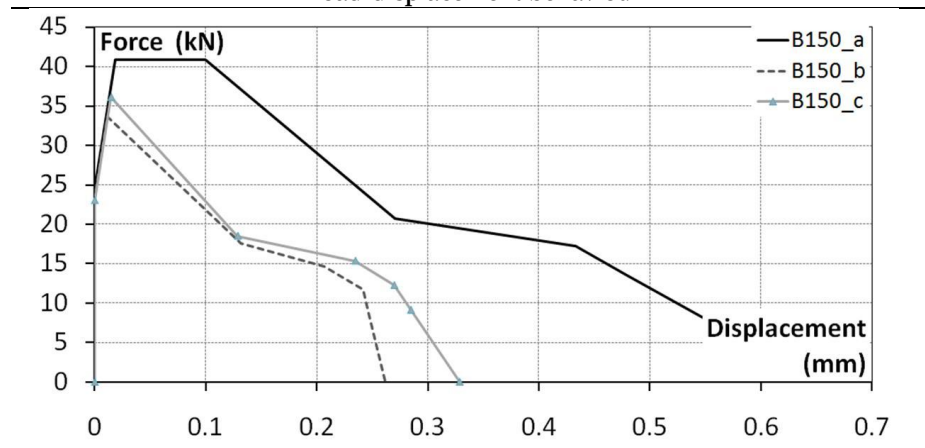
After the tests, it was observed the collapse mode experienced by both sides of each specimen, hereinafter labelled side A and B, respectively.

Table 8.3 Failure modes and load-displacement curves for B150.

B150_a		B150_b		B150_c	
Ultimate load (kN)		Ultimate load (kN)		Ultimate load (kN)	
40.835		33.7		36.12	
A side	B side	A side	B side	A side	B side
Delamin.	Delamin.	Delamin.	Delamin.	Delamin.	Delamin.









Load-displacement behaviour

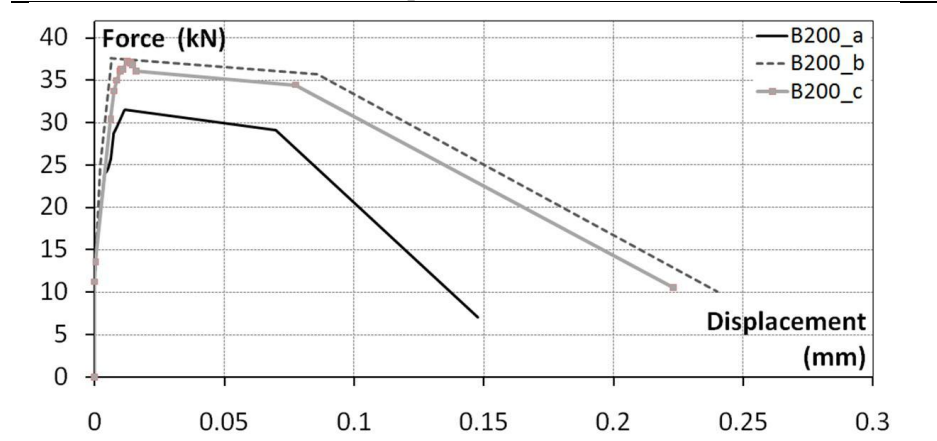


From Table 8.3 to 8.5, all collapse modes are described. The main collapse mode observed after tests was the delamination of the CFR lamina, with the crack propagating within the FRP plate. These cracks are determined by the separation of some carbon fibers from the resin matrix.

Table 8.4 Failure modes and load-displacement curves for B200.

B200_a		B200_b		B200_c	
Ultimate load (kN)		Ultimate load (kN)		Ultimate load (kN)	
31.61		37.625		37.295	
A side	B side	A side	B side	A side	B side
Adhesive/ Delamin.	Adhesive/ Delamin.	Adhesive/ Delamin.	Delamin.	Adhesive/ Delamin.	Adhesive/ Delamin.
					

Load-displacement behaviour









Indeed, it can be observed that the main part of specimens present a thin layer of fiber attached to the adhesive layer after the failure. This kind of failure mode means that in such FRP-to-steel bonded joints, the adhesive

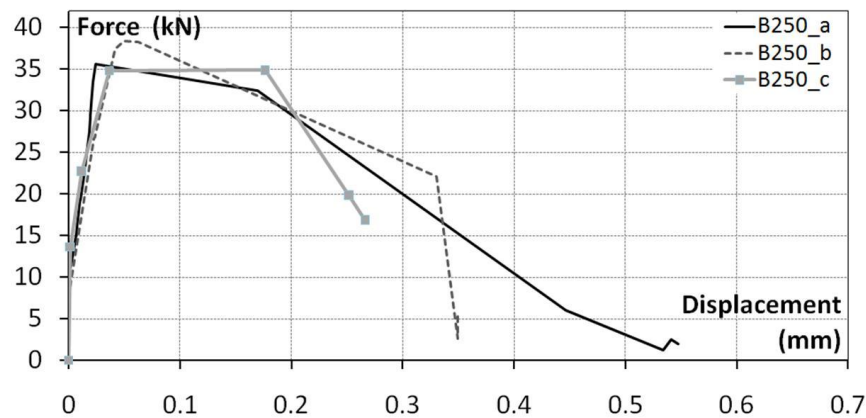
and the FRP-to-adhesive and the adhesive-to-steel layers can be stronger than interfaces between fibers and matrix within the FRP lamina.

Table 8.5 Failure modes and load-displacement curves for B250.

B250_a		B250_b		B250_c	
Ultimate load (kN)		Ultimate load (kN)		Ultimate load (kN)	
36.12		38.41		34.825	
A side	B side	A side	B side	A side	B side
Adhesive/ Delamin.	Delamin.	Adhesive/ Delamin.	Adhesive/ Delamin.	Delamin.	Adhesive/ Delamin.

Load-displacement behaviour



These failure modes are to that observed in previous research (Xia et al., 2005). Initially, debonding occurred at the loaded end within the adhesive layer. As debonding propagated, failure moved towards the FRP layer separating the carbon fibres from the resin matrix or moved within the interface of the adhesive and the FRP plate.

Another kind of collapse that can occur is the cohesive failure within the adhesive layer. In this case, the cracks start and propagate within the adhesive layer. A thin layer of adhesive was attached to the FRP lamina after failure. This failure is not observed in tests, but a combination of the delamination and the cohesive failure was observed, denoted as “adhesive/delamination”. In this case, adhesive failure occurred after the delamination crack had propagated over a substantial part of the interface towards the free end of the FRP lamina.

The pure debonding failure, i.e. the FRP-to-adhesive and the adhesive-to-steel interfaces failure, were not observed. This demonstrates the strong bond capacity of the adhesive to the cleaned FRP lamina and to the roughened steel.

8.3 CONCLUSIVE REMARKS

This work shows the results of an experimental activity devoted to investigate the behaviour of CFRP strengthening on ancient steel elements. First of all, some simple bonding tests were performed to study the influence of different bonding length on the type of collapse and the ductility of failure. The performed tests showed that the bonding length has a notable influence on the failure mode. When the bonding length is equal to the value recommended from code (EN 10025, CNR-DT 200/2004); the type of collapse is adhesive/delamination, and the connection develops a considerable ductility before failure. When the bonding length is greater, the same type of failure occurs, but the connection develops ductility greater than the 200 mm ones. If the length is smaller, a pure delamination failure occurred.

9 APPENDIX

In the present appendix, all the experimental results are reported. First of all, the geometrical characteristics and the experimental set-up is describe, then the load displacement curves, the mechanical characteristics, the photos and the kind of collapse is reported.

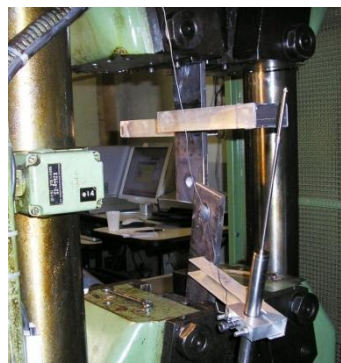
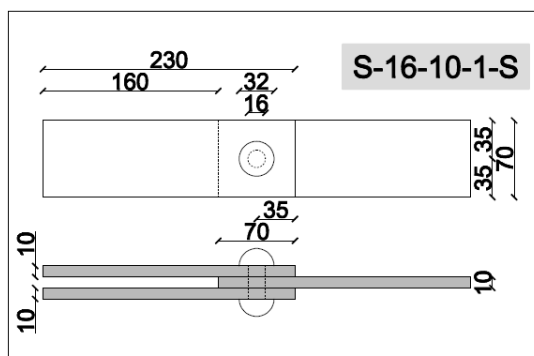
The experimental test machine is a universal electro-mechanical Zwick/Roell testing machine and is characterized by:

- the maximum load reached is 600 kN.
- the total machine stroke is 500 mm
- the displacement rate in elastic range is 0,01 mm/s, in the plastic range is 0,1 mm/s.
- the acquisition frequency is equal to 10 Hz.
- The relative in-plane displacement of tested specimens was measured by means of a pair of LVDT (Linear Variable Differential Transformer) characterized by a displacement range of ± 150 mm and positioned 30 mm from both ends of the regions where plate discontinuities occur in all specimens

S-16-10-1-A

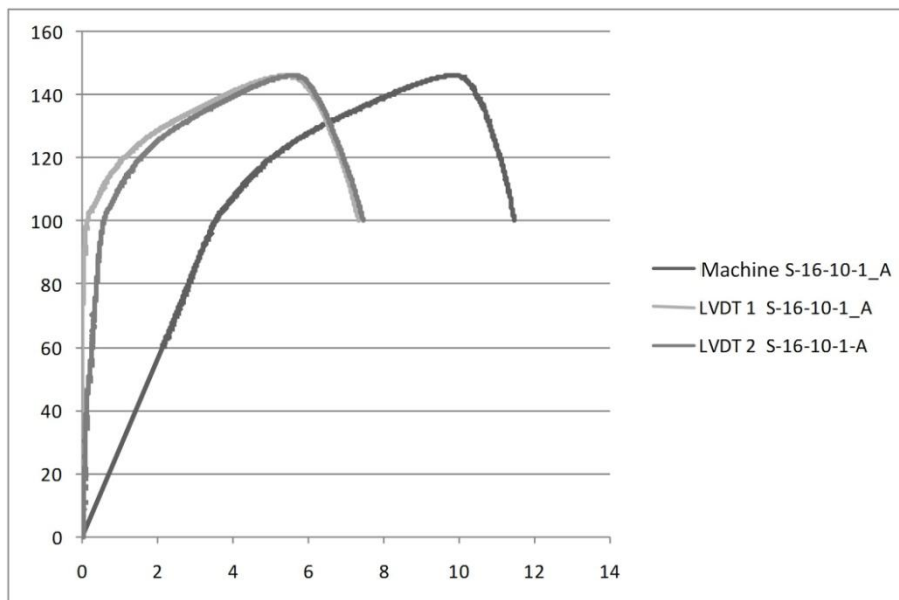
Specimen tag	S	U	Width plate (mm)	70
S-16-10-1-A	✓		Dist. from edge (mm)	35
Rivet diam. (mm)	16		Rivet pitch (mm)	—
Thickness plate (mm)	10		Rivet no.	1

PHOTOS



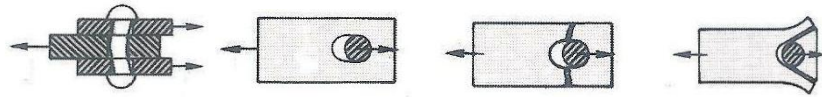
Test Information: The hole in the center plate was subjected to an ovalization: dimensions: 16x18,82 mm

RESULTS



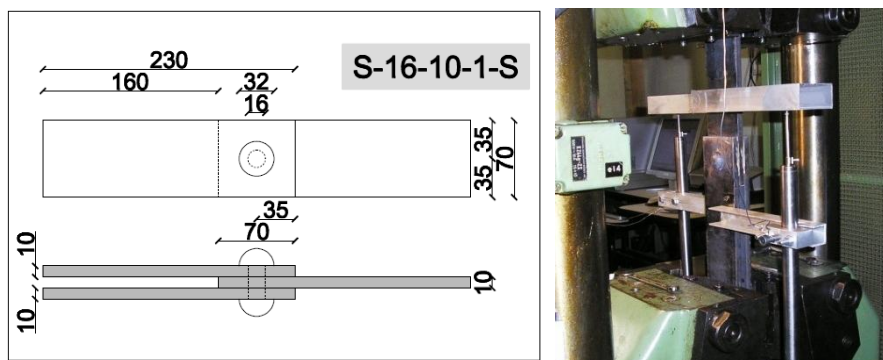


Peak: [kN]	$F_p = 146,08$	$d_{pav} = 9,89$	$d_{p1} = 5,41$	$d_{p2} = 5,61$
Elastic limit: [kN]	$F_{yaverage} = 96,69$	$d_{yaverage} = 3,15$	$d_{y1average} = 0,06$	$d_{y2average} = 0,46$
Ultimate: [kN]	$F_u = 116,87$	$d_{uav} = 11,16$	$d_{u1} = 6,95$	$d_{u2} = 7,04$
Stiffness: [kN/mm]		$K_{av} = 28,2$	$K_{LVD1} = 1500,1$	$K_{LVD2} = 135,18$

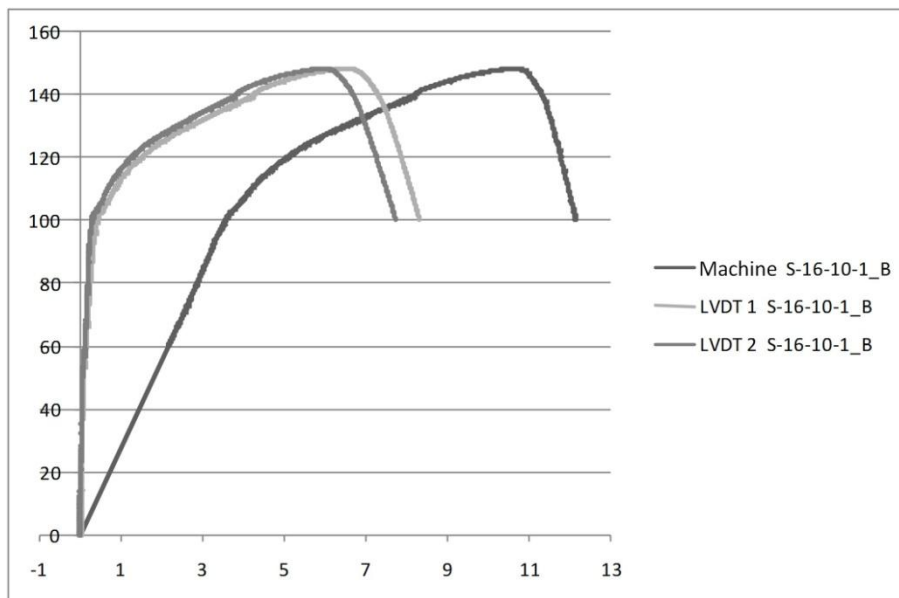
COLLAPSE MODE☒ Rivet Shear☐ Bearing☐ Tension☐ Shear out

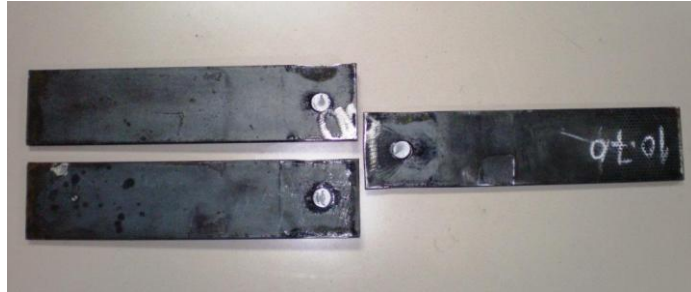
S-16-10-1-B

Specimen tag	S	U	Width plate (mm)	70
S-16-10-1-B	✓		Dist. from edge (mm)	35
Rivet diam. (mm)	16		Rivet pitch (mm)	—
Thickness plate (mm)	10		Rivet no.	1

PHOTOS

Test Information: The hole in the center plate was subjected to an ovalization: dimensions: 16x18,82 mm

RESULTS



Peak: [kN]	$F_p = 147,99$	$d_{pav} = 10,63$	$d_{p1} = 6,53$	$d_{p2} = 5,98$
Elastic limit: [kN]	$F_{yaverage} = 98,70$	$d_{yaverage} = 3,51$	$d_{y1average} = 0,39$	$d_{y2average} = 0,3$
Ultimate: [kN]	$F_u = 118,39$	$d_{uav} = 11,81$	$d_{u1} = 7,88$	$d_{u2} = 7,30$
Stiffness: [kN/mm]		$K_{av} = 28,01$	$K_{LVD1} = 139,84$	$K_{LVD2} = 212,74$

COLLAPSE MODE

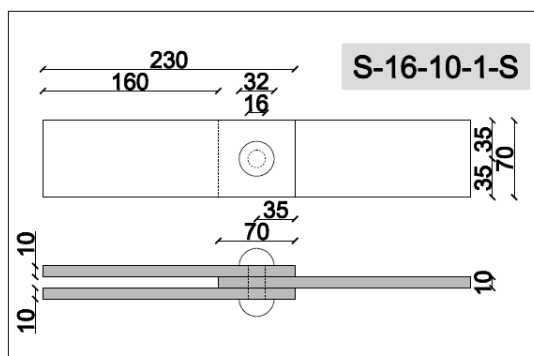
☒ Rivet Shear
 ☐ Bearing
 ☐ Tension
 ☐ Shear out



S-16-10-1-C

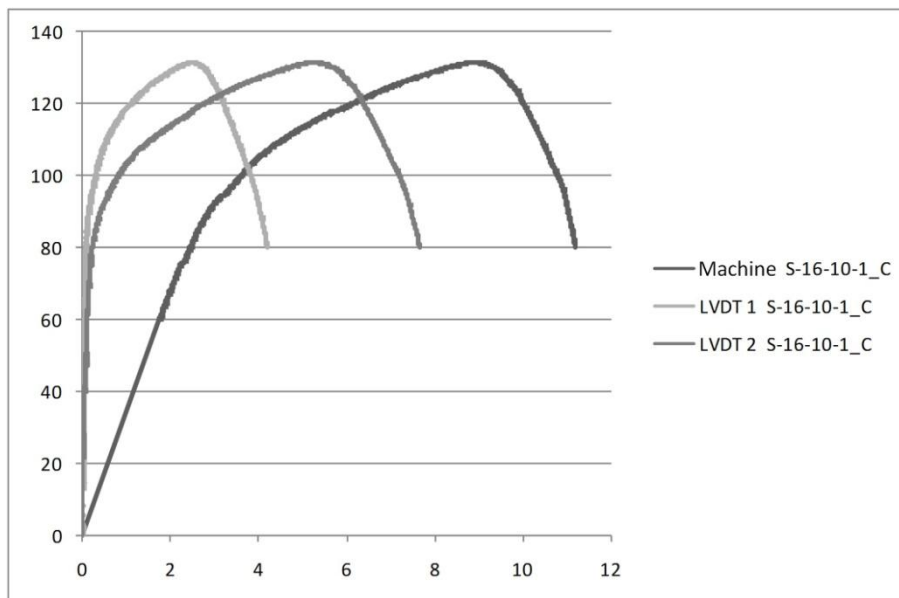
Specimen tag	S	U	Width plate (mm)	70
S-16-10-1-C	✓		Dist. from edge (mm)	35
Rivet diam. (mm)	16		Rivet pitch (mm)	—
Thickness plate (mm)	10		Rivet no.	1

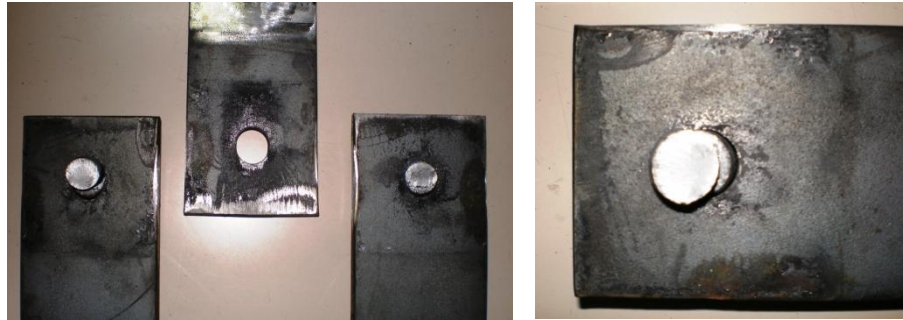
PHOTOS



Test Information: The hole in the center plate was subjected to an ovalization:
dimensions: 16x18 mm

RESULTS

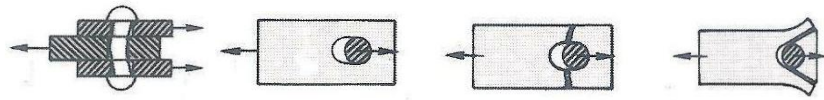




Peak: [kN]	$F_p = 131,43$	$d_{pav} = 8,94$	$d_{p1} = 2,51$	$d_{p2} = 5,29$
Elastic limit: [kN]	$F_{yaverage} = 81,38$	$d_{yaverage} = 2,52$	$d_{y1average} = 0,09$	$d_{y2medio} = 0,25$
Ultimate: [kN]	$F_u = 105,15$	$d_{uav} = 10,60$	$d_{u1} = 3,68$	$d_{u2} = 7,00$
Stiffness: [kN/mm]		$K_{av} = 34,06$	$K_{LVD1} = 500,63$	$K_{LVD2} = 218,85$

COLLAPSE MODE

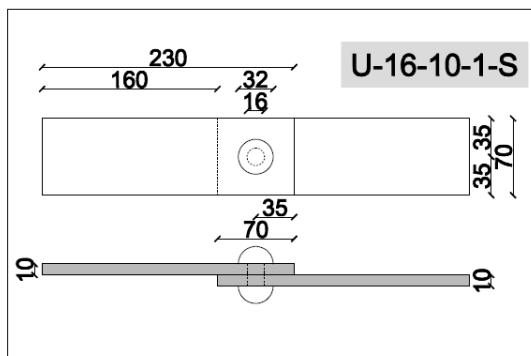
☒ Rivet Shear
 ☐ Bearing
 ☐ Tension
 ☐ Shear out



U-16-10-1-A

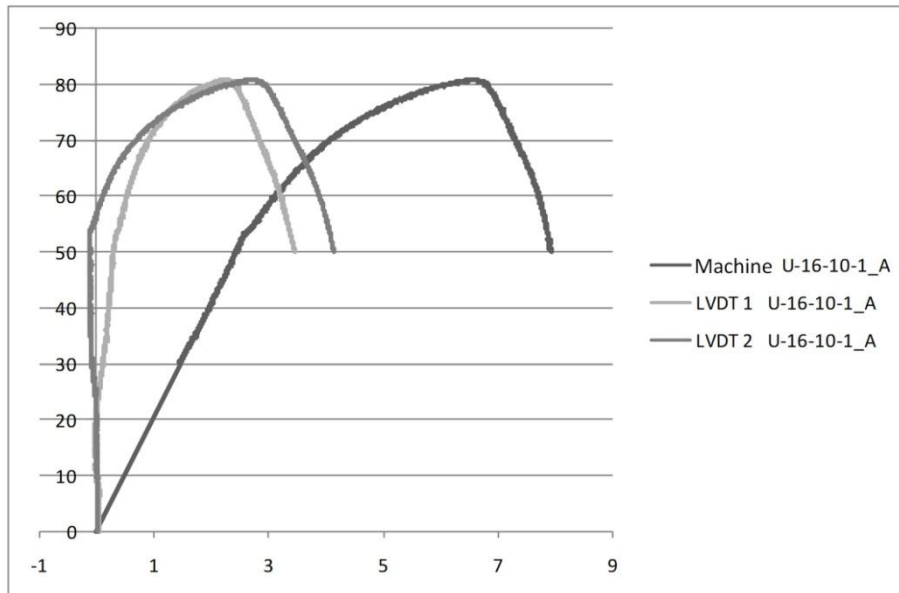
Specimen tag	S	U	Width plate (mm)	70
U-16-10-1-A		✓	Dist. from edge (mm)	35
Rivet diam. (mm)	16		Rivet pitch (mm)	—
Thickness plate (mm)	10		Rivet no.	1

PHOTOS



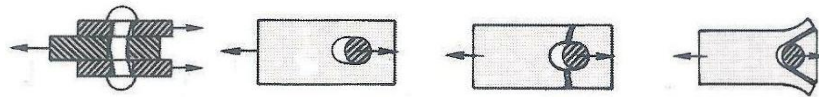
Test Information:

RESULTS





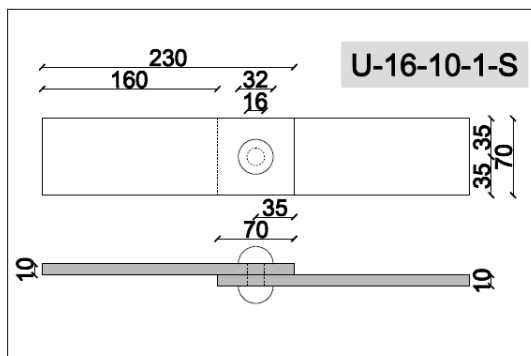
Peak: [kN]	$F_p = 80,02$	$d_{pav} = 6,57$	$d_{p1} = 2,25$	$d_{p2} = 2,74$
Elastic limit: [kN]	$F_{yaverage} = 52,67$	$d_{yaverage} = 2,55$	$d_{y1average} = 0,34$	$d_{y2average} = -0,1$
Ultimate: [kN]	$F_u = 64,65$	$d_{uav} = 7,54$	$d_{u1} = 3,05$	$d_{u2} = 3,72$
Stiffness: [kN/mm]		$K_{av} = 20,06$	$K_{LVD1} = 115,15$	$K_{LVD2} = -$

COLLAPSE MODE☒ Rivet Shear☐ Bearing☐ Tension☐ Shear out

U-16-10-1-B

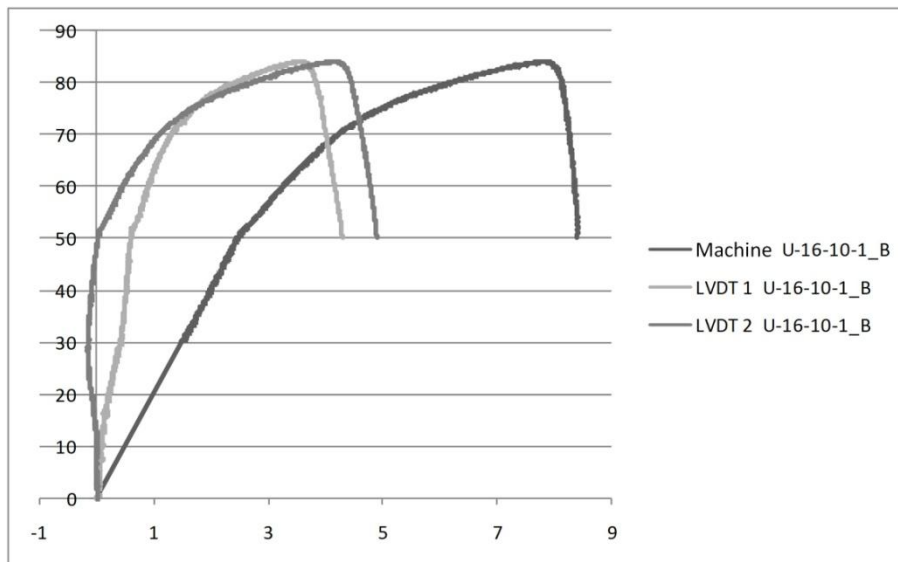
Specimen tag	S	U	Width plate (mm)	70
U-16-10-1-B		✓	Dist. from edge (mm)	35
Rivet diam. (mm)	16		Rivet pitch (mm)	—
Thickness plate (mm)	10		Rivet no.	1

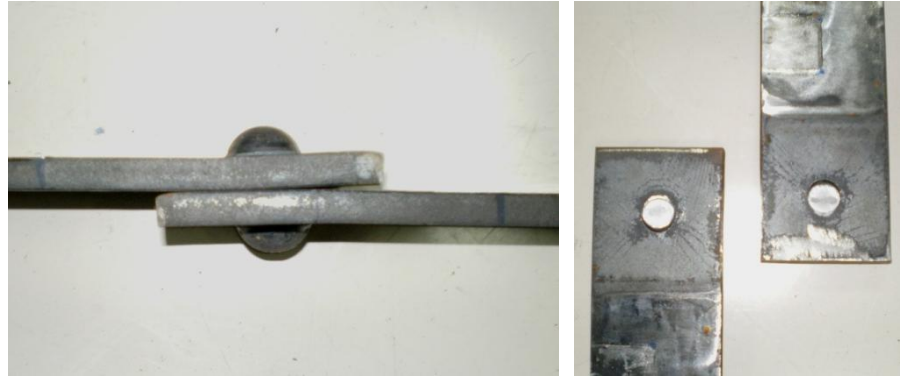
PHOTOS



Test Information: out of plane plastic deformation for each plate equal to 1,1 mm

RESULTS

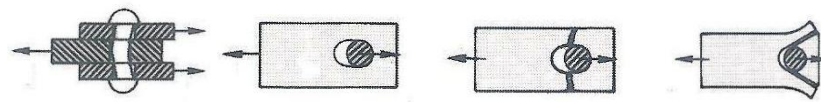




Peak: [kN]	$F_p = 83,95$	$d_{pav} = 7,80$	$d_{p1} = 3,52$	$d_{p2} = 4,13$
Elastic limit: [kN]	$F_{yaverage} = 50,68$	$d_{yaverage} = 2,52$	$d_{y1average} = 0,61$	$d_{y2average} = 0,04$
Ultimate: [kN]	$F_u = 67,16$	$d_{uav} = 8,30$	$d_{u1} = 4,04$	$d_{u2} = 4,68$
Stiffness: [kN/mm]		$K_{av} = 20,39$	$K_{LVD1} = 108,58$	$K_{LVD2} = -$

COLLAPSE MODE

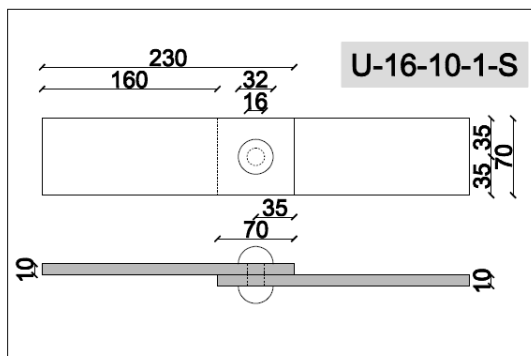
☒ Rivet Shear
 ☐ Bearing
 ☐ Tension
 ☐ Shear out



U-16-10-1-C

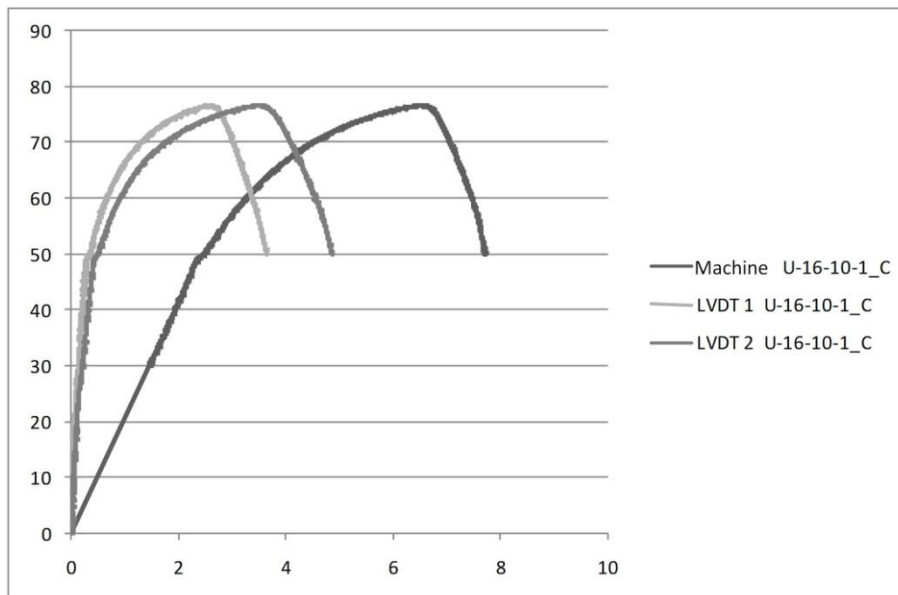
Specimen tag	S	U	Width plate (mm)	70
U-16-10-1-C		✓	Dist. from edge (mm)	35
Rivet diam. (mm)	16		Rivet pitch (mm)	—
Thickness plate (mm)	10		Rivet no.	1

PHOTOS



Test Information: out of plane plastic deformation for each plate equal to 1,1 mm

RESULTS

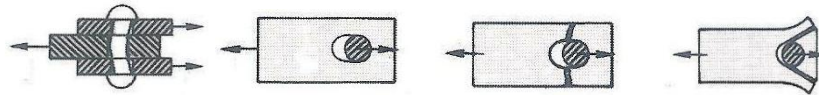




Peak: [kN]	$F_p = 76,71$	$d_{pav} = 6,54$	$d_{p1} = 2,61$	$d_{p2} = 3,51$
Elastic limit: [kN]	$F_{yaverage} = 49,02$	$d_{yaverage} = 2,35$	$d_{y1average} = 0,28$	$d_{y2average} = 0,42$
Ultimate: [kN]	$F_u = 61,37$	$d_{uav} = 7,41$	$d_{u1} = 3,33$	$d_{u2} = 4,49$
Stiffness: [kN/mm]		$K_{av} = 20,41$	$K_{LVD1} = 128,52$	$K_{LVD2} = 145,97$

COLLAPSE MODE

☒ Rivet Shear
 ☐ Bearing
 ☐ Tension
 ☐ Shear out

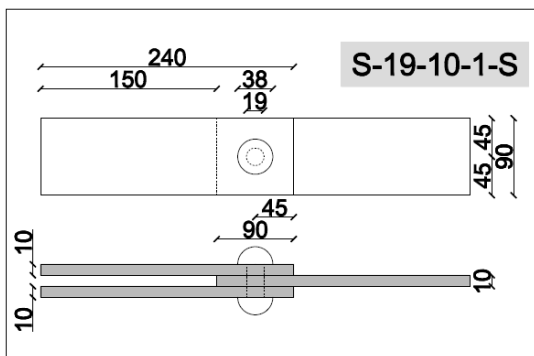


Appendix

S-19-10-1-A

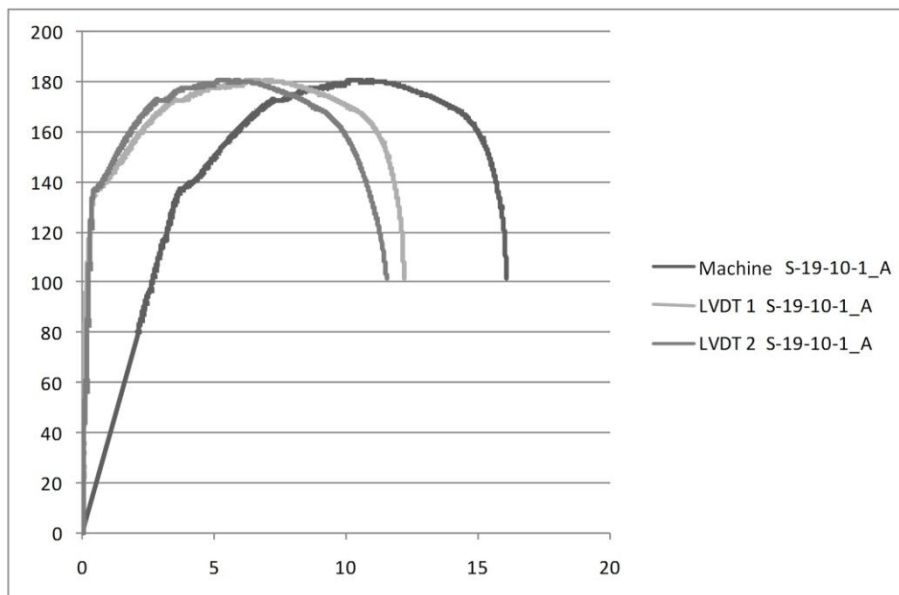
Specimen tag	S	U	Width plate (mm)	90
S-19-10-1-A	✓		Dist. from edge (mm)	45
Rivet diam. (mm)	19		Rivet pitch (mm)	—
Thickness plate (mm)	10		Rivet no.	1

PHOTOS



Test Information: plastic deformations and bearing of the inner plate, final plate width = 97 mm

RESULTS

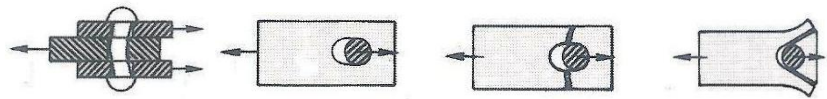




Peak: [kN]	$F_p = 180,45$	$d_{pav} = 10,23$	$d_{p1} = 6,36$	$d_{p2} = 5,24$
Elastic limit: [kN]	$F_{yaverage} = 136,01$	$d_{yaverage} = 3,66$	$d_{y1average} = 0,49$	$d_{y2average} = 0,43$
Ultimate: [kN]	$F_u = 144,36$	$d_{uav} = 15,58$	$d_{u1} = 11,74$	$d_{u2} = 10,60$
Stiffness: [kN/mm]		$K_{av} = 37,51$	$K_{LVD1} = 784,4$	$K_{LVD2} = 328,6$

COLLAPSE MODE

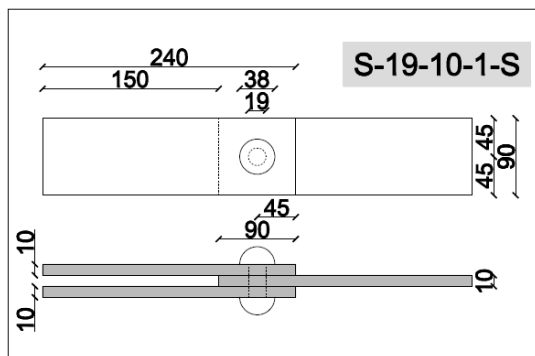
☐ Rivet Shear
 ☒ Bearing
 ☐ Tension
 ☐ Shear out



S-19-10-1-B

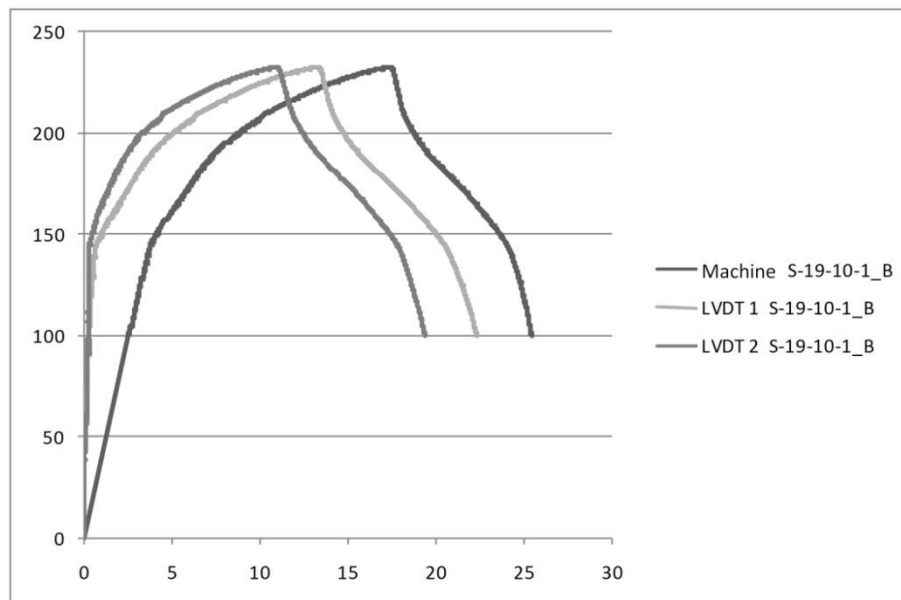
Specimen tag	S	U	Width plate (mm)	90
S-19-10-1-B	✓		Dist. from edge (mm)	45
Rivet diam. (mm)	19		Rivet pitch (mm)	—
Thickness plate (mm)	10		Rivet no.	1

PHOTOS



Test Information: plastic deformations and bearing of the inner plate, final plate width = 107 mm

RESULTS





Peak: [kN]	$F_p = 232,35$	$d_{pav} = 17,33$	$d_{p1} = 13,26$	$d_{p2} = 10,90$
Elastic limit: [kN]	$F_{yaverage} = 141,70$	$d_{yaverage} = 3,67$	$d_{y1average} = 0,62$	$d_{y2average} = 0,29$
Ultimate: [kN]	$F_u = 185,88$	$d_{uav} = 19,88$	$d_{u1} = 15,99$	$d_{u2} = 13,61$
Stiffness: [kN/mm]		$K_{av} = 39,14$	$K_{LVD1} = 69,34$	$K_{LVD2} = 222,2$

COLLAPSE MODE

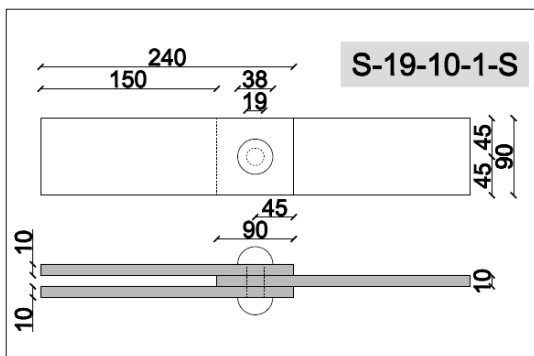
☐ Rivet Shear
 ☒ Bearing
 ☐ Tension
 ☐ Shear out



S-19-10-1-C

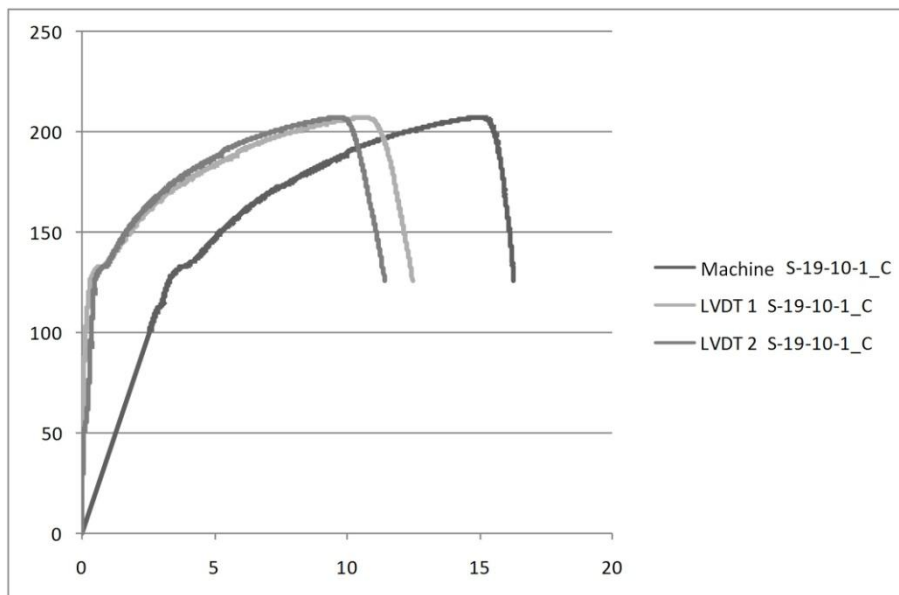
Specimen tag	S	U	Width plate (mm)	90
S-19-10-1-C	✓		Dist. from edge (mm)	45
Rivet diam. (mm)	19		Rivet pitch (mm)	—
Thickness plate (mm)	10		Rivet no.	1

PHOTOS



Test Information: plastic deformations and bearing of the inner plate, final plate width = 92 mm; ovaled hole final dimensions = 27x19 mm

RESULTS

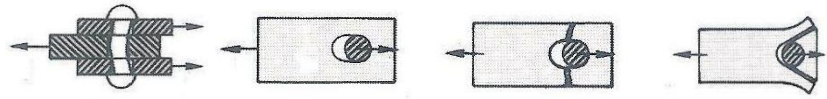




Peak: [kN]	$F_p = 207,12$	$d_{pav} = 14,95$	$d_{p1} = 10,56$	$d_{p2} = 9,63$
Elastic limit: [kN]	$F_{yaverage} = 130,02$	$d_{yaverage} = 3,53$	$d_{y1average} = 0,44$	$d_{y2average} = 0,61$
Ultimate: [kN]	$F_u = 165,69$	$d_{uav} = 16,03$	$d_{u1} = 11,93$	$d_{u2} = 10,86$
Stiffness: [kN/mm]		$K_{av} = 39,02$	$K_{LVD1} = 724,95$	$K_{LVD2} = 246,02$

COLLAPSE MODE

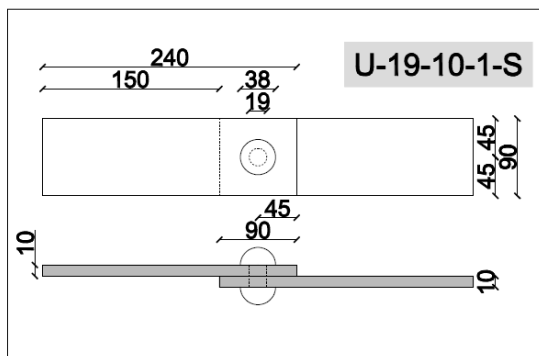
☐ Rivet Shear
 ☒ Bearing
 ☐ Tension
 ☐ Shear out



U-19-10-1-A

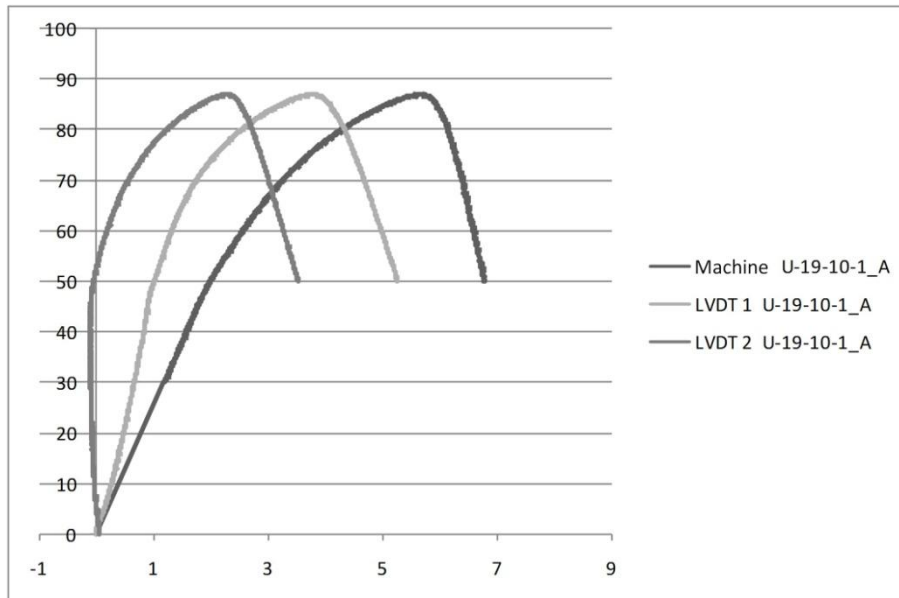
Specimen tag	S	U	Width plate (mm)	90
U-19-10-1-A		✓	Dist. from edge (mm)	45
Rivet diam. (mm)	19		Rivet pitch (mm)	—
Thickness plate (mm)	10		Rivet no.	1

PHOTOS



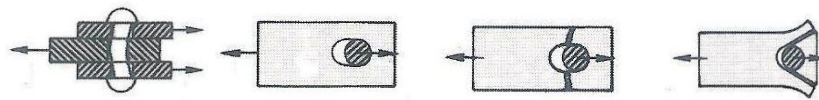
Test Information

RESULTS





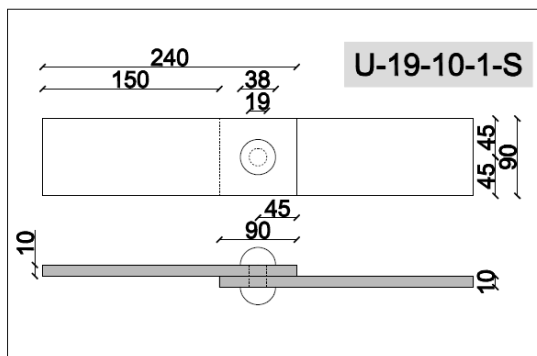
Peak: [kN]	$F_p = 86,99$	$d_{pav} = 5,65$	$d_{p1} = 3,79$	$d_{p2} = 2,29$
Elastic limit: [kN]	$F_{yaverage} = 47,36$	$d_{yaverage} = 1,86$	$d_{y1average} = 0,94$	$d_{y2average} = -0,08$
Ultimate: [kN]	$F_u = 69,59$	$d_{uav} = 6,39$	$d_{u1} = 4,68$	$d_{u2} = 3,02$
Stiffness: [kN/mm]		$K_{av} = 25,38$	$K_{LVD1} = 59,52$	$K_{LVD2} = -$

COLLAPSE MODE☒ Rivet Shear☐ Bearing☐ Tension☐ Shear out

U-19-10-1-B

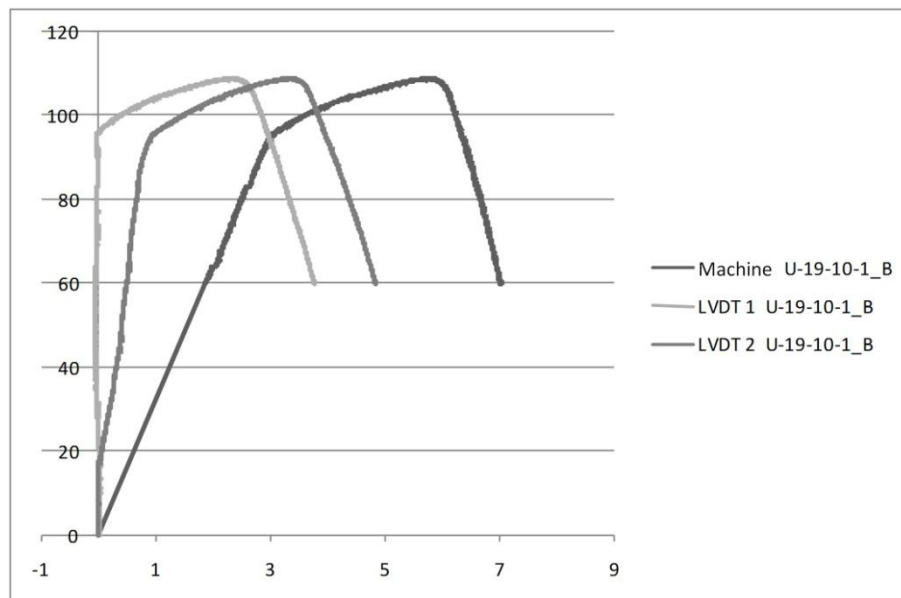
Specimen tag	S	U	Width plate (mm)	90
U-19-10-1-B		✓	Dist. from edge (mm)	45
Rivet diam. (mm)	19		Rivet pitch (mm)	—
Thickness plate (mm)	10		Rivet no.	1

PHOTOS



Test Information: out of plane plastic displacement for each plate: 1.1 mm; all holes are oveled, final dimensions: 21x19 mm

RESULTS





Peak: [kN]	$F_p = 108,93$	$d_{pav} = 5,77$	$d_{p1} = 2,34$	$d_{p2} = 3,35$
Elastic limit: [kN]	$F_{yaverage} = 95,34$	$d_{yaverage} = 3,02$	$d_{y1average} = -0,03$	$d_{y2average} = 0,95$
Ultimate: [kN]	$F_u = 87,14$	$d_{uav} = 6,50$	$d_{u1} = 3,17$	$d_{u2} = 4,19$
Stiffness: [kN/mm]		$K_{av} = 32,07$	$K_{LVDT1} = -$	$K_{LVDT2} = 113,52$

COLLAPSE MODE

☒ Rivet Shear
 ☐ Bearing
 ☐ Tension
 ☐ Shear out



U-19-10-1-C

Specimen tag	S	U	Width plate (mm)	90
U-19-10-1-C		✓	Dist. from edge (mm)	45
Rivet diam. (mm)	19		Rivet pitch (mm)	—
Thickness plate (mm)	10		Rivet no.	1

PHOTOS

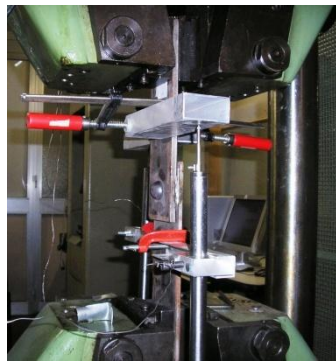
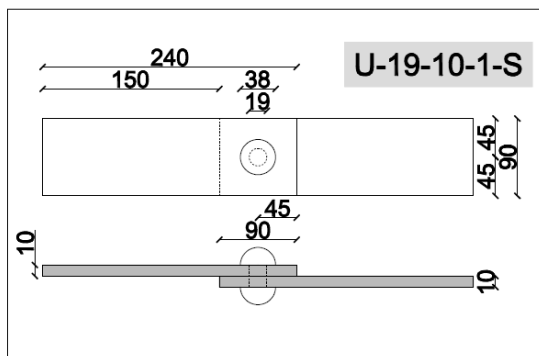
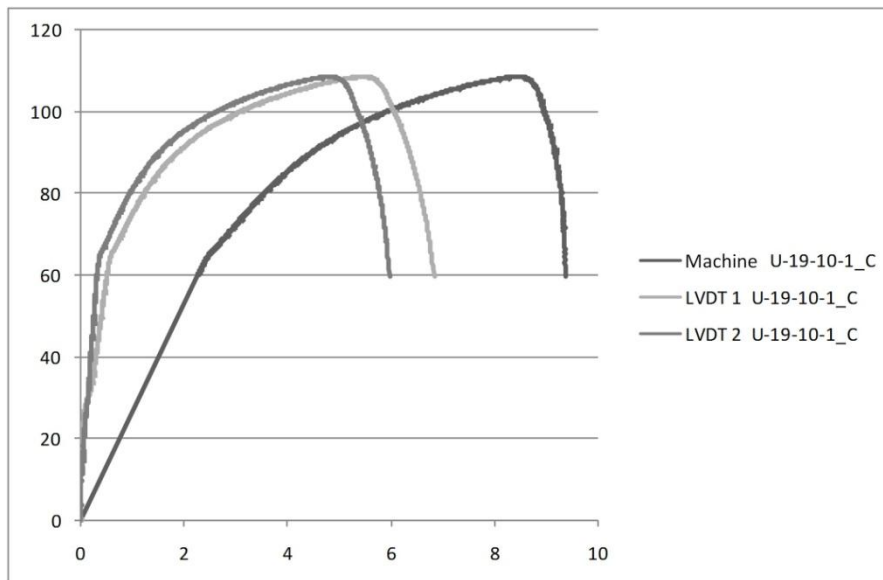
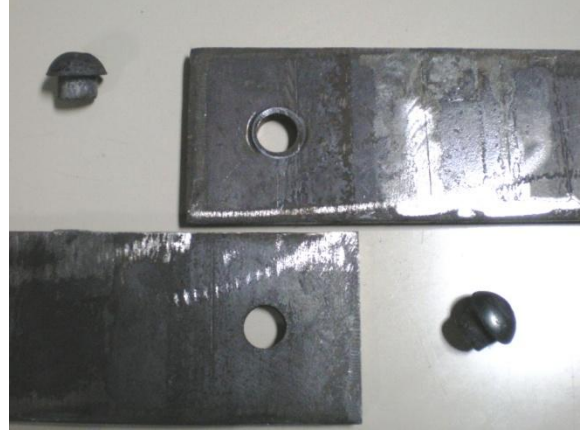
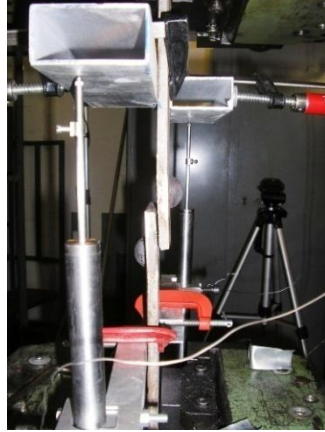
**Test Information:**

plate 1: out of plane displacement = 1.7 mm, ovaled hole dimesions = 19,8x21 mm

plate 2: out of plane displacement = 1.6 mm, ovaled hole dimesions = 21,3x20 mm

RESULTS



Peak: [kN]	$F_p = 108,52$	$d_{pavm} = 8,42$	$d_{p1} = 5,44$	$d_{p2} = 4,79$
Elastic limit: [kN]	$F_{yaverage} = 64,00$	$d_{yaverage} = 2,42$	$d_{y1average} = 0,57$	$d_{y2average} = 0,36$
Ultimate: [kN]	$F_u = 86,82$	$d_{uav} = 9,20$	$d_{u1} = 6,42$	$d_{u2} = 5,66$
Stiffness: [kN/mm]		$K_{av} = 25,9$	$K_{LVD1} = 89,67$	$K_{LVD2} = 183,46$

COLLAPSE MODE

☒ Rivet Shear

☐ Bearing

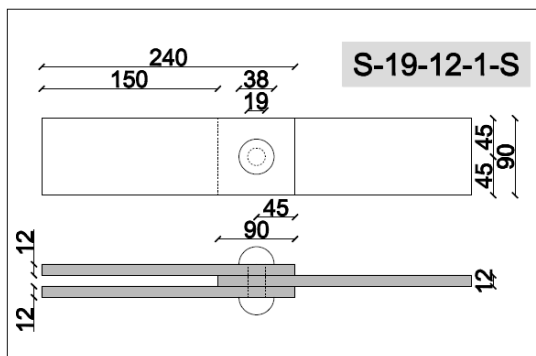
☐ Tension

☐ Shear out


S-19-12-1-A

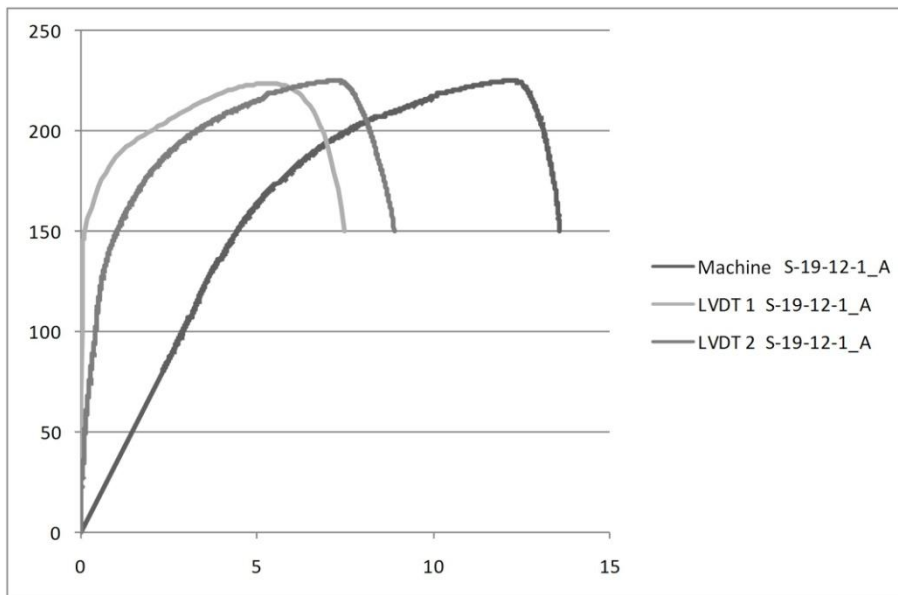
Specimen tag	S	U	Width plate (mm)	90
S-19-12-1-A	✓		Dist. from edge (mm)	45
Rivet diam. (mm)	19		Rivet pitch (mm)	—
Thickness plate (mm)	12		Rivet no.	1

PHOTOS



Test Information: The hole in the center plate was subjected to an ovalization: dimensions: 19x23 mm

RESULTS





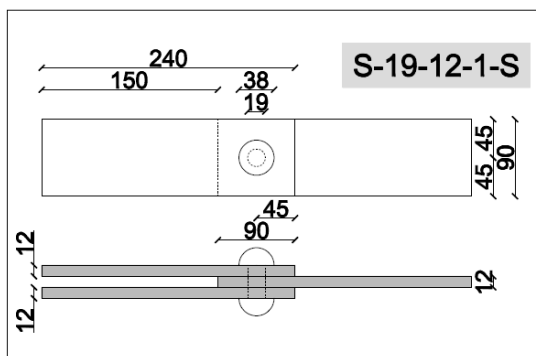
Peak: [kN]	$F_p = 225,16$	$d_{pav} = 12,23$	$d_{p1} = 5,83$	$d_{p2} = 7,24$
Elastic limit: [kN]	$F_{yaverage} = 126,70$	$d_{yaverage} = 3,6$	$d_{y1average} = 0,02$	$d_{y2average} = 0,59$
Ultimate: [kN]	$F_u = 180,13$	$d_{uav} = 13,36$	$d_{u1} = 7,21$	$d_{u2} = 8,51$
Stiffness: [kN/mm]		$K_{av} = 34,63$	$K_{LVDT1} = 2693$	$K_{LVDT2} = 164,45$

COLLAPSE MODE

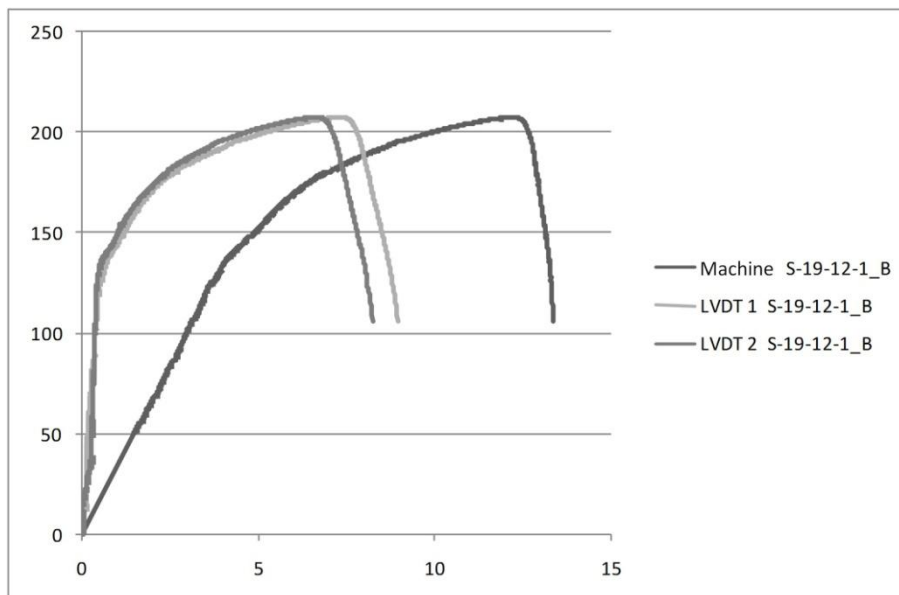
- ☐ Rivet Shear ☒ Bearing ☐ Tension ☐ Shear out
-
- ☒ Rivet Shear ☐ Bearing ☐ Tension ☐ Shear out

S-19-12-1-B

Specimen tag	S	U	Width plate (mm)	90
S-19-12-1-B	✓		Dist. from edge (mm)	45
Rivet diam. (mm)	19		Rivet pitch (mm)	—
Thickness plate (mm)	12		Rivet no.	1

PHOTOS

Test Information: The hole in the center plate was subjected to an ovalization: dimensions: 19x22,5 mm

RESULTS



Peak: [kN]	$F_p = 207,19$	$d_{pav} = 12,13$	$d_{p1} = 7,28$	$d_{p2} = 6,58$
Elastic limit: [kN]	$F_{yaverage} = 125,35$	$d_{yaverage} = 3,74$	$d_{y1average} = 0,56$	$d_{y2average} = 0,44$
Ultimate: [kN]	$F_u = 165,74$	$d_{uav} = 13,00$	$d_{u1} = 8,30$	$d_{u2} = 7,59$
Stiffness: [kN/mm]		$K_{av} = 33,75$	$K_{LVD1} = 249,18$	$K_{LVD2} = 676,82$

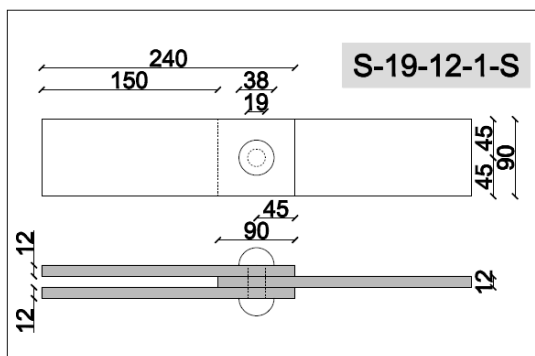
COLLAPSE MODE

- ☐ Rivet Shear ☒ Bearing ☐ Tension ☐ Shear out
-
- ☒ Rivet Shear ☐ Bearing ☐ Tension ☐ Shear out

S-19-12-1-C

Specimen tag	S	U	Width plate (mm)	90
S-19-12-1-C	✓		Dist. from edge (mm)	45
Rivet diam. (mm)	19		Rivet pitch (mm)	—
Thickness plate (mm)	12		Rivet no.	1

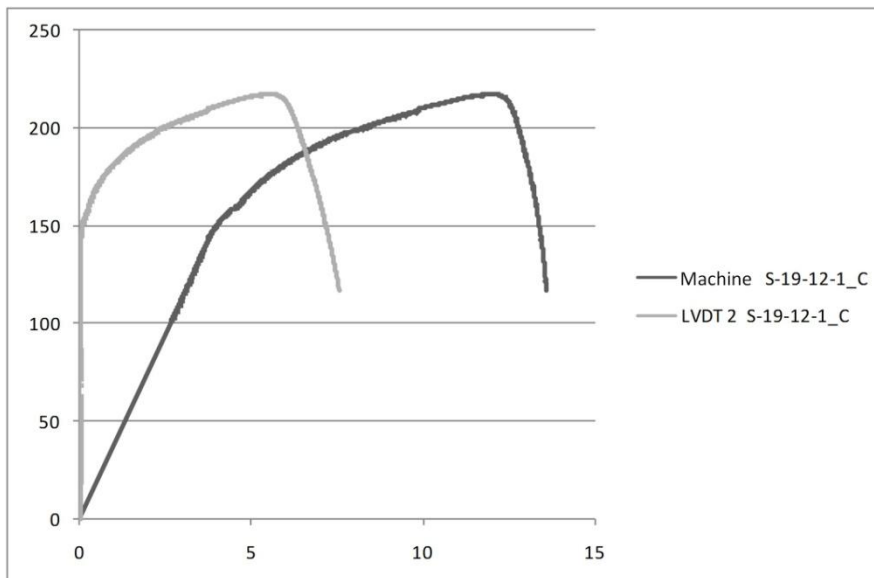
PHOTOS



Test Information:

The hole in the center plate was subjected to an ovalization: dimensions: 19x23,5 mm; plastic deformations and bearing of the inner plate, final plate width = 97 mm

RESULTS





Peak: [kN]	$F_p = 217,19$	$d_{pav} = 12,02$	$d_{p1} =$	$d_{p2} = 5,53$
Elastic limit: [kN]	$F_{yaverage} = 149,00$	$d_{yaverage} = 3,97$	$d_{y1average} =$	$d_{y2average} = 0,09$
Ultimate: [kN]	$F_u = 173,75$	$d_{uav} = 13,17$	$d_{u1} =$	$d_{u2} = 6,82$
Stiffness: [kN/mm]		$K_{av} = 37,62$	$K_{LVD1} =$	$K_{LVD2} = 2693,8$

COLLAPSE MODE

☐ Rivet Shear
 ☒ Bearing
 ☐ Tension
 ☐ Shear out

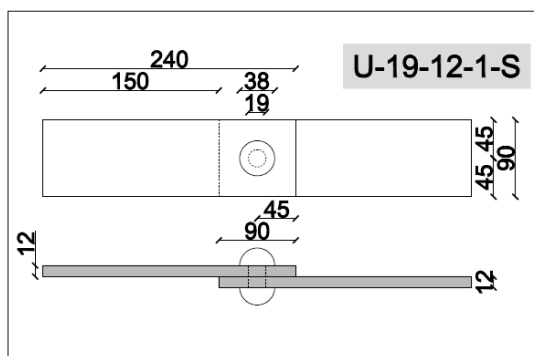


☒ Rivet Shear
 ☐ Bearing
 ☐ Tension
 ☐ Shear out

U-19-12-1-A

Specimen tag	S	U	Width plate (mm)	90
U-19-12-1-A		✓	Dist. from edge (mm)	45
Rivet diam. (mm)	19		Rivet pitch (mm)	—
Thickness plate (mm)	12		Rivet no.	1

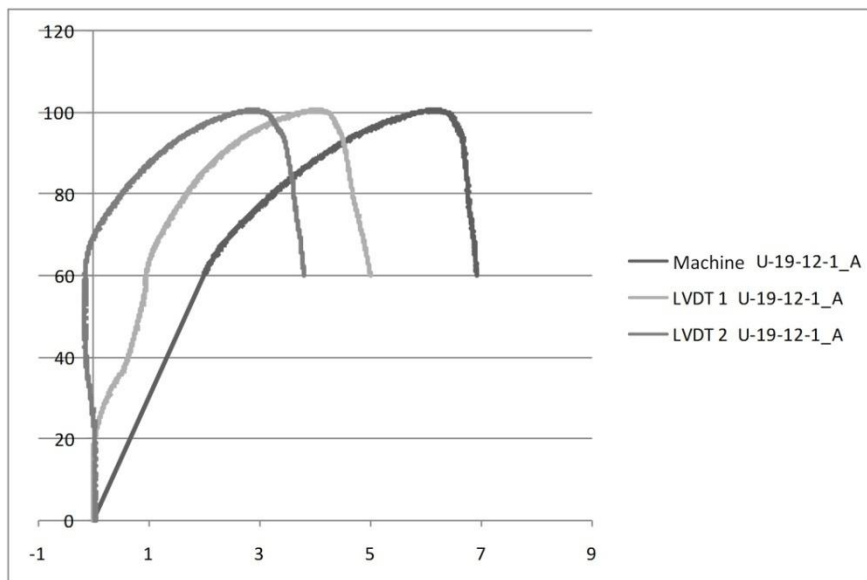
PHOTOS



Test Information:

The hole in all plates was subjected to an ovalization: dimensions: 19x21 mm;
Out of plane plastic deformations of all plate equal to 0.5 mm

RESULTS





Peak: [kN]	$F_p = 100,63$	$d_{pav} = 6,15$	$d_{p1} = 4,40$	$d_{p2} = 2,89$
Elastic limit: [kN]	$F_{yaverage} = 60,07$	$d_{yaverage} = 1,98$	$d_{y1average} = 0,95$	$d_{y2average} = -0,14$
Ultimate: [kN]	$F_u = 80,50$	$d_{uav} = 6,77$	$d_{u1} = 4,68$	$d_{u2} = 3,62$
Stiffness: [kN/mm]		$K_{av} = 29,96$	$K_{LVD1} = 57,94$	$K_{LVD2} = -$

COLLAPSE MODE

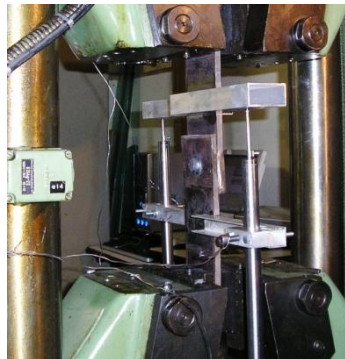
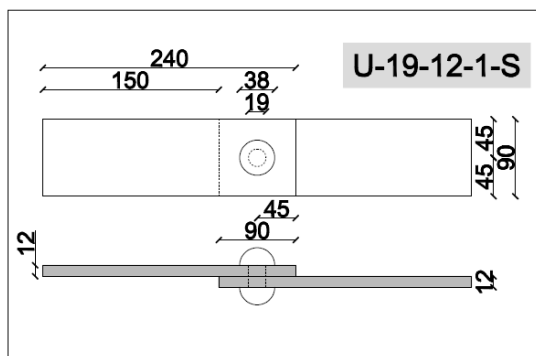
☒ Rivet Shear
 ☐ Bearing
 ☐ Tension
 ☐ Shear out



U-19-12-1-B

Specimen tag	S	U	Width plate (mm)	90
U-19-12-1-B		✓	Dist. from edge (mm)	45
Rivet diam. (mm)	19		Rivet pitch (mm)	—
Thickness plate (mm)	12		Rivet no.	1

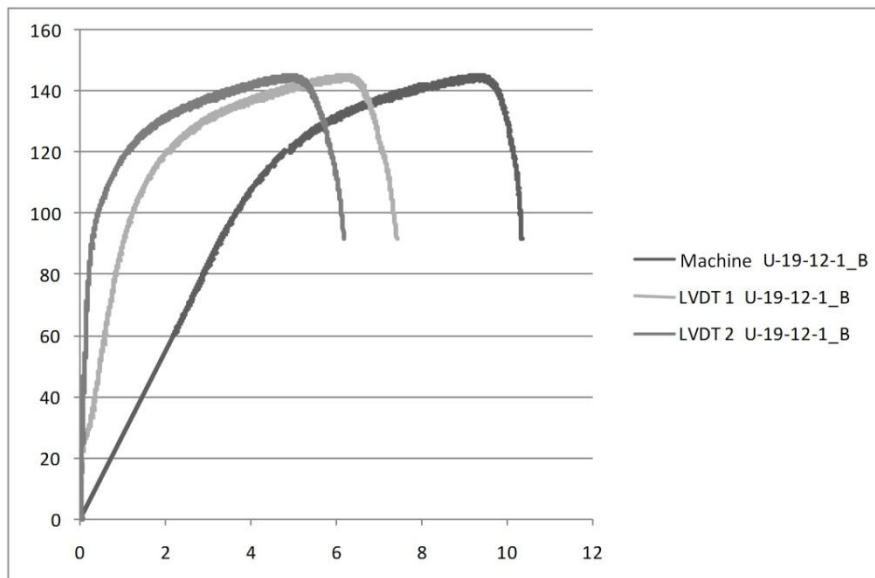
PHOTOS

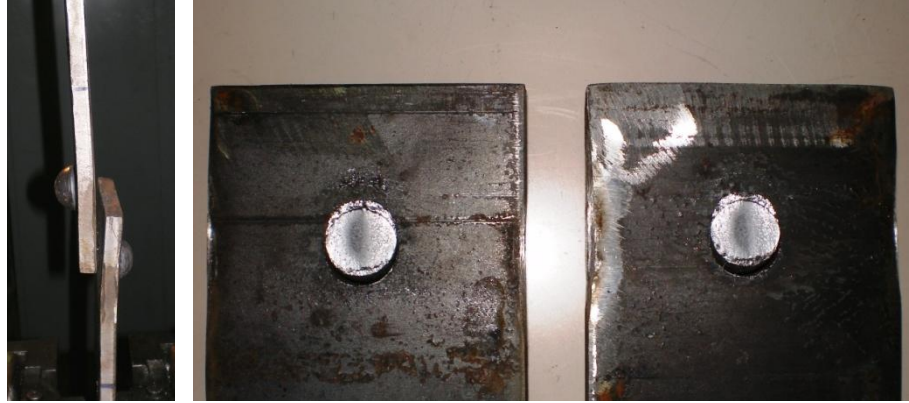


Test Information:

The hole in all plates was subjected to an ovalization: dimensions: 19x22 mm;
Out of plane plastic deformations of all plate equal to 2 mm

RESULTS





Peak: [kN]	$F_p = 145,28$	$d_{pav} = 9,29$	$d_{p1} = 6,20$	$d_{p2} = 4,90$
Elastic limit: [kN]	$F_{yaverage} = 87,37$	$d_{yaverage} = 3,14$	$d_{y1average} = 0,97$	$d_{y2average} = 0,25$
Ultimate: [kN]	$F_u = 116,22$	$d_{uav} = 10,20$	$d_{u1} = 7,19$	$d_{u2} = 5,94$
Stiffness: [kN/mm]		$K_{av} = 27,44$	$K_{LVD1} = 82,46$	$K_{LVD2} = 326,05$

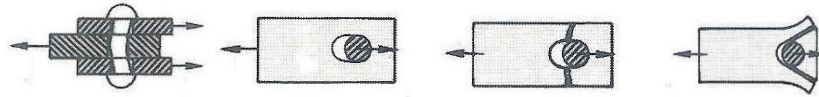
COLLAPSE MODE

☒ Rivet Shear

☐ Bearing

☐ Tension

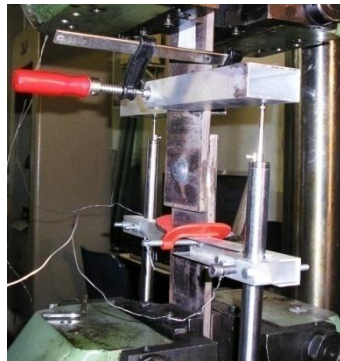
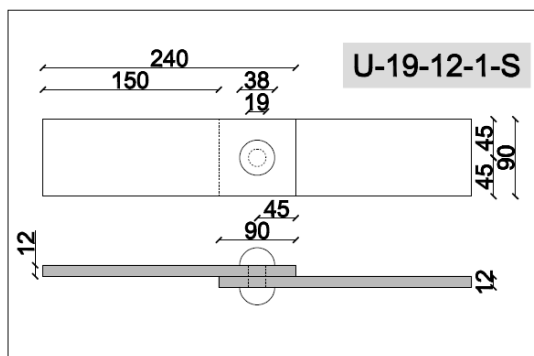
☐ Shear out



U-19-12-1-C

Specimen tag	S	U	Width plate (mm)	90
U-19-12-1-C		✓	Dist. from edge (mm)	45
Rivet diam. (mm)	19		Rivet pitch (mm)	—
Thickness plate (mm)	12		Rivet no.	1

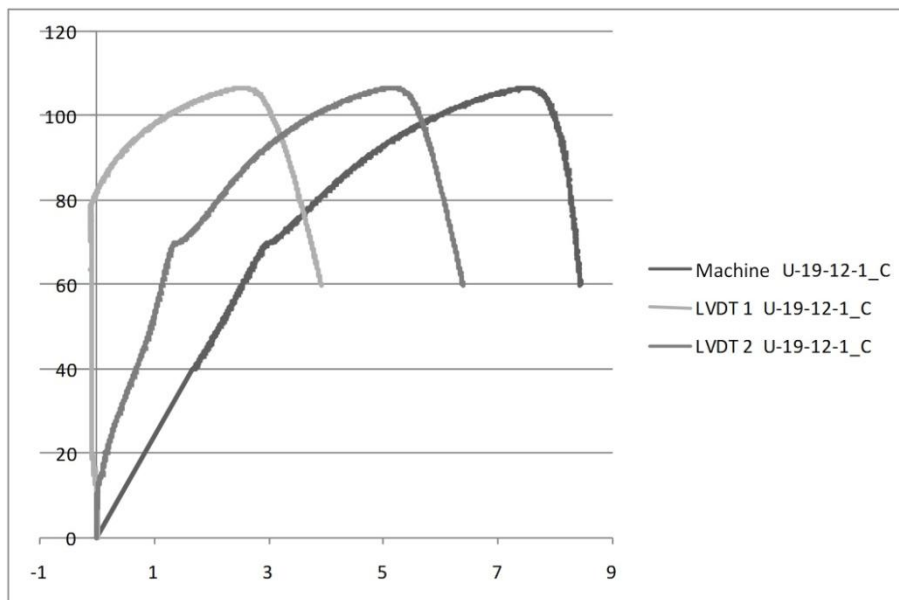
PHOTOS

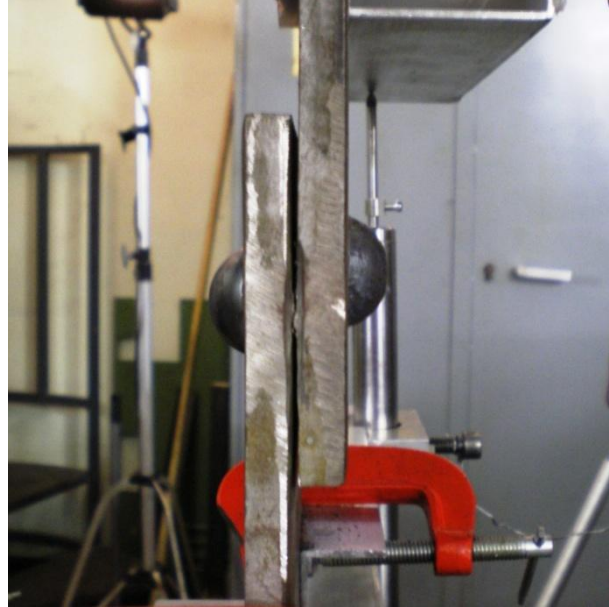


Test Information:

The hole in all plates was subjected to an ovalization: dimensions: 20x21 mm

RESULTS





Peak: [kN]	$F_p = 106,84$	$d_{pav} = 7,45$	$d_{p1} = 2,49$	$d_{p2} = 5,12$
Elastic limit: [kN]	$F_{yaverage} = 73,36$	$d_{yaverage} = 3,32$	$d_{y1average} = -0,1$	$d_{y2average} = 1,7$
Ultimate: [kN]	$F_u = 85,47$	$d_{uav} = 8,23$	$d_{u1} = 3,45$	$d_{u2} = 5,98$
Stiffness: [kN/mm]		$K_{av} = 23,72$	$K_{LVDT1} = -$	$K_{LVDT2} = 47,32$

COLLAPSE MODE

☒ Rivet Shear

☐ Bearing

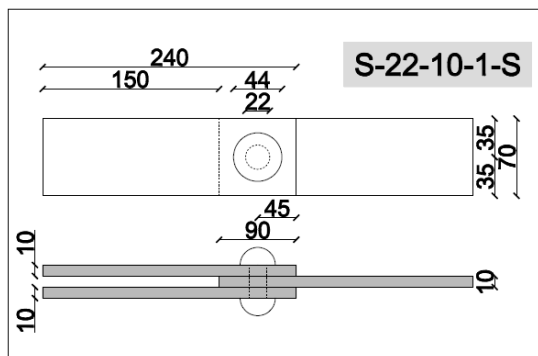
☐ Tension

☐ Shear out


S-22-10-1-A

Specimen tag	S	U	Width plate (mm)	70
S-22-10-1-A	✓		Dist. from edge (mm)	35
Rivet diam. (mm)	22		Rivet pitch (mm)	—
Thickness plate (mm)	10		Rivet no.	1

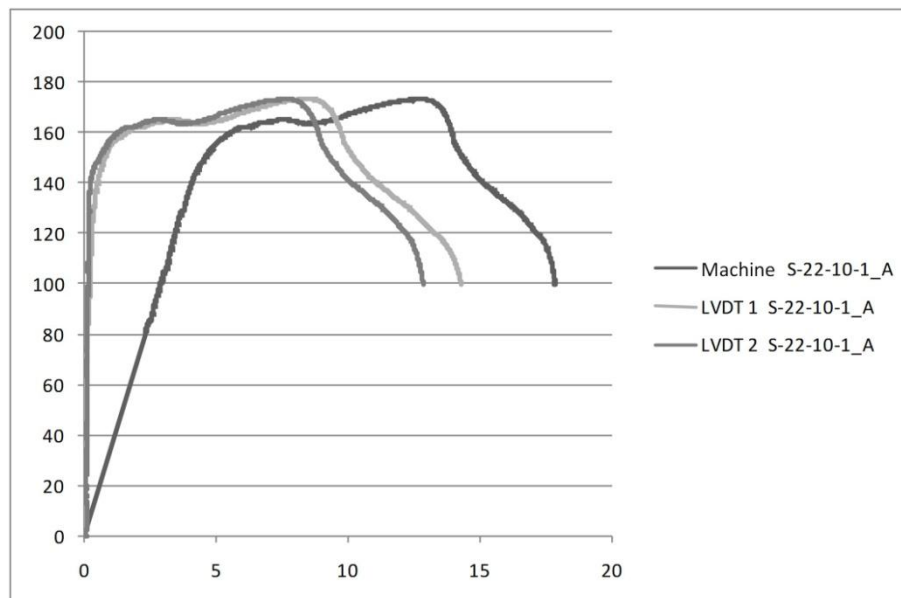
PHOTOS

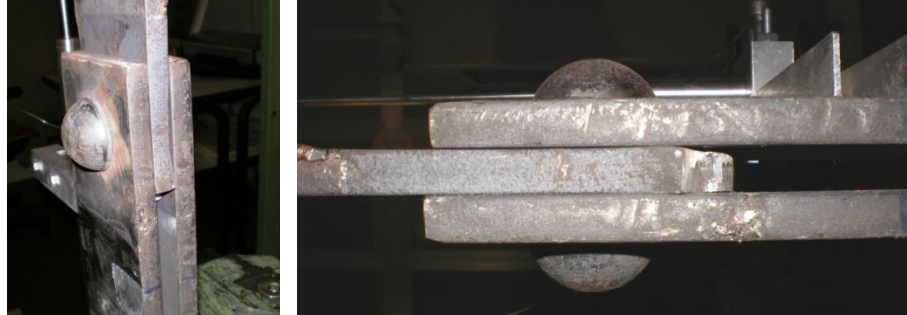


Test Information:

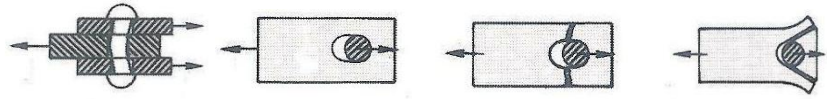
plastic deformations and bearing of the inner plate, final plate width = 82.5 mm

RESULTS





Peak: [kN]	$F_p = 173,59$	$d_{pav} = 12,65$	$d_{p1} = 8,41$	$d_{p2} = 7,59$
Elastic limit: [kN]	$F_{yaverage} = 133,35$	$d_{yaverage} = 3,86$	$d_{y1medio} = 0,41$	$d_{y2average} = 0,19$
Ultimate: [kN]	$F_u = 138,87$	$d_{uav} = 15,26$	$d_{u1} = 11,26$	$d_{u2} = 10,28$
Stiffness: [kN/mm]		$K_{av} = 34,63$	$K_{LVD1} = 207,13$	$K_{LVD2} = 908,98$

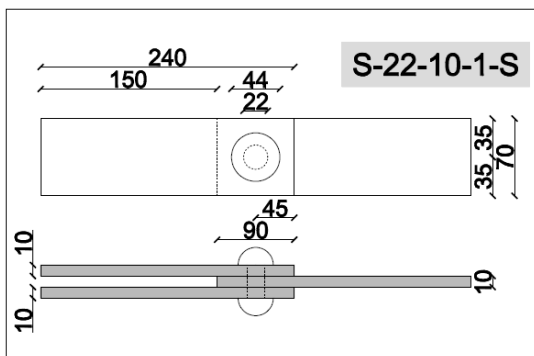
COLLAPSE MODE☐ Rivet Shear☒ Bearing☐ Tension☐ Shear out

Appendix

S-22-10-1-B

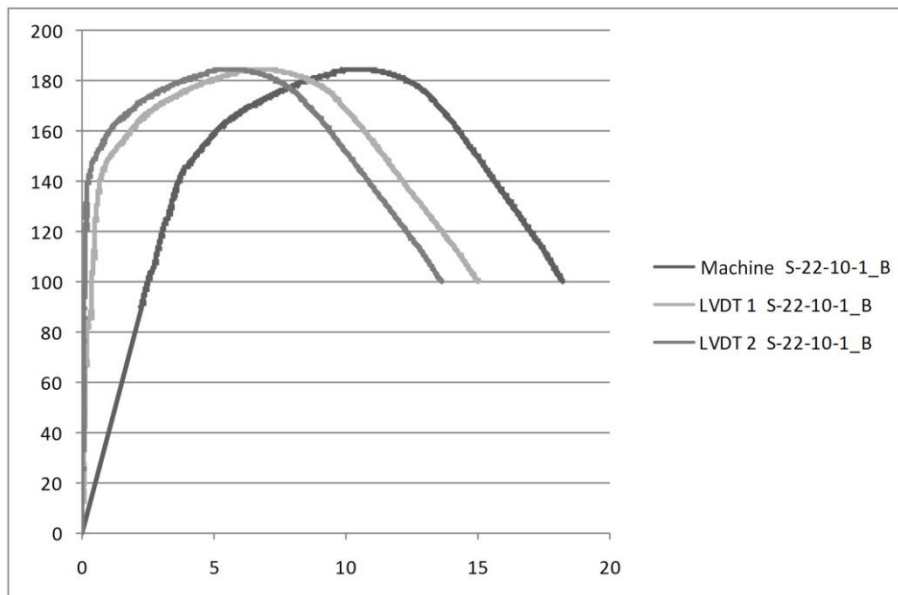
Specimen tag	S	U	Width plate (mm)	70
S-22-10-1-B	✓		Dist. from edge (mm)	35
Rivet diam. (mm)	22		Rivet pitch (mm)	—
Thickness plate (mm)	10		Rivet no.	1

PHOTOS



Test Information:

RESULTS





Peak: [kN]	$F_p = 184,57$	$d_{pav} = 10,19$	$d_{p1} = 4,47$	$d_{p2} = 5,38$
Elastic limit: [kN]	$F_{yaverage} = 138,70$	$d_{yaverage} = 3,58$	$d_{y1average} = 0,64$	$d_{y2average} = 0,2$
Ultimate: [kN]	$F_u = 147,66$	$d_{uav} = 15,09$	$d_{u1} = 11,59$	$d_{u2} = 10,29$
Stiffness: [kN/mm]		$K_{av} = 40,33$	$K_{LVD1} = 404,18$	$K_{LVD2} = 872,87$

COLLAPSE MODE

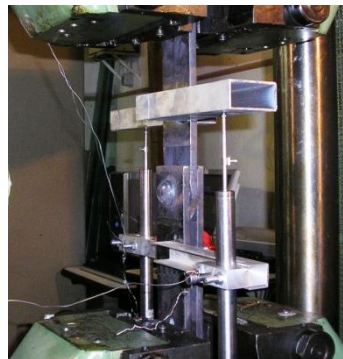
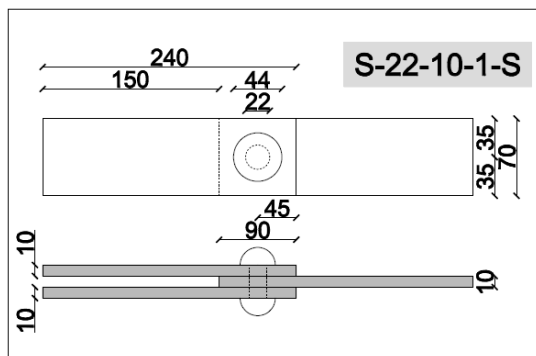
☐ Rivet Shear
 ☒ Bearing
 ☐ Tension
 ☐ Shear out



S-22-10-1-C

Specimen tag	S	U	Width plate (mm)	70
S-22-10-1-C	✓		Dist. from edge (mm)	35
Rivet diam. (mm)	22		Rivet pitch (mm)	—
Thickness plate (mm)	10		Rivet no.	1

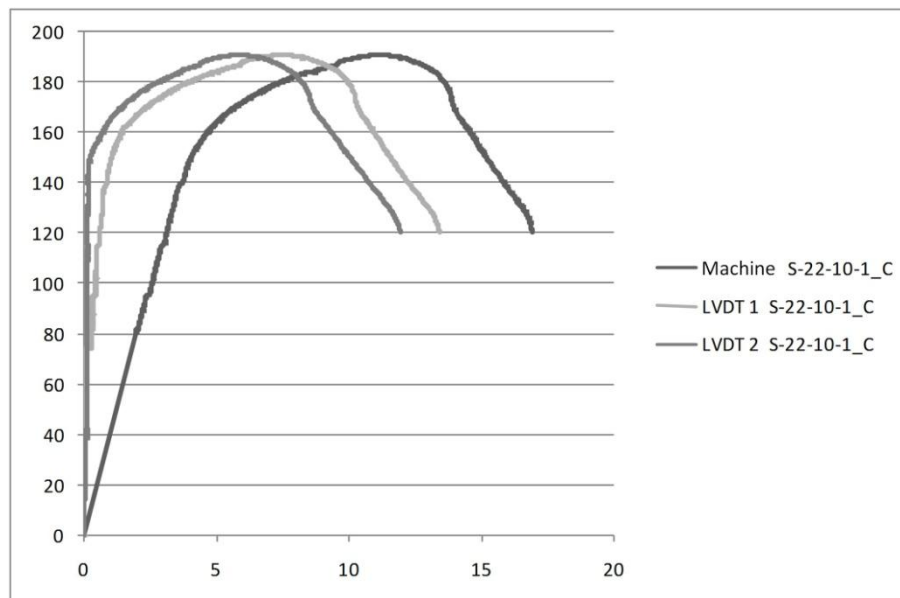
PHOTOS

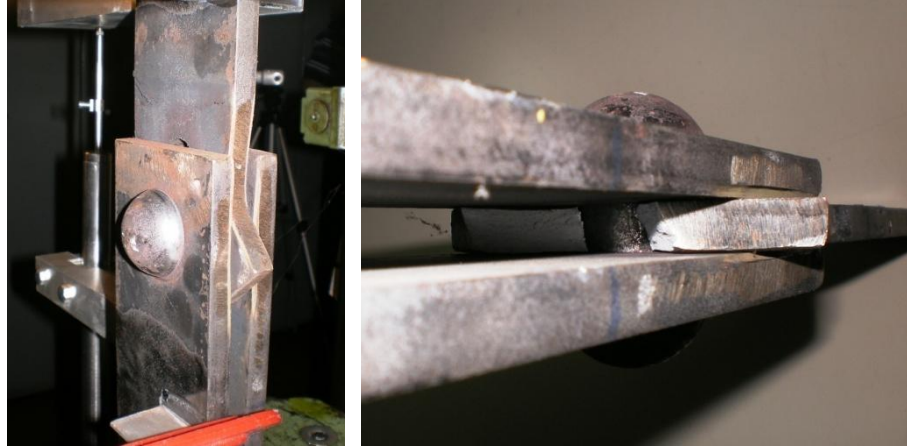


Test Information:

plastic deformations and bearing of the inner plate, final plate width = 91.5 mm

RESULTS





Peak: [kN]	$F_p = 190,89$	$d_{pav} = 11,25$	$d_{p1} = 7,57$	$d_{p2} = 5,96$
Elastic limit: [kN]	$F_{yaverage} = 136,01$	$d_{yaverage} = 3,51$	$d_{y1average} = 0,73$	$d_{y2average} = 0,18$
Ultimate: [kN]	$F_u = 152,71$	$d_{uav} = 15,03$	$d_{u1} = 11,38$	$d_{u2} = 9,85$
Stiffness: [kN/mm]		$K_{av} = 40,4$	$K_{LVD1} = 946,08$	$K_{LVD2} = 566,11$

COLLAPSE MODE

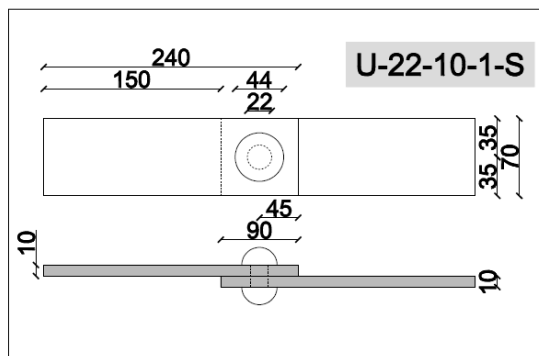
☐ Rivet Shear
 ☒ Bearing
 ☐ Tension
 ☐ Shear out



U-22-10-1-A

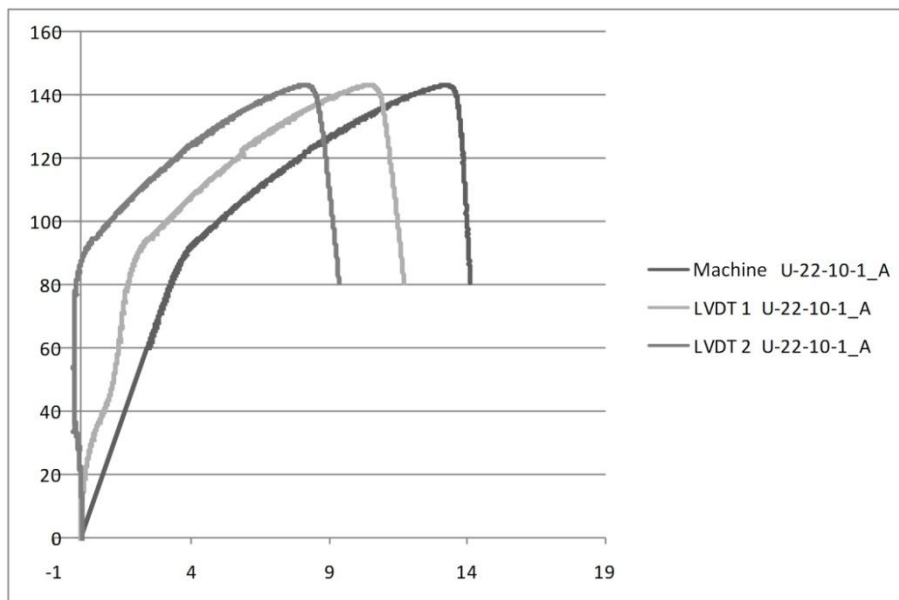
Specimen tag	S	U	Width plate (mm)	70
U-22-10-1-A	✓		Dist. from edge (mm)	35
Rivet diam. (mm)	22		Rivet pitch (mm)	—
Thickness plate (mm)	10		Rivet no.	1

PHOTOS



Test Information: oveled hole dimesions of all plates = 22x27 mm
 plate 1: out of plane displacement=1.7 mm; plate 2: out of plane displacement=1.6 mm.

RESULTS





Peak: [kN]	$F_p = 143,13$	$d_{pav} = 13,22$	$d_{p1} = 10,51$	$d_{p2} = 8,14$
Elastic limit: [kN]	$F_{yaverage} = 79,34$	$d_{yaverage} = 3,2$	$d_{y1average} = 1,71$	$d_{y2average} = -0,16$
Ultimate: [kN]	$F_u = 114,51$	$d_{uav} = 13,87$	$d_{u1} = 11,32$	$d_{u2} = 8,95$
Stiffness: [kN/mm]		$K_{av} = 24,81$	$K_{LVD1} = 73,54$	$K_{LVD2} = -$

COLLAPSE MODE

☒ Rivet Shear

☐ Bearing

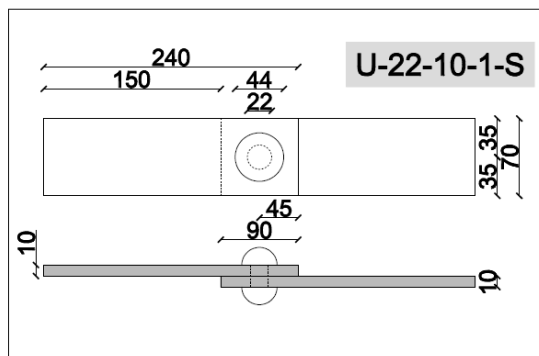
☐ Tension

☐ Shear out

U-22-10-1-B

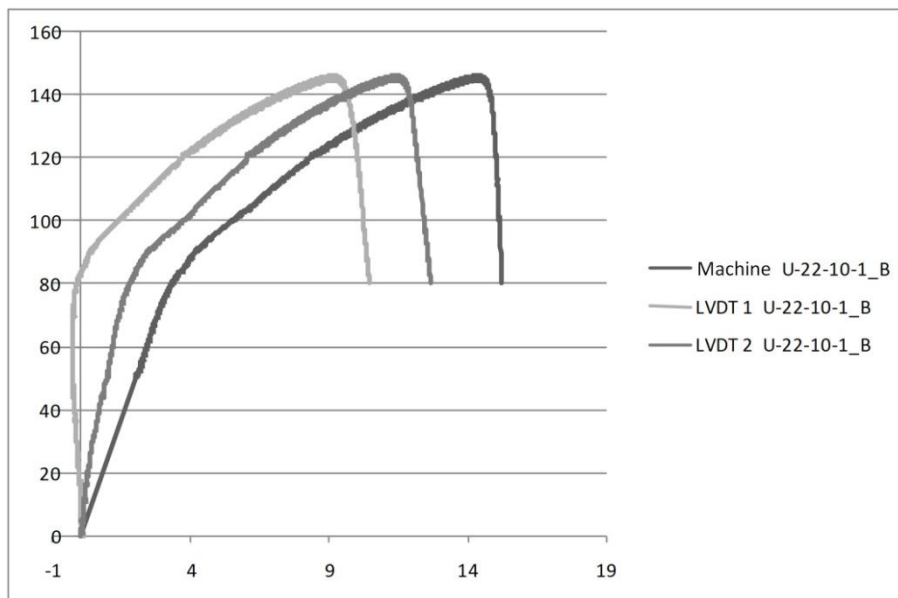
Specimen tag	S	U	Width plate (mm)	70
U-22-10-1-B	✓		Dist. from edge (mm)	35
Rivet diam. (mm)	22		Rivet pitch (mm)	—
Thickness plate (mm)	10		Rivet no.	1

PHOTOS



Test Information: oveled hole dimesions of all plates = 22x25 mm
out of plane displacement of all plates = 4 mm.

RESULTS





Peak: [kN]	$F_p = 146,43$	$d_{pav} = 14,41$	$d_{p1} = 9,18$	$d_{p2} = 11,45$
Elastic limit: [kN]	$F_{yaverage} = 76,02$	$d_{yaverage} = 3,05$	$d_{y1average} = -0,22$	$d_{y2average} = 1,56$
Ultimate: [kN]	$F_u = 117,14$	$d_{uav} = 15,01$	$d_{u1} = 10,01$	$d_{u2} = 12,17$
Stiffness: [kN/mm]		$K_{av} = 25,36$	$K_{LVDT1} = -$	$K_{LVDT2} = 51,4$

COLLAPSE MODE

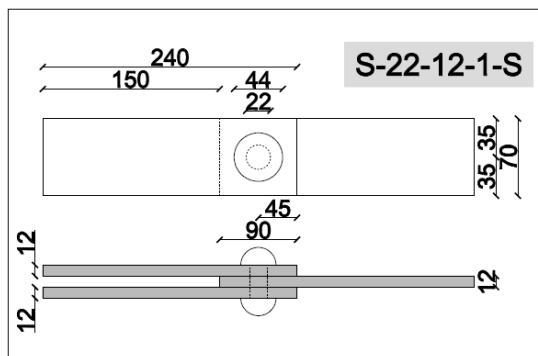
☒ Rivet Shear
 ☐ Bearing
 ☐ Tension
 ☐ Shear out



S-22-12-1-A

Specimen tag	S	U	Width plate (mm)	70
S-22-12-1-A	✓		Dist. from edge (mm)	35
Rivet diam. (mm)	22		Rivet pitch (mm)	—
Thickness plate (mm)	12		Rivet no.	1

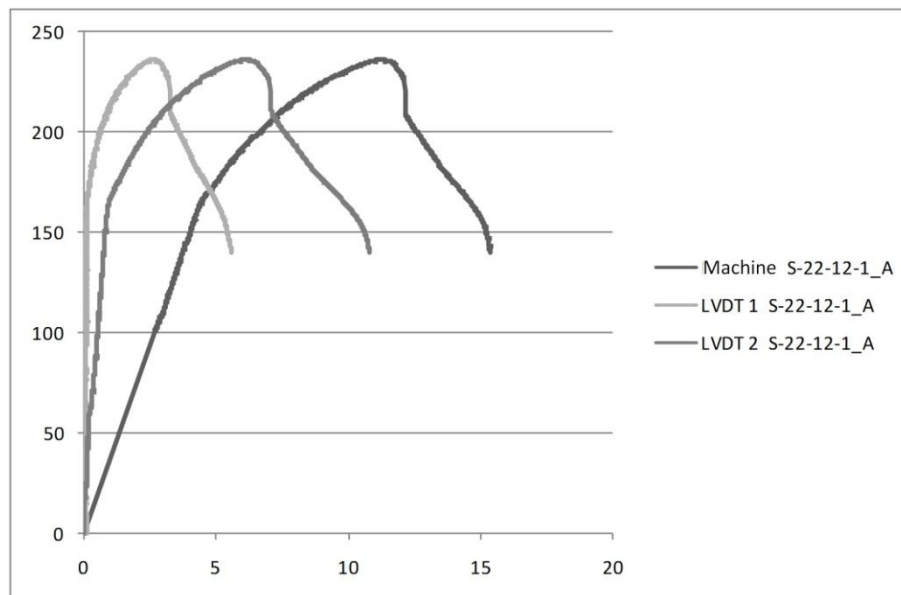
PHOTOS



Test Information:

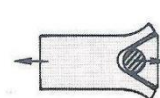
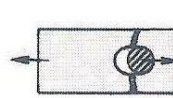
plastic deformations and bearing of the inner plate, final plate width = 91 mm

RESULTS





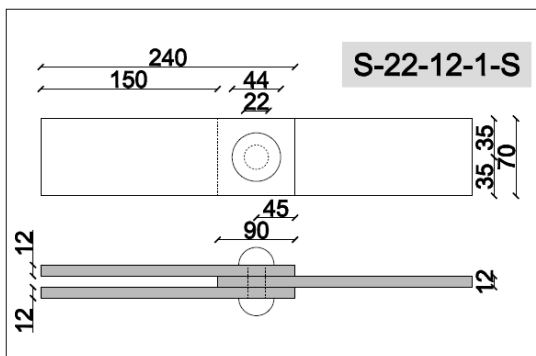
Peak: [kN]	$F_p = 236,18$	$d_{pav} = 11,17$	$d_{p1} = 2,58$	$d_{p2} = 6,05$
Elastic limit: [kN]	$F_{yaverage} = 156,72$	$d_{yaverage} = 4,2$	$d_{y1average} = 0,11$	$d_{y2average} = 0,84$
Ultimate: [kN]	$F_u = 188,94$	$d_{uav} = 13,17$	$d_{u1} = 4,00$	$d_{u2} = 8,22$
Stiffness: [kN/mm]		$K_{av} = 37,2$	$K_{LVD1} = 1876,2$	$K_{LVD2} = 156,39$

COLLAPSE MODE☐ Rivet Shear☒ Bearing☐ Tension☐ Shear out

S-22-12-1-B

Specimen tag	S	U	Width plate (mm)	70
S-22-12-1-B	✓		Dist. from edge (mm)	35
Rivet diam. (mm)	22		Rivet pitch (mm)	—
Thickness plate (mm)	12		Rivet no.	1

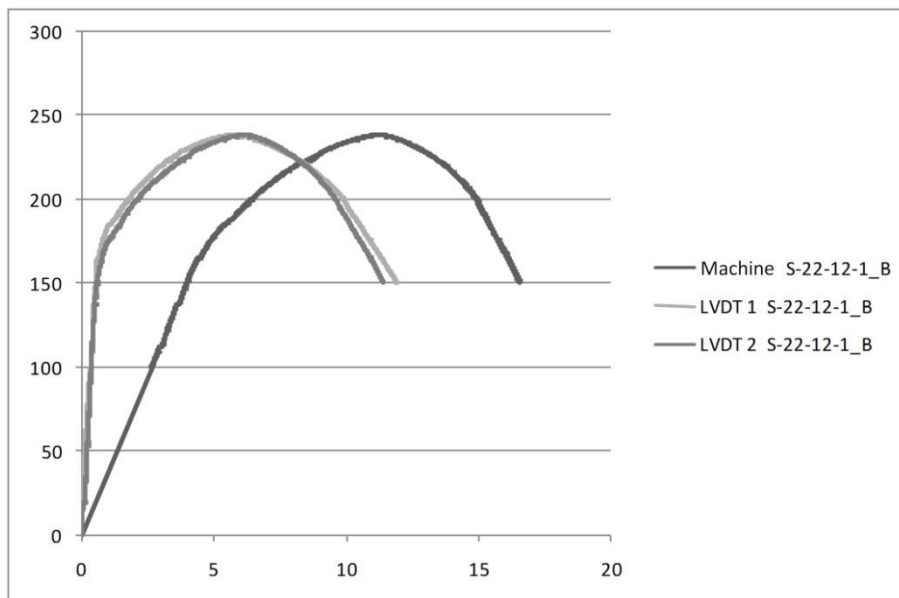
PHOTOS



Test Information:

plastic deformations and bearing of the inner plate, final plate width = 75 mm

RESULTS





Peak: [kN]	$F_p = 238,23$	$d_{pav} = 11,29$	$d_{p1} = 5,84$	$d_{p2} = 6,19$
Elastic limit: [kN]	$F_{yaverage} = 153,36$	$d_{yaverage} = 4,04$	$d_{y1average} = 0,52$	$d_{y2average} = 0,6$
Ultimate: [kN]	$F_u = 190,59$	$d_{uav} = 15,18$	$d_{u1} = 10,22$	$d_{u2} = 9,88$
Stiffness: [kN/mm]		$K_{av} = 37,89$	$K_{LVD1} = 248,68$	$K_{LVD2} = 265,17$

COLLAPSE MODE

☐ Rivet Shear

☒ Bearing

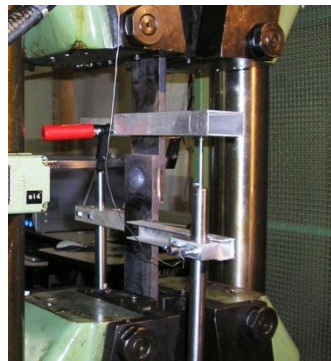
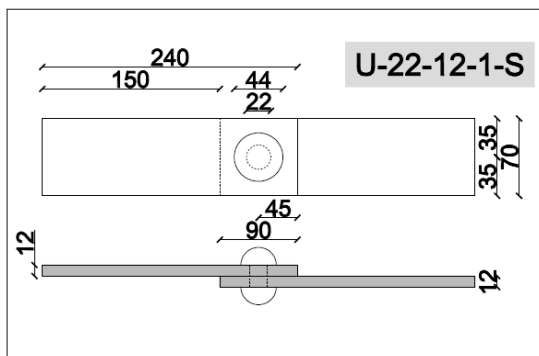
☐ Tension

☐ Shear out


U-22-12-1-A

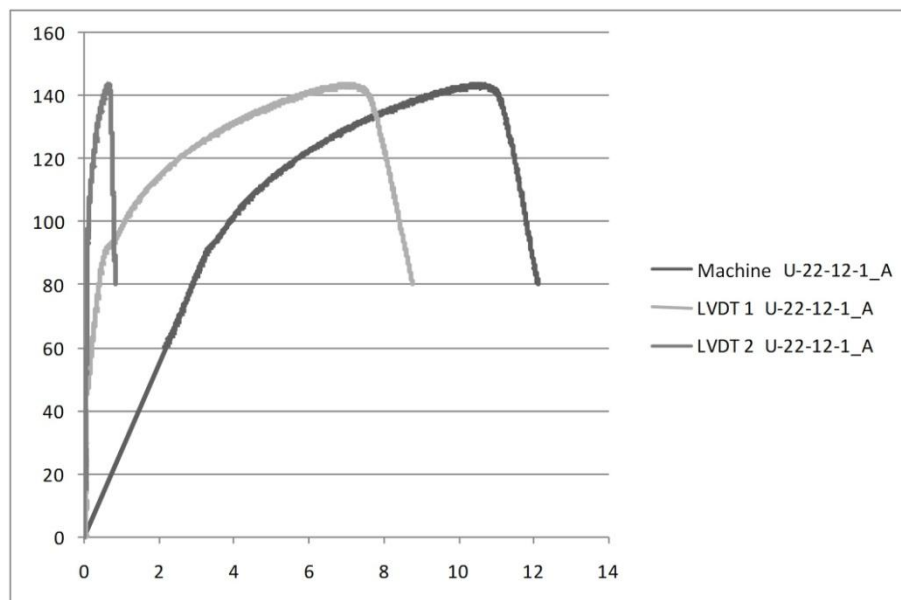
Specimen tag	S	U	Width plate (mm)	70
U-22-12-1-A		✓	Dist. from edge (mm)	35
Rivet diam. (mm)	22		Rivet pitch (mm)	—
Thickness plate (mm)	12		Rivet no.	1

PHOTOS



Test Information: oveled hole dimesions of all plates = 22x25 mm
out of plane displacement of all plates = 4 mm.

RESULTS





Peak: [kN]	$F_p = 143,39$	$d_{pav} = 10,51$	$d_{p1} = 7,01$	$d_{p2} = 0,64$
Elastic limit: [kN]	$F_{yaverage} = 94,67$	$d_{yaverage} = 3,59$	$d_{y1average} = 0,86$	$d_{y2average} = 0,1$
Ultimate: [kN]	$F_u = 114,87$	$d_{uav} = 11,58$	$d_{u1} = 8,17$	$d_{u2} = 0,75$
Stiffness: [kN/mm]		$K_{av} = 27,66$	$K_{LVD1} = 103,62$	$K_{LVD2} = 1249,9$

COLLAPSE MODE

☒ Rivet Shear

☐ Bearing

☐ Tension

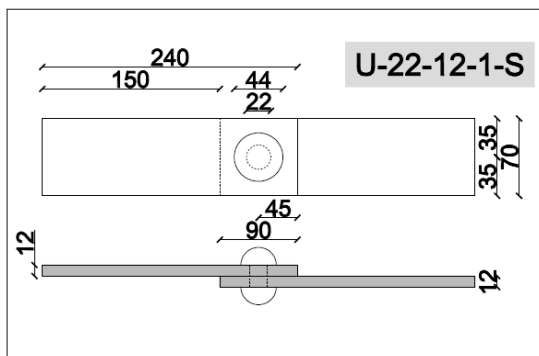
☐ Shear out



U-22-12-1-B

Specimen tag	S	U	Width plate (mm)	70
U-22-12-1-B		✓	Dist. from edge (mm)	35
Rivet diam. (mm)	22		Rivet pitch (mm)	—
Thickness plate (mm)	12		Rivet no.	1

PHOTOS

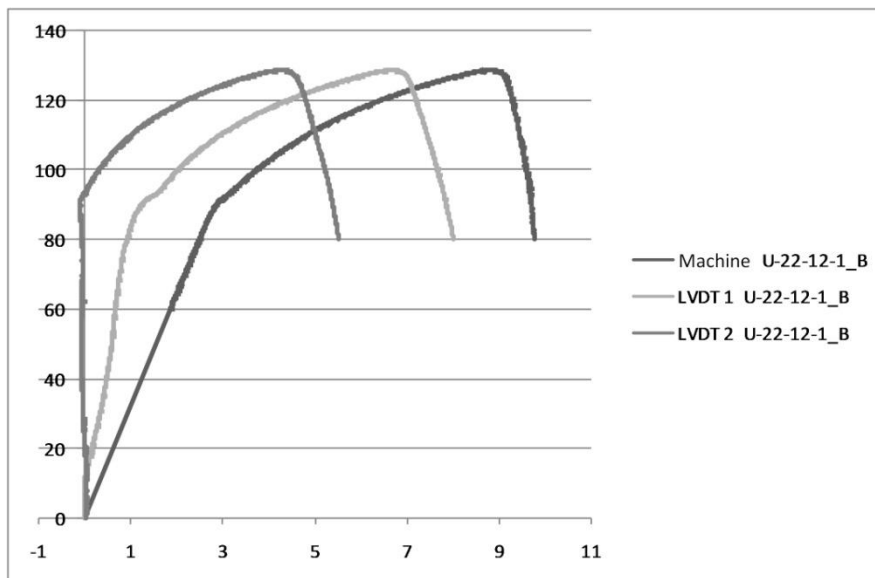


Test Information:

plate1: ovaled hole dimesions=22.3x24 mm; plate2: ovaled hole dimesions=22.5x24 mm

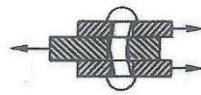
plate1: out of plane displacement = 5 mm; plate1: out of plane displacement = 4.5 mm;

RESULTS





Peak: [kN]	$F_p = 128,74$	$d_{pav} = 8,81$	$d_{p1} = 6,67$	$d_{p2} = 4,27$
Elastic limit: [kN]	$F_{yaverage} = 84,70$	$d_{yaverage} = 2,66$	$d_{y1average} = 1,04$	$d_{y2average} = -0,06$
Ultimate: [kN]	$F_u = 102,99$	$d_{uav} = 9,55$	$d_{u1} = 7,59$	$d_{u2} = 5,17$
Stiffness: [kN/mm]		$K_{av} = 32,1$	$K_{LVD1} = 96,81$	$K_{LVD2} = -$

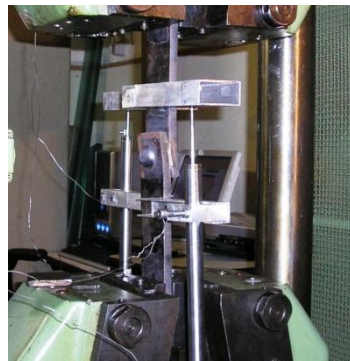
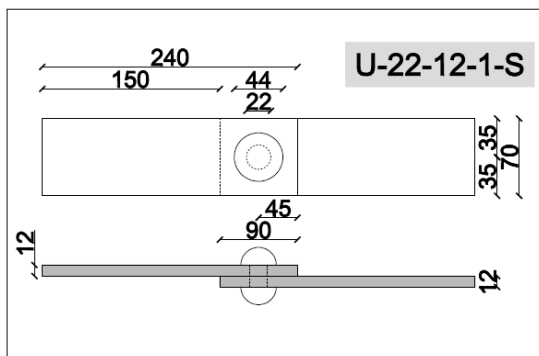
COLLAPSE MODE☒ Rivet Shear☐ Bearing☐ Tension☐ Shear out

Appendix

U-22-12-1-C

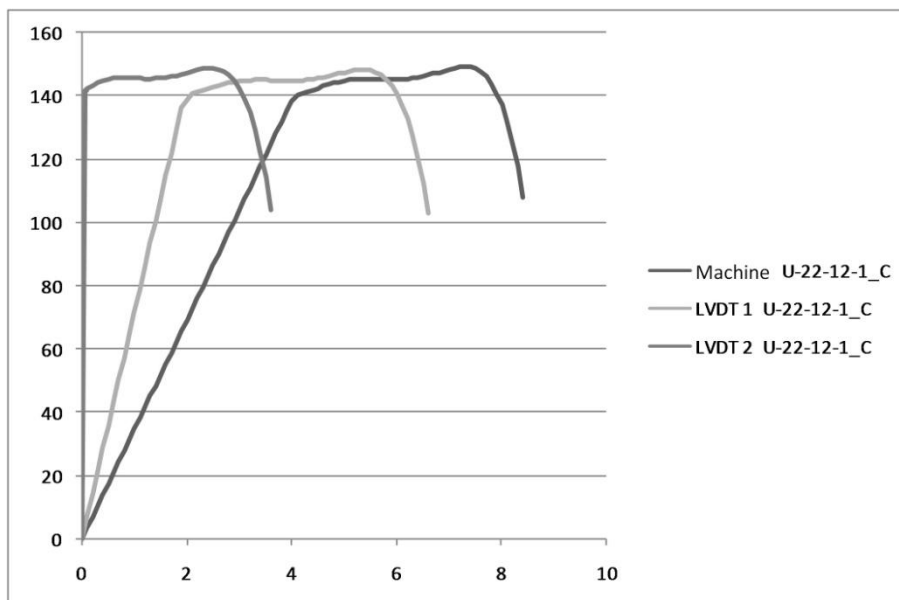
Specimen tag	S	U	Width plate (mm)	70
U-22-12-1-C		✓	Dist. from edge (mm)	35
Rivet diam. (mm)	22		Rivet pitch (mm)	—
Thickness plate (mm)	12		Rivet no.	1

PHOTOS



Test Information:

RESULTS





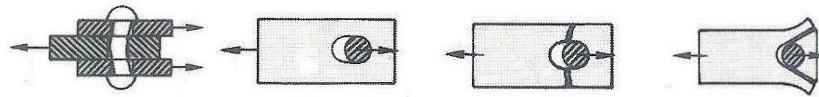
Peak: [kN]	$F_p = 148,61$	$d_{pav} = 7,33$	$d_{p1} = 5,40$	$d_{p2} = 2,46$
Elastic limit: [kN]	$F_{yaverage} = 137,36$	$d_{yaverage} = 3,95$	$d_{y1average} = 1,83$	$d_{y2average} = 0,03$
Ultimate: [kN]	$F_u = 118,89$	$d_{uav} = 8,10$	$d_{u1} = 6,10$	$d_{u2} = 3,36$
Stiffness: [kN/mm]		$K_{av} = 34,79$	$K_{LVD1} = 96,81$	$K_{LVD2} = 4578,6$

COLLAPSE MODE

☒ Rivet Shear

☐ Bearing

☐ Tension

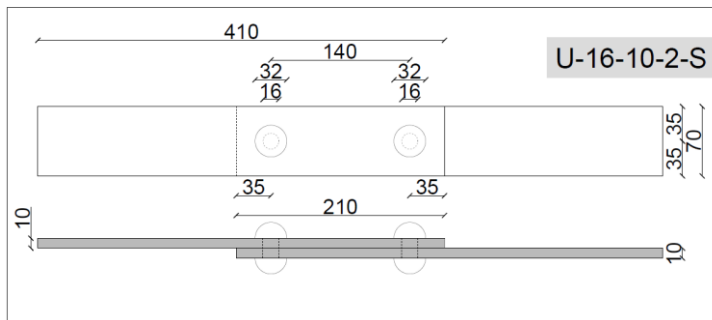
☐ Shear out


Appendix

U-16-10-2-A

Specimen tag	S	U	Width plate (mm)	70
U-16-10-2-A		✓	Dist. from edge (mm)	35
Rivet diam. (mm)	16		Rivet pitch (mm)	140
Thickness plate (mm)	10		Rivet no.	2

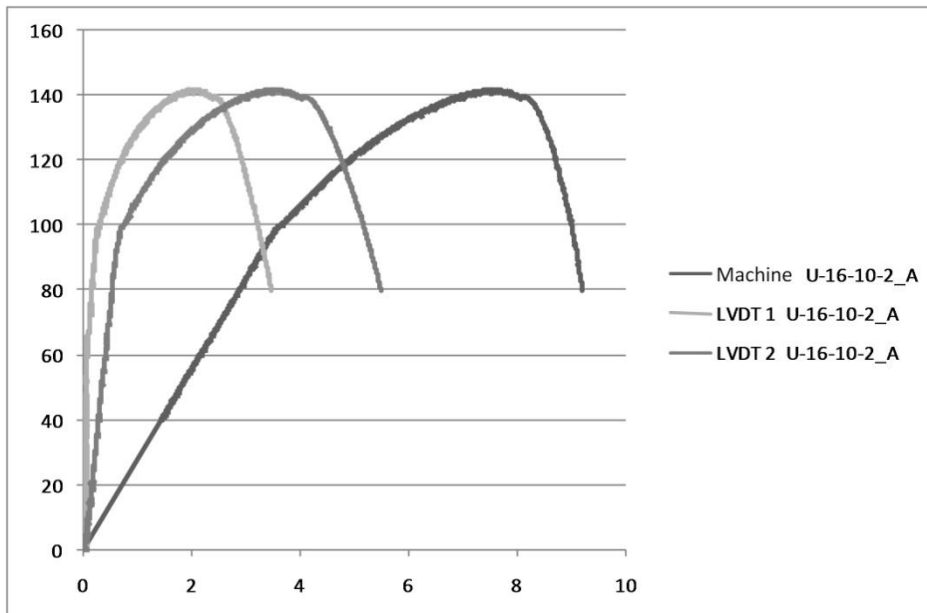
PHOTOS



Test Information:

Out of plane displacement for all plates = 8.5 mm

RESULTS





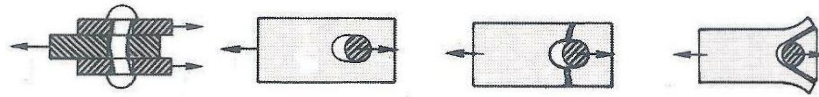
Peak: [kN]	$F_p = 141,87$	$d_{pav} = 7,59$	$d_{p1} = 2,04$	$d_{p2} = 3,51$
Elastic limit: [kN]	$F_{yaverage} = 98,68$	$d_{yaverage} = 3,53$	$d_{y1average} = 0,26$	$d_{y2average} = 0,69$
Ultimate: [kN]	$F_u = 113,50$	$d_{uav} = 8,80$	$d_{u1} = 3,03$	$d_{u2} = 4,90$
Stiffness: [kN/mm]		$K_{av} = 27,41$	$K_{LVD1} = 143,74$	$K_{LVD2} = 137,73$

COLLAPSE MODE

☒ Rivet Shear

☐ Bearing

☐ Tension

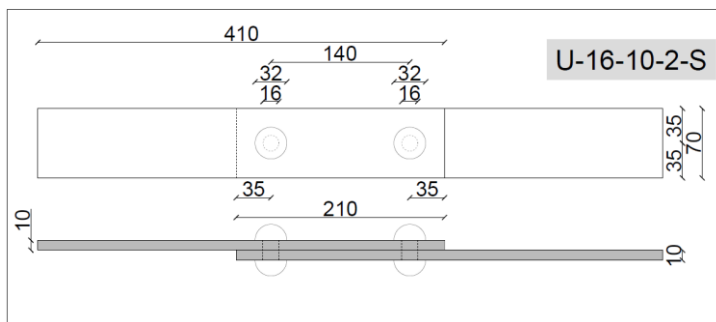
☐ Shear out


Appendix

U-16-10-2-B

Specimen tag	S	U	Width plate (mm)	70
U-16-10-2-B		✓	Dist. from edge (mm)	35
Rivet diam. (mm)	16		Rivet pitch (mm)	140
Thickness plate (mm)	10		Rivet no.	2

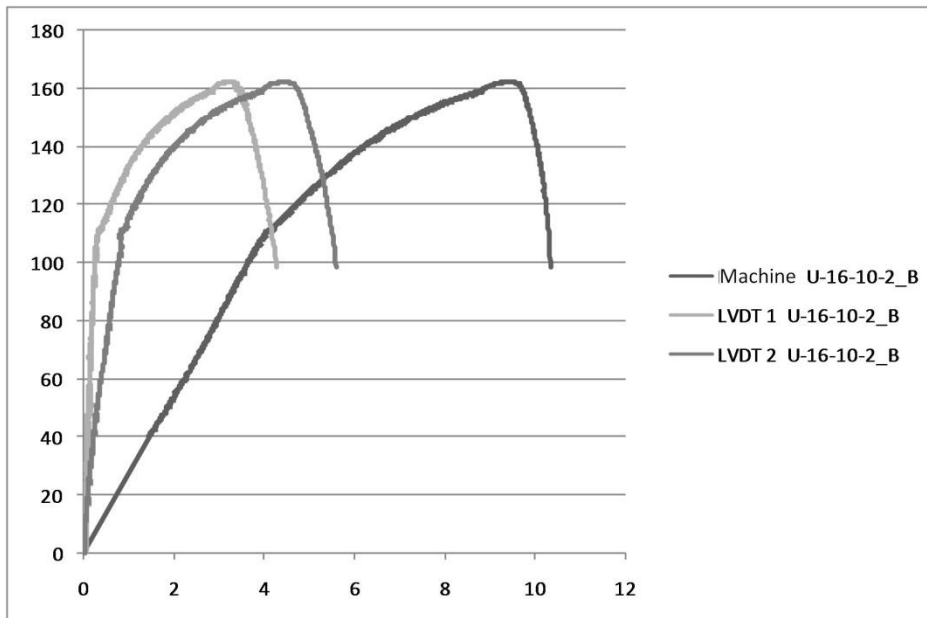
PHOTOS



Test Information:

Out of plane displacement for all plates = 9 mm

RESULTS





Peak: [kN]	$F_p = 162,23$	$d_{pav} = 9,41$	$d_{p1} = 3,23$	$d_{p2} = 4,44$
Elastic limit: [kN]	$F_{yaverage} = 105,36$	$d_{yaverage} = 3,83$	$d_{y1average} = 0,28$	$d_{y2average} = 0,83$
Ultimate: [kN]	$F_u = 129,79$	$d_{uav} = 10,15$	$d_{u1} = 3,94$	$d_{u2} = 5,27$
Stiffness: [kN/mm]		$K_{av} = 27,29$	$K_{LVD1} = 316,62$	$K_{LVD2} = 106,85$

COLLAPSE MODE

☒ Rivet Shear

☐ Bearing

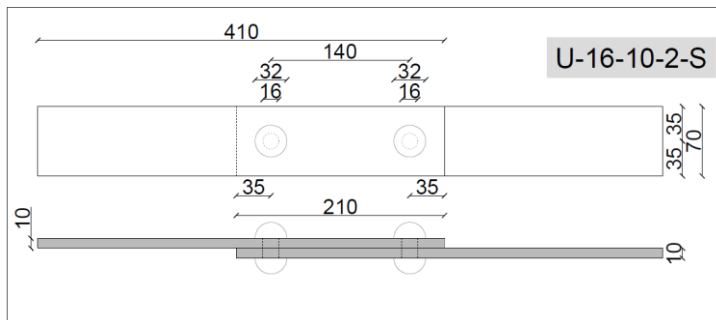
☐ Tension

☐ Shear out


U-16-10-2-C

Specimen tag	S	U	Width plate (mm)	70
U-16-10-2-C		✓	Dist. from edge (mm)	35
Rivet diam. (mm)	16		Rivet pitch (mm)	140
Thickness plate (mm)	10		Rivet no.	2

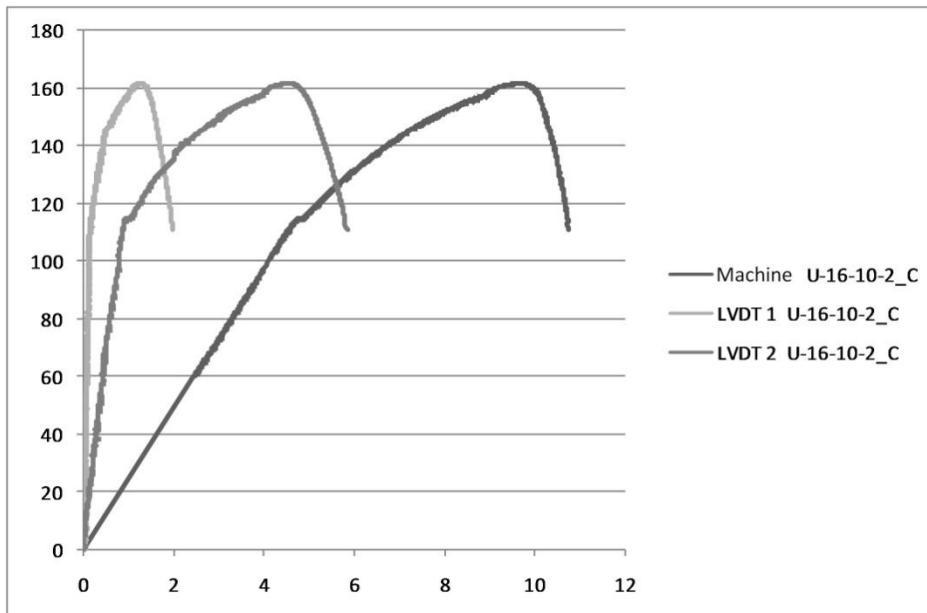
PHOTOS



Test Information:

Out of plane displacement for all plates = 8.5 mm

RESULTS





Peak: [kN]	$F_p = 161,37$	$d_{pav} = 9,61$	$d_{p1} = 1,26$	$d_{p2} = 4,50$
Elastic limit: [kN]	$F_{yaverage} = 110,68$	$d_{yaverage} = 4,53$	$d_{y1average} = 0,16$	$d_{y2average} = 0,89$
Ultimate: [kN]	$F_u = 129,10$	$d_{uav} = 10,52$	$d_{u1} = 1,83$	$d_{u2} = 5,54$
Stiffness: [kN/mm]		$K_{av} = 24,39$	$K_{LVD1} = 715,5$	$K_{LVD2} = 122,82$

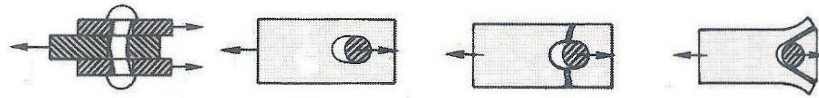
COLLAPSE MODE

☒ Rivet Shear

☐ Bearing

☐ Tension

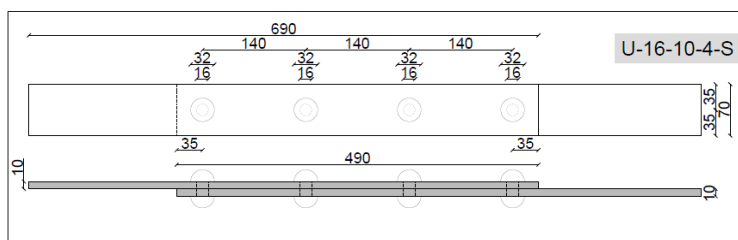
☐ Shear out



U-16-10-4-A

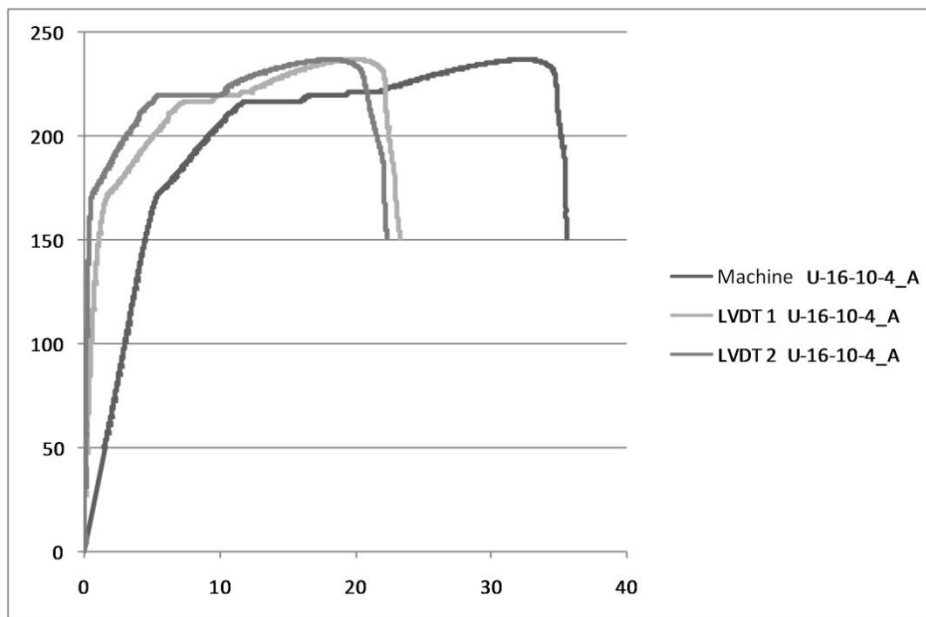
Specimen tag	S	U	Width plate (mm)	70
U-16-10-4-A		✓	Dist. from edge (mm)	35
Rivet diam. (mm)	16		Rivet pitch (mm)	140
Thickness plate (mm)	10		Rivet no.	4

PHOTOS

**Test Information:**

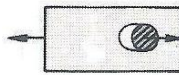
The failed plate width, at yielding, is equal to 62,54 mm; The unfailed plate width, at yielding, is equal to 63,8 mm; the hole width is equal to 17,51 mm.

RESULTS





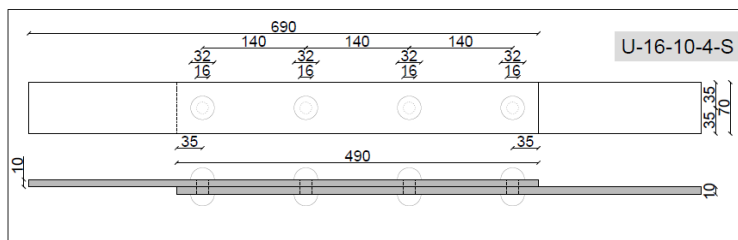
Peak: [kN]	$F_p = 236,56$	$d_{pav} = 32,29$	$d_{p1} = 19,82$	$d_{p2} = 18,11$
Elastic limit: [kN]	$F_{yaverage} = 166,69$	$d_{yaverage} = 5,13$	$d_{y1average} = 1,49$	$d_{y2average} = 0,48$
Ultimate: [kN]	$F_u = 189,25$	$d_{uav} = 35,40$	$d_{u1} = 22,70$	$d_{u2} = 22,10$
Stiffness: [kN/mm]		$K_{av} = 33,31$	$K_{LVD1} = 146,66$	$K_{LVD2} = 270,44$

COLLAPSE MODE☐ Rivet Shear☐ Bearing☒ Tension☐ Shear out

U-16-10-4-B

Specimen tag	S	U	Width plate (mm)	70
U-16-10-4-B		✓	Dist. from edge (mm)	35
Rivet diam. (mm)	16		Rivet pitch (mm)	140
Thickness plate (mm)	10		Rivet no.	4

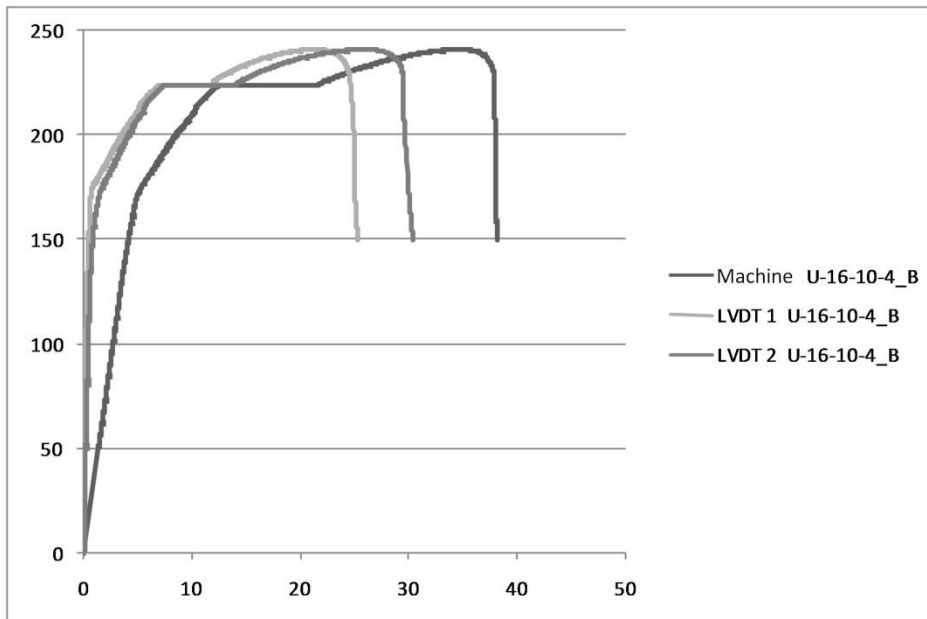
PHOTOS



Test Information:

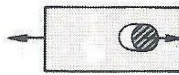
The failed plate width, at yielding, is equal to 61,1 mm; The unfailed plate width, at yielding, is equal to 62,9 mm; the hole width is equal to 17,5 mm.

RESULTS





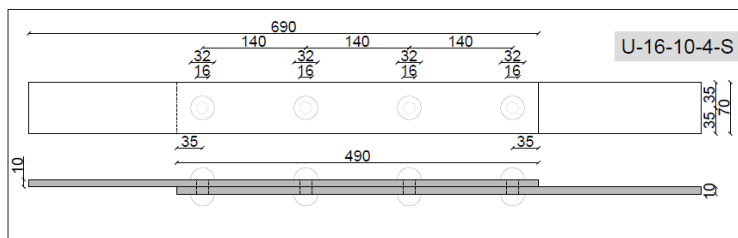
Peak: [kN]	$F_p = 241,13$	$d_{pav} = 34,45$	$d_{p1} = 21,23$	$d_{p2} = 25,78$
Elastic limit: [kN]	$F_{yaverage} = 168,69$	$d_{yaverage} = 4,84$	$d_{y1average} = 0,66$	$d_{y2average} = 1,36$
Ultimate: [kN]	$F_u = 192,90$	$d_{uav} = 37,90$	$d_{u1} = 24,90$	$d_{u2} = 29,70$
Stiffness: [kN/mm]		$K_{av} = 36,04$	$K_{LVD1} = 161,85$	$K_{LVD2} = 216,93$

COLLAPSE MODE☐ Rivet Shear☐ Bearing☒ Tension☐ Shear out

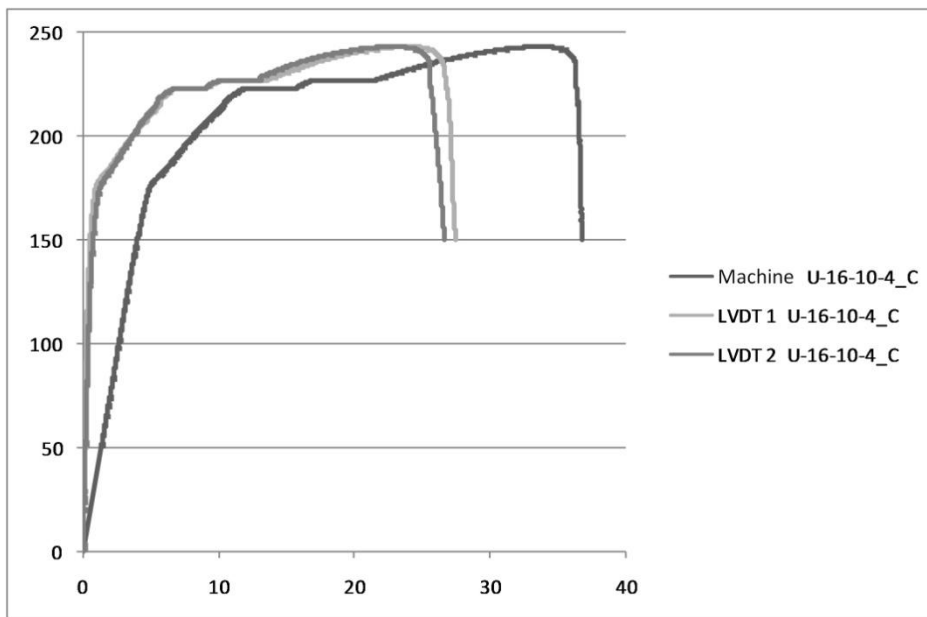
U-16-10-4-C

Specimen tag	S	U	Width plate (mm)	70
U-16-10-4-C		✓	Dist. from edge (mm)	35
Rivet diam. (mm)	16		Rivet pitch (mm)	140
Thickness plate (mm)	10		Rivet no.	4

PHOTOS

**Test Information:**

The failed plate width, at yielding, is equal to 63,7 mm; The unfailed plate width, at yielding, is equal to 64,4 mm; the hole width is equal to 17 mm.

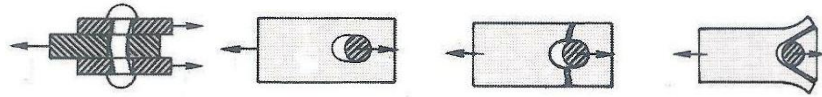
RESULTS



Peak: [kN]	$F_p = 242,85$	$d_{pav} = 33,73$	$d_{p1} = 23,91$	$d_{p2} = 22,90$
Elastic limit: [kN]	$F_{yaverage} = 170,68$	$d_{yaverage} = 4,7$	$d_{y1average} = 0,81$	$d_{y2average} = 1,1$
Ultimate: [kN]	$F_u = 194,28$	$d_{uav} = 36,60$	$d_{u1} = 27,10$	$d_{u2} = 26,10$
Stiffness: [kN/mm]		$K_{av} = 37,66$	$K_{LVD1} = 166,58$	$K_{LVD2} = 234,8$

COLLAPSE MODE

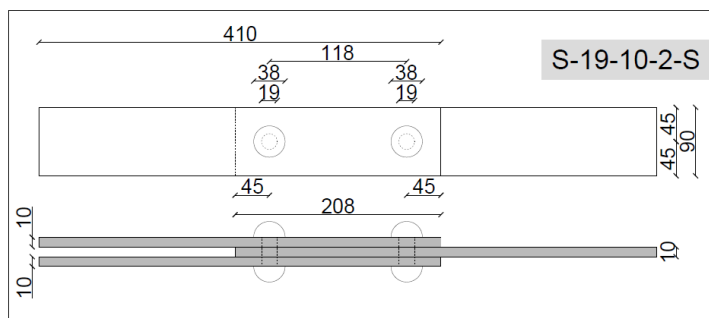
☐ Rivet Shear
 ☐ Bearing
 ☒ Tension
 ☐ Shear out



S-19-10-2-A

Specimen tag	S	U	Width plate (mm)	90
S-19-10-2-C	✓		Dist. from edge (mm)	45
Rivet diam. (mm)	19		Rivet pitch (mm)	118
Thickness plate (mm)	10		Rivet no.	2

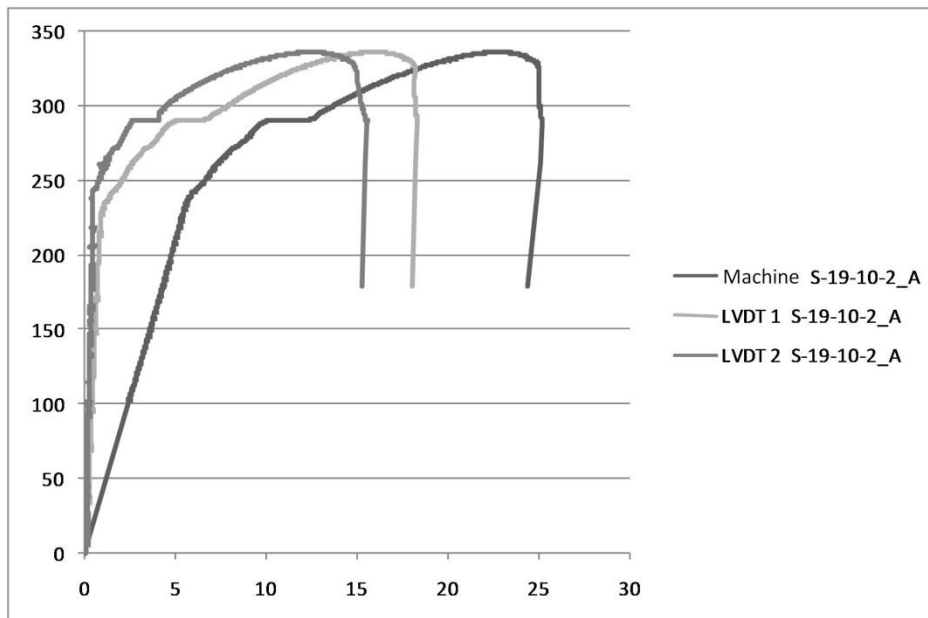
PHOTOS

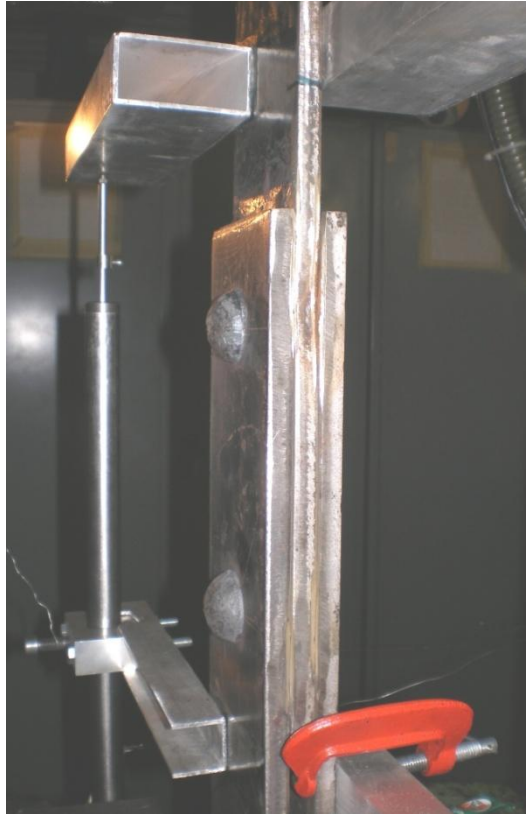


Test Information:

The inner plate width, at yielding, is equal to 82,8 mm.

RESULTS





Peak: [kN]	$F_p = 336,63$	$d_{pav} = 22,74$	$d_{p1} = 15,96$	$d_{p2} = 12,52$
Elastic limit: [kN]	$F_{yaverage} = 236,69$	$d_{yaverage} = 5,67$	$d_{y1average} = 1,24$	$d_{y2average} = 0,44$
Ultimate: [kN]	$F_u = 269,30$	$d_{uav} = 25,10$	$d_{u1} = 18,10$	$d_{u2} = 15,50$
Stiffness: [kN/mm]		$K_{av} = 42$	$K_{LVD1} = 272,45$	$K_{LVD2} = 564,9$

COLLAPSE MODE

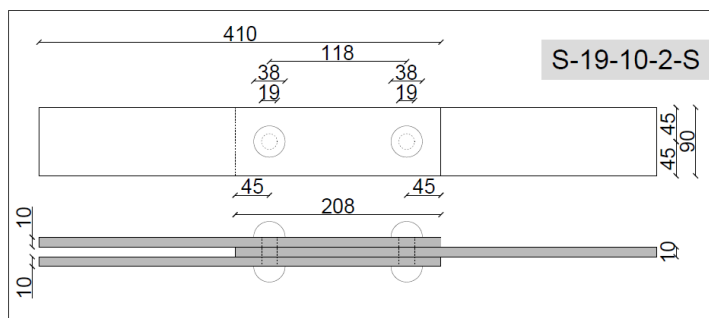
☐ Rivet Shear
 ☐ Bearing
 ☒ Tension
 ☐ Shear out



S-19-10-2-B

Specimen tag	S	U	Width plate (mm)	90
S-19-10-2-B	✓		Dist. from edge (mm)	45
Rivet diam. (mm)	19		Rivet pitch (mm)	118
Thickness plate (mm)	10		Rivet no.	2

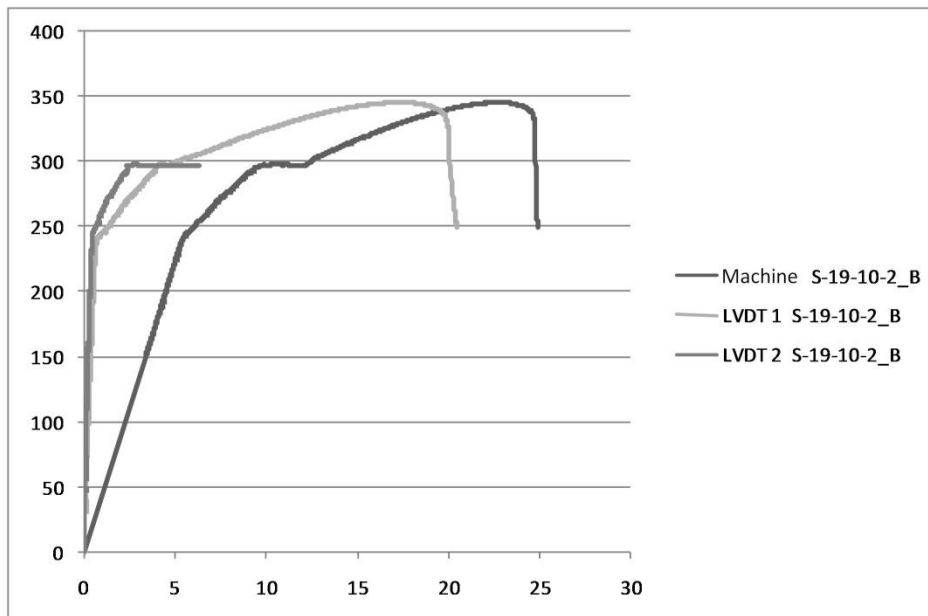
PHOTOS



Test Information:

The inner plate width, at yielding, is equal to 82,8 mm; the hole width is equal to 17 mm.

RESULTS

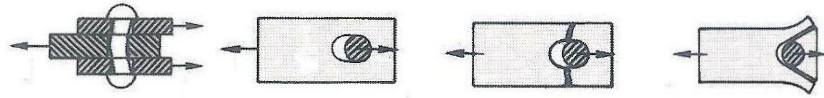




Peak: [kN]	$F_p = 346,02$	$d_{pav} = 22,74$	$d_{p1} = 17,34$	$d_{p2} = -$
Elastic limit: [kN]	$F_{yaverage} = 240,71$	$d_{yaverage} = 5,4$	$d_{y1average} = 0,76$	$d_{y2average} = 0,43$
Ultimate: [kN]	$F_u = 276,82$	$d_{uav} = 24,80$	$d_{u1} = 20,20$	$d_{u2} = -$
Stiffness: [kN/mm]		$K_{av} = 44,75$	$K_{LVD1} = 355,96$	$K_{LVD2} = 502,63$

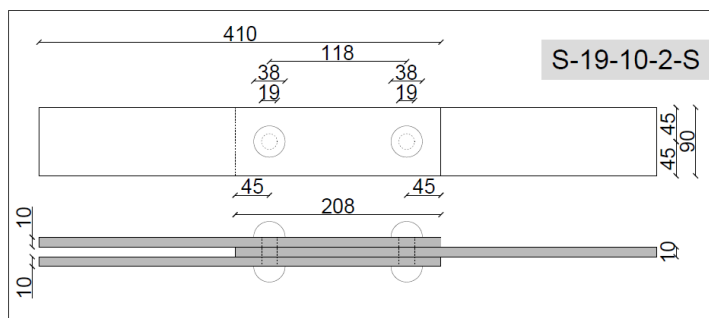
COLLAPSE MODE

☐ Rivet Shear
 ☐ Bearing
 ☒ Tension
 ☐ Shear out

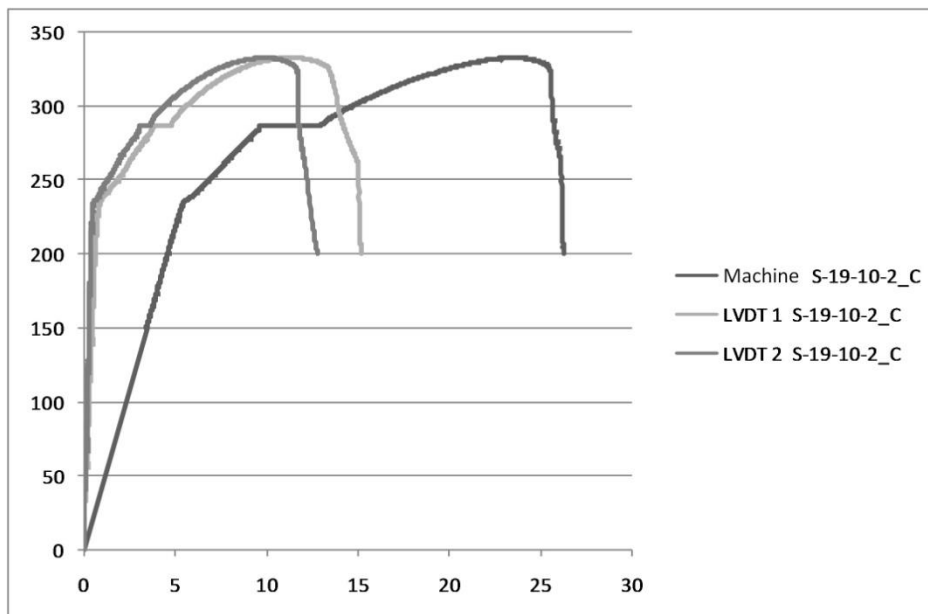


S-19-10-2-C

Specimen tag	S	U	Width plate (mm)	90
S-19-10-2-C	✓		Dist. from edge (mm)	45
Rivet diam. (mm)	19		Rivet pitch (mm)	118
Thickness plate (mm)	10		Rivet no.	2

PHOTOS**Test Information:**

The failed plate width, at yielding, is equal to 82,43 mm; The unfailed plate width, at yielding, is equal to 83,26 mm; the hole width is equal to 20,46 mm.

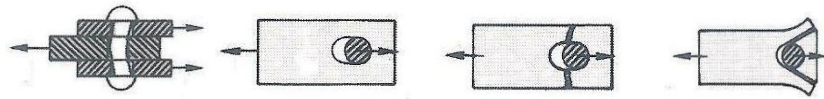
RESULTS



Peak: [kN]	$F_p = 332,60$	$d_{pav} = 23,35$	$d_{p1} = 11,14$	$d_{p2} = 9,78$
Elastic limit: [kN]	$F_{yaverage} = 230,69$	$d_{yaverage} = 5,31$	$d_{y1average} = 0,8$	$d_{y2average} = 0,46$
Ultimate: [kN]	$F_u = 266,08$	$d_{uav} = 26,10$	$d_{u1} = 14,80$	$d_{u2} = 12,10$
Stiffness: [kN/mm]		$K_{av} = 43,72$	$K_{LVD1} = 299,48$	$K_{LVD2} = 574,86$

COLLAPSE MODE

☐ Rivet Shear
 ☐ Bearing
 ☒ Tension
 ☐ Shear out



U-19-10-2-A_90mm

Specimen tag	S	U	Width plate (mm)	90
U-19-10-2-A_90mm		✓	Dist. from edge (mm)	45
Rivet diam. (mm)	19		Rivet pitch (mm)	118
Thickness plate (mm)	10		Rivet no.	2

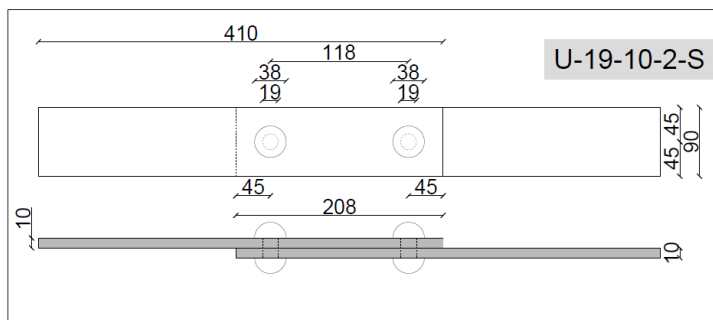
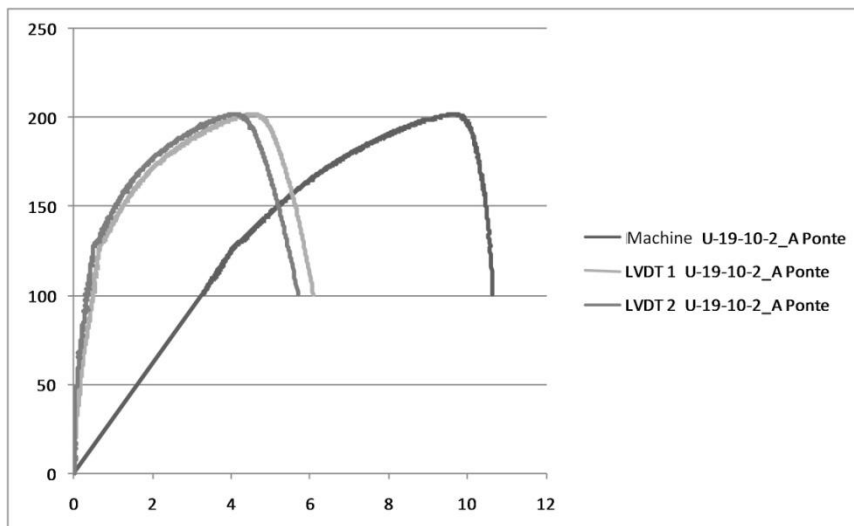
PHOTOS**Test Information:**

Plate 1: out of plane displacement =11 mm, Plate 2: out of plane displacement =12.3 mm.
Plate 1: side A hole deformed dimensions=19,69x20,04 mm; side B hole deformed dimensions=20,14x21,04 mm;
Plate 2: side A hole deformed dimensions=19,85x21 mm; side B hole deformed dimensions=19,72x20,75 mm.

RESULTS



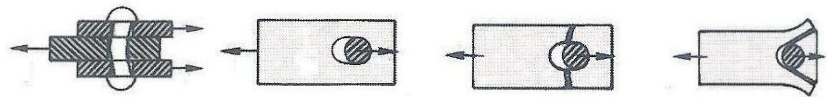
Peak: [kN]	$F_p = 201,55$	$d_{pav} = 9,69$	$d_{p1} = 4,59$	$d_{p2} = 4,10$
Elastic limit: [kN]	$F_{yaverage} = 128,68$	$d_{yaverage} = 4,13$	$d_{y1average} = 0,7$	$d_{y2average} = 0,54$
Ultimate: [kN]	$F_u = 161,24$	$d_{uav} = 10,40$	$d_{u1} = 5,52$	$d_{u2} = 5,05$
Stiffness: [kN/mm]		$K_{av} = 30,68$	$K_{LVD1} = 155,2$	$K_{LVD2} = 217,29$

COLLAPSE MODE

☒ Rivet Shear

☐ Bearing

☐ Tension

☐ Shear out


U-19-10-2-B_90mm

Specimen tag	S	U	Width plate (mm)	90
U-19-10-2-B_90mm		✓	Dist. from edge (mm)	45
Rivet diam. (mm)	19		Rivet pitch (mm)	118
Thickness plate (mm)	10		Rivet no.	2

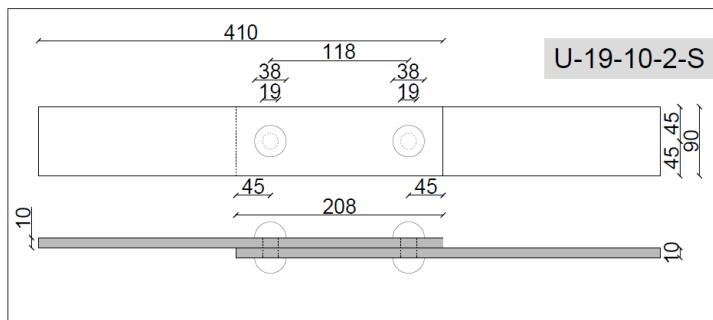
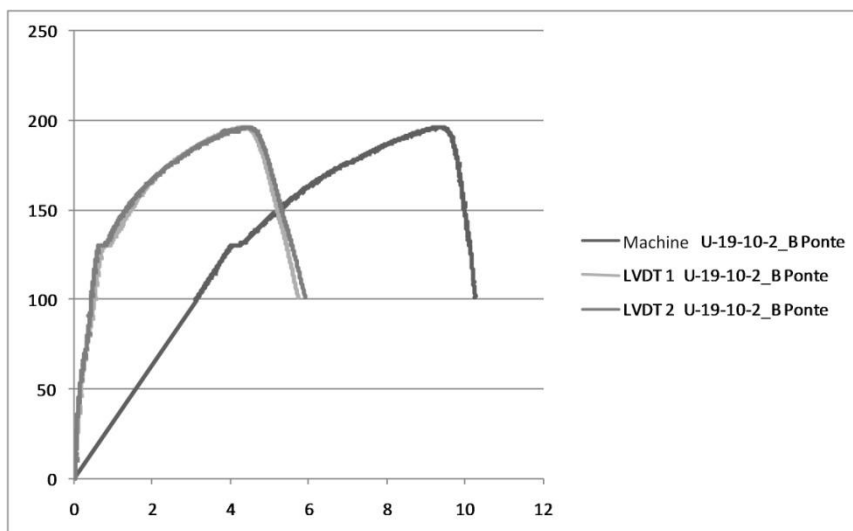
PHOTOS**Test Information:**

Plate 1: out of plane displacement=10.4mm, Plate 2: out of plane displacement=9.85 mm.

Plate 1: side A hole deformed dimensions=20,42x20,98 mm; side B hole deformed dimensions=20,14x21,04 mm;

Plate 2: side A hole deformed dimensions=19,20x20,6 mm; side B hole deformed dimensions= 19,68x20,52 mm.

RESULTS



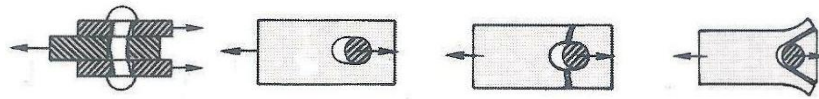
Peak: [kN]	$F_p = 196,22$	$d_{pav} = 9,32$	$d_{p1} = 4,32$	$d_{p2} = 4,40$
Elastic limit: [kN]	$F_{yaverage} = 126,69$	$d_{yaverage} = 3,9$	$d_{y1average} = 0,71$	$d_{y2average} = 0,6$
Ultimate: [kN]	$F_u = 156,97$	$d_{uav} = 9,93$	$d_{u1} = 5,11$	$d_{u2} = 5,22$
Stiffness: [kN/mm]		$K_{av} = 31,93$	$K_{LVD1} = 263,22$	$K_{LVD2} = 340,22$

COLLAPSE MODE

☒ Rivet Shear

☐ Bearing

☐ Tension

☐ Shear out


U-19-10-2-C_90mm

Specimen tag	S	U	Width plate (mm)	90
U-19-10-2-C_90mm		✓	Dist. from edge (mm)	45
Rivet diam. (mm)	19		Rivet pitch (mm)	118
Thickness plate (mm)	10		Rivet no.	2

PHOTOS

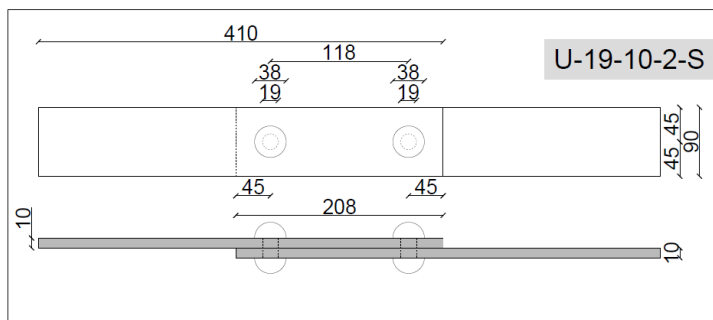
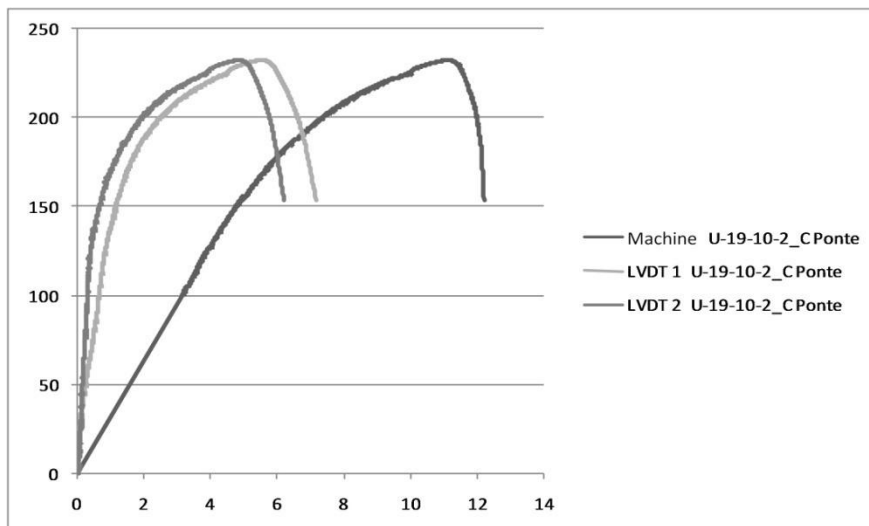
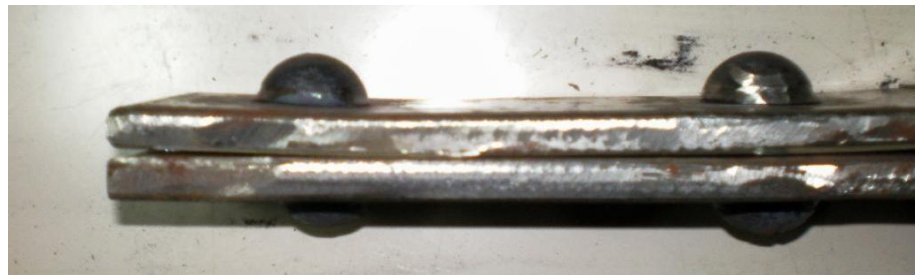
**Test Information:**

Plate 1: out of plane displacement=15,04mm, Plate 2: out of plane displacement=14,1mm.

Plate 1: side A hole deformed dimensions=19,82x20,70 mm; side B hole deformed dimensions=19,91x21,88 mm;

Plate 2: side A hole deformed dimensions=19,79x21,22 mm; side B hole deformed dimensions= 19,35x20,8 mm.

RESULTS



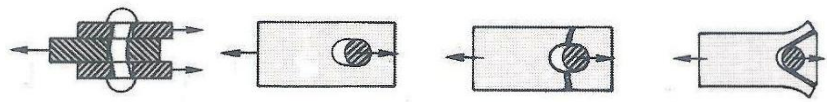
Peak: [kN]	$F_p = 232,35$	$d_{pav} = 11,17$	$d_{p1} = 5,56$	$d_{p2} = 4,88$
Elastic limit: [kN]	$F_{yaverage} = 126,70$	$d_{yaverage} = 3,95$	$d_{y1average} = 0,86$	$d_{y2average} = 0,42$
Ultimate: [kN]	$F_u = 185,88$	$d_{uav} = 12,12$	$d_{u1} = 6,84$	$d_{u2} = 5,95$
Stiffness: [kN/mm]		$K_{av} = 31,58$	$K_{LVD1} = 137,4$	$K_{LVD2} = 338,13$

COLLAPSE MODE

☒ Rivet Shear

☐ Bearing

☐ Tension

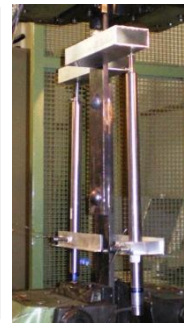
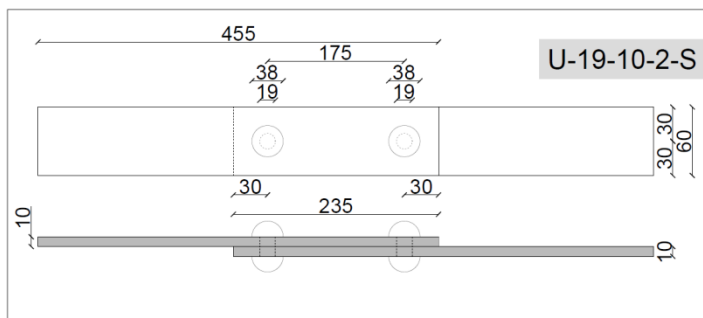
☐ Shear out


Appendix

U-19-10-2-A_60mm

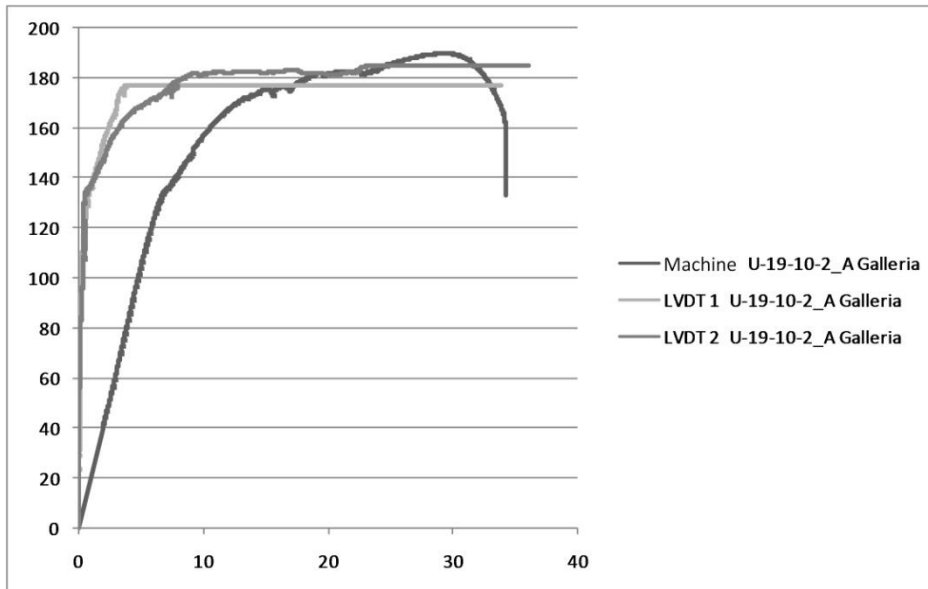
Specimen tag	S	U	Width plate (mm)	60
U-19-10-2-A_60mm		✓	Dist. from edge (mm)	30
Rivet diam. (mm)	19		Rivet pitch (mm)	175
Thickness plate (mm)	10		Rivet no.	2

PHOTOS



Test Information:

RESULTS

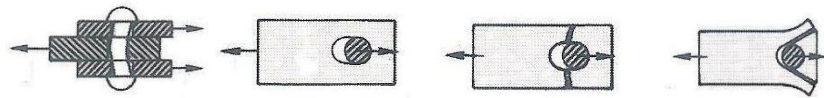




Peak: [kN]	$F_p = 190,09$	$d_{pav} = 29,26$	$d_{p1} = -$	$d_{p2} = -$
Elastic limit: [kN]	$F_{yaverage} = 128,68$	$d_{yaverage} = 6,33$	$d_{y1average} = 0,64$	$d_{y2average} = 0,41$
Ultimate: [kN]	$F_u = 152,07$	$d_{uav} = 34,20$	$d_{u1} = -$	$d_{u2} = -$
Stiffness: [kN/mm]		$K_{av} = 20,72$	$K_{LVD1} = 431,06$	$K_{LVD2} = 280,92$

COLLAPSE MODE

☐ Rivet Shear
 ☐ Bearing
 ☒ Tension
 ☐ Shear out

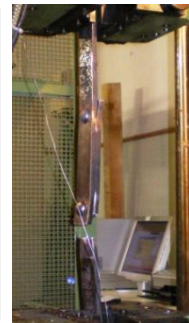
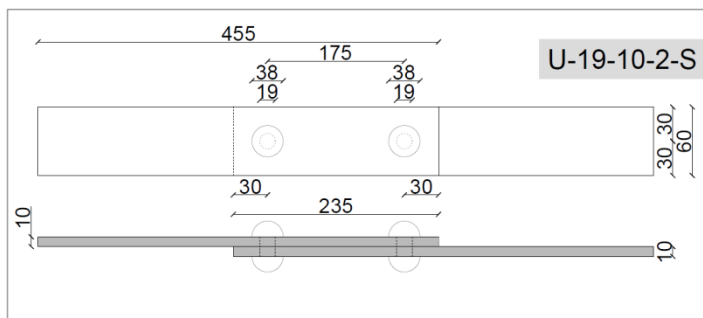


Appendix

U-19-10-2-B_60mm

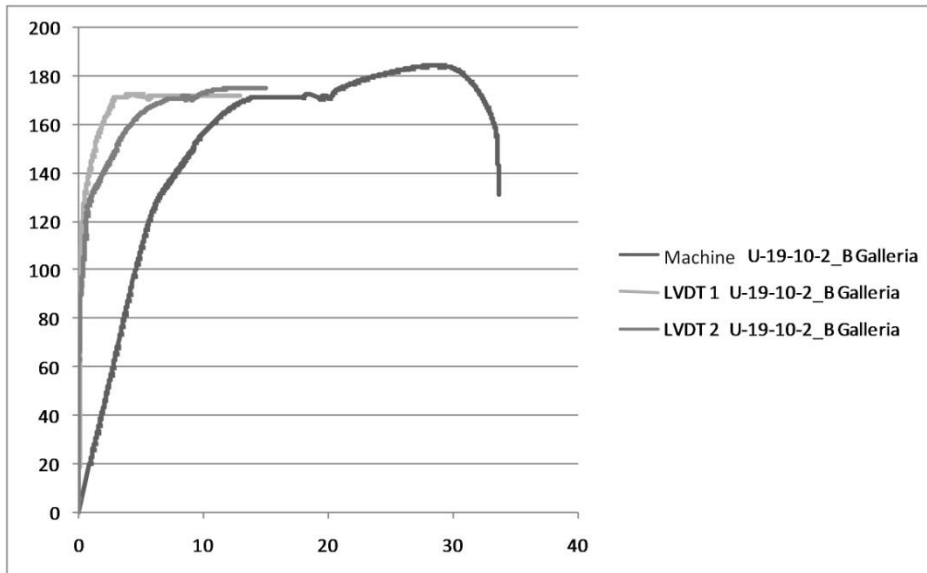
Specimen tag	S	U	Width plate (mm)	60
U-19-10-2-B_60mm		✓	Dist. from edge (mm)	30
Rivet diam. (mm)	19		Rivet pitch (mm)	175
Thickness plate (mm)	10		Rivet no.	2

PHOTOS



Test Information:

RESULTS

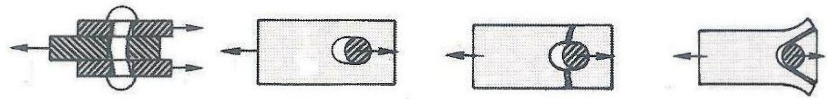




Peak: [kN]	$F_p = 184,23$	$d_{pav} = 28,44$	$d_{p1} = -$	$d_{p2} = -$
Elastic limit: [kN]	$F_{yaverage} = 123,36$	$d_{yaverage} = 5,89$	$d_{y1average} = 0,37$	$d_{y2average} = 0,67$
Ultimate: [kN]	$F_u = 147,38$	$d_{uav} = 33,66$	$d_{u1} = -$	$d_{u2} = -$
Stiffness: [kN/mm]		$K_{av} = 21,77$	$K_{LVD1} = 748,08$	$K_{LVD2} = 696,04$

COLLAPSE MODE

☐ Rivet Shear
 ☐ Bearing
 ☒ Tension
 ☐ Shear out

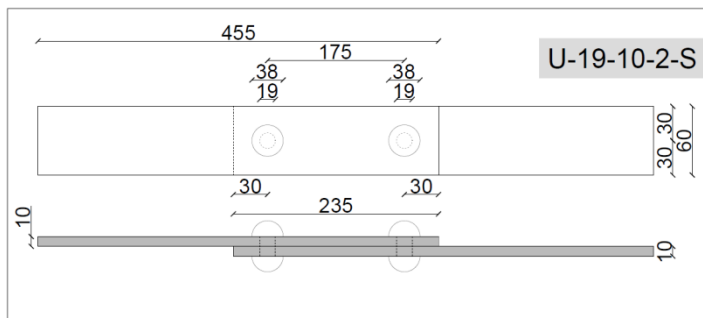


Appendix

U-19-10-2-C_60mm

Specimen tag	S	U	Width plate (mm)	60
U-19-10-2-C_60mm		✓	Dist. from edge (mm)	30
Rivet diam. (mm)	19		Rivet pitch (mm)	175
Thickness plate (mm)	10		Rivet no.	2

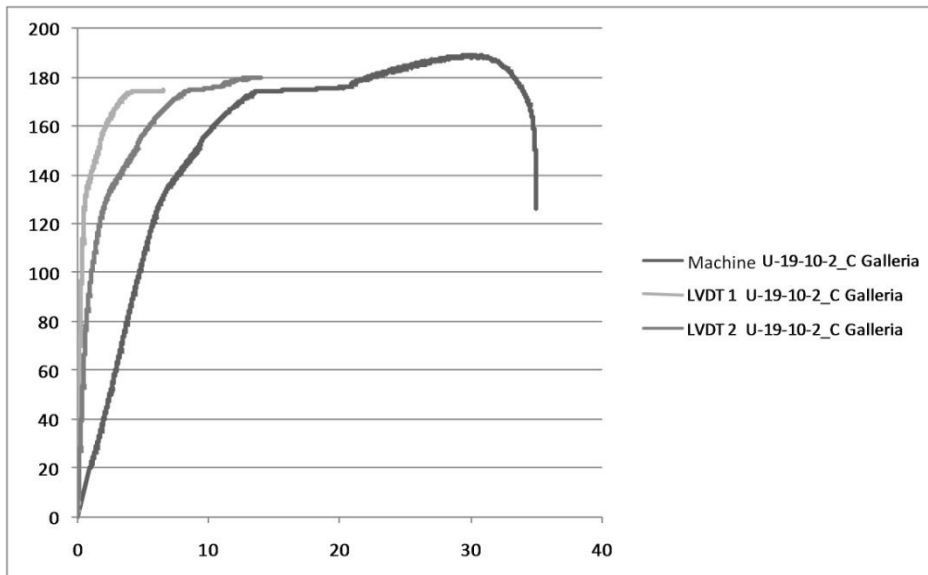
PHOTOS



Test Information:

Out of plane displacement for all plates = 2 mm.

RESULTS





Peak: [kN]	$F_p = 188,92$	$d_{pav} = 29,60$	$d_{p1} = -$	$d_{p2} = -$
Elastic limit: [kN]	$F_{yaverage} = 121,34$	$d_{yaverage} = 5,61$	$d_{y1average} = 0,46$	$d_{y2average} = 1,73$
Ultimate: [kN]	$F_u = 151,13$	$d_{uav} = 34,67$	$d_{u1} = -$	$d_{u2} = -$
Stiffness: [kN/mm]		$K_{av} = 22,14$	$K_{LVD1} = 403,99$	$K_{LVD2} = 101,77$

COLLAPSE MODE

☐ Rivet Shear
 ☐ Bearing
 ☒ Tension
 ☐ Shear out

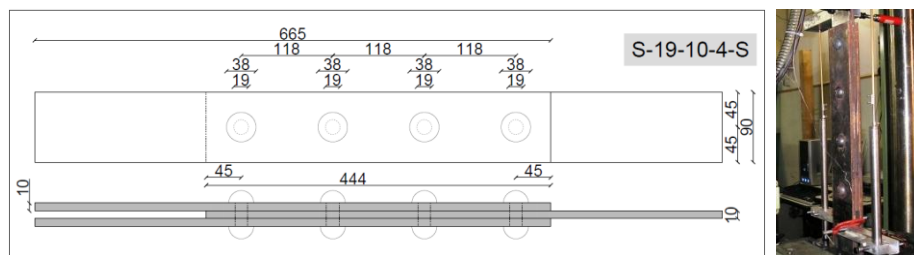


Appendix

S-19-10-4-A

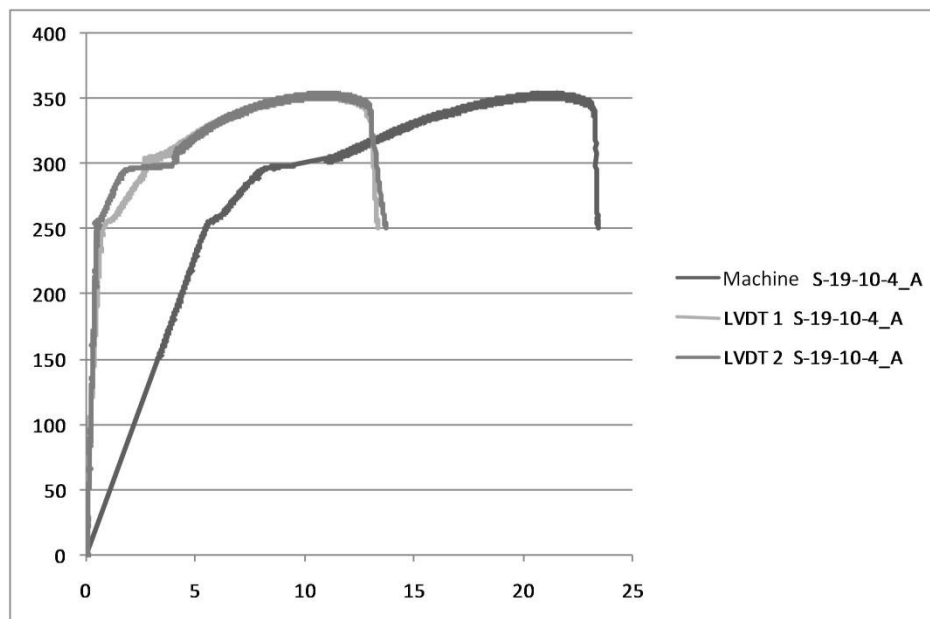
Specimen tag	S	U	Width plate (mm)	90
S-19-10-4-A	✓		Dist. from edge (mm)	45
Rivet diam. (mm)	19		Rivet pitch (mm)	118
Thickness plate (mm)	10		Rivet no.	4

PHOTOS



Test Information:

RESULTS

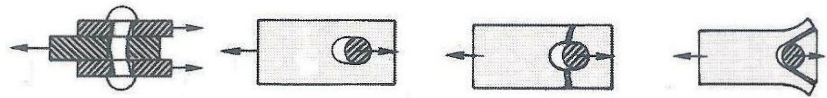




Peak: [kN]	$F_p = 354,63$	$d_{pav} = 20,98$	$d_{p1} = 10,66$	$d_{p2} = 10,71$
Elastic limit: [kN]	$F_{yaverage} = 254,04$	$d_{yaverage} = 5,56$	$d_{y1average} = 0,89$	$d_{y2average} = 0,58$
Ultimate: [kN]	$F_u = 283,70$	$d_{uav} = 23,30$	$d_{u1} = 15,20$	$d_{u2} = 13,40$
Stiffness: [kN/mm]		$K_{av} = 45,92$	$K_{LVD1} = 288,89$	$K_{LVD2} = 520,91$

COLLAPSE MODE

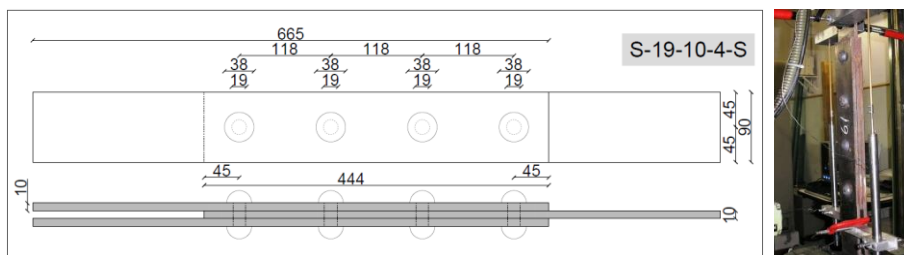
☐ Rivet Shear
 ☐ Bearing
 ☒ Tension
 ☐ Shear out



S-19-10-4-B

Specimen tag	S	U	Width plate (mm)	90
S-19-10-4-B	✓		Dist. from edge (mm)	45
Rivet diam. (mm)	19		Rivet pitch (mm)	118
Thickness plate (mm)	10		Rivet no.	4

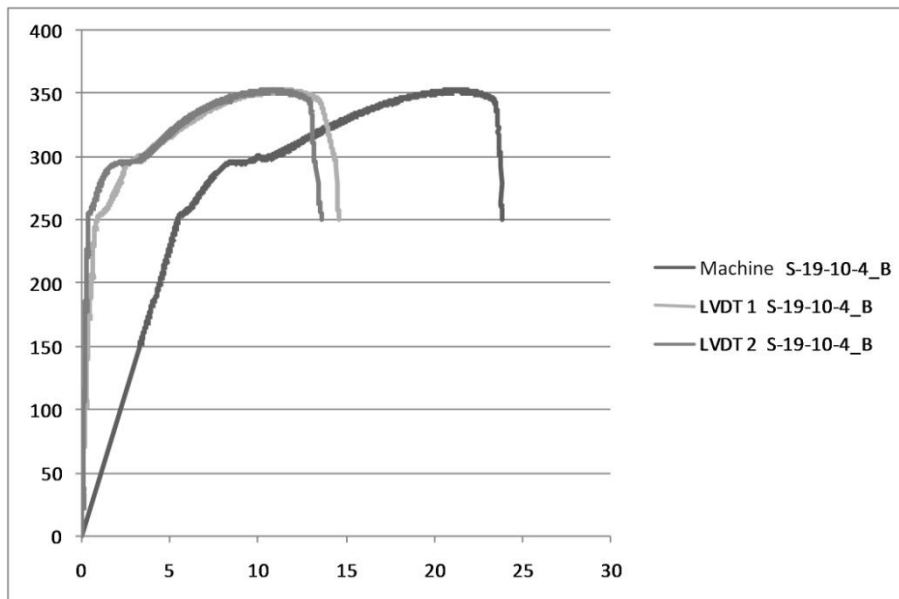
PHOTOS



Test Information:

The inner plate width, at yielding, is equal to 82.1 mm; The unfailed plate width, at yielding, is equal to 83.1 mm; the hole width is equal to 21.1 mm.

RESULTS

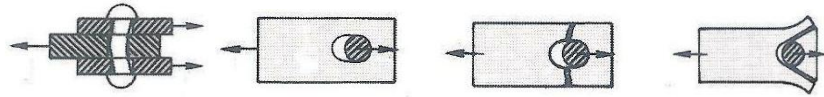




Peak: [kN]	$F_p = 353,27$	$d_{pav} = 21,20$	$d_{p1} = 11,27$	$d_{p2} = 10,76$
Elastic limit: [kN]	$F_{yaverage} = 251,45$	$d_{yaverage} = 5,48$	$d_{y1average} = 0,91$	$d_{y2average} = 0,33$
Ultimate: [kN]	$F_u = 282,62$	$d_{uav} = 23,80$	$d_{u1} = 14,40$	$d_{u2} = 13,30$
Stiffness: [kN/mm]		$K_{av} = 45,95$	$K_{LVD1} = 374,7$	$K_{LVD2} = 394,52$

COLLAPSE MODE

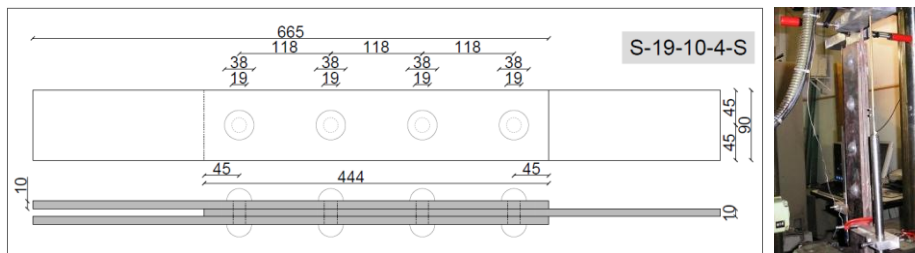
☐ Rivet Shear
 ☐ Bearing
 ☒ Tension
 ☐ Shear out



S-19-10-4-C

Specimen tag	S	U	Width plate (mm)	90
S-19-10-4-C	✓		Dist. from edge (mm)	45
Rivet diam. (mm)	19		Rivet pitch (mm)	118
Thickness plate (mm)	10		Rivet no.	4

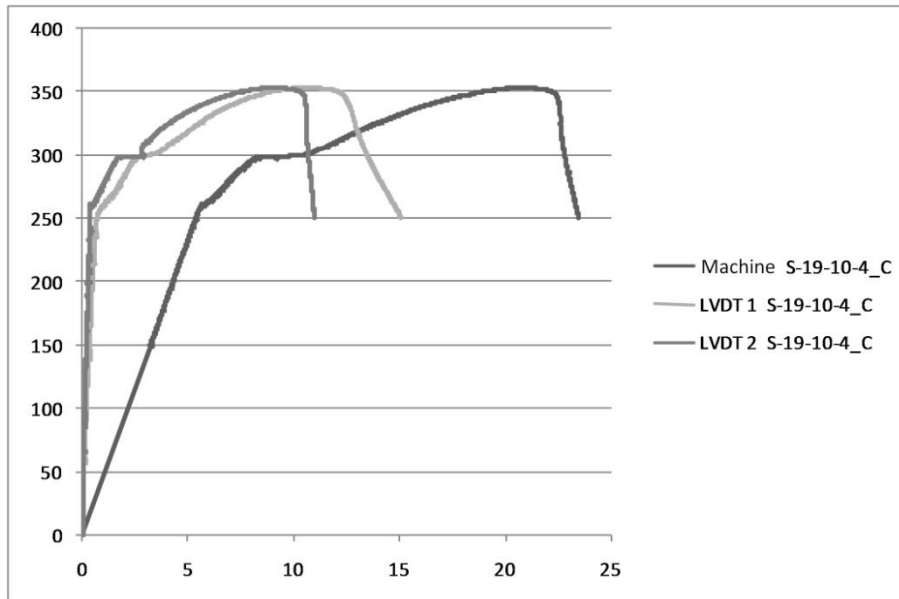
PHOTOS



Test Information:

The inner plate width, at yielding, is equal to 82.5 mm; The unfailed plate width, at yielding, is equal to 85.3 mm; the hole width is equal to 21.2 mm.

RESULTS





Peak: [kN]	$F_p = 352,96$	$d_{pav} = 20,67$	$d_{p1} = 10,45$	$d_{p2} = 8,93$
Elastic limit: [kN]	$F_{yaverage} = 256,67$	$d_{yaverage} = 5,56$	$d_{y1average} = 0,87$	$d_{y2average} = 0,4$
Ultimate: [kN]	$F_u = 282,37$	$d_{uav} = 23,10$	$d_{u1} = 14,10$	$d_{u2} = 10,80$
Stiffness: [kN/mm]		$K_{av} = 46,47$	$K_{LVD1} = 325,54$	$K_{LVD2} = 578,94$

COLLAPSE MODE

☐ Rivet Shear

☐ Bearing

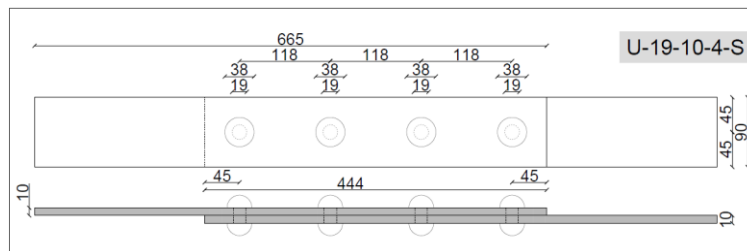
☒ Tension

☐ Shear out

U-19-10-4-A_90mm

Specimen tag	S	U	Width plate (mm)	90
U-19-10-4-A_90mm		✓	Dist. from edge (mm)	45
Rivet diam. (mm)	19		Rivet pitch (mm)	118
Thickness plate (mm)	10		Rivet no.	4

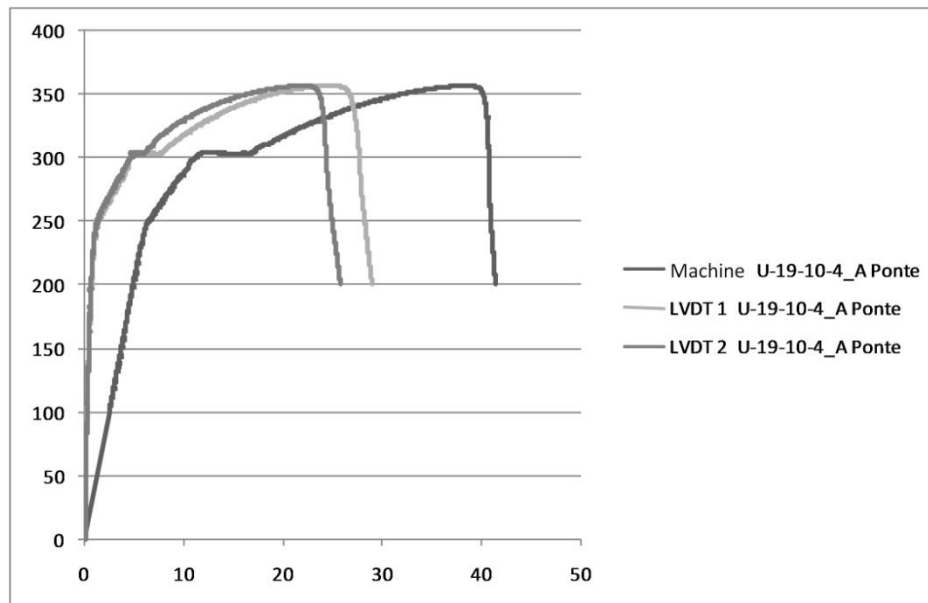
PHOTOS



Test Information:

The failed plate width, at yielding, is equal to 81.6 mm; The unfailed plate width, at yielding, is equal to 83.4 mm; the hole width is equal to 21.9 mm.

RESULTS





Peak: [kN]	$F_p = 356,61$	$d_{pav} = 38,13$	$d_{p1} = 24,52$	$d_{p2} = 21,71$
Elastic limit: [kN]	$F_{yaverage} = 250,01$	$d_{yaverage} = 6,42$	$d_{y1average} = 1,34$	$d_{y2average} = 1,24$
Ultimate: [kN]	$F_u = 285,28$	$d_{uav} = 40,80$	$d_{u1} = 27,80$	$d_{u2} = 24,50$
Stiffness: [kN/mm]		$K_{av} = 40,02$	$K_{LVD1} = 200,56$	$K_{LVD2} = 251,46$

COLLAPSE MODE

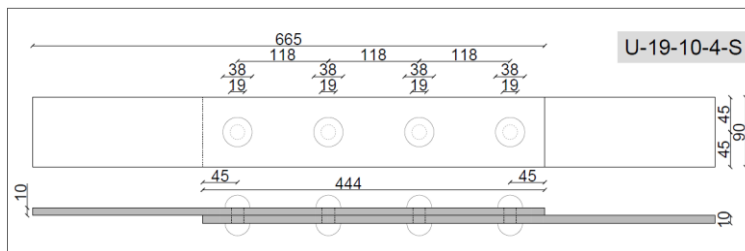
☐ Rivet Shear
 ☐ Bearing
 ☒ Tension
 ☐ Shear out



U-19-10-4-B_90mm

Specimen tag	S	U	Width plate (mm)	90
U-19-10-4-B_90mm		✓	Dist. from edge (mm)	45
Rivet diam. (mm)	19		Rivet pitch (mm)	118
Thickness plate (mm)	10		Rivet no.	4

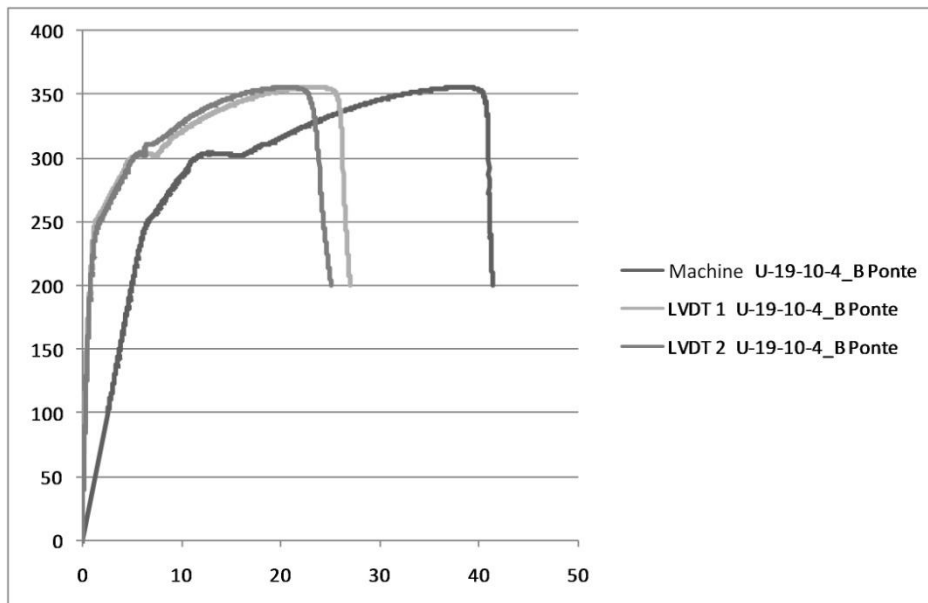
PHOTOS



Test Information:

The failed plate width, at yielding, is equal to 82.3 mm; The unfailed plate width, at yielding, is equal to 83 mm; the hole width is equal to 20.1 mm.

RESULTS

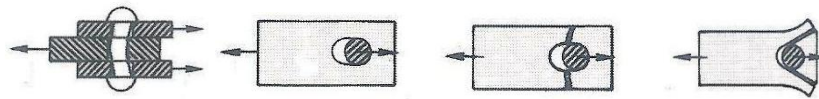




Peak: [kN]	$F_p = 355,52$	$d_{pav} = 38,24$	$d_{p1} = 23,44$	$d_{p2} = 20,63$
Elastic limit: [kN]	$F_{yaverage} = 243,38$	$d_{yaverage} = 6,22$	$d_{y1average} = 1,16$	$d_{y2average} = 1,43$
Ultimate: [kN]	$F_u = 284,42$	$d_{uav} = 40,90$	$d_{u1} = 26,30$	$d_{u2} = 23,90$
Stiffness: [kN/mm]		$K_{av} = 39,42$	$K_{LVD1} = 135,95$	$K_{LVD2} = 193,2$

COLLAPSE MODE

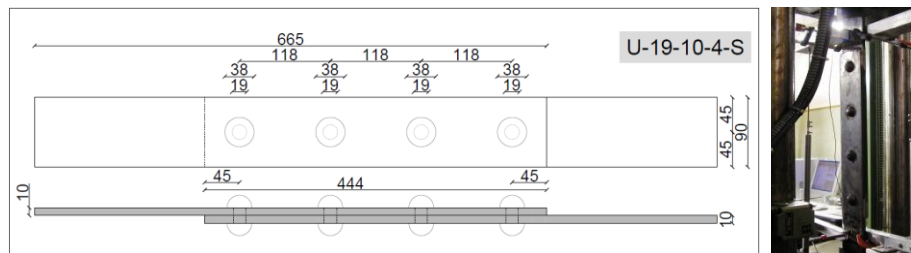
☐ Rivet Shear
 ☐ Bearing
 ☒ Tension
 ☐ Shear out



U-19-10-4-C_90mm

Specimen tag	S	U	Width plate (mm)	90
U-19-10-4-C_90mm		✓	Dist. from edge (mm)	45
Rivet diam. (mm)	19		Rivet pitch (mm)	118
Thickness plate (mm)	10		Rivet no.	4

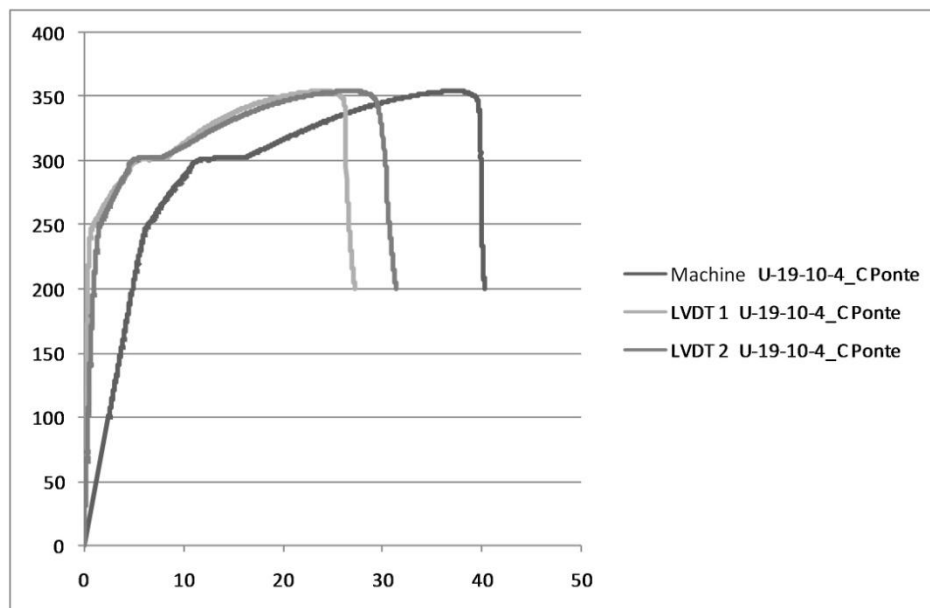
PHOTOS



Test Information:

The failed plate width, at yielding, is equal to 82.1 mm; the hole width is equal to 23 mm.

RESULTS





Peak: [kN]	$F_p = 355,12$	$d_{pav} = 37,13$	$d_{p1} = 23,84$	$d_{p2} = 26,71$
Elastic limit: [kN]	$F_{yaverage} = 246,67$	$d_{yaverage} = 6,12$	$d_{y1average} = 0,68$	$d_{y2average} = 1,44$
Ultimate: [kN]	$F_u = 284,10$	$d_{uav} = 39,90$	$d_{u1} = 26,40$	$d_{u2} = 30,40$
Stiffness: [kN/mm]		$K_{av} = 40,78$	$K_{LVD1} = 220,61$	$K_{LVD2} = 223,65$

COLLAPSE MODE

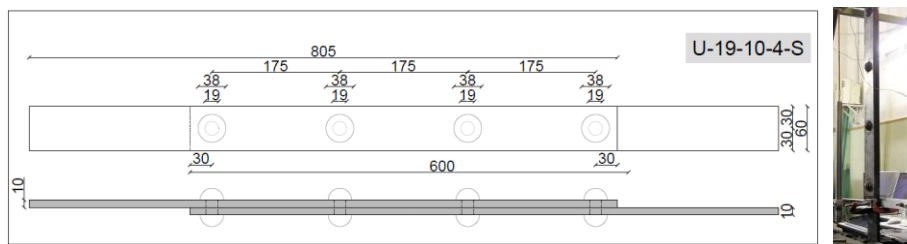
☐ Rivet Shear
 ☐ Bearing
 ☒ Tension
 ☐ Shear out



U-19-10-4-A_60mm

Specimen tag	S	U	Width plate (mm)	60
U-19-10-4-A_60mm		✓	Dist. from edge (mm)	30
Rivet diam. (mm)	19		Rivet pitch (mm)	175
Thickness plate (mm)	10		Rivet no.	4

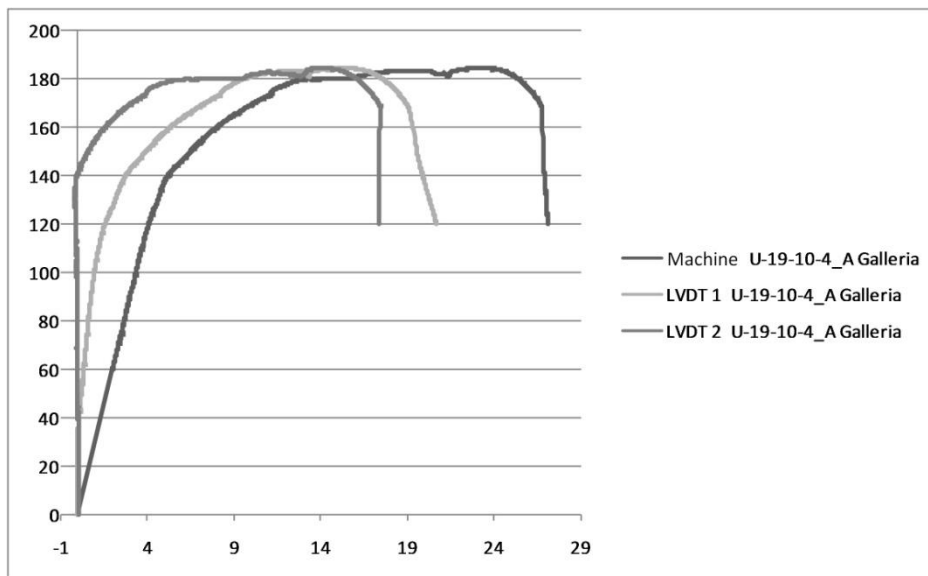
PHOTOS



Test Information:

The failed plate width, at yielding, is equal to 52.1 mm; the unfailed plate width, at yielding, is equal to 55 mm; the hole width is equal to 21.5 mm.

RESULTS

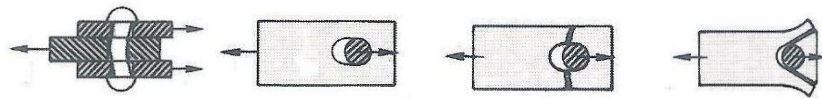




Peak: [kN]	$F_p = 184,37$	$d_{pav} = 23,01$	$d_{p1} = 15,14$	$d_{p2} = 13,91$
Elastic limit: [kN]	$F_{yaverage} = 122,69$	$d_{yaverage} = 4,21$	$d_{y1average} = 1,75$	$d_{y2average} = -0,11$
Ultimate: [kN]	$F_u = 147,50$	$d_{uav} = 26,70$	$d_{u1} = 19,60$	$d_{u2} = 17,30$
Stiffness: [kN/mm]		$K_{av} = 29,74$	$K_{LVD1} = 75,36$	$K_{LVD2} = -$

COLLAPSE MODE

☐ Rivet Shear
 ☐ Bearing
 ☒ Tension
 ☐ Shear out

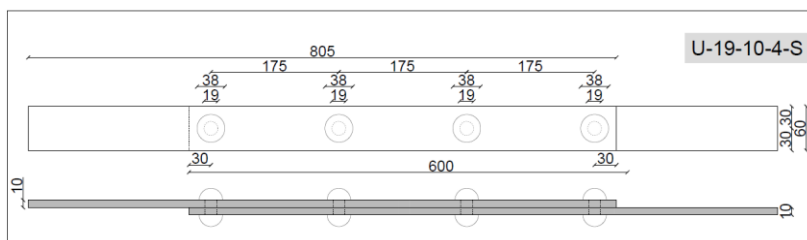


Appendix

U-19-10-4-B_60mm

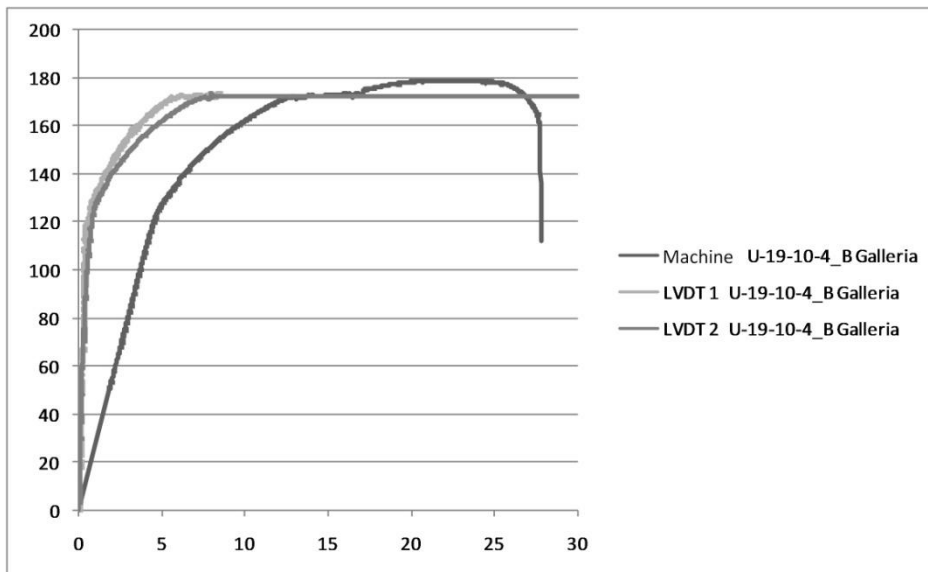
Specimen tag	S	U	Width plate (mm)	60
U-19-10-4-A_60mm		✓	Dist. from edge (mm)	30
Rivet diam. (mm)	19		Rivet pitch (mm)	175
Thickness plate (mm)	10		Rivet no.	4

PHOTOS



Test Information:

RESULTS





Peak: [kN]	$F_p = 178,42$	$d_{pav} = 20,55$	$d_{p1} = -$	$d_{p2} = -$
Elastic limit: [kN]	$F_{yaverage} = 121,34$	$d_{yaverage} = 4,61$	$d_{y1average} = 0,67$	$d_{y2average} = 0,84$
Ultimate: [kN]	$F_u = 142,74$	$d_{uav} = 27,70$	$d_{u1} = -$	$d_{u2} = -$
Stiffness: [kN/mm]		$K_{av} = 27,06$	$K_{LVD1} = 304,14$	$K_{LVD2} = 195,09$

COLLAPSE MODE

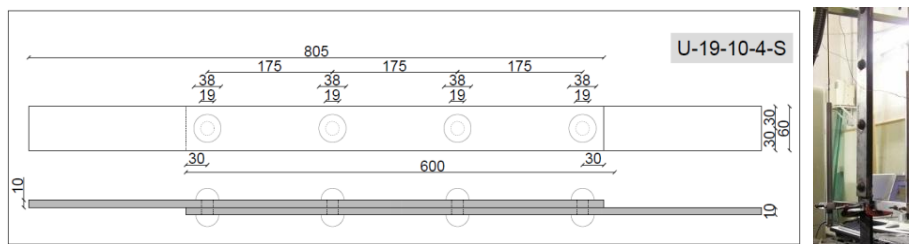
☐ Rivet Shear
 ☐ Bearing
 ☒ Tension
 ☐ Shear out



U-19-10-4-C_60mm

Specimen tag	S	U	Width plate (mm)	60
U-19-10-4-C_60mm		✓	Dist. from edge (mm)	30
Rivet diam. (mm)	19		Rivet pitch (mm)	175
Thickness plate (mm)	10		Rivet no.	4

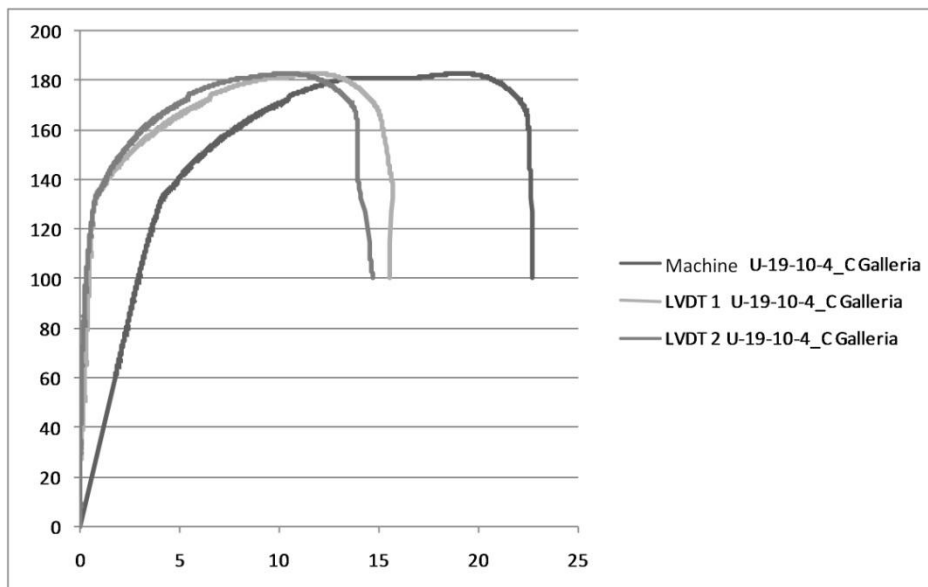
PHOTOS

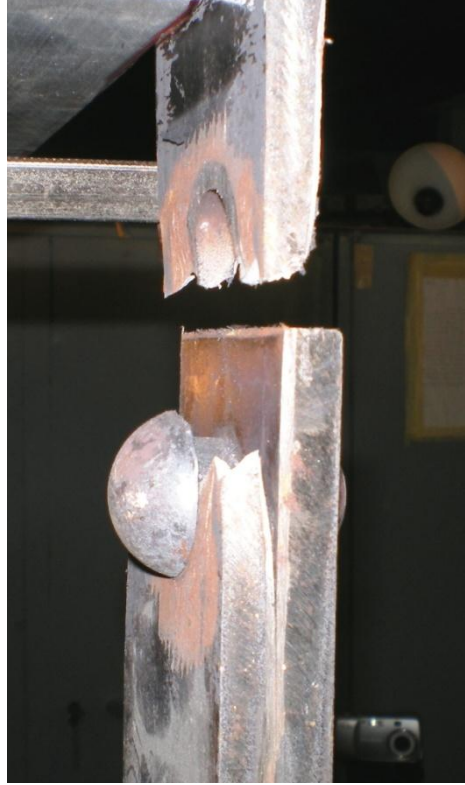


Test Information:

The failed plate width, at yielding, is equal to 52,6 mm; the unfailed plate width, at yielding, is equal to 54,1 mm; the hole width is equal to 22 mm. La larghezza del piatto

RESULTS

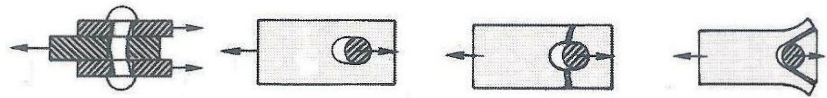




Peak: [kN]	$F_p = 183,07$	$d_{pav} = 18,96$	$d_{p1} = 11,69$	$d_{p2} = 10,27$
Elastic limit: [kN]	$F_{yaverage} = 130,70$	$d_{yaverage} = 4,02$	$d_{y1average} = 0,71$	$d_{y2average} = 0,72$
Ultimate: [kN]	$F_u = 146,46$	$d_{uav} = 22,50$	$d_{u1} = 15,40$	$d_{u2} = 13,90$
Stiffness: [kN/mm]		$K_{av} = 34,39$	$K_{LVD1} = 180,56$	$K_{LVD2} = 430,16$

COLLAPSE MODE

☐ Rivet Shear
 ☐ Bearing
 ☒ Tension
 ☐ Shear out

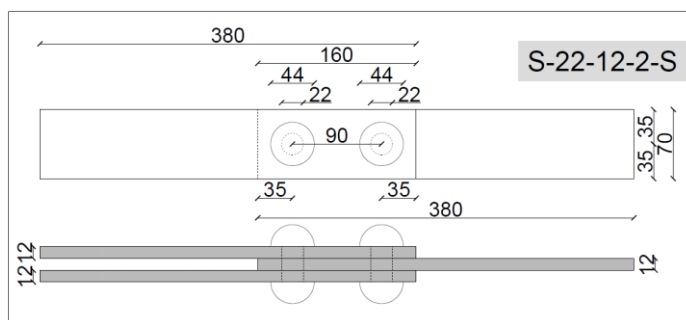


Appendix

S-22-12-2-A

Specimen tag	S	U	Width plate (mm)	70
S-22-12-2-A	✓		Dist. from edge (mm)	35
Rivet diam. (mm)	22		Rivet pitch (mm)	90
Thickness plate (mm)	12		Rivet no.	2

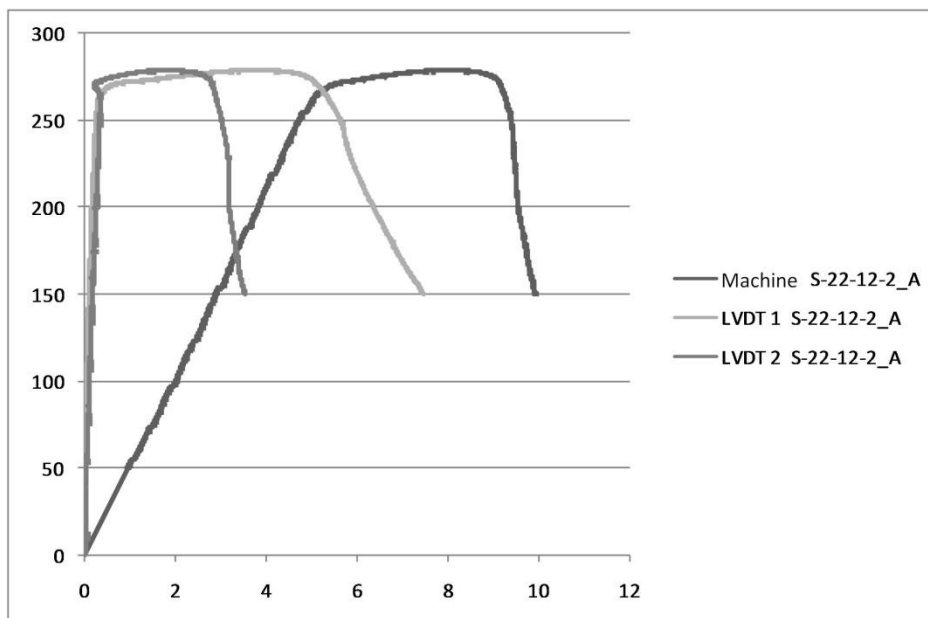
PHOTOS



Test Information:

The inner plate width, at yielding, is equal to 63.7 mm; the hole deformed dimensions = 22x24,02 mm.

RESULTS





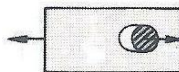
Peak: [kN]	$F_p = 278,89$	$d_{pav} = 7,97$	$d_{p1} = 3,73$	$d_{p2} = 1,76$
Elastic limit: [kN]	$F_{yaverage} = 257,38$	$d_{yaverage} = 4,93$	$d_{y1average} = 0,92$	$d_{y2average} = 0,35$
Ultimate: [kN]	$F_u = 223,11$	$d_{uav} = 9,48$	$d_{u1} = 5,95$	$d_{u2} = 3,17$
Stiffness: [kN/mm]		$K_{av} = 52,75$	$K_{LVD1} = 681$	$K_{LVD2} = 699,98$

COLLAPSE MODE

☐ Rivet Shear

☐ Bearing

☒ Tension

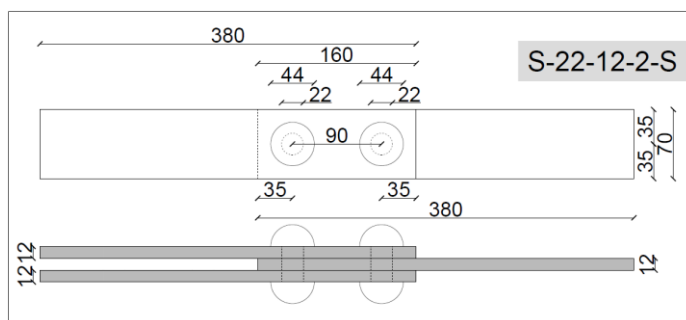
☐ Shear out


Appendix

S-22-12-2-B

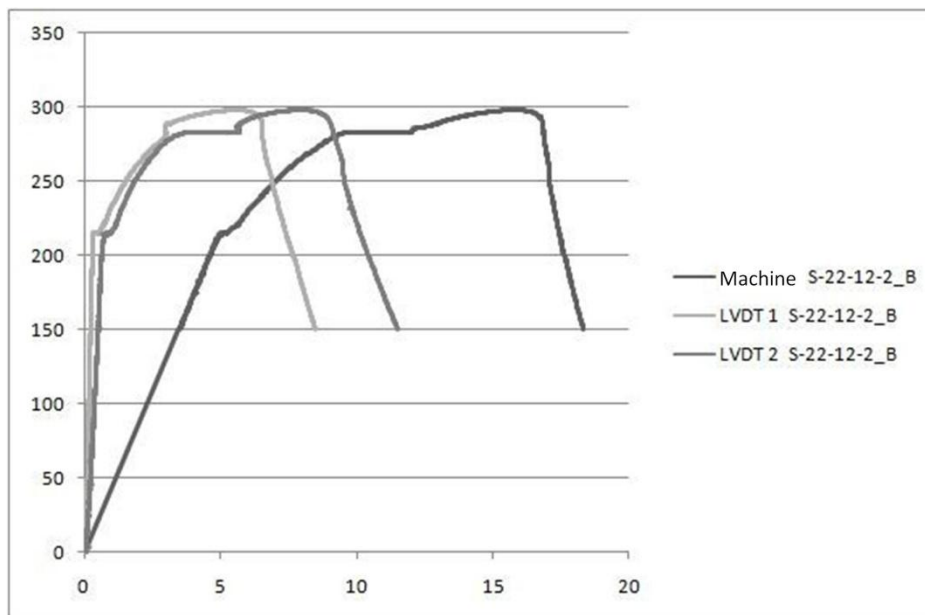
Specimen tag	S	U	Width plate (mm)	70
S-22-12-2-B	✓		Dist. from edge (mm)	35
Rivet diam. (mm)	22		Rivet pitch (mm)	90
Thickness plate (mm)	12		Rivet no.	2

PHOTOS



Test Information:

RESULTS





Peak: [kN]	$F_p = 298,35$	$d_{pav} = 15,73$	$d_{p1} = 5,52$	$d_{p2} = 7,90$
Elastic limit: [kN]	$F_{yaverage} = 212,70$	$d_{yaverage} = 4,91$	$d_{y1average} = 0,28$	$d_{y2average} = 0,72$
Ultimate: [kN]	$F_u = 238,68$	$d_{uav} = 17,70$	$d_{u1} = 7,05$	$d_{u2} = 9,72$
Stiffness: [kN/mm]		$K_{av} = 43,35$	$K_{LVD1} = 802,14$	$K_{LVD2} = 364,96$

COLLAPSE MODE

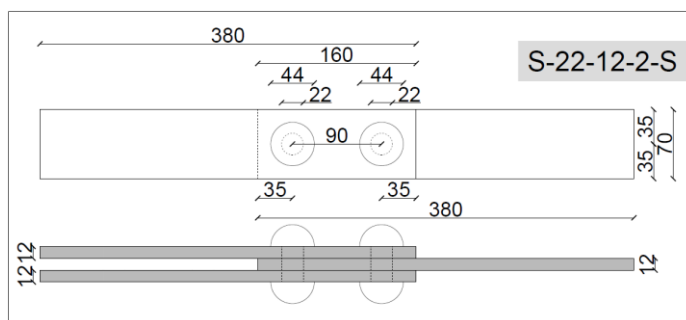
☐ Rivet Shear
 ☐ Bearing
 ☒ Tension
 ☐ Shear out



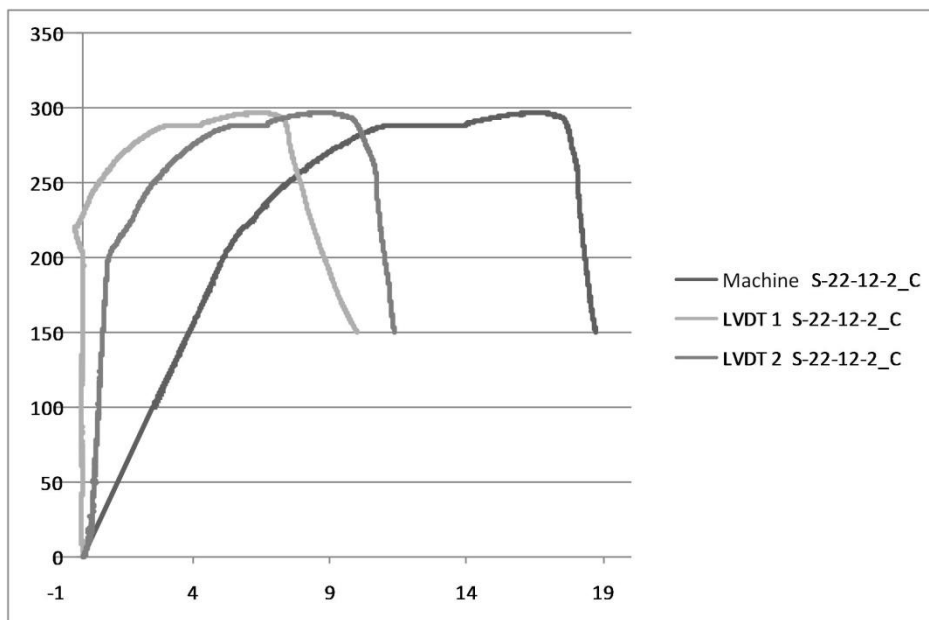
S-22-12-2-C

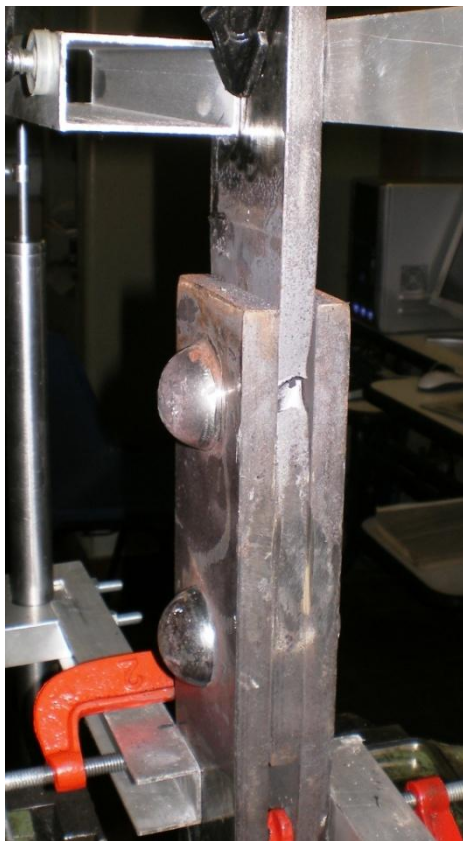
Specimen tag	S	U	Width plate (mm)	70
S-22-12-2-C	✓		Dist. from edge (mm)	35
Rivet diam. (mm)	22		Rivet pitch (mm)	90
Thickness plate (mm)	12		Rivet no.	2

PHOTOS

**Test Information:**

The failed plate width, at yielding, is equal to 63,25 mm; the unfailed plate width, at yielding, is equal to 64 mm; the hole deformed width =23.28 mm

RESULTS



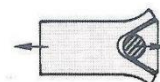
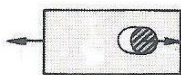
Peak: [kN]	$F_p = 296,89$	$d_{pav} = 16,63$	$d_{p1} = 6,51$	$d_{p2} = 8,84$
Elastic limit: [kN]	$F_{yaverage} = 210,02$	$d_{yaverage} = 5,47$	$d_{y1average} = -0,16$	$d_{y2average} = 1,25$
Ultimate: [kN]	$F_u = 237,51$	$d_{uav} = 18,14$	$d_{u1} = 8,12$	$d_{u2} = 10,75$
Stiffness: [kN/mm]		$K_{av} = 39$	$K_{LVDT1} = -$	$K_{LVDT2} = 279,3$

COLLAPSE MODE

☐ Rivet Shear

☐ Bearing

☒ Tension

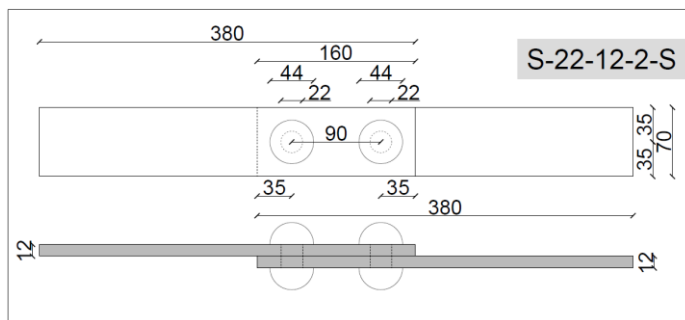
☐ Shear out


Appendix

U-22-12-2-A

Specimen tag	S	U	Width plate (mm)	70
U-22-12-2-A		✓	Dist. from edge (mm)	35
Rivet diam. (mm)	22		Rivet pitch (mm)	90
Thickness plate (mm)	12		Rivet no.	2

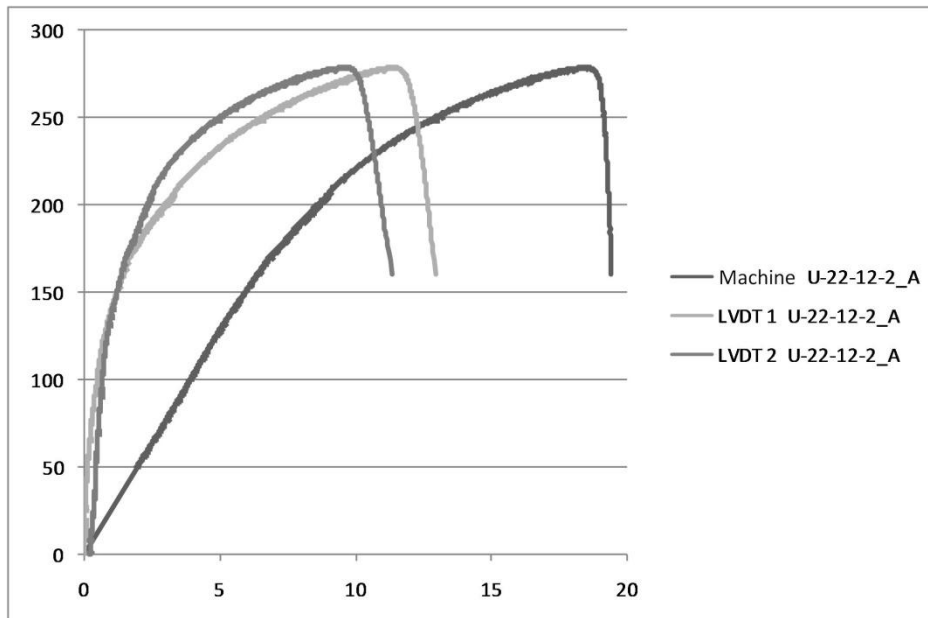
PHOTOS



Test Information:

Out of plane displacement for each plate = 17 mm.

RESULTS





Peak: [kN]	$F_p = 279,05$	$d_{pav} = 18,43$	$d_{p1} = 11,34$	$d_{p2} = 9,58$
Elastic limit: [kN]	$F_{yaverage} = 170,02$	$d_{yaverage} = 6,82$	$d_{y1average} = 1,66$	$d_{y2average} = 1,54$
Ultimate: [kN]	$F_u = 223,24$	$d_{uav} = 19,29$	$d_{u1} = 12,49$	$d_{u2} = 10,76$
Stiffness: [kN/mm]		$K_{av} = 25,51$	$K_{LVD1} = 379,16$	$K_{LVD2} = 202,33$

COLLAPSE MODE

☒ Rivet Shear

☐ Bearing

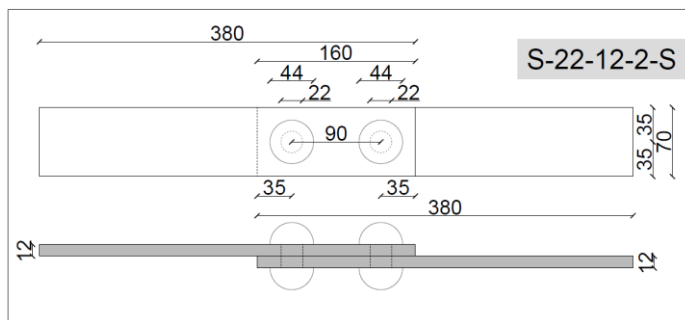
☐ Tension

☐ Shear out


U-22-12-2-B

Specimen tag	S	U	Width plate (mm)	70
U-22-12-2-B		✓	Dist. from edge (mm)	35
Rivet diam. (mm)	22		Rivet pitch (mm)	90
Thickness plate (mm)	12		Rivet no.	2

PHOTOS



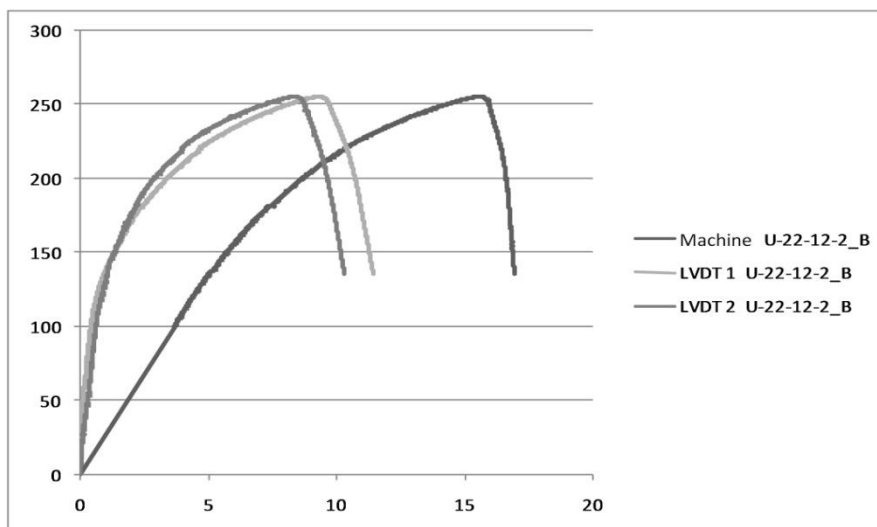
Test Information:

Plate 1: out of plane displacement=16,03mm, Plate 2: out of plane displacement=17,5mm.

Plate 1: side A hole deformed dimensions=22,5x23,6 mm; side B hole deformed dimensions=22,62x25,9 mm;

Plate 2: side A hole deformed dimensions=23,06x24,3 mm; side B hole deformed dimensions= 22,77x26,02 mm.

RESULTS

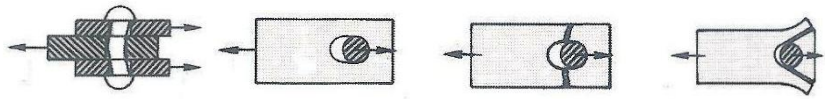




Peak: [kN]	$F_p = 255,24$	$d_{pav} = 15,61$	$d_{p1} = 9,33$	$d_{p2} = 8,42$
Elastic limit: [kN]	$F_{yaverage} = 150,06$	$d_{yaverage} = 5,72$	$d_{y1average} = 1,32$	$d_{y2average} = 1,32$
Ultimate: [kN]	$F_u = 204,20$	$d_{uav} = 16,56$	$d_{u1} = 10,64$	$d_{u2} = 9,61$
Stiffness: [kN/mm]		$K_{av} = 27,12$	$K_{LVD1} = 152,53$	$K_{LVD2} = 154,41$

COLLAPSE MODE

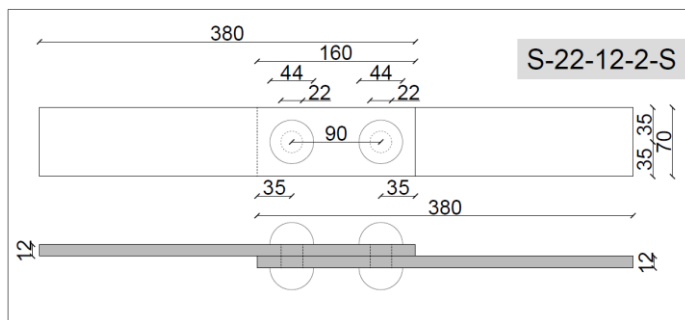
☒ Rivet Shear ☐ Bearing ☐ Tension ☐ Shear out



U-22-12-2-C

Specimen tag	S	U	Width plate (mm)	70
U-22-12-2-C		✓	Dist. from edge (mm)	35
Rivet diam. (mm)	22		Rivet pitch (mm)	90
Thickness plate (mm)	12		Rivet no.	2

PHOTOS



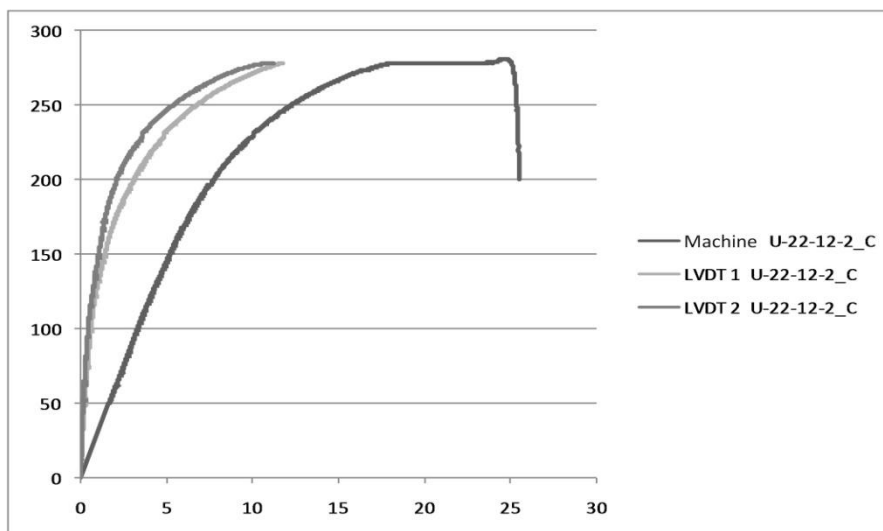
Test Information:

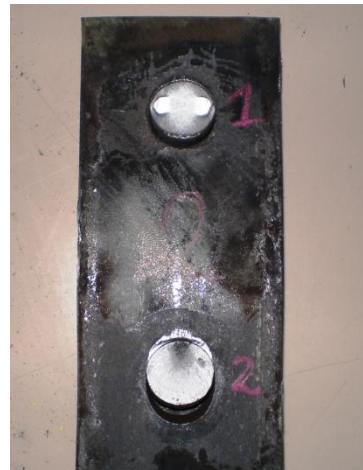
Plate 1: out of plane displacement=18,06mm, Plate 2: out of plane displacement=17,4mm.

Plate 1: side A hole deformed dimensions=22,6x24,27 mm; side B hole deformed dimensions=22,25x27,3 mm;

Plate 2: side A hole deformed dimensions=22,5x24 mm; side B hole deformed dimensions= 22,42x27,05 mm.

RESULTS





Peak: [kN]	$F_p = 280,77$	$d_{pav} = 25,13$	$d_{p1} = -$	$d_{p2} = -$
Elastic limit: [kN]	$F_{yaverage} = 170,72$	$d_{yaverage} = 6,57$	$d_{y1average} = 1,92$	$d_{y2average} = 1,36$
Ultimate: [kN]	$F_u = 224,62$	$d_{uav} = 25,93$	$d_{u1} = -$	$d_{u2} = -$
Stiffness: [kN/mm]		$K_{av} = 26,52$	$K_{LVD1} = 134,49$	$K_{LVD2} = 187,38$

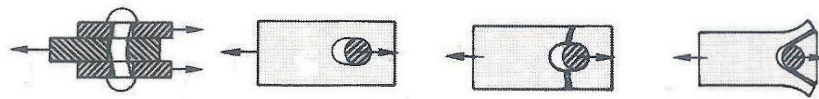
COLLAPSE MODE

☒ Rivet Shear

☐ Bearing

☐ Tension

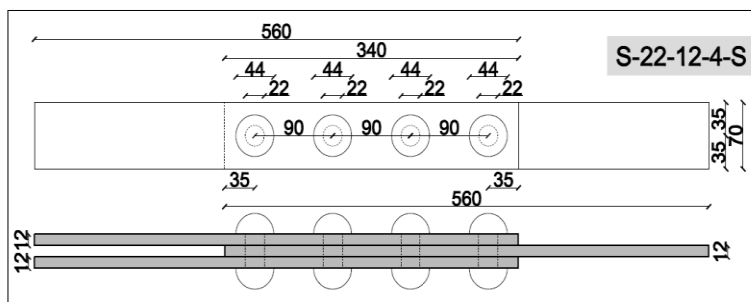
☐ Shear out



S-22-12-4-A

Specimen tag	S	U	Width plate (mm)	70
S-22-12-4-A	✓		Dist. from edge (mm)	35
Rivet diam. (mm)	22		Rivet pitch (mm)	90
Thickness plate (mm)	12		Rivet no.	4

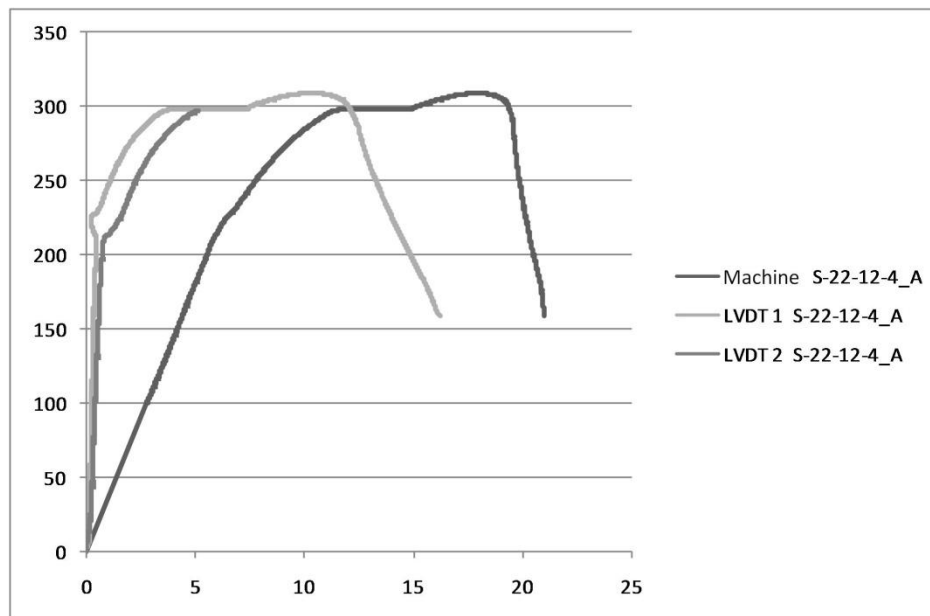
PHOTOS



Test Information:

The inner plate width, at yielding, is equal to 68 mm.

RESULTS





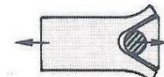
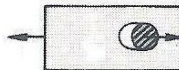
Peak: [kN]	$F_p = 308,94$	$d_{pav} = 17,83$	$d_{p1} = 10,26$	$d_{p2} = -$
Elastic limit: [kN]	$F_{yaverage} = 210,71$	$d_{yaverage} = 5,81$	$d_{y1average} = 0,46$	$d_{y2average} = 0,8$
Ultimate: [kN]	$F_u = 247,15$	$d_{uav} = 19,80$	$d_{u1} = 13,30$	$d_{u2} = -$
Stiffness: [kN/mm]		$K_{av} = 36,17$	$K_{LVD1} = 609,74$	$K_{LVD2} = 366,45$

COLLAPSE MODE

☐ Rivet Shear

☐ Bearing

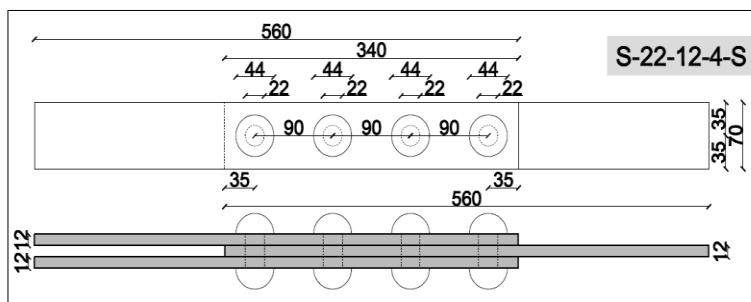
☒ Tension

☐ Shear out


S-22-12-4-B

Specimen tag	S	U	Width plate (mm)	70
S-22-12-4-B	✓		Dist. from edge (mm)	35
Rivet diam. (mm)	22		Rivet pitch (mm)	90
Thickness plate (mm)	12		Rivet no.	4

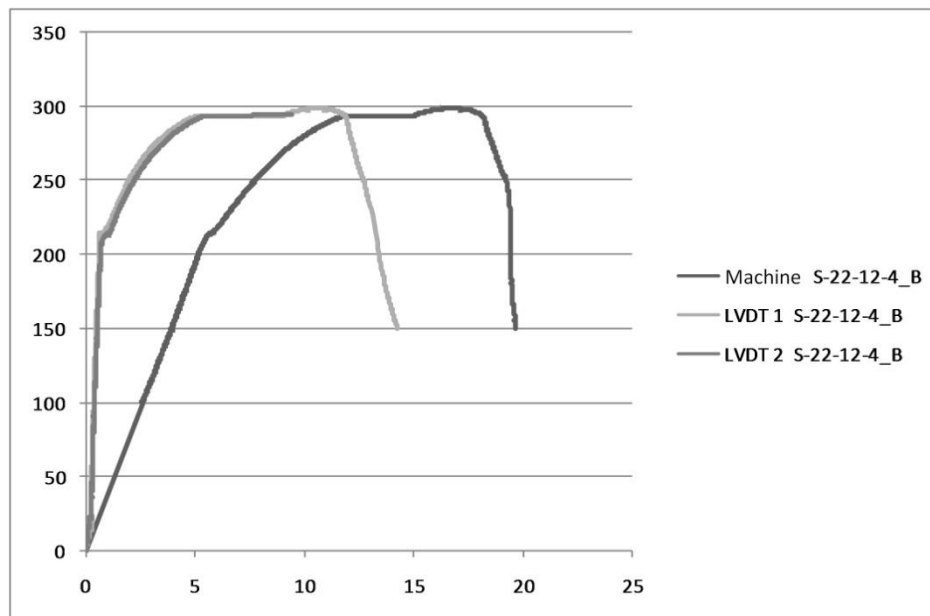
PHOTOS

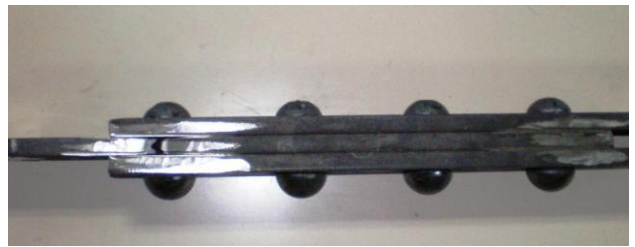


Test Information:

The inner plate width, at yielding, is equal to 68 mm.

RESULTS





Peak: [kN]	$F_p = 298,54$	$d_{pav} = 16,68$	$d_{p1} = 10,52$	$d_{p2} = -$
Elastic limit: [kN]	$F_{yaverage} = 211,38$	$d_{yaverage} = 5,5$	$d_{y1average} = 0,62$	$d_{y2average} = 0,81$
Ultimate: [kN]	$F_u = 238,83$	$d_{uav} = 19,30$	$d_{u1} = 12,80$	$d_{u2} = -$
Stiffness: [kN/mm]		$K_{av} = 38,88$	$K_{LVD1} = 458,15$	$K_{LVD2} = 326,6$

COLLAPSE MODE

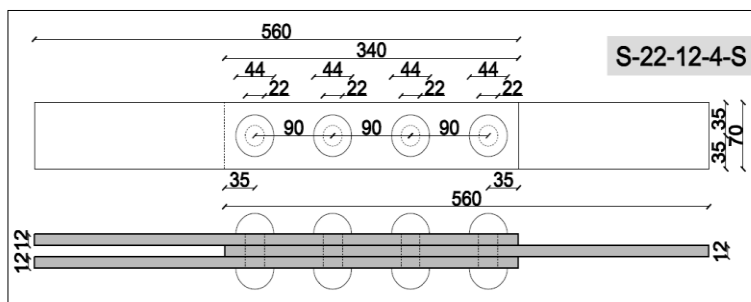
☐ Rivet Shear
 ☐ Bearing
 ☒ Tension
 ☐ Shear out



S-22-12-4-C

Specimen tag	S	U	Width plate (mm)	70
S-22-12-4-C	✓		Dist. from edge (mm)	35
Rivet diam. (mm)	22		Rivet pitch (mm)	90
Thickness plate (mm)	12		Rivet no.	4

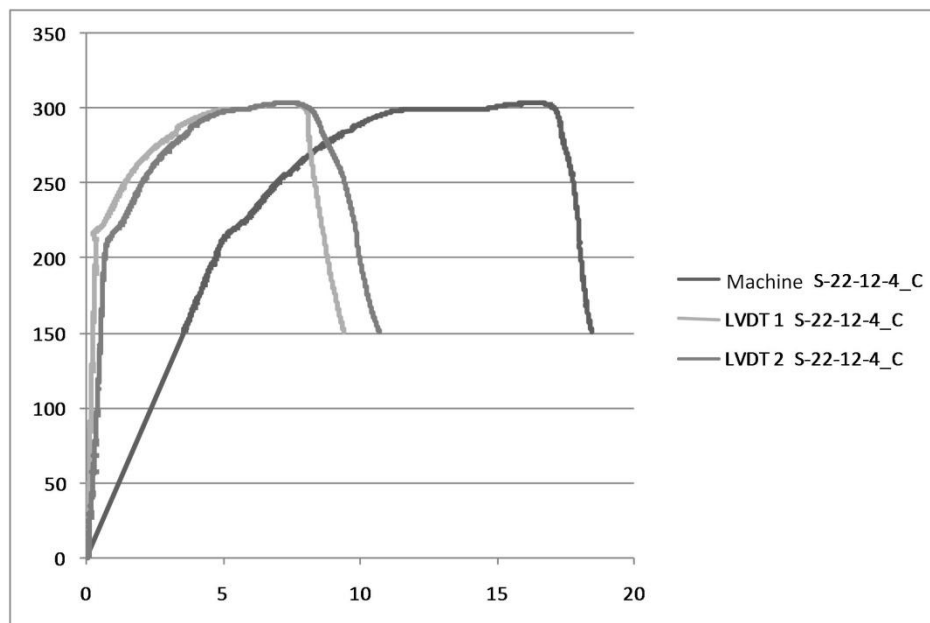
PHOTOS



Test Information:

The inner plate width, at yielding, is equal to 63.16 mm, the unfailed plate width, at yielding, is equal to 64.9 mm; the hole width is equal to 23.1 mm.

RESULTS

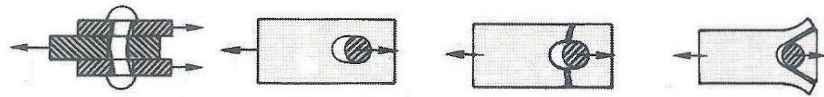




Peak: [kN]	$F_p = 303,50$	$d_{pav} = 16,26$	$d_{p1} = 7,24$	$d_{p2} = 7,24$
Elastic limit: [kN]	$F_{yaverage} = 209,37$	$d_{yaverage} = 4,92$	$d_{y1average} = 0,36$	$d_{y2average} = 0,75$
Ultimate: [kN]	$F_u = 242,80$	$d_{uav} = 17,80$	$d_{u1} = 8,40$	$d_{u2} = 9,50$
Stiffness: [kN/mm]		$K_{av} = 42,36$	$K_{LVD1} = 596,62$	$K_{LVD2} = 313,69$

COLLAPSE MODE

☐ Rivet Shear
 ☐ Bearing
 ☒ Tension
 ☐ Shear out

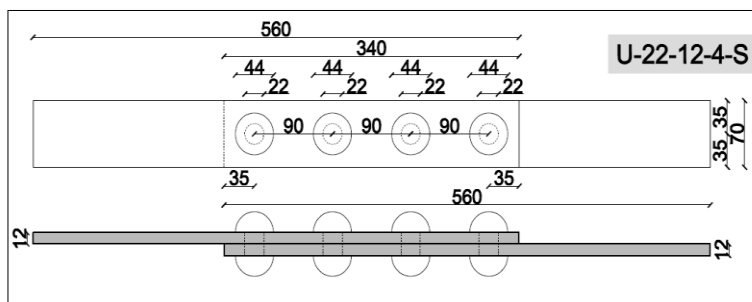


Appendix

U-22-12-4-A

Specimen tag	S	U	Width plate (mm)	70
U-22-12-4-A		✓	Dist. from edge (mm)	35
Rivet diam. (mm)	22		Rivet pitch (mm)	90
Thickness plate (mm)	12		Rivet no.	4

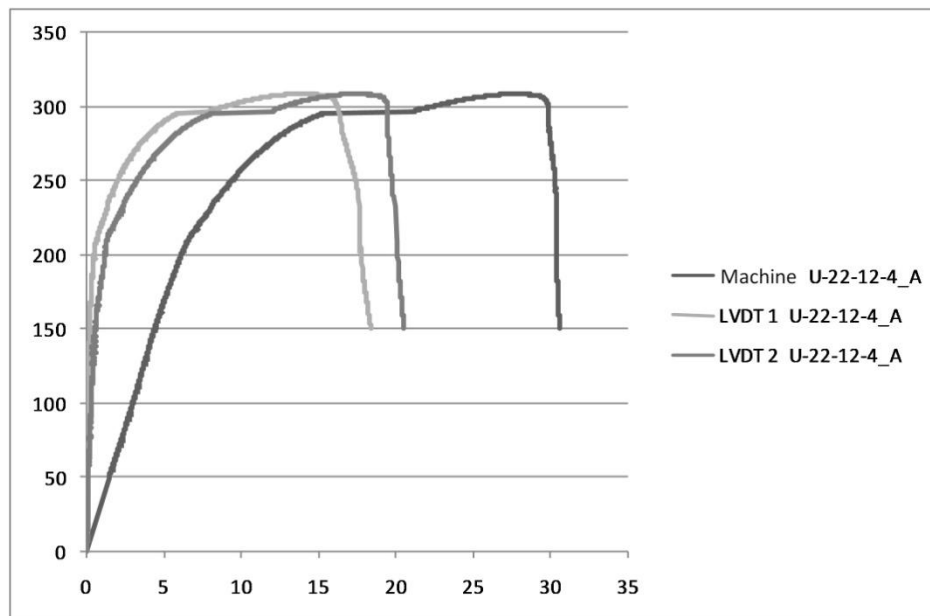
PHOTOS



Test Information:

Plastic out of plane displacement for each plate = 11 mm.

RESULTS





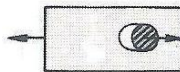
Peak: [kN]	$F_p = 308,94$	$d_{pav} = 27,77$	$d_{p1} = 13,93$	$d_{p2} = 17,40$
Elastic limit: [kN]	$F_{yaverage} = 201,34$	$d_{yaverage} = 6,16$	$d_{y1average} = 0,5$	$d_{y2average} = 1,2$
Ultimate: [kN]	$F_u = 247,15$	$d_{uav} = 30,30$	$d_{u1} = 17,50$	$d_{u2} = 19,70$
Stiffness: [kN/mm]		$K_{av} = 34,26$	$K_{LVD1} = 777,58$	$K_{LVD2} = 220,89$

COLLAPSE MODE

☐ Rivet Shear

☐ Bearing

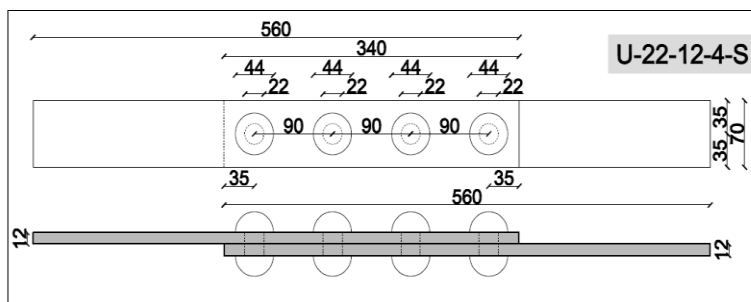
☒ Tension

☐ Shear out


U-22-12-4-B

Specimen tag	S	U	Width plate (mm)	70
U-22-12-4-B		✓	Dist. from edge (mm)	35
Rivet diam. (mm)	22		Rivet pitch (mm)	90
Thickness plate (mm)	12		Rivet no.	4

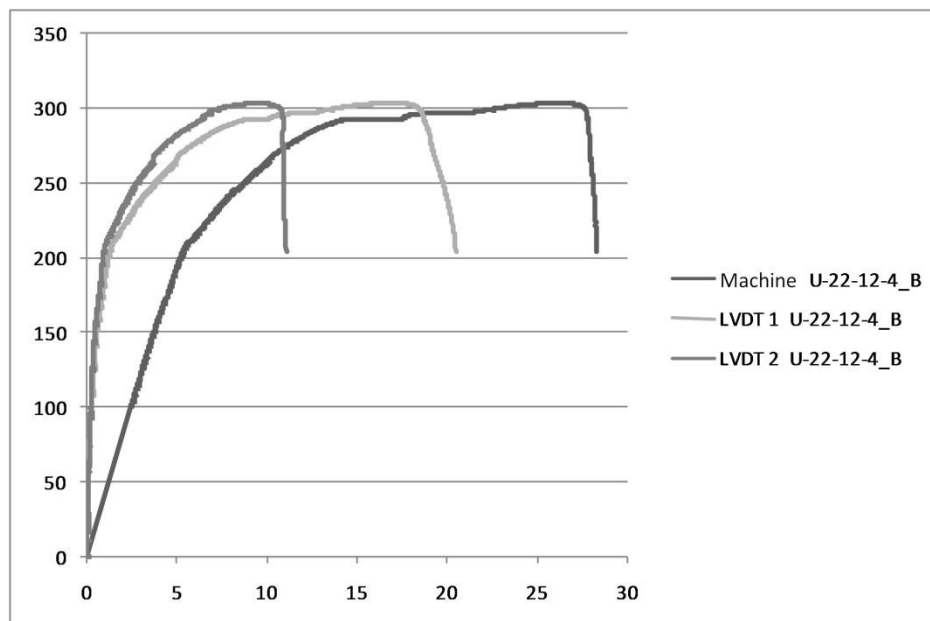
PHOTOS



Test Information:

The inner plate width, at yielding, is equal to 64 mm, the unfailed plate width, at yielding, is equal to 63.8 mm; the hole width is equal to 23,68 mm.

RESULTS





Peak: [kN]	$F_p = 303,59$	$d_{pav} = 26,06$	$d_{p1} = 16,84$	$d_{p2} = 9,48$
Elastic limit: [kN]	$F_{yaverage} = 200,68$	$d_{yaverage} = 5,23$	$d_{y1average} = 1,22$	$d_{y2average} = 0,91$
Ultimate: [kN]	$F_u = 242,87$	$d_{uav} = 28,10$	$d_{u1} = 19,90$	$d_{u2} = 10,90$
Stiffness: [kN/mm]		$K_{av} = 40,51$	$K_{LVD1} = 386,12$	$K_{LVD2} = 326,64$

COLLAPSE MODE

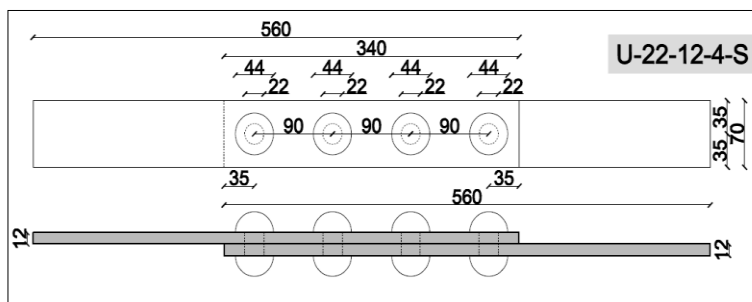
☐ Rivet Shear
 ☐ Bearing
 ☒ Tension
 ☐ Shear out



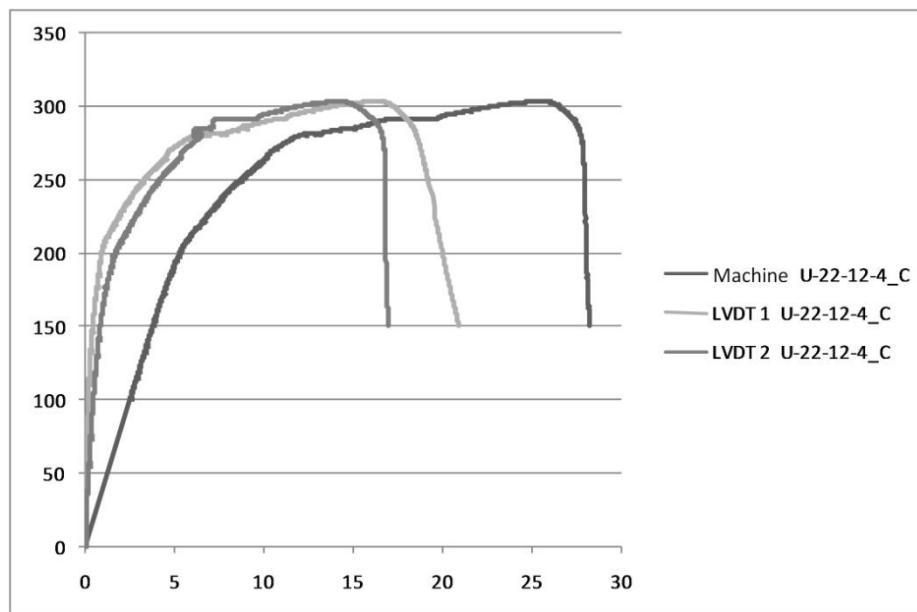
U-22-12-4-C

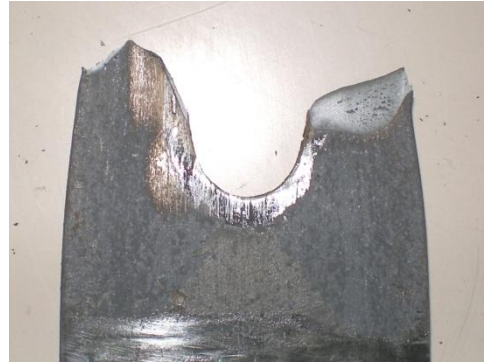
Specimen tag	S	U	Width plate (mm)	70
U-22-12-4-C		✓	Dist. from edge (mm)	35
Rivet diam. (mm)	22		Rivet pitch (mm)	90
Thickness plate (mm)	12		Rivet no.	4

PHOTOS

**Test Information:**

The inner plate width, at yielding, is equal to 64.2 mm, the unfailed plate width, at yielding, is equal to 65.1 mm; the hole width is equal to 23,13 mm.

RESULTS



Peak: [kN]	$F_p = 303,66$	$d_{pav} = 25,54$	$d_{p1} = 16,29$	$d_{p2} = 14,16$
Elastic limit: [kN]	$F_{yaverage} = 202,69$	$d_{yaverage} = 5,4$	$d_{y1average} = 0,98$	$d_{y2average} = 0,78$
Ultimate: [kN]	$F_u = 249,93$	$d_{uav} = 27,90$	$d_{u1} = 19,10$	$d_{u2} = 16,70$
Stiffness: [kN/mm]		$K_{av} = 39,55$	$K_{LVD1} = 370,33$	$K_{LVD2} = 193,03$

COLLAPSE MODE

☐ Rivet Shear
 ☐ Bearing
 ☒ Tension
 ☐ Shear out



Appendix

REFERENCES

- ABAQUS, Inc. (2010). ABAQUS Analysis User's Manual, v. 6.5.
- Al-Emrani M., Kliger R. (2003). FE analysis of stringer-to-floor-beam connections in riveted railway bridges. *Journal of Constructional Steel Research* No. 59: 803–818, ELSEVIER.
- Bailey DJ, Stevenson R. (1979). High strength low carbon sheet steel by thermo-mechanical treatment: 1. Strengthening mechanisms. *Metal Mater Trans*, 10(1):47–55.
- Ballio, G. and Mazzolani, F.M. (1983). “*Theory and design of steel structures*”, Chapman and Hall Ltd, London, ISBN 0-412-23660-5.
- Bassetti A., Nussbaumer A., Hirt M.A. (2000). Crack repair and fatigue life extension of riveted bridge members using composite materials. Proc intern. *symp. on bridge engineering conference, ESE-LABSE-FIB*, Sharm El Sheikh, Egypt.
- Batho C., Bateman EH. (1934). Investigations on bolts and bolted joints. *Second report of the steel structures research committee*. London.
- Billington D. P. (1983). *The tower and the bridge*, Princeton University press.
- Bresler B., Lyn T. Y. (1960). *Design of Steel Structures*. John Wiley & Sons, Inc., New York.
- Cadei JMC, Stratford TJ, Hollaway LC, Duckett WG. (2004). Strengthening Metallic structures using externally bonded fibre-reinforced polymers. *Publication C595, Construction Industry Research and Information Association (CIRIA)*, London, UK.
- CNR-DT 200/2004. Istruzioni per la Progettazione, l'Esecuzione ed il Controllo di Interventi di Consolidamento Statico mediante l'utilizzo di Compositi Fibrorinforzati. *Technical delivery*.
- Cooper T. (1889). American railroad bridges. *Trans.*, ASCE, 21 (July), 1-54.
- D'Aniello M., Portioli F., Fiorino L., Landolfo R. (2010). Experimental investigation on shear behaviour of riveted connections in steel structures, *Engineering Structures* 33: 516–531.
- Darnell V.C. (1984). Directory of American bridge-building companies 1840-1900. *Occasional publ. No. 4*. Soc. of Industrial Archeology, Washington, D.C.
- De Jonge A.E.R. (1945). Riveted joints. *Am. Soc. Of Mech. Engrs.*, New York, N.Y.
- Duggal S. K. (2000). *Design of steel structures*. Tata McGraw-Hill, ISBN 0-07-463095-4.

References

- EN 10025 (2004). Hot rolled products of non-alloy structural steels. Technical delivery conditions for flat products. *Committee ref. ISE 12*.
- EN 1993:1-8 (2005). Eurocode 3 design of steel structures part 1.8 “Design of joints”. Brussels: CEN.
- Esposto M. (2008). “*PTED beam-to-column connections for steel moment resisting frames: structural identification based on numerical analyses*”. Doctoral dissertation, University of Naples “Federico II”, Italy.
- European Committee for Standardisation (2002). EN 1990: Eurocode: basis of structural design. Brussels.
- Fernandes A. A., Castro P. T., Figueiredo M. and Oliveira F. (2004) Structural integrity evaluation of highway riveted bridges. In: Bridge Maintenance, SAFETY and Management (IABMAS’04); Proc. Intern. Conf., Kyoto, 18-22 October 2004. (E.Watanabe et al. , Ed.). Balkema, Rotterdam: 839–841.
- Fisher JW, Yoshida N. (1969). Large bolted and riveted shingle splices. *J Struct Div, ASCE*; 96(ST9).
- Gasparini D., Simons D. (1997). American truss bridge connections in the 19th century. II: 1850-1900. *Journal of Performance of Constructed Facilities*, Vol 11, n. 3.
- Gray G.E. (1897). Notes on early practice in bridge building. *Trans., ASCE*, 37 (June), 1-16.
- Greiner J.E. (1895),. What is the life of an iron railroad bridge? *Trans., ASCE*, 34 (Oct), 294-346.
- Guerrieri M.R., Di Lorenzo G., Landolfo R. (2005). Influence of atmospheric corrosion on the XIX century “iron” structures: assessment of damage for Umberto I Gallery in Naples. *Proc. of XX CTA Conference*, Ischia (Italy) 26-28 September.
- Hechtman R.A. (1948). A study of the effects of heating and driving conditions on hot driven structural steel rivets. *Off. of nav. res. project. University of Illinois*.
- Hohlwegler B (1993). Korrosion von Stählen aus eisernen Konstruktionen des 19. Jahrhunderts, Mineralogische und metallographische Untersuchungen an historischen Eisen und an daraus resultierenden Korrosionsprodukten. *Dissertation Universität Karlsruhe (TH)*. [in German].
- Hrennikoff A. (1934). Work of rivets in riveted joints. *Trans ASCE*;99:437–49.
- Iwankiw N, Sghlafly T. (1982). Effect of hole-making on the strength of double lap joints. *Eng J, AISC*;III–IV:170–8.
- Koegler RK, Schnitt A. (1943). Effects of yielding on perforations on a wing tension surface. *J Aeronaut Sci*;10:273–84.
- Kulak G.L., Fisher J.W., Struik J.H.A. (1987). *Guide to design criteria for bolted and riveted joints*. 2nd ed. New York: John Wiley & Sons; 1987.
- Liu H., Al-Mahaidi R., Zhao X.L. (2009). Experimental study of fatigue crack growth behaviour in adhesively reinforced steel structures, *Engineering Structures* 90: 12–20.

- Mackanness C. (2006). *Bridging Sydney*, Historic Houses Trust of New South Wales.
- Malina J, Stanková H, Drnek J, Nový Z, Mašek B. (2005). Influence of thermomechanical treatment on the steel C45 fatigue properties. *In: Proc. of 13th inte. Scientific conference CO-MAT-TECH*.
- Mang F, Bucak Ö. (1996). Tauglichkeit und Lebensdauer von bestehenden Stahlbauwerken. Kapitel 18 in Stahlbau Handbuch 1, Teil B; Stahlbau-Ein Handbuch für Studium und Praxis, 3 Bände. Herausgegeben vom Deutschen Stahlbau- Verband-Köln. Stahlbau-Verlagsgesellschaft mbH Köln. [in German].
- Marmo R., D'Aniello M., Portioli F., Landolfo R. (2010). Finite element modelling of lap shear riveted connections in fire. *Proc. of International Conference on Urban Habitat Constructions Under Catastrophic events Final Conference*, COST Action C26, Napoli, 16-18 September.
- Marrullier E. (1925). Costruzione degli Edifizi. UTET, Torino.
- Masi F. (1996). Costruire in acciaio. Hoepli, Milano.
- Mercur J. (1891). Rivets, riveted joints and pin connected joints. *U.S.M.A. Publ.*, West Point, N.Y.
- Moreno J., Valiente A. (2004). Stress intensity factor in riveted steel beam. *Engineering Failure Analysis*, No. 11:777-787, ELSEVIER.
- Moreno J., Valiente A. (2006). Cracking induced failure of old riveted steel beams. *Engineering Failure Analysis* No. 13: 247–259, ELSEVIER.
- Munse WH, Cox HC. (1956). The static strength of rivets subjected to combined tension and shear. *Engineering experiment station bulletin 437*. Urbana: University of Illinois.
- Munse WH. (1970). Final report on riveted and bolted structural joints project IHR-5 *Illinois cooperative highway research program*. Urbana: University of Illinois.
- Nack JK, Gareth T. (1983). Evolution of multiphase structures and their influence on mechanical properties of low carbon steels. *In: Proc. of int. conference on technology and application of HSLA steels*.
- Parrilli M. (2010). *Vulnerability of historic metallic structures and reversible consolidation technologies with FRP*. Doctoral dissertation, University of Naples “Federico II”, Italy.
- PROHITECH—earthquake protection of historical buildings by reversible mixed technologies. (2005). <http://www.prohitech.com/>.
- RFI (2000) Istruzioni 44M specifica tecnica relativa al collaudo dei materiali ed alla costruzione delle strutture metalliche per ponti ferroviari e cavalcavia. [in Italian].
- RFI (1991) steel structure division of Naples. Internal bulletin. [in Italian].
- Ryall M.J., Parke G.A.R., Harding J.E. (2000). *Manual of Bridge Engineering*, Thomas Telford.

- Sarraf M., Bruneau M. (1996). Cyclic testing of existing and retrofitted riveted seat angle connections. *Journal of structural engineering*, Vol. 122, No. 7, July.
- SB3.4. (2007) Condition assessment and inspection of steel railway bridges, including stress measurements in riveted, bolted and welded structures. *Background document D3.4 to "guideline for condition assessment and inspection"*. Prepared by Sustainable bridges—a project within EU FP6. [Available from: www.sustainablebridges.net].
- Schenker L, Salmon CG, Johnston BG. (1954). Structural steel connections. *AFSWP rep. no. 352. Ann Arbor*: Department of Civil Engineering. University of Michigan.
- Schutz FW. (1952). *The efficiency of riveted structural joints*. Doctoral dissertation. University of Illinois.
- Shoukry Z, Haisch WT. (1970). Bolted connections with varied hole diameters. *J Struct Div, ASCE*; 96(ST6).
- Simmons D.A. (1989). Bridge building on a national scale: the King Iron Bridge and Manufacturing Company. *J. Soc. For Industrial Archeology*, 15(2), 23-39.
- Snijder HH, Ungermann D, Stark JWB, Sedlacek G, Bijlaard FSK, Hemmert-Halswick A. (1988). Evaluation of test results on bolted connections in order to obtain strength functions and suitable model factors—part A: results. Eurocode no. 3—part 1—background documentation. *Document 6.01. Brussels: Commission of the European Communities*; [Chapter 6].
- Stier W, Kosteas D, Graf U. (1983). Ermüdungsverhalten von Brücken aus Schweißeisens. *Der Stahlbau* 5. [in German].
- Stratford T.J., Chen J.F. (2005) Designing for tapers and defects in FRP-strengthened metallic structures. *Proc intern. symp. on bond behaviour of FRP in structures, BBFS2005*, Hong Kong, China.
- Sustainable bridges. (2006). Guideline for load and resistance assessment of existing european railway bridges—advices on the use of advanced methods. *European research project under the EU 6th framework programme*. <http://www.sustainablebridges.net/>.
- Tessarotto M. G. (1952). *Saldatura e chiodatura*. Gorlich Ed. Milan.
- Valtinat G, Huhn H. (2004). Bolted connections with hot dip galvanized steel members with punched holes. In: *Proc. of connections in steel structures*. p. 297–309.
- Vermes W. (2007). Designing and Performance of riveted bridge connections. In: *Proc. of Ohio Transportation Engineering Conference*, 24 October.
- Waddell J.A.L. (1888). Chapter II: general specifications. *The designing of ordinary highway bridges*, Third ed. John Wiley & Sons, New York, N.Y.
- Waddell J.A.L. (1889). Discussion of “American Railroad Bridges”, by T. Cooper. *Trans., ASCE*, 21 (Dec), 566-607.
- Xia S.H., Teng J.G. (2005). Behaviour of FRP-to-steel bonded joints. *Proc intern. symp. on bond behaviour of FRP in structures, BBFS2005*, Hong Kong, China.

- Yong-xin Y., Qing-rui Y., Fu-ming P. (2005). Experimental research on bond behaviour of CFRP to steel. *Proc intern. Symp. On bond behaviour of FRP in Structures, BBFS2005*, Hong Kong, China.
- Zhao X., Zhang L. (2007). State-of-the-art review on FRP strengthened steel structures, *Engineering Structures* 29: 1808–1823.
- Zienkiewicz, O.C., Taylor, R.L. and Zhu, J.Z. (2004). “*The Finite Element Method: its basis and fundamentals*” (sixth edition).